The use of genetically modified mouse models for investigations of mechanisms of arterial stiffness

By:

Kayla Dawn Viegas (BEng, MSc)

A thesis accepted for the degree of

DOCTOR OF PHILOSOPHY

The Australian School of Advanced Medicine

Faculty of Human Sciences

Macquarie University

September 2014

Declaration of originality

I hereby declare that the work presented in this thesis entitled "*The use of genetically modified mouse models for investigations of mechanisms of arterial stiffness*" has not been submitted for a degree nor has it been submitted as part of the requirements for a degree to any other university or institution other than Macquarie University. The majority of the work in this thesis was conducted in the Australian School of Advanced Medicine under the supervision of Prof Alberto Avolio and Dr. Mark Butlin. Some of the work was also undertaken at the Victor Chang Cardiac Research Institute under the supervision of Dr. Siiri Iismaa and in the Department of Anaesthesia and Critical Care Medicine at Johns Hopkins University under the supervision of Prof Dan E Berkowitz and Dr. Lakshmi Santhanam. I declare that the contents of this thesis represent the original experimentation and written work of the candidate except where due acknowledgements are made.

This work was carried out with ethical approval from: the Animal Care and Ethics Committee of Macquarie University (ARA 2011/002, ARA, 2011/017, ARA, 2011/036); the Garvan/St. Vincent's Animal Ethics Committee (12_29); and the Johns Hopkins University Animal Care and Use Committee (MO13M258).

Kayla Dawn Viegas

Declaration of contributions

Chapter 7

The implantation of osmotic mini pumps and measurement of tail-cuff blood pressure was performed by Konrad Vandegaer. The transthoracic echocardiography was performed by Djahida Bedja. All other experimental work and all data analysis were performed by the candidate.

Appendix

The surgeries performed in the study comparing passive and active changes in blood pressure on PWV in the rat aorta were performed by the candidate, Dr. Mark Butlin, and George Lindesay.

Acknowledgements

Thank you to my supervisor, Prof Alberto Avolio for your guidance, support, and philosophical life lessons throughout my candidature. Thank you also for checking your UNSW email after moving to Macquarie or else who knows where I would have ended up. Thank you to my co-supervisor, Dr. Mark Butlin for your mentorship and help throughout this thesis, especially in the experimental design and in the early days where you sat with me during my initial 8 hour-long surgeries. I would never have been able to complete this academic and ***EMOTIONAL*** journey without you two. Thank you for believing in me before I believed in myself. Not only have you been teachers, you've been friends.

Thank you to the Australian Government and Macquarie University for giving me the International Postgraduate Research Scholarship and the Macquarie University Research Excellence Scholarship throughout my candidature. Thank you to the Skipper family for providing me with funding to present my work at the European Society for Hypertension conference and to visit the Berkowitz Lab at Johns Hopkins University. Also thank you to ASAM for providing a top up scholarship which has removed the financial stress of being an international student in Sydney.

I've learned so many different things from so many different people here at ASAM, but a few in particular stand out that I want to thank. Dr. Andrea Gaede taught me so much about surgery and was the first person to let me cannulate a rat artery and vein all by myself. She also held my hand through the terrifying experience of trying to do an IP injection in the mouse, and then did it herself when I was almost in tears. Dr. Sarah Hemley, in addition to providing great advice, taught me LOTS about histology which was instrumental in this thesis. Andrew Hammond taught me everything I know about how to use a myograph, and he made me the best ever ECG electrodes which I used throughout my surgeries. Omar Al-Adhami showed me how to do the calcium assay, to use an organ bath, and too many other

things to list. George Lindsay let me sit in on countless hours of surgery, was my first physiology teacher, and showed me how to use Spike about 10 times. Dr. Melissa Farnham developed a practice mouse protocol so I could perfect my surgical techniques and gave me great tips and advice regarding mouse handling and surgery. Thanks also to Dr. Lindsay Parker for teaching me how to use a microscope.

I can't thank enough Dr. Siiri Iismaa for always helping me ***IMMEDIATELY*** whenever I needed anything, from TG2 advice to getting me mice that I desperately needed and all the bureaucracy associated with doing animal work at a new institution.

Special thanks to Prof Dan Berkowitz and Dr. Lakshmi Santhanam for allowing me to spend two months in their brilliant lab at Hopkins to collect some wonderful data for this thesis. I owe a big thank you to Konrad Vandegaer for doing all the implantations and tail cuff blood pressure measurements in my mice and Djahida Bedja for performing such great echoes. There would be no Chapter 7 without the collective effort from all of you.

I would also like to extend my thanks to many of the academic and research staff at ASAM who have given me support, advice, and encouragement: Ann Goodchild, Paul Pilowsky, Mark Connor, Simon McMullan, Anita Turner, and Rochelle Boyd.

My family is the best and have always been so supportive of me moving across the world for this massive undertaking. Mom and Dad, thank you for your love, for listening to me, and always telling me how amazing I am (when I feel anything but). Leanne, you always make me smile and your emails have brought me lots of happiness from across the world. Grandma, Grandpa, and Susan, thank you for your love and encouragement. I'm so lucky to have such a wonderful family.

I am lucky enough to also have the best friends ever, whose constant love, support, and hugs have helped me to get through this, both from Canada and Australia. There are a few people

who I would like to specially mention: Megan Hancock, Sarah Wisniewski, Andrea Gaede, Francesca Giudici, Helena Klanjscek, Oldooz Dianat, and Sarah Hemley.

Last, but certainly not least, I have to thank Xavi, for loving me and taking care of my psychological health throughout the last couple of years. I warned you from the beginning that I was “impatient and grumpy” and this PhD certainly exasperated that, but you have endured it all in the most caring and supportive way and I don’t think I would have come this far without you. T’estimo molt!

Publications

Peer reviewed articles

[1] S.M. Jung, S. Jandu, J Steppan, A. Belkin, S.S. An, A. Pak, E.Y. Choi, D. Nyhan, M. Butlin, **K. Viegas**, A.P. Avolio, D.E. Berkowitz, L. Santhanam, Increased Tissue Transglutaminase Activity Contributes to Central Vascular Stiffness in eNOS Knockout Mice., American Journal of Physiology. Heart and Circulatory Physiology. (2013).

[2] A.P. Avolio, M. Butlin, Y.-Y. Liu, **K. Viegas**, B. Avadhanam, G. Lindesay, Regulation of arterial stiffness: Cellular, molecular and neurogenic mechanisms, Artery Research. 5 (2011) 122–127.

Conference abstracts published in journals

[3] **K.D. Viegas**, M. Butlin, A.P. Avolio, Characterisation of the pressure dependency of pulse wave velocity in the mouse aorta, Journal of Hypertension. 30 (2012) e159.

[4] G. Lindesay, **K.D. Viegas**, M. Butlin, A.P. Avolio, Sympathetic activity contributes to abdominal aortic compliance and wall distensibility in rats, Journal of Hypertension. 29 (2011) e485.

[5] M. Butlin, G. Lindesay, **K.D. Viegas**, I. Tan, A.P. Avolio, Cardiovascular parameters other than mean arterial pressure are predictive of dynamics changes in aortic stiffness in the rat, Artery Research. 5 (2011) 160.

[6] M. Butlin, A. Hammond, G. Lindesay, **K. Viegas**, A.P. Avolio, In-vitro and in-vivo use of vasoactive agents in characterising aortic stiffness in rats: testing the assumptions, Journal of Hypertension. 30 (2012) e42.

[7] **K.D. Viegas**, G. Lindesay, M. Butlin, A.P. Avolio, Aortic stiffness is dependent on direction of mean arterial pressure change, Hypertension. 60 (2012) 497.

[8] **K.D. Viegas**, M. Butlin, A.P. Avolio, Effect of tissue transglutaminase (TG2) on cardiac and vascular function in young TG2 knockout mice, Artery Research. 6 (2012) 183.

Conference abstracts published in proceedings

[9] **K.D. Viegas**, M. Butlin, L. Santhanam, D.E. Berkowitz, A.P. Avolio, Transglutaminase 2 does not have intrinsic effect on in-vivo pressure-dependent stiffness in healthy adult mice, 23rd European Meeting on Hypertension and Cardiovascular Protection. (2013).

[10] **K. Viegas**, M. Butlin, A.P. Avolio, Cardiovascular parameters other than mean arterial pressure are also predictive of dynamic changes in aortic stiffness in the mouse, 23rd European Meeting on Hypertension and Cardiovascular Protection. (2013).

[11] G. Lindesay, **K.D. Viegas**, M. Butlin, A.P. Avolio, Sympathetic denervation decreases aortic compliance in rats, High Blood Pressure Research Council of Australia Meeting. (2010).

Abstract

Arterial stiffness is an independent risk factor for cardiovascular morbidity and mortality. With age, the large arteries become stiffer, leading to hypertension, left ventricular hypertrophy, end organ damage, and cardiovascular disease. However, the underlying cellular and molecular mechanisms leading to increased arterial stiffness remain largely unknown. The scope of the work presented in this thesis encompasses the use of genetically modified mouse models to explore potential mechanisms of vascular stiffness. A novel, high-fidelity technique of estimating aortic stiffness by pulse wave velocity (PWV) in the mouse was developed and used to characterise the pressure-dependency of PWV in the mouse aorta. Transglutaminase 2 (TG2) is a multifunctional enzyme which was hypothesized to play a role in arterial stiffness due to its ability to crosslink various structural proteins in the extracellular matrix. Pressure-dependent PWV, vascular reactivity, aortic geometry and calcification, and cardiac function were investigated in $TG2^{-/-}$ and wild type (WT) mice. Findings suggest that TG2 plays a role in arterial stiffness at high blood pressures and left ventricular hypertrophy. The apolipoprotein E knockout ($apoE^{-/-}$) mouse is a widely used model of human atherosclerosis. *In vivo* PWV measurements demonstrated increased stiffness in $apoE^{-/-}$ mice compared to control as early as 12 weeks of age. Endothelial dysfunction through an impaired relaxation response to acetylcholine was also observed. A study of the effects of early aging on vascular stiffness in the mouse was also performed. Between the ages of 12 and 36 weeks a significant increase in aortic stiffness was observed in WT mice. A slight but insignificant increase in PWV was observed in the $apoE^{-/-}$ mouse suggesting that the rate of change of PWV is strain dependent. The nitric oxide synthase inhibitor, L-NAME, was used to induce both increased TG2 activity and endothelial dysfunction, with the hypothesis that this would increase arterial stiffness. In $TG2^{-/-}$ mice and WT control, no differences in cardiovascular function were observed after L-NAME treatment. However, in 12 week old $apoE^{-/-}$ mice, L-NAME administration reduced PWV, suggesting the presence of compensatory mechanisms that account for the lack of nitric oxide bioavailability. This thesis provides new insights into potential mechanisms of increased vascular stiffness. More importantly, it highlights the utility of the genetically modified mouse as a tool for interrogating novel pathways to arterial stiffness, and a new method with which to do so. Use of this technique could lead to the identification of novel therapeutic targets for the treatment of vascular stiffness.

Table of Contents

Declaration of originality i

Declaration of contributions ii

Acknowledgements iii

Publications vi

Abstract viii

Table of Contents ix

List of Figures xvi

List of Tables xxvi

List of Abbreviations xxviii

Chapter 1 Introduction *1*

Chapter 2 Literature Review *7*

2.1 Arterial function 7

2.2 Pressure wave reflection 8

2.3 Arterial stiffness 9

2.4 Measuring arterial stiffness 9

2.4.1 Measurement of pulse wave velocity in the mouse 12

2.5 Arterial structure 20

2.6 Factors influencing large artery stiffness 22

2.6.1 Age and blood pressure 23

2.6.2 Structural components 23

2.6.3 Arterial remodelling 24

2.6.4 Advanced glycation end products 26

2.6.5 Calcification 27

2.6.6 Atherosclerosis 28

2.6.7 Other extrinsic factors 30

2.7 Endothelial function 31

2.7.1 S-Nitrosylation 32

2.7.2 Nitric oxide inhibition 33

2.8 Transglutaminase 2 37

2.9 Apolipoprotein E 45

2.10 Aging 48

2.11 Hypotheses and specific aims 49

2.11.1 Refining measurement of PWV in the mouse 49

2.11.2 Transglutaminase 2 50

2.11.3 Apolipoprotein E 52

2.11.4 Aging 52

Chapter 3 Aortic pulse wave velocity measurement in the mouse: method development 55

3.1 Housing and anaesthesia 56

3.2 Calculation of PWV 56

3.3 Assessment of PWV measurement techniques 57

3.3.1 PWV measurement using Doppler flow 58

3.3.2 Use of fluid filled pressure catheters 59

3.3.3 PWV measurement using an intravascular catheter and applanation tonometry 59

3.3.4 Intra-vascular pressure measurement of PWV 63

3.4 Vasoactive control of blood pressure 64

3.5 Altering blood pressure: Effect of SNP on the mouse aortic PWV 67

3.5.1 Methods 67

3.5.1.1 Animals 67

3.5.1.2 Infusion rates and venous return 67

3.5.1.3 Active and passive lowering of blood pressure 68

3.5.1.4 Data and statistical analysis 68

3.5.2 Results 68

3.5.2.1 Infusion rates and venous return 68

3.5.2.2 Vasoactive control of blood pressure: Directional dependence in the PWV-MAP relationship 69

3.5.2.3 Comparison of passive and active pressure changes 71

3.6 Discussion 72

Chapter 4 Characterisation of pressure dependency of aortic PWV in the mouse 77

4.1 Introduction 77

4.2 Methods 77

4.2.1 Animals 77

4.2.2 Incremental stiffness along the length of the mouse aorta 78

4.2.3 Pressure dependent PWV relationship 78

4.2.4 Cardiovascular parameters predictive of dynamic changes in PWV 79

4.2.5 Data and statistical analysis 79

4.3 Results 79

4.3.1 Incremental stiffness along the length of the mouse aorta 80

4.3.2 Pressure dependent PWV relationship 83

4.3.3 Cardiovascular parameters predictive of dynamic changes in PWV 85

4.4 Discussion 86

Chapter 5 Effect of transglutaminase 2 on arterial stiffness 89

5.1 Methods 90

5.1.1 Animals 90

5.1.2 L-NAME administration 90

5.1.3 PWV measurement 90

5.1.4 Baroreflex sensitivity 91

5.1.5 Tissue dissection and preparation 91

5.1.6 Wire Myography 92

5.1.6.1 Tensile testing 92

5.1.7 Calcium quantification assay 93

5.1.8 Histological analysis 94

5.1.9 Statistical Analysis 94

5.2 Results 95

5.2.1 Baseline Characteristics 95

5.2.2 Pulse Wave Velocity 96

5.2.3 Baroreflex sensitivity 103

5.2.4 Tensile testing 103

5.2.5 Vascular Studies 104

5.2.5.1 Smooth muscle contraction 104

5.2.5.2 Smooth muscle cell relaxation 107

5.2.5.3 Endothelium-dependent relaxation 109

5.2.6 Calcification Assay 112

5.2.7 Histology 113

5.3 Discussion 114

Chapter 6 Transglutaminase 2 and arterial stiffness: effect of increased duration of NOS inhibition 123

6.1 Methods 123

6.1.1 Animals 123

6.1.2 L-NAME treatment 124

6.1.3 Cardiac Function – Transthoracic echocardiography 124

6.1.4 PWV Measurement 125

6.1.5 Histological analysis 125

6.1.6 Statistical Analysis 125

6.2 Results 126

6.2.1 Baseline Characteristics 126

6.2.2 Cardiac function 127

6.2.3 Pulse Wave Velocity 129

6.2.4 Baroreflex Sensitivity 136

6.2.5 Histology 136

6.3 Discussion 138

Chapter 7 Arterial stiffness in apolipoprotein E knockout mice 145

7.1 Methods 146

7.1.1 Animals 146

7.2.2 L-NAME treatment 146

7.2.3 Experimental procedures 146

7.2.4 Statistics and data analysis 147

7.2 Results 147

7.2.1 Baseline characteristics 147

7.2.2 Pulse wave velocity 148

7.2.3 Baroreflex sensitivity 151

7.2.4 Tensile testing 152

7.2.5 Vascular reactivity 153

7.2.5.1 Smooth muscle cell contraction 153

7.2.5.2 Smooth muscle cell relaxation 155

7.2.5.3 Endothelium-dependent relaxation 157

7.2.6 Calcification assay 160

7.2.7 Histology 160

7.3 Discussion 162

Chapter 8 Effect of age on pressure-dependent PWV in the mouse 171

8.1 Methods 172

8.1.1 Animals 172

8.1.2 Experimental procedures 172

8.1.3 Statistical Analysis 172

8.2 Results: preliminary analysis of the dependence of PWV on age 173

8.3 Results: effect of age on WT and apoE$^{-/-}$ mice 174

8.3.1 Baseline characteristics 175

8.3.2 Pulse wave velocity 175

8.3.3 Baroreflex sensitivity 179

8.3.4 Tensile testing 179

8.3.4 Vascular reactivity 180

8.3.4.1 Smooth muscle cell contraction 180

8.3.4.2 Smooth muscle cell relaxation 182

8.3.4.3 Endothelium-dependent relaxation 184

8.3.5 Histology 187

8.4 Discussion 190

8.4.1 Preliminary analysis of the dependence of PWV on age 190

8.4.2 The effect of age on WT and apoE$^{-/-}$ mice 191

Chapter 9 Conclusion 197

9.1 Summary 198

9.1.1 Development of the method to measure aortic PWV in the mouse 198

9.1.2 Characterizing the pressure-dependent PWV in the mouse 199

9.1.3 The effect of transglutaminase 2 on arterial stiffness 199

9.1.4 Characterizing the PWV-MAP relationship in the apolipoprotein E$^{-/-}$ mouse 200

9.1.5 The effect of early aging on arterial stiffness in the mouse 201

9.2 Limitations and future directions 202

9.3 Concluding remarks 206

Appendices 209

A1: Measuring PWV using an intravascular catheter and an extravascular tonometer____209

A2: Measurement of aortic PWV in the rat: effects of vasoactive agents on the measurement 211

A2.1 Introduction _____211

A2.2 Methods _____211

A2.2.1 Animals _____211

A2.2.2 Surgical preparation _____212

A2.2.3 PWV over active and passive changes in blood pressure _____212

A2.2.4 Data and statistical analysis _____213

A2.3 Results _____213

A2.4 Discussion _____214

A3: Comparison of PWV-MAP curves in TG2$^{-/-}$ and WT mice measured at Macquarie University and Johns Hopkins University._____215

A4: Mouse demographics used for PWV-age study _____217

A5: Final Ethics Approval Letters _____219

References ***_____221***

List of Figures

Figure 1: Computation of AIx from an arterial pressure waveform. 11

Figure 2: Diagram showing the structure of the large elastic arteries (Reproduced from Ross and Pawlina, 2010 (58)).....21

Figure 3: Atherosclerosis development and progression. (a) Local inflammation and injury cause endothelial dysfunction. This results in the adhesion of circulating blood cells and increased permeability. (b) Fatty streaks are formed in the intima as increased transendothelial migration of monocytes occurs where they differentiate into macrophages, digest lipids, and become foam cells. Plaque formation progresses with continued infiltration by inflammatory cells and extracellular lipids, migration of VSMC, and deposition of ECM components. (c) Eventually, a necrotic core forms within the lesion comprised of apoptotic and necrotic cells, cell debris, and cholesterol. This is surrounded by a fibrous cap comprised of VSMC embedded in a collagen matrix. (d) With time, thinning of the fibrous cap occurs which leads to plaque rupture, thrombosis, and stroke. (Reproduced from Weber et al 2008 (86)). 29

Figure 4: TG2 activity in response to tissue injury and inflammation. Under normal physiological conditions TG2 activity is latent. Environmental stress causes increased intracellular Ca^{2+}, inflammatory molecules, and reduced NO bioavailability. Collectively, this causes upregulation of TG2 activity. This can cause massive intracellular crosslinking leading to apoptosis (crosslinking designated by dashed crossed lines). Decreased S-nitrosylation of TG2 caused by a reduction in NO leads to externalization of TG2 where it mediates the formation of crosslinks of ECM proteins. These crosslinks play a role in various physiological and pathological processes, including arterial stiffness. Other downstream effects of increased TG2 activity involve elevated TGFβ, increased deposition of collagen and fibronectin, and possible calcification. 45

Figure 5: The hypothesized role of TG2 in regulating arterial stiffness.....51

Figure 6: Surgical preparation to measure PWV in the rat. A dual pressure sensor catheter is positioned in the aorta via the femoral artery. Two simultaneously recorded pressure waveforms are measured by the two pressure transducers located a known distance apart. PWV is calculated by dividing this distance by the time it takes for the pressure wave to propagate down the aorta (Equation 3.1).....57

Figure 7: Doppler velocity signals from the aortic arch and the abdominal aorta in an anaesthetized mouse using a 2 mm diameter 20 MHz probe. The vertical red line corresponds to the R wave of the ECG and is used to measure velocity pulse arrival times for determination of PWV. The abdominal aortic flow waveform is inverted due to the direction that the vessel was insonated. 58

Figure 8: Schematic of the method employed by Wang et al (51) where the proximal sensor is placed in the aortic arch via the carotid artery. Applanation of the abdominal aorta to obtain the distal signal was via a pressure sensor placed either beneath, or held upon the abdominal aorta. 60

Figure 9: Devices used to record distal tonometric pressure. Although not exactly to scale, the image offers the reader an indication of the relative sizes of the two measuring devices.....60

Figure 10: Spike trace showing (from bottom to top) the ECG, proximal pressure P1 (intravascular pressure), distal pressure P2 (extravascular pressure), HR, MAP, TT, 2nd derivative of proximal pressure, and 2nd derivative of distal pressure. The second derivative of distal pressure does not yield well-defined peaks which may introduce errors into TT determination. 61

Figure 11: Spike trace of data acquired using an intravascular and an extravascular catheter. From the bottom up: ECG signal, proximal pressure, distal pressure, MAP, TT, HR, second derivative of P1, and second derivative of P2. Clearly defined feet can be determined from the peaks of the second derivatives. 62

Figure 12: Photograph showing the surgical preparation for measurement of PWV in the mouse. The face is completely covered by a nose cone delivering a continuous flow of isoflurane anaesthesia. The 3 ECG leads are positioned subcutaneously at the two forelimbs and one rear hind limb. The dual pressure catheter is inserted into the aorta via the right femoral artery. A polyethylene cannula is positioned in the left femoral vein for fluids administration. 63

Figure 13: Example recording demonstrating how TT was obtained on a beat-to-beat basis within the Spike software using custom scripts. Cursors '0' and '1' are set up to detect the R-wave of the ECG signal. Within this boundary, cursors '2' and '3' detect the feet of the proximal and distal pressure waves by locating the peak of their second derivative. TT is then calculated as the time difference between cursors '3' and '2' and PWV calculated using Equation 3.1 (distance = 3 cm). Shown on this trace from bottom to top is the ECG, distal blood pressure, proximal blood pressure, HR derived from the ECG, MAP from the proximal signal, TT, the second derivative of the proximal pressure, and the second derivative of the distal pressure. 64

Figure 14: Spike trace during a PE infusion and the following return to baseline values. From bottom to top: ECG, distal pressure (P1), proximal pressure (P2), HR, MAP, and TT. As pressure increases, HR and TT both drop, and slowly rise to baseline as pressure decreases. 65

Figure 15: Spike trace during an SNP infusion and the following return to baseline values. From bottom to top: ECG, distal pressure (P1), proximal pressure (P2), HR, MAP, and TT. In this case, as pressure decreases, HR and TT increase. 66

Figure 16: Sample plot of the PWV-MAP relationship from a single mouse. 66

Figure 17: The directional dependence of PWV on MAP for a pressure range of 100 – 125 mmHg. This pressure range was achieved by PE infusion. Data was analysed using two-way ANOVA with repeated measures in both directions followed by Sidak's multiple comparisons test. The two factors were pressure and direction of pressure change (i.e. up or down). The analysis showed that pressure, direction of pressure change, and the interaction between the two factors was significant. *$p<0.05$. 70

Figure 18: The directional dependence of PWV on MAP for a pressure range of 65 – 90 mmHg. This pressure range was achieved by SNP infusion. Data were analysed using two-way ANOVA with repeated measures in both directions followed by Sidak's multiple comparisons test. The two factors were pressure and direction of pressure change (i.e. up or down). The analysis showed that pressure, direction of pressure change, and the interaction between the two factors was significant. *$p<0.05$. 70

Figure 19: PWV-MAP relationship measured for both SNP infusion (SNP) and reduced venous return via occlusion of the vena cava (VO). While PWV changes with pressure induced by both reduced venous return and SNP infusion, there were no significant differences between the two methods of lowering MAP.....72

Figure 20: An example of a pressure waveform recorded from the aortic arch using a high-fidelity pressure catheter. Catheters are capable of measuring high frequency components, such as the incisura, which is shown in this figure. High frequency components are important in TT measurement. 78

Figure 21: The shape of the pressure waveform changes as it travels down the length of the aorta. The distance from the aortic arch is indicated on the diagram. The waveform on the right (P2) was detected by the distal pressure sensor located 3cm away from the proximal sensor. The waveforms measured by the two sensors at a position of 30mm from the aortic arch are very similar, indicating that the presence of the catheter itself is not significantly interfering with the pressure waveforms. All waveforms are aligned at the pressure waveform foot (that is, the delay of the distal waveform is not indicated). 81

Figure 22: Relationship between MAP and distance of the proximal pressure sensor from the aortic arch. MAP did not differ significantly between any of the locations along the aorta. Data were analysed using one-way ANOVA and Tukey's multiple comparisons test. 82

Figure 23: Relationship between PWV and distance from the aortic arch. PWV was not significantly different between any of the locations in the aorta as determined using one-way ANOVA followed by Tukey's multiple comparisons test. 82

Figure 24: Graph of the PPA-MAP relationship. PPA remains approximately constant around 1.03 for pressures of 85 mmHg and above. PPA drops steadily as pressure decreases below this value. Using one-way ANOVA followed by Dunnett's multiple comparisons test, PPA becomes significantly different from the value of 1.028 at 85 mmHg at pressures of 70, 65, and 60 mmHg. *$p<0.05$. 83

Figure 25: PWV-MAP curve fitted with a second order polynomial: $PWV=0.0003228(MAP)^2 – 0.03447(MAP) + 3.569$. $R^2=0.9939$. This indicates that the sensitivity of PWV to changes in MAP increases linearly with pressure. Regression was fitted to average data points. 84

Figure 26: The sensitivity of PWV to changes in MAP increases linearly with MAP. 84

Figure 27: Relationship between PWV and (A) MAP and HR, (B) PP and max dP/dt. These plots indicate an interaction between terms (e.g. HR sensitivity of PWV is greater at higher MAP). 85

Figure 28: PWV-MAP relationship in WT and $TG2^{-/-}$ mice. PWV was higher in WT mice at pressures of 126 mmHg and higher. *$p<0.05$.....97

Figure 29: PWV-MAP relationship for L-NAME treated and control WT animals. No statistical difference between L-NAME and control animals was observed. 98

Figure 30: PWV-MAP relationship for L-NAME treated and control $TG2^{-/-}$ animals. No statistical difference between L-NAME and control animals was observed. 98

Figure 31: PWV-MAP relationship for L-NAME treated WT and TG2$^{-/-}$ mice. No statistical difference between L-NAME and control animals was observed. 99

Figure 32: Sensitivity of PWV to changes in MAP increases linearly with pressure. The sensitivity at low (60 mmHg) medium (90mm Hg) and high (120 mmHg) MAP was not different between strain or treatment groups (2-way ANOVA followed by Tukey's multiple comparisons test). 100

Figure 33: PPA-MAP relationship for WT and TG2$^{-/-}$ mice. While both strain and pressure were detected as significant sources of variation in PPA, the post-hoc test did not reveal any statistically significant pressure bins. There is a trend of increased PPA in the TG2 mice between pressures of 80 and 100mmHg. 101

Figure 34: PPA-MAP relationship for L-NAME administered and control WT mice. The L-NAME administered animals appear to have a higher PPA compared to controls. Similar to the data presented in Figure 6, both treatment and pressure were detected as significant sources of variation in PPA; however, post-hoc tests did not detect any statistically significant pressure bins. 101

Figure 35: PPA-MAP relationship for L-NAME administered and control TG2$^{-/-}$ mice. L-NAME administered mice show a trend towards higher PPA compared to control. There were no statistically significant differences detected. 102

Figure 36: PPA-MAP relationship for L-NAME administered WT and TG2$^{-/-}$ mice. There were no significant differences detected between strains. 102

Figure 37: BRS in response to PE administration in WT, TG2$^{-/-}$ and L-NAME treated mice. 103

Figure 38: The stress-strain curves (A) and E_{inc} at a strain of 0.1 (B) for control and L-NAME treated WT and TG2$^{-/-}$ mice. No significant differences were observed. 104

Figure 39: Maximal contraction to PE in thoracic (A) and abdominal (B) segments isolated from the four different mice groups. Treatment with L-NAME impaired vascular smooth muscle contractile response significantly only in the thoracic sections from the WT mice; however, there was a similar trend in all groups studied. *P<0.05. 105

Figure 40: Contractile response to PE (A) and EC_{50} values (B) in the thoracic aorta of L-NAME administered and control TG2$^{-/-}$ and WT mice. *P<0.05 for untreated versus L-NAME administered mice, †P<0.05 for untreated versus L-NAME treated WT mice only. 106

Figure 41: Contractile response to PE (A) and EC_{50} values (B) in the abdominal aorta of L-NAME administered and control TG2$^{-/-}$ and WT mice. *P<0.05 for untreated versus L-NAME treated mice, †P<0.05 for untreated versus L-NAME treated WT mice only. 106

Figure 42: Maximum force of contraction to PE (A) and EC_{50} values (B) for rings taken from the thoracic and abdominal aortas. *p<0.05 107

Figure 43: Relaxation response to SNP (A) and EC50 values (B) in the thoracic aorta of L-NAME treated and untreated TG2-/- and WT mice. The curves from the L-NAME treated animals were slightly shifted to the right; however, there were no differences in maximal response to SNP, *P<0.05 for untreated versus L-NAME treated TG2-/- mice only in graph

A. The EC50 values were reduced in L-NAME treated animals compared to control *P<0.05 as indicated in graph B. In both graphs no strain differences were observed. 108

Figure 44: Relaxation response to SNP (A) and EC50 values (B) in the abdominal aorta of L-NAME treated and untreated TG2-/- and WT mice. The curves from the L-NAME treated animals were slightly shifted to the right; however, there were no differences in maximal response to SNP, *P<0.05 for untreated versus L-NAME treated TG2-/- mice only, †P<0.05 for both WT and TG2-/- treated versus untreated mice in graph A. The EC50 values were reduced in L-NAME treated animals compared to control *P<0.05 as indicated in graph B. There were no differences observed between WT and TG2-/- mice (both control and L-NAME treated). 108

Figure 45: EC50 values from the thoracic and abdominal aortas. No differences were observed. 109

Figure 46: Maximum relaxation to ACh in thoracic (A) and abdominal (B) segments isolated from the four different mice groups. Treatment with L-NAME impaired the endothelium-dependent response significantly only in the thoracic sections from the WT mice, and in the abdominal sections from both WT and $TG2^{-/-}$ mice; however, there was a similar trend in untreated $TG2^{-/-}$ mice as well. *P<0.05. 110

Figure 47: Relaxation response to ACh (A) and EC50 values (B) in the thoracic aorta of L-NAME treated and untreated $TG2^{-/-}$ and WT mice. There were no differences observed between control WT and $TG2^{-/-}$ animals. The curves from the L-NAME treated animals were shifted to the right and in both strains of mice, the relaxation response was severely impaired, †P<0.05 for untreated versus L-NAME treated WT mice only, *P<0.05 for untreated versus L-NAME treated WT and $TG2^{-/-}$ mice, #P<0.05 for L-NAME-treated WT versus TG2-/- mice in graph A. The EC_{50} values were significantly different between L-NAME treated WT and $TG2^{-/-}$ mice *P<0.05 as indicated in graph B. 111

Figure 48: Relaxation response to ACh (A) and EC50 values (B) in the thoracic aorta of L-NAME treated and untreated $TG2^{-/-}$ and WT mice. There were no differences observed between control WT and $TG2^{-/-}$ animals. In both strains of mice, the relaxation response was severely impaired in L-NAME treated animals, *P<0.05 for untreated versus L-NAME treated WT and $TG2^{-/-}$ mice in graph A. The EC_{50} values were not significantly different between any of the 4 groups. 111

Figure 49: Maximum relaxation to ACh (expressed as a percentage of complete relaxation) (A) and EC50 values (B) for rings taken from the thoracic and abdominal aortas. *p<0.05. 112

Figure 50: Aortic calcium content. There were no significant differences between any groups examined. 112

Figure 51: Representative images of histological cross-sections of thoracic aorta stained with H&E from control and L-NAME treated WT and $TG2^{-/-}$ mice. Bar: 100μm. 113

Figure 52: The media-to-lumen ratio (A) and the medial thickness (B) of the thoracic aortas from control and L-NAME treated WT and $TG2^{-/-}$ mice. No significant differences were detected. 114

Figure 53: Graphical representation of parameters from echocardiography studies showing (A) left ventricle end diastolic diameter (LVEDD), (B) left ventricle end systolic diameter

(LVESD), (C) ejection fraction (EF), (D) ratio of septal thickness (IVSD) and wall thickness (LVPWD), (E) left ventricular mass (LV mass), and fractional shortening (FS) in WT, $TG2^{-/-}$, WT + L-NAME, $TG2^{-/-}$+ L-NAME mice. *p<0.05.....128

Figure 54: Representative m-mode echocardiography images from WT (A), WT + L-NAME (B), $TG2^{-/-}$ (C), and $TG2^{-/-}$ + L-NAME (D).....129

Figure 55: PWV is not different between WT and $TG2^{-/-}$ mice at any given MAP. 130

Figure 56: PWV-MAP relationship between L-NAME treated and untreated WT mice. There were no statistically significant differences between groups.....130

Figure 57: PWV-MAP relationship for $TG2^{-/-}$ mice. L-NAME had no effect on the pressure-dependent PWV. 131

Figure 58: There were no differences in the PWV-MAP relationship between WT and $TG2^{-/-}$ mice treated with L-NAME. 131

Figure 59: Sensitivity of PWV to changes in MAP increases linearly with pressure. The sensitivity at low (60 mmHg) and medium (90 mmHg) MAP was not different between strain or treatment groups. At high (120 mmHg) MAP, WT-L-NAME animals had decreased pressure-sensitivity compared to treated and untreated $TG2^{-/-}$ mice (2-way ANOVA followed by Tukey's multiple comparisons test). *p<0.05.....132

Figure 60: Relationship between PWV and distance from the aortic arch. PWV was not significantly different between any of the locations in the aorta or between strains as determined using two-way ANOVA followed by Tukey's multiple comparisons test. 133

Figure 61: PPA-MAP relationship for WT and $TG2^{-/-}$ mice. As previously demonstrated, PPA remains around 1 at MAP above 80 mmHg and begins to steadily decline as pressure is reduced. WT mice have significantly higher PPA at pressures between 65 and 70 mmHg; however, this trend is apparent at pressures less than 85mmHg. *p<0.05. 134

Figure 62: PPA-MAP relationship between L-NAME treated and untreated WT mice. There were no differences detected at any level of MAP. 134

Figure 63: PPA-MAP relationship between L-NAME treated and untreated $TG2^{-/-}$ mice. There were no differences detected at any level of MAP. 135

Figure 64: PPA-MAP relationship for WT and $TG2^{-/-}$ mice given L-NAME. WT mice have significantly higher PPA at pressures between 60and 70 mmHg. *p<0.05.....135

Figure 65: BRS in response to PE administration in anaesthetized mice. 136

Figure 66: Representative images of histological sections of thoracic aorta stained with H&E in WT, $TG2^{-/-}$ control mice and mice given L-NAME for 4 weeks. Bar: 100μm. 137

Figure 67: Thoracic aorta media-to-lumen ratio (A) and medial thickness (B) in control and L-NAME treated WT and $TG2^{-/-}$ mice. The wall-to-lumen ratio was significantly greater in WT mice given L-NAME compared to WT controls. No other significant differences were found. *p<0.05. 138

Figure 68: PWV-MAP relationships for WT, apoE$^{-/-}$ and apoE$^{-/-}$ treated with L-NAME. ApoE$^{-/-}$ mice had significantly higher PWV at pressures of 95 mmHg and above. L-NAME treatment lowered PWV in apoE$^{-/-}$ mice to that of controls, and significantly reduced it at pressures of 60-65 mmHg. *P<0.05, WT vs. apoE-/-, #P<0.05, WT vs. apoE$^{-/-}$ + L-NAME; †P<0.05, apoE$^{-/-}$ vs. apoE$^{-/-}$ + L-NAME. 149

Figure 69: Sensitivity of PWV to changes in MAP increases linearly with pressure. At low MAP (60 mmHg), apoE$^{-/-}$ mice + L-NAME had significantly increased pressure sensitivity compared to WT mice. At medium (90 mmHg) and high (120 mmHg) MAP pressure sensitivity was significantly higher in the apoE$^{-/-}$ mice. *P<0.05, WT vs. apoE$^{-/-}$, #P<0.05, WT vs. apoE$^{-/-}$ + L-NAME; †P<0.05, apoE$^{-/-}$ vs. apoE$^{-/-}$ + L-NAME. 150

Figure 70: Relationship between PWV and distance from the aortic arch. PWV was not significantly different between any of the locations in the aorta or between strains. 150

Figure 71: PPA-MAP relationship for C57, apoE-/- , and apoE-/- given L-NAME mice. No differences were detected at any of the MAPs. Data was analysed using two-way ANOVA followed by Tukey's multiple comparisons test. 151

Figure 72: BRS in response to PE administration in anaesthetized mice. 152

Figure 73: The stress-strain curves (A) and E_{inc} at a strain of 0.1 (B) for WT, apoE$^{-/-}$, and apoE$^{-/-}$ given L-NAME. ApoE$^{-/-}$ mice had a significantly higher incremental elastic modulus at a strain of 0.1 compared to WT and L-NAME treated apoE$^{-/-}$ mice. *p<0.05. 152

Figure 74: Maximal contraction to PE in thoracic (A) and abdominal (B) segments isolated from the three different mice groups ex vivo. Treatment with L-NAME impaired vascular smooth muscle contractile response significantly only in the thoracic sections from the apoE$^{-/-}$ mice; however, there was a similar trend in the abdominal sections as well: *P<0.05. 153

Figure 75: Contractile response to PE (A) and EC_{50} values (B) in the thoracic aorta. No differences in the dose-response curve or EC_{50} values were noted between groups. 154

Figure 76: Contractile response to PE (A) and EC_{50} values (B) in the abdominal aorta. No differences in the dose-response curve or EC_{50} values were noted between groups. 154

Figure 77: Maximum force of contraction to PE (A) and EC50 values (B) for rings taken from the thoracic and abdominal aortas. *p<0.5 155

Figure 78: Relaxation response to SNP (A) and EC_{50} values (B) in the thoracic aorta. The curves from the control and L-NAME treated apoE$^{-/-}$ mice were slightly shifted to the right; however, there were no differences in maximal response to SNP, *P<0.05 WT versus apoE, # P<0.05 WT versus apoE$^{-/-}$ + L-NAME in graph A. The EC_{50} values were reduced in control and L-NAME treated apoE$^{-/-}$ mice compared to control *P<0.05 as indicated in graph B. ...156

Figure 79: Relaxation response to SNP (A) and EC50 values (B) in the abdominal aorta. No significant differences were observed. 156

Figure 80: EC50 values from the thoracic and abdominal aortas. No differences were observed. 157

Figure 81: Maximum relaxation to ACh in thoracic (A) and abdominal (B) aortic segments. Relaxation to ACh was completely abolished in both L-NAME treated and untreated apoE$^{-/-}$ mice. Animals administered with L-NAME had aortic rings that displayed constriction instead of relaxation. *P<0.05.....157

Figure 82: Relaxation response to ACh (A) and EC_{50} values (B) in the thoracic aorta of L-NAME treated and untreated apoE$^{-/-}$ and WT mice. The relaxation response from the apoE$^{-/-}$ mice (both L-NAME treated and untreated) were completely abolished, *P<0.05 for untreated and L-NAME treated apoE$^{-/-}$ versus WT mice in graph A. The EC_{50} values were not significantly different; however, as previously mentioned the EC_{50} values from the apoE/- mice reflect a value for the constriction, not relaxation, curve.....158

Figure 83: Relaxation response to ACh (A) and EC_{50} values (B) in the abdominal aorta of L-NAME treated and untreated apoE$^{-/-}$ and WT mice. The relaxation response from the apoE$^{-/-}$ mice (both L-NAME treated and untreated) were completely abolished, *P<0.05 for untreated and L-NAME treated apoE$^{-/-}$ versus WT mice in graph A. The EC_{50} values were not significantly different; however, as previously mentioned the EC_{50} values from the apoE$^{-/-}$ mice reflect a value for the constriction, not relaxation, curve.....159

Figure 84: Maximum relaxation to ACh (expressed as a percentage of complete relaxation) (A) and EC_{50} values (B) for rings taken from the thoracic and abdominal aortas. No location-related differences were detected.....159

Figure 85: Aortic calcium content. There were no significant differences detected between any groups examined. 160

Figure 86: Representative images off histological cross sections of thoracic aortas from WT, apoE$^{-/-}$, and apoE$^{-/-}$ - L-NAME mice. Bar: 100μm. 161

Figure 87: The media-to-lumen ratio (A) and the medial thickness (B) of WT, apoE$^{-/-}$, and apoE$^{-/-}$ -L-NAME mice. No significant differences were detected. 162

Figure 88: Relationship between age and PWV for three different values of MAP. Each data point represents values from an individual mouse. For each MAP group, data was fitted with a line. The equations for each of the lines can be found in Table 14. 174

Figure 89: PWV-MAP relationship for WT and apoE$^{-/-}$ mice at ages 12 and 36 weeks. WT mice aged 36 weeks have higher PWV at 100 mmHg compared to WT control. ApoE$^{-/-}$ mice aged 36 weeks do not have significantly higher PWV than apoE$^{-/-}$ mice aged 12 weeks or WT mice aged 36 weeks. *p<0.05 for WT mice 36 weeks vs. 12 weeks.....176

Figure 90: The pressure sensitivity of PWV increases with pressure. No significant changes with age were observed in WT and apoE$^{-/-}$ mice. In addition, there were no significant differences between WT and apoE$^{-/-}$ at 36 weeks of age.....177

Figure 91: Relationship between PWV and distance from the aortic arch. PWV was significantly higher in old WT mice compared to all other groups at the most proximal location to the heart. *p<0.05. 178

Figure 92: PPA-MAP relationship for WT mice and apoE$^{-/-}$ mice at ages 12 and 36 weeks. There were no significant differences detected between any of the groups studied.....178

Figure 93: Drug-induced BRS was not different between groups. 179

Figure 94: The stress-strain curves (A) and E_{inc} at a strain of 0.1 (B) for old and young WT apoE$^{-/-}$ mice. The incremental elastic modulus increased significantly in old WT mice compared to young WT mice. *p<0.05 179

Figure 95: Maximal contraction to PE in thoracic (A) and abdominal (B) segments isolated from the three different mice groups *ex vivo*. Old apoE$^{-/-}$ mice aged had an impaired vascular smooth muscle contractile response significantly only in the thoracic sections compared to young apoE$^{-/-}$ mice. No changes were observed in the abdominal rings *P<0.05. 180

Figure 96: Contractile response to PE (A) and EC_{50} values (B) in the thoracic aorta. With the exception of a slight shift to the left in the dose-response curve from the old WT mice, no differences were observed in the dose-response curves of EC_{50} values. *p<0.05 for old versus young WT mice. 181

Figure 97: Contractile response to PE (A) and EC_{50} values (B) in the abdominal aorta. There is a shift to the right in the dose-response curve and reduced EC_{50} values between 36 week old animals and 12 week old animals. (A) *p<0.05 WT – 12 weeks versus WT – 36 weeks; †p<0.05 apoE$^{-/-}$ - 12 weeks versus apoE$^{-/-}$ - 36 weeks. (B) *p<0.05 181

Figure 98: Maximum force of contraction to PE (A) and EC_{50} values (B) for rings taken from the thoracic and abdominal aortas. There were no differences in maximum contractile forces between thoracic and abdominal sections. The EC_{50} values were significantly lower in all groups. 182

Figure 99: Relaxation response to SNP (A) and EC_{50} values (B) in the thoracic aorta. While there was a slight shift to the right of the old WT and young apoE$^{-/-}$ mice, none of the groups had any impairment in their smooth muscle relaxation responses. Old apoE$^{-/-}$ mice had a slightly higher EC_{50} value compared to young apoE$^{-/-}$ mice. (A) *p<0.05 between young and old apoE$^{-/-}$ mice; †p<0.05 between 36 week old WT and apoE$^{-/-}$ mice; $^{\#}$p<0.05 between young and old WT mice. (B) *p<0.05. 183

Figure 100: Relaxation response to SNP (A) and EC_{50} values (B) in the abdominal aorta. While the relaxation response was not impaired in any of the four groups examined, mice that were 36 weeks old had reduced sensitivity to SNP as indicated by a right-ward shift in the dose-response curves and reduced EC_{50} values. (A) *p<0.05 between young and old apoE$^{-/-}$ mice; $^{\#}$p<0.05 between young and old WT mice. (B) *p<0.05. 183

Figure 101: EC_{50} values from the thoracic and abdominal aortas. At 12 weeks of age, thoracic sections had reduced sensitivity to SNP compared to abdominal sections. At 36 weeks of age, abdominal sections have reduced sensitivity to SNP compared to thoracic sections. *p<0.05. 184

Figure 102: Maximum relaxation to ACh in thoracic (A) and abdominal (B) aortic segments. Relaxation to ACh was completely abolished in apoE$^{-/-}$ mice. No significant differences were observed between old and young mice or between old WT and apoE$^{-/-}$ mice. 185

Figure 103: Relaxation response to ACh (A) and EC50 values (B) in the thoracic aorta of 12 and 36 week old apoE$^{-/-}$ and WT mice. The relaxation response from the apoE-/- mice was completely abolished. Though not statically significant, the relaxation to ACh was reduced in the old WT mice compared to young WT mice. The EC50 values were not significantly

different; however, as previously mentioned the EC_{50} values from the $apoE^{-/-}$ mice do not exist as there was no dose response. 186

Figure 104: Relaxation response to ACh (A) and EC50 values (B) in the abdominal aorta of 12 and 36 week old $apoE^{-/-}$ and WT mice. The relaxation response from the $apoE^{-/-}$ mice was completely abolished. The old WT mice had reduced endothelium dependent responses, although this was not significant. The EC_{50} values were significantly lower in the old WT mice compared to the young WT mice; however, as previously mentioned the EC_{50} values from the $apoE^{/-}$ mice are invalid. (A) *p<0.05 for young versus old WT mice; †p<0.05 for old $apoE^{-/-}$ versus WT mice. (B) *p<0.05. 186

Figure 105: Maximum relaxation to ACh (expressed as a percentage of complete relaxation) (A) and EC50 values (B) for rings taken from the thoracic and abdominal aortas. No location-related differences were detected. 187

Figure 106: Photograph of an aorta from an old $apoE^{-/-}$ where lesions are clearly visible (A) and an aortic cross-section stained with H&E from an old $apoE^{-/-}$ mouse with an obvious lesion (B). Lesions are indicated with arrows. 188

Figure 107: Representative images of histological cross sections of thoracic aortas from 12 and 36 week old WT and $apoE^{-/-}$ mice. Bar: 100 μm. 189

Figure 108: The media-to-lumen ratio (A) and the media thickness (B) of young and old WT and $apoE^{-/-}$ mice. No differences were detected in the media-to-lumen ratio between groups. Old WT mice had significantly greater medial thickness compared to young WT mice. No other significant differences were observed. *p<0.05. 190

Figure 109: PWV-MAP curves obtained using two different measuring techniques as previously described. Intra/Extra refers to one proximal sensor placed into the arch via the carotid and one distal sensor placed underneath the abdominal aorta to record extravascular tonometric pressure. Dual refers to one dual pressure sensor placed in the aortic arch via the femoral artery. The data was analysed with 2-way ANOVA followed by Sidak's multiple comparisons test. There were no significant differences at any of the pressure bins. 210

Figure 110: With the exception of three pressure bins, no significant difference was found in arterial stiffness achieved with the vasoactive agents or with the venous occlusion methods of blood pressure manipulation.*p<0.05. 214

Figure 111: Comparison of the PWV-MAP relationship for WT and $TG2^{-/-}$ mice between experiments performed at JHU and MQ. There were only difference found occurred at a pressure of 125mmHg where WT mice from MQ had higher PWV than those from JHU (two-way ANOVA followed by Tukey's multiple comparisons test) *p<0.05 for WT (JHU) versus WT (MQ). 215

List of Tables

Table 1: Summary of the different methods employed to measure arterial stiffness and their advantages and disadvantages. 19

Table 2: Comparison between baseline values for HR, MAP, PP, and PWV between baseline and during saline infusion at 0.1 ml/min. Data are shown as mean ± SD. 69

Table 3: AUC of the PWV-MAP relationship. It can be seen that the AUC is significantly greater while pressure is increasing as compared to decreasing for both PE and SNP infusions. Units are m·s-1·mmHg. 71

Table 4: Baseline cardiovascular parameters for the SJL mice. 71

Table 5: Baseline cardiovascular characteristics 80

Table 6: Cardiovascular parameters that significantly affected PWV.....85

Table 7: Baseline cardiovascular characteristics. Data are presented as mean ± SD. No statistical differences between groups were observed. 96

Table 8: PWV-MAP relationships are described by a quadratic equation. 99

Table 9: Blood pressure and heart rate obtained from a tail-cuff apparatus. Data are presented as mean ± SD. *p<0.05 $TG2^{-/-}$ versus WT, †p<0.05 $TG2^{-/-}$ versus $TG2^{-/-}$ + L-NAME, #p<0.05 WT + L-NAME versus $TG2^{-/-}$ + L-NAME. 126

Table 10: Baseline cardiovascular characteristics. Data are presented as mean ± SD. *p<0.05 with respect to WT animals. #p<0.05 with respect to $TG2^{-/-}$ animals. †p<0.05 with respect to WT – L-NAME treated animals. 127

Table 11: PWV-MAP relationships are described by a quadratic equation. 132

Table 12: Baseline cardiovascular characteristics. Data are presented as mean ± SD. *p<0.05 $apoE^{-/-}$ vs. WT, †p<0.05 $apoE^{-/-}$ - L-NAME vs. WT. 148

Table 13: PWV-MAP relationships are described by a quadratic equation. 149

Table 14: Comparison of our PWV measurement in $apoE^{-/-}$ to those taken from the literature. 164

Table 15: Equations of the linear regression for the PWV-age relationship for each of the three MAPs. 174

Table 16: Baseline cardiovascular characteristics (one-way ANOVA followed by Tukey's multiple comparisons test). *p<0.05 with respect to WT mice 12 weeks old; †p<0.05 with respect to $apoE^{-/-}$ mice 12 weeks old. $^{\#}$p<0.05 with respect to $WT^{-/-}$ mice 36 weeks old. 175

Table 17: The PWV-MAP relationships in all four groups are well described by a quadratic equation. This indicates that sensitivity of PWV to changes in MAP increases linearly with pressure. 176

Table 18: Body weight (g) of mice from JHU versus MQ. While $TG2^{-/-}$ mice have similar weights in both labs, WT mice from JHU are larger than from MQ, although this only reached statistical significance in the WT – L-NAME group. *p<0.05.....216

Table 19: Left ventricular weight normalized by body weight ($g/g \cdot 10^{-3}$) of mice from JHU versus MQ. In all cases, LVW/BW is smaller in mice from MQ compared to JHU; however this did not reach statistical significance in the WT – L-NAME group. *p<0.05.....216

Table 20: Summary details of mice used for aging analysis. Dual refers to measurements made with a dual pressure sensor. *Int/Ext* refers to measurements made with two separate sensors: one placed intravascularly and the other placed extravascularly as a tonometer. *Iso* is isoflurane, *U* is urethane, pent is sodium pentobarbital, and *A* refers to the administration of atropine which was sometimes required to reduce respiratory difficulties. 217

List of Abbreviations

8HQ	8 hydroxy-quinoline
ACh	acetylcholine
AGE	advanced glycation end products
AIx	augmentation index
ANOVA	analysis of variance
apoE	apolipoprotein E
AUC	area under the curve
BRS	baroreflex sensitivity
BW	body weight
CMR	cardiovascular magnetic resonance
CPC	ortho-cresophthalein complexone
Cys	cysteine
DBP	diastolic blood pressure
E_{inc}	incremental elastic modulus
EC	endothelial cells
EC_{50}	half maximal effective concentration
ECG	electrocardiogram
ECM	extracellular matrix
EDHF	endothelium derived hyperpolarizing factor
EF	ejection fraction
eNOS	endothelial nitric oxide synthase
ESRD	end stage renal disease
F	French
FS	fractional shortening
GTP	guanosine triphosphate
H&E	haematoxylin and eosin

HLU	hind limb unweighting
HR	heart rate
IC	internal circumference
IVSD	interventricular septal thickness at end diastole
JHU	Johns Hopkins University
KCl	potassium chloride
L-NMMA	N^G-monomethyl-L-arginine
L-NAME	N^G-nitro-L-arginine methyl ester
LV	left ventricle
LVEDD	left ventricle chamber diameter at end diastole
LVESD	left ventricle chamber diameter at end systole
LVPWD	left ventricular posterior wall thickness at end diastole
MAP	mean arterial pressure
max dP/dt	maximum of the first time derivative of pressure
MQ	Macquarie University
MRI	magnetic resonance imaging
NO	nitric oxide
NOS	nitric oxide synthase
PE	phenylephrine
PP	pulse pressure
PPA	pulse pressure amplification
PWV	pulse wave velocity
ROS	reactive oxygen species
SA	specific aim
SBP	systolic blood pressure
SD	standard deviation
SEM	standard error of the mean
SHR	spontaneously hypertensive rat

SNP	sodium nitroprusside
TG2	transglutaminase 2
TGF-β	transforming growth factor beta
TT	transit time
WT	wild type
VO	venous occlusion
VSMC	vascular smooth muscle cells
Z	impedance
ρ	density

Chapter 1

Introduction

Despite significant advances in scientific research and clinical medicine, cardiovascular disease remains the major cause of death worldwide (1). It claimed the lives of almost 45,600 Australians (31% of all deaths) in 2011 alone and remains a huge burden on the health care system and the economy (2).

With age, blood vessels undergo various structural and functional changes which result in increased arterial stiffness. Increased arterial stiffness directly causes increased systolic blood pressure, which places a greater workload on the heart and subsequent left ventricular hypertrophy, which eventually leads to impaired coronary perfusion (3).

It is now accepted that large artery stiffness, as measured by pulse wave velocity (PWV) is an independent risk factor associated with increased cardiovascular morbidity and mortality. Blacher et al found that aortic stiffness, measured by PWV, was highly associated with the presence and extent of atherosclerosis and is a strong marker of cardiovascular risk in hypertensive patients (4). It has also been shown to be an independent predictor of stroke in a population with essential hypertension (5). Aortic PWV has been shown to be a significant predictor of all-cause and cardiovascular mortality in patients with essential hypertension (6). Measures of arterial stiffness also have prognostic value in patients suffering end-stage renal disease (ESRD). In ESRD patients, both carotid arterial stiffness, estimated by the

incremental elastic modulus (7), and aortic PWV (8) are strong independent predictors of all-cause and cardiovascular mortality. Furthermore, the addition of PWV measurements provide added prognostic power above and beyond conventional cardiovascular risk factors in ESRD patients (9). In elderly patients (aged 70 to 100 years) aortic PWV is a predictor of cardiovascular death (10). Finally, aortic PWV also predicts all-cause and cardiovascular mortality in multiethnic patients with type 2 diabetes (11).

However, the significance of large artery stiffness is not relevant only in higher risk or diseases groups. It has been shown that aortic PWV is a strong predictor of coronary heart disease and stroke in a large population of apparently healthy subjects (12). Another community based sample found that aortic PWV was associated with increased risk for a first cardiovascular event and addition of PWV to standard risk factors resulted in improved risk classification (13). Decreased arterial elasticity in the common carotid artery in a large sample of normotensive subjects was associated with a 15% greater risk of hypertension, independent of other risk factors or baseline blood pressure (14). Higher aortic PWV is also associated with increased cardiovascular mortality, coronary heart disease, and stroke in healthy, well-functioning, older adults (15).

The main structural components of the vessel wall are elastin, collagen, and vascular smooth muscle cells (VSMC). The elasticity of the arteries displays non-linear behaviour. At low distending pressures, the tension in the vessel wall is taken up primarily by elastin, which is highly distensible. However, with increasing pressure and stretch, the much stiffer collagen fibres unfold and gradually take up more of the tension created in the wall, causing the vessel to become increasingly stiffer. By adjusting their tone, VSMC can modulate the distribution of pressure between the collagen and elastin, thereby affecting stiffness as well.

With age, the VSMC in the large arteries migrate, proliferate and experience changes in their contractile state, contributing to vascular remodelling, whereby the vessel walls become

thicker and the lumen diameter increases. In the aging vasculature, there is also an increased collagen-to-elastin ratio, elastin fragmentation, disorganization, calcification, and crosslinking of collagen. Inflammation, oxidative stress, various pathologies, and many other factors can influence these changes, all of which cause the arteries to become stiffer. The importance of arterial stiffness in the clinical setting is quite evident; however, the causative cellular and molecular mechanisms remain the subject of great speculation. The stiffening of large arteries currently lacks any therapy for the prevention or reversal of the condition. Therapies that could target aortic stiffness would offer a powerful and novel pathway in combating cardiovascular diseases. It is necessary to elucidate the cellular and molecular mechanisms underlying aortic stiffening in order to develop new therapies for the prevention and treatment of cardiovascular diseases.

The shared physiology of the human and mouse makes the mouse a suitable animal for modelling these complex disease states. Furthermore, the ability to manipulate the entire mouse genome allows the isolation of specific genes and the investigation of how their downstream effects may influence arterial stiffness. This will allow better understanding of the mechanisms responsible for arterial stiffness and how they are regulated on a cellular and molecular level.

Obtaining cardiovascular measurements in the mouse can be technically challenging due to their small size and fast heart rate. To date, methods of quantification of aortic stiffness in the mouse are largely non-invasive and thus suffer from certain inaccuracies. Furthermore, no method exists for measuring aortic stiffness across a range of physiological blood pressures. This is an important metric for isobaric comparison of functional stiffness between different animal models of cardiovascular pathologies. It is also important to realise the pressure sensitivity of aortic stiffness as blood pressure is an acutely changing parameter.

This thesis presents a novel method for invasively measuring pressure-dependent aortic stiffness, estimated by PWV, in the anaesthetized mouse. Other *in vivo* hemodynamic parameters and *ex vivo* measures of vascular function are also presented (Chapters 3 and 4). In Chapter 3 some of the major limitations to using this surgical method are addressed in the mouse model.

Recent data suggest that the multifunctional enzyme, transglutaminase 2 (TG2) plays a significant role in mediating large artery stiffness by its ability to crosslink proteins in the extracellular matrix (ECM) (16). In Chapters 5 and 6, aortic stiffness and function and cardiac function are assessed in TG2 knockout mice compared to wild type controls. *In vitro*, it has been shown that nitric oxide (NO) regulates TG2 activity (17). Therefore, the cardiovascular effects of NO inhibition are also explored.

While vascular stiffening occurs with aging, it is also highly correlated with the presence of severe atherosclerosis (18). The apoE$^{-/-}$ mouse is a widely used model of atherosclerosis; however, the pressure-dependent PWV has not yet been investigated in this animal model. Chapter 7 presents this data together with other hemodynamic and functional results.

The effect of aging on large artery stiffness in humans is well-established (19). It is less clear in the mouse model. In Chapter 8, some preliminary data on aging and PWV in wild type, apoE$^{-/-}$ and other strains of mice are investigated in order to elucidate whether the use of the mouse as a model of large artery vascular remodelling with age is a suitable analogue for the aging human vasculature.

Collectively, this thesis provides insight into the pressure dependent characteristics and hemodynamic parameters of the mouse aorta. On a broad scale it examines the potential influence of two extracellular matrix modifications on functional arterial stiffness in the mouse: *(i)* increased crosslinking of ECM proteins and *(ii)* atherosclerotic plaque development. The influence of both aging and endothelial dysfunction, characterised by a

reduced bioavailability of NO, is also briefly explored. While further research is required to substantiate the findings presented in this thesis, this work has contributed to elucidating possible mechanisms which lead to increased stiffness. Most importantly, this thesis validates a new method to measure pressure-dependent PWV which can be used in virtually any mouse model relevant to cardiovascular disease. This opens new avenues of research to investigate mechanisms underlying the development of large artery stiffness utilising the powerful tool of the genetically modified mouse.

Chapter 2

Literature Review

2.1 Arterial function

The arterial system serves two major functions. First, it acts as a conduit to deliver oxygenated, nutrient-rich blood from the heart to all the organs, tissues, and cells of the body. Second, it acts as a cushion to dampen the pulsations generated by the beating heart, such that flow at the level of the capillaries is continuous. The human arterial system is very well adapted to perform these functions efficiently and effectively (20).

The cushioning function is highly dependent on arterial compliance, or the ability of arteries to stretch and recoil. The structure and composition of the vessel wall confers viscoelastic properties. Due to this viscoelasticity, arterial compliance (that is, a change in volume for a given change in pressure), has non-linear behaviour, which gives the artery the elasticity it requires to function well at physiological pressures, while also providing tensile strength, which allows it to withstand higher, perhaps pathological, pressures without over-distending (21).

2.2 Pressure wave reflection

The arterial pressure waveform can be considered to consist of two waveforms: a forward travelling wave due to the ejection of blood from the heart, and a backward travelling reflected wave which is the summation of reflections that occur at branch points, changes in vessel diameter or stiffness, and at the arteriolar level of the vasculature. The resultant waveform is thus a function of both the geometry of the vessel wall and its mechanical properties, namely, stiffness (3, 22).

Both the arrival time and the magnitude of the reflected wave contribute to increased systolic blood pressure and arterial stiffness (3). In young, distensible arteries, the wave speed is slower, and the resulting reflected wave reaches the heart mainly during diastole. This provides improved conditions for coronary flow, and a reduced left ventricular pressure load. Conversely, in older, stiff arteries, where the pressure waves travel much faster, the reflected wave returns to the heart during systole. In fact, arrival of the reflected wave during diastole is extraordinarily rare in adult populations. This causes both increased systolic pressure and pulse pressure, thus placing an increased workload on the heart which eventually results in left ventricular hypertrophy and impaired coronary perfusion (22-24).

Furthermore, the elasticity of the young arteries cushions the pulsations such that flow is virtually steady once it reaches the microvasculature. However, in the aged arteries, the increase in stiffness results in an inability of the large arteries to completely absorb pulsations, and thus the flow in the microvasculature is pulsatile and with time causes end organ damage, especially in the brain and kidneys (20, 24).

2.3 Arterial stiffness

Stiffness can be broadly defined as the resistance of an elastic material to deformation. In the context of the arterial system, stiffness refers to the resistance of the arteries to stretch in response to a distending pressure (imposed by the ejection of blood from the heart). Thus, the heart would expend more energy to eject the same volume of blood into the stiffer aorta, as there is a higher resistance to expansion (25).

Stiffness is a mechanical property of the arteries that varies with location, geometry, and pressure. In engineering terms, the inherent stiffness of a material is described by its Elastic modulus, which is defined as the ratio of stress (the force applied per unit area) to strain (the resulting deformation due to the applied force), within an elastic region. Due to the non-linearity of the vessel wall, the Elastic modulus increases with stress, so it is more useful to use the incremental Elastic modulus, E_{inc}. This essentially defines the Elastic modulus for a given pressure and can be calculated as the slope of the stress-strain curve (26).

2.4 Measuring arterial stiffness

As the clinical importance of arterial stiffness has continued to rise (13), many methods to measure and assess different aspects of stiffness have been developed (25, 26). The following discussion will outline some of the relationships used to characterise arterial stiffness, and then review how these are being measured in the murine model.

When the left ventricle contracts, it ejects a bolus of blood into the aorta, creating a pressure pulse wave that travels along the arteries at a velocity (pulse wave velocity, PWV) that is proportional to the material stiffness and geometry of the vessel wall. The relationship between PWV and material stiffness is defined by the Moens-Korteweg equation (2.1):

$$PWV = \sqrt{\frac{E_{inc}h}{2\rho r}} \quad (2.1)$$

where E_{inc} is the elastic modulus of the vessel, h is the wall thickness, r the radius, and ρ is the density of the blood. It is important to note that this relationship is essentially valid under conditions of a thin wall. In addition, E_{inc} is proportional to PWV only for non-significant changes in the vessel wall geometry ratio of wall thickness to radius (h/r).

PWV is the distance, L, travelled by a wave divided by the time, Δt, taken to travel that distance:

$$PWV = \frac{L}{\Delta t} \quad (2.2)$$

Equation 2.2 requires a system without reflections, which is not the case in the vasculature. However, aortic PWV can be determined by measuring the time delay of a pressure wave diastolic "foot" between a proximal and distal site a known distance apart. This is due to the fact that there is little or no interference from the reflected waves during the period of the cardiac cycle in which the "foot" occurs (27), that is, late diastole and early systole. This method of estimating stiffness is used throughout this study. In fact, one of the main aims of this work was to establish an *in vivo*, invasive technique to obtain PWV via the foot-to-foot method in the mouse.

There are several reasons for this. Primarily, our group and others have been able to demonstrate the validity and relative ease and accuracy of this technique in intact animals as small as the rat (28, 29). Furthermore, in the clinical setting, PWV is the most common method of assessing vascular stiffness, as it has been demonstrated to have a significant relationship with cardiovascular morbidity and mortality (6, 13). Application of this technique to the mouse would open up avenues of research into genetic and thus molecular mechanisms that determine functional changes in large artery stiffness.

Augmentation index (AIx), although not a direct measure of stiffness itself, is a measure of wave reflection that is itself dependent on arterial stiffness. As previously mentioned, in a stiffer vessel the reflected wave arrives early, augmenting pressure in mid to late systole. AIx is calculated as the ratio of this "augmentation pressure" and the pulse pressure directly from the aortic pressure waveform (Figure 1).

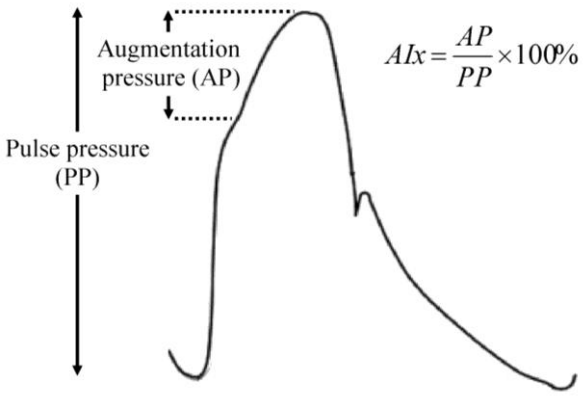

Figure 1: Computation of AIx from an arterial pressure waveform.

Compliance, *C*, and distensibility are inverse parameters of stiffness and can be calculated according to the following formulas if the dimensions of the artery can be recorded (via ultrasound for example) simultaneously with pressure.

$$C = \frac{\Delta V}{\Delta P} = \frac{\Delta D}{\Delta P} \tag{2.3}$$

$$distensibility = \frac{\Delta V}{V_d \times \Delta P} = \frac{\Delta D}{D_d \times \Delta P} \tag{2.4}$$

where V_d is the original or diastolic volume, ΔV the change in volume, and ΔP the change in pressure. Distensibility is essentially compliance normalized by the original size of the arterial segment. Because of this, a highly distensible vessel that has a small volume may actually have a far lower level of compliance. Compliance and distensibility measurements can also be made using diameter, *D*, in place of volume.

When the large central arteries are compliant, such as in a healthy young subject, the arterial waveform is amplified as it travels toward the periphery. The level of amplification is influenced by large artery stiffness, total peripheral resistance, and impedance changes along the length of the artery which affect the wave reflection characteristics. As the large arteries stiffen, this amplification is reduced due to the reduced difference in stiffness of central and peripheral conduit arteries. Therefore, pulse pressure amplification (PPA) (calculated as the distal pulse pressure divided by the proximal pulse pressure) also provides an indication of vessel stiffness. Pulse pressure can also be used as an indirect measure of stiffness because its value depends on stroke volume, arterial compliance, and pressure wave reflection.

2.4.1 Measurement of pulse wave velocity in the mouse

Due to the availability of various technologies and their relative ease of use, PWV has been successfully measured in a wide range of species including human (19), monkeys (30), sheep (31), dogs (32), rabbits (33), rats (29), and even snakes (34), wombats (35) and kangaroos (36)! This section will discuss the various techniques that have been employed to estimate arterial stiffness by PWV in the mouse, as well as the advantages and limitations of each method.

A key question to consider is: why the mouse? There are many technical challenges associated with making cardiovascular measurements in mice that primarily arise from their small size and rapid heart rate. However, the ability to manipulate the entire mouse genome allows the study of how individual genes and their downstream effects may influence arterial stiffness. This could eventually lead to the identification of novel mechanisms and signalling pathways that cause increased stiffness. By studying these mechanisms, it may be possible to discover new therapeutic targets that delay the process of vascular aging.

One of the most common, non-invasive ways of measuring PWV in the mouse is by using Doppler ultrasound. Doppler instruments measure blood velocity by detecting the difference

in frequency between an emitted burst of ultrasound and the returning echoes from moving blood (37). Hartley et al have developed a technique which uses high resolution Doppler probes to measure blood velocity in the heart and in numerous locations throughout the arterial tree. There is a plethora of data that can be derived from these signals, including indices of ventricular function, arterial resistance, compliance, and wave reflection (38). PWV is obtained by recording velocity signals from two sites, separated by a known distance, and measuring the difference in pulse arrival times with a high-fidelity ECG used as a timing reference. The two velocity signals can either be measured sequentially or simultaneously (37).

The evident advantage of this technique is its non-invasiveness and ease of use. Since it is not a terminal procedure, Doppler measurements can be made longitudinally to study aging, disease progression or treatment efficacy over time. This also allows individual animals to be their own controls. It has successfully been applied to study many genetically modified mouse models (39-45).

However, there are inherent limitations with using Doppler to assess PWV. First, one must ensure that the obtained velocity and ECG waveforms are crisp and clean (noise free) in order to accurately detect the upstroke of velocity (equivalent to the foot of the pressure wave form). Whilst accurate foot detection in the Doppler frequency shift waveform presents some problems, one of the principle sources of error arises from the inability to precisely measure the distance along the aorta between the two measurement locations which are marked on the surface of the skin. Further error is accumulated when accounting for the probe angle and sample volume depth. A straight line between the two measurement points is also assumed but the aorta itself lies along a curved path. When sequential velocity measurements are made (pulse transit time is calculated using a single probe to the first measurement site followed by the second site), any changes to the pre-ejection time, stiffness, or blood pressure that may

occur between the two measurements will impact the results (37). These measurements are often operator dependent as they are susceptible to artefact introduced by probe positioning. Finally, in the majority of studies that use Doppler to measure PWV, blood pressure is not measured simultaneously, and is often also measured noninvasively with a tail-cuff apparatus which has many inaccuracies itself and cannot accurately measure diastolic blood pressure (46). Blood pressure often varies with strain and/or treatment and these differences must be accounted for when measuring PWV which, due to the elastic properties of arteries, varies with pressure (47).

Another potentially useful method of measuring PWV in mice involves the use of magnetic resonance imaging (MRI). New, high-field MRI systems with high signal-to-noise ratios that are available now allow for the high spatial and temporal resolution required to obtain cardiovascular measurements in the mouse. Parczyk et al demonstrated the feasibility of using a cardiovascular magnetic resonance (CMR) transit time method to determine murine aortic PWV using blood flow waveforms (48). This method functions under the same basic principle as that used with Doppler ultrasound; the upstroke of the flow velocity in this case is determined from the MR image that can be obtained at multiple locations known distances apart along the length of the aorta. They used a CMR system with a field strength of 17.6T. Their measurements suggested that maximal distances between measurement sites should be used in order to minimize uncertainties. Herold et al used a 17.6T high field MRI to determine PWV by measuring the cross-sectional area and through-plane velocity, called a flow-area approach, in the ascending and descending aorta in mice (49). Using a 7T animal scanner, an undersampled, asymmetric echo radial phase contrast MR technique was developed by Zhao et al to measure through-plane blood flow velocity at axial slices along the descending aorta (50). The PWV and time averaged wall shear stress (WSS) were then calculated from the spatiotemporal flow data.

A limitation of the transit time method for determining PWV is that it gives an average value over a relatively long section of the aorta. However, PWV changes along the aorta, especially in models of atherosclerosis where plaques tend to form in localized areas. The flow area approach using MRI is able to measure the local PWV at different positions on the aorta, thus overcoming this limitation. It also provides accurate morphological information simultaneously. A further benefit of using MRI is the improved image quality which allows for a more precise measurement of the vessel cross sectional area compared to ultrasound methods (49).

One of the most obvious disadvantages of using MRI to quantify PWV is the cost. At a more fundamental level, the pulse waveform measured by MRI is constructed by repeated sampling across multiple cardiac cycles in order to "construct" the waveform. This is required due to the temporal limitations of sampling with MRI. Motional artefacts (which may occur due to respiration under anaesthesia) may occur and affect the calculation of flow velocity. However, these can often be detected and excluded from analysis (48). In order to apply the flow-area approach, one must acquire the data over what is assumed to be a wave-reflection free period of the cardiac cycle which limits the length of time data can be acquired for in each cardiac cycle. Signal loss may also occur during measurements acquired during early systole (the assumed wave-reflection free period). The flow-area method also renders the measurements very susceptible to changes in heart rate; in fact, if it varies by more than 5ms (approximately 5% of the cardiac cycle) over the course of the experiment, the PWV measurements are not reliable (49). Finally, none of the reported findings from the MRI studies presented here reported blood pressure measurements. It would likely be difficult to simultaneously measure blood pressure within the confines of the MRI machines.

PWV has also been determined tonometrically (44). A 2F pressure sensor was positioned underneath both the aortic arch and the abdominal aorta. If the vessel was appropriately

applanated by the pressure sensor, a clear foot from the pressure wave could be obtained and used to calculate transit time for PWV determination. Taking this a step further, in a study by Wang et al, pulse transit time was measured using two high-fidelity pressure sensors, one placed in the aortic arch via the carotid artery, and the second placed underneath the abdominal aorta to record *extravascular* tonometric pressure (51). The distance between the two sensors was measured post-mortem using a damp cotton thread laid along the length of the aorta that was marked and measured with a ruler, and then PWV could be calculated.

These were both significantly important studies, especially the second (Wang et al) because it allowed for the simultaneous measurement of blood pressure and PWV. However, it involves highly invasive surgery, and recording the tonometric pressure requires that the aorta must be applanated which could affect the results through changes in hemodynamics and measured pressure waveforms.

A custom-made, dual-sensor conductance catheter has also been successfully used to simultaneously acquire arterial input impedance, arterial function, and ventricular-vascular interaction in mice (52). In this study PWV was derived from the relationship:

$$PWV = \frac{ZA}{\rho} \tag{2.5}$$

where Z is the measured aortic characteristic impedance, ρ is the density of blood assumed to be 1060 kg/m^3, and A is the aortic cross sectional area assumed to be 1.13 mm^2 (constant diameter of 1.2 mm).

The greatest advantage from this study is the ability to measure aortic pressure and flow at the same time. Numerous cardiac and arterial properties can be derived from these data which provide a complete description of the state of the murine cardiovascular system. However, it is a highly invasive procedure. The thorax must be opened and the catheter positioned in the left ventricle (via a left ventricular apical stab) such that the distal tip of the catheter is in the

aortic root and the proximal electrode within the endocardial wall of the left ventricular apex. Then an aortic flow probe must be positioned around the descending aorta in order to calibrate the conductance catheter. The measurements are highly dependent on this calibration, which is a limitation to the study as the flow probe should ideally be positioned around the ascending aorta where the catheter is located, but this is extremely difficult to achieve, especially without distorting the signal. This also highlights the fact that PWV can only be measured from the proximal aorta and not at discrete locations along the full length of the aortic trunk. The use of a constant cross-sectional area, based on the assumed value of D = 1.2 mm may also introduce errors into the determination of PWV. Finally, the open-thorax setting may affect the transmural aortic pressure, and thus PWV, AIx, Z, and other indices, although the authors indicate that this is unlikely (52).

Maizel et al used Millar Mikro-tip 1.4F pressure transducers to measure invasive PWV. The first transducer was positioned in the aortic arch via the right carotid artery and the second was positioned either directly in the abdominal aorta or via the femoral artery. PWV was determined using the foot-to-foot method and averaging at least 10 consecutive, normal cardiac cycles. Once euthanized, the entire aorta was exposed and the distance between the two transducers was measured with a cotton thread (53).

Again, this study provides pressure and PWV at the same time, which is crucial. It is also much less invasive than the tonometric methods previously discussed. However, it is still quite invasive as it requires opening the neck and possibly the abdomen. Further, they did not measure pressure-dependent PWV. There is also the possibility of human error being introduced in the measurement between the two pressure transducers.

The final method of mouse PWV measurement reported in the literature involves the use of polyethylene cannulas chronically implanted in mice under anaesthesia into the descending aorta, the abdominal aorta, and the abdominal vena cava. The aortic cannulas of non-

anesthetized, freely moving mice were connected to low-volume pressure transducers. An algorithm calculated central mean aortic blood pressure, pulse pressure, and heart rate. PWV was calculated as the distance between the 2 cannula tips (measured in situ after post-mortem fixation by sticking a damp cotton thread onto the aorta) divided by transit time. Transit times were measured online for 4-second periods by an algorithm that systematically shifted in time the peripheral pressure waveform with respect to the central pressure waveform and then determined the value of the time shift giving the highest correlation. After baseline hemodynamic measurements were made, central MAP was reduced in a stepwise manner by infusion of sodium nitroprusside (SNP). At each stabilized step, 15 measurements of aortic blood pressure and transit time were performed and averaged. PWV was expressed as a function of MAP by using an exponential model (54).

This study by Marque et al (54) is significant as it provided pressure-dependent PWV data in the mouse aorta for the first time. Another advantage is the acquisition of data in the non-anaesthetized animal as anaesthetic agents are known to have cardiovascular effects. However, once again, this would be a highly invasive, technically challenging surgery. Error is also introduced when measuring the distance between the tips of the two cannulas.

High-fidelity solid state pressure catheters have the sensors mounted at the tip of the catheter so that pressure can be directly measured at the desired location, whereas fluid-filled catheters transmit the pressure pulse along a tube filled with physiological fluid to an external sensor. This system introduces a certain degree of error when compared to the solid state catheters. At high frequencies, such as in the mouse cardiovascular system, with fluid-filled pressure-transducers the pressure amplitude may become affected and detection of pressure changes is not as accurate as in the high-fidelity solid pressure sensors. The fluid filled lines are capable of developing air bubbles which may further affect the frequency response (55). Newer

technology minimizes these problems (56); nonetheless, both the precision of measurement and easier surgical placement render the solid-state catheters a better choice.

There have been many attempts to characterise PWV in the murine aorta. However, many studies do not provide simultaneous measurements of blood pressure. Of those that do, the surgeries are often highly invasive, complex procedures. Current high-fidelity dual pressure sensors are available which can provide a transit time resolution of 0.5 msec. This range of resolution provides an accuracy of PWV determination between 3-5%. With this technology, pressure-dependent PWV could be obtained in a minimally invasive way with few sources of error.

A summary of the advantages and disadvantages for the various arterial stiffness measurement techniques is outlined in Table 1 below.

Table 1: Summary of the different methods employed to measure arterial stiffness and their advantages and disadvantages.

Method used to estimate PWV	Advantages	Disadvantages	References
Doppler ultrasound	- Non-invasive - Ability to do longitudinal studies - Each animal can be its own control	- Cannot accurately measure distance between measurement points - Error due to probe angle and sample volume depth - Operator dependent - Often not accompanied by simultaneous blood pressure measurements	(37, 38, 46, 47)
MRI	- Non-invasive - Ability to do longitudinal studies - Each animal can be its own control - Can measure stiffness at discrete locations along the length of the aorta	- Cost - Subject to motion artefacts from respiration - Susceptible to changes in heart rate - No studies have reported simultaneous blood pressure measurements	(48-50)
Two pressure catheters placed tonometrically a known distance apart	- High fidelity signals	- Highly invasive - Blood pressure cannot be measured intravascularly - Vessels must be applanated in which could affect local hemodynamics	(44)
One pressure catheter placed intravascularly, one placed tonometrically a known distance apart	- Simultaneous blood pressure measurements - High fidelity signals	- Highly invasive - Vessels must be applanated which could affect local hemodynamics	(51)

Method used to estimate PWV	Advantages	Disadvantages	References
Estimated from impedance measurements but a custom catheter	- Ability to measure pressure and flow	- Highly invasive - Measurements can only be obtained from the proximal aorta - Calibration of catheter cannot be obtained at the site of measurement	(52)
Two single intravascular pressure catheters a known distance apart	- Simultaneous blood pressure measurements - High fidelity signals	- Highly invasive	(53)
Two fluid-filled pressure transducers chronically implanted a known distance apart	- Simultaneous blood pressure measurements - Ability to make measurements in the non-anaesthetized animal	- Highly invasive - Signals are not as accurate as high-fidelity pressure catheters - Error when measuring distance between two locations - May develop air bubbles	(54)
Dual pressure sensor	- Simultaneous blood pressure measurements - Accurate distance measurement between two sensors - High fidelity signals	- Minimally invasive	This study

2.5 Arterial structure

The composition of the arterial wall changes significantly, becoming stiffer, from proximal to the distal aorta (24). This enables the aorta to perform its primary functions optimally and for effective ventricular-vascular coupling.

The arterial wall can essentially be divided into two types of constituents: *(i)* the extracellular matrix (ECM), which includes structural proteins, such as elastin and collagen that largely determine the passive mechanical properties of the arterial wall, and *(ii)* the cellular component, primarily endothelial and vascular smooth muscle cells (VSMC), which can dynamically alter the local mechanical properties of the vessel. Structurally, the arterial wall is organized into three layers, the intima, the media, and the adventitia (Figure 2). The intima, the inner-most layer, consists of the endothelium. Though it contributes little structurally, through various signalling pathways and mechanotransduction mechanisms, the intima can

trigger changes that influence the stiffness of the arterial wall. The media varies greatly with location in the arterial tree, and its state and composition essentially dictate the functional stiffness of the vessel wall. The main structural components of the media are elastin, collagen, and VSMC, and they are arranged within concentric layers, embedded within an extracellular matrix. The adventitia is composed primarily of collagen, fibroblasts, and connective tissue and its contribution to vessel stiffness is increasingly being realised (22). The collagen in the adventitia also becomes important in preventing vessel rupture at extremely high blood pressures (57).

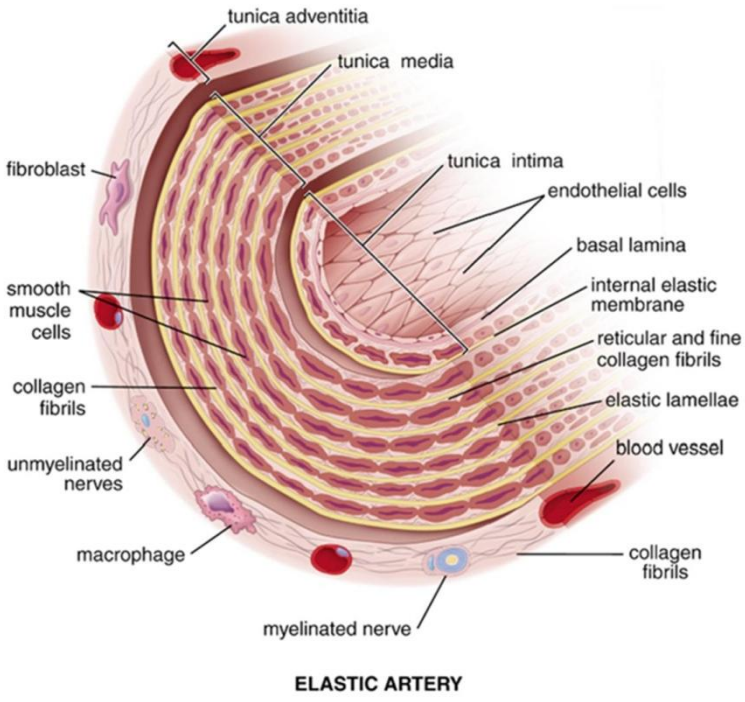

Figure 2: Diagram showing the structure of the large elastic arteries (Reproduced from Ross and Pawlina, 2010 (58)).

As previously mentioned, arteries are non-linearly elastic, i.e. they become stiffer as they are distended (3). Within physiological pressures, elastin, which confers the arterial wall with the majority of its elasticity, bears the majority of the distending forces. However, at higher pressures, collagen, which provides tensile strength, becomes increasingly recruited, stiffening the vessel wall, and thereby preventing it from over-stretching. VSMCs, by

adjusting their level of tone, can also influence wall stiffness. Whereas in resistance vessels, VSMC contraction causes a significant reduction in lumen diameter, this is not the case in the aorta. VSMC contraction modulates stiffness in the aorta by redistributing the tensile forces between collagen and elastin (22). From the proximal aorta to more distal sections, the quantity of elastin decreases, while the amount of collagen and density of VSMCs increases (the arteries become more muscular and stiffer). Naturally occurring crosslinks between the structural proteins of the ECM, as well as cell-matrix interactions play an important role in determining vessel stiffness. This will be discussed in more detail in Section 2.6.

2.6 Factors influencing large artery stiffness

With age, the arteries become stiffer. The severity of this depends on a variety of risk factors, such as the presence of complex disease states (diabetes, atherosclerosis, and renal dysfunction), lifestyle (salt and alcohol intake, smoking, exercise), and genetic factors (abnormalities of connective tissue, Marfan syndrome). The interactions between the structural and cellular components of the vessel wall that maintain its mechanical properties become uniquely altered under these varying conditions causing a reduction in vascular compliance. The ensuing changes in local hemodynamic forces, such as wall shear stress and intraluminal pressure, exacerbate the pathophysiology.

However, even after adjusting for classical risk factors, including blood pressure and age, arterial stiffness is still an important predictor of cardiovascular mortality. This suggests that other genetic factors play an important role in increased vascular stiffness and its downstream effects (59). Several studies have identified candidate genes which may be involved in the pathogenesis of arterial stiffness (60). These have been extensively reviewed and will not be elaborated on in this discussion (60-62). However, the underlying molecular mechanisms and the specific genes which contribute to stiffening of the arteries remain largely unknown.

2.6.1 Age and blood pressure

The stiffness of an artery is a function of its intraluminal pressure. As pressure is increased, less extensible collagen fibres are recruited, thus leading to a reduction in compliance (3). Therefore, it is crucial when assessing arterial stiffness that the direct effects of blood pressure are taken into account.

However, aging is the dominant risk factor for cardiovascular disease (63). With age, the aorta dilates and becomes stiffer. Vascular aging is generally associated with two pathological processes which influence the elastic properties of the vessel wall: medial degeneration and intimal changes which lead to atherosclerosis. This is characterised by an increase in collagen and a decrease in elastin content, as well as migration and proliferation of medial VSMCs (22). Hypertension, which is both a cause and consequence of increased stiffness, accelerates the effects of aging (19), thus creating a vicious cycle.

2.6.2 Structural components

As previously mentioned, the balance between collagen and elastin is a significant factor that dictates the elasticity of the arteries. This balance is normally maintained by a slow process of protein production and degradation. When it becomes disrupted, with age or inflammation for example, an overproduction of collagen and a decrease in elastin levels occurs causing an increase in stiffness (23). Hypertension also stimulates the over-production of collagen (64).

Elastin fragmentation, disorganization, and degradation are characteristic of stiffened arteries. This occurs with age and mechanical fatigue due to the continuous beating of the heart, and is also responsible for the dilation of the arteries. Furthermore, elastin content decreases with age, and because it is so stable and there is virtually no elastin synthesis in adulthood, (having a half-life in humans of more than 40 years (65), and no detectable synthesis in the mouse after 21 days (66)), it is unlikely that damaged elastin will be replaced (22). Some studies

have also suggested that increased oxidative stress and cytokines (as seen in aging or inflammation) could activate elastase, which would add to the elastin degradation (67). The increase in pulse pressure caused by increased arterial stiffness would also exacerbate the degeneration of elastin, thus creating a type of positive feedback loop (60).

VSMCs modify their contractile state in response to changes in mean arterial and pulse pressure, which can indirectly affect stiffness by increasing peripheral resistance and blood pressure, or directly affect stiffness by redistribution of tensile forces. Medial VSMC abundance can also have an influence on wall stiffness. Studies have shown that, with age, the quantity of medial VSMCs declines. Fibrotic scars appear to take the place of the VSMCs while the remaining ones become hypertrophied and embedded in a "collagen capsule" (67). Under pathological conditions, VSMCs experience changes in their normal contractile state and their synthetic, mitotic, and migratory activity, which eventually leads to intimal and medial remodelling (22). By its ability to regulate VSM tone via the release of vasoactive mediators and growth factors, the endothelium can influence arterial stiffness. Endothelial cells become dysfunctional with aging, inflammation, and other pathologies which have downstream effects on the local arterial properties. This will be discussed in more detail in Section 2.7.

Aortic stiffness, however, cannot fully be explained by changes in elastin, collagen, and smooth muscle cell content. Thus it has proven to be very important and intriguing to investigate the interactions between the cellular components of the vessel walls and the structural elements, namely the various proteins that comprise the ECM.

2.6.3 Arterial remodelling

The cells which comprise the vessel wall are sensitive to the local hemodynamic environment. When hemodynamic forces such as pressure and flow are altered (in various cardiovascular pathologies), this results in changes in gene expression, activation of signalling pathways, and

ultimately modifications in the arterial wall in order to account for the new conditions. This is termed arterial or vascular remodelling. This process involves modifications of the ECM itself and its interactions with the surrounding cells, including cell migration, proliferation and death as well as synthesis and degradation of the ECM (68).

When vessels are exposed to increased blood pressure, the arteries remodel by increasing wall thickness in order to normalize tensile forces. This process of remodelling eventually results in the increased deposition of ECM proteins, especially collagen, which then directly augments arterial stiffness, causing a further elevation in blood pressure and eventually left ventricular hypertrophy (57). Left ventricular hypertrophy is also a form of remodelling and it occurs as a compensatory mechanism allowing the heart to accommodate the increased strain caused by increased blood pressure. Accumulation of other matrix proteins in the vessel wall can also influence stiffness, including heparan sulphate, proteoglycans, and fibronectin (68). So while arterial remodelling is in fact a physiological response to altered pressure and/or flow (and often initially increases compliance), it often becomes pathological, contributing to various cardiovascular pathologies such as hypertension, atherosclerosis, and end-organ damage.

When flow is altered, arteries respond firstly with an acute vasodilation (when flow is increased) or constriction (when flow is decreased). This is followed by a structural reorganization of the medial component of the vascular wall as flow changes persist (69). Essentially the vessel becomes fixed in its modified diameter to accommodate the blood flow changes and to normalize wall shear stress. When inward remodelling occurs in the resistance arteries, it causes an increase in total peripheral resistance which then augments blood pressure. This is in part caused by structural changes in the vessel wall characterised by a reduction in lumen diameter and an increased wall-to-lumen ratio. Studies have found that increased smooth muscle tone is the primary instigator of inward remodelling in resistance

arteries. This is supported by the fact that hypertension is often associated with increased sympathetic activity (which causes increased vascular tone). It is important to note that in order for vessels to remain in their rearranged geometries, existing crosslinks in the proteins that comprise the vessel wall must be broken and new ones created (70). Small artery remodelling indirectly affects large arterial stiffness by raising blood pressure, which eventually turns into a vicious cycle.

2.6.4 Advanced glycation end products

The accumulation of advanced glycation end products (AGEs) in the vessel wall with age and disease causes arterial stiffening (71). Plasma concentration of AGEs is also related to increased aortic stiffness as measured by PWV, independent of age and blood pressure (72). AGEs are derived from the non-enzymatic reaction between glucose and proteins in the arterial wall. Over time, the products of these reactions undergo complex chemical rearrangements which result in AGEs. AGEs can then react with amino groups on neighbouring proteins to form crosslinks that are stable and highly resistant to breakdown (73). Collagen and elastin are highly susceptible to AGE accumulation due to their low turnover. This increased crosslinking of collagen contributes to its accumulation in the vessel wall (67). AGE-crosslinked collagen is also stiffer and less susceptible to hydrolytic turnover (23). Collagen crosslinking in the arteries and myocardium leads to a loss of elasticity, increased stiffness, and myocardial diastolic dysfunction. This is supported by the fact that the AGE inhibitor, aminoguanidine, has been shown to slow or prevent both age- and diabetes-related arterial and myocardial stiffening (74, 75). Furthermore, compounds which can break AGE crosslinks have been shown to reverse decreases in myocardial and vascular compliance (76-78). It is evident that collagen crosslinking plays a highly important role in increased arterial stiffness.

2.6.5 Calcification

Various pathologies have been shown to influence medial elastocalcinosis, including hypertension (79), Type 2 diabetes (80), and end stage renal disease (81). Calcium is increasingly deposited in the arterial wall with age. This takes on two forms: intimal atherosclerotic plaque calcification and medial elastocalcinosis (67).

A relationship between aortic calcification and stiffness has been demonstrated in rat by our group and others (67, 82). In fact, Dao et al found that at least one third of an observed increase in arterial stiffness was due to medial elastocalcinosis (67). *Ex vivo* compliance is also significantly reduced in calcified rat aortas depending on the severity of calcification. Interestingly in this study, VSMC and endothelial function were not altered by medial calcification (83). Treating rats with vitamin D_3 + nicotine drastically increases calcium content in the aorta and significantly increases pulse pressure, which may be considered a surrogate marker for increased aortic stiffness (84). However, these rats also experienced endothelial dysfunction, which may have been responsible for the changes observed in pulse pressure. Nakamura et al studied the correlation between brachial-ankle PWV and the length of abdominal aortic calcification (AAC) on X-ray films in 97 patients. They found that AAC length was a significant determinant of PWV, independently of age and blood pressure (85). On the other hand, Maizel et al observed that chronic renal failure (CRF) status and absence of apoE increase aortic intimal and medial calcification but there is no correlation between this and diastolic dysfunction, left ventricular mass, or PWV (53). This was supported by the fact that stiffness values were not different between wild type (WT) and apoE$^{-/-}$ mice with CRF despite the fact that there was a significant difference in calcification. There were no differences in collagen or elastin content in either model, which often confounds results. For example, severe elastocalcinosis may induce destruction of elastic fibres, which is the cause of increases in stiffness rather than the deposition of calcium itself. Thus, while aortic

calcification is associated with various cardiovascular pathologies, its individual contribution to vascular stiffness still remains highly unknown.

2.6.6 Atherosclerosis

Events that lead to diminishing the integrity of the endothelium elicit local unhealthy genetic changes and inflammatory responses. This promotes the adhesion of circulating leukocytes and activated platelets to these regions and increased permeability to plasma lipids, such as low-density lipoprotein (LDL). Monocytes accumulate in the intima where they differentiate into macrophages, become loaded with oxidized LDL, and become foam cells. Eventually this forms fatty streaks in the arterial wall which initiate atherosclerotic plaque formation. Continued infiltration by inflammatory and immune cells (including T cells and mast cells) and extracellular lipids forms a necrotic core within the lesion. This is covered by a fibrous cap comprised of VSMC and collagen. Plaque progression occurs as cells within the lesion secrete cytokines and growth factors, and ECM components continue to accumulate causing intimal thickening and a narrowing of the arterial lumen diameter. With time, the fibrous cap may thin and rupture, which can ultimately lead to a heart attack or stroke. Aneurysms may also form as the arteries remodel to compensate for the intimal thickening (86-89). This is described in (Figure 3).

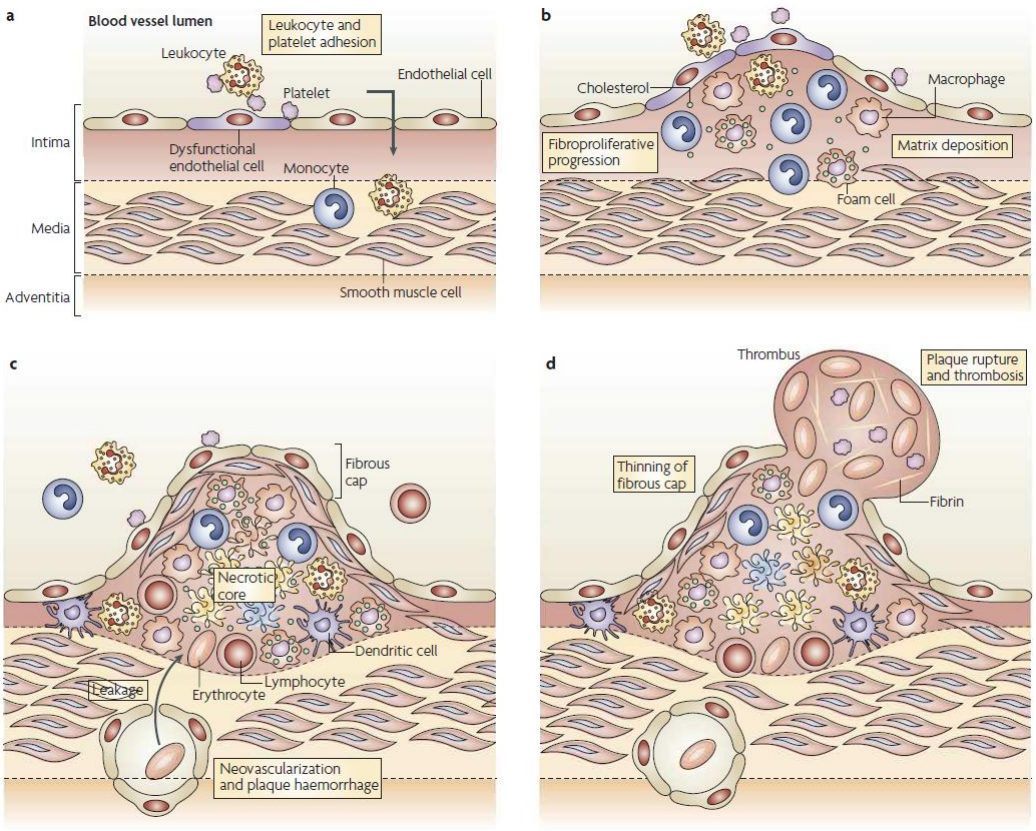

Figure 3: Atherosclerosis development and progression. (a) Local inflammation and injury cause endothelial dysfunction. This results in the adhesion of circulating blood cells and increased permeability. (b) Fatty streaks are formed in the intima as increased transendothelial migration of monocytes occurs where they differentiate into macrophages, digest lipids, and become foam cells. Plaque formation progresses with continued infiltration by inflammatory cells and extracellular lipids, migration of VSMC, and deposition of ECM components. (c) Eventually, a necrotic core forms within the lesion comprised of apoptotic and necrotic cells, cell debris, and cholesterol. This is surrounded by a fibrous cap comprised of VSMC embedded in a collagen matrix. (d) With time, thinning of the fibrous cap occurs which leads to plaque rupture, thrombosis, and stroke. (Reproduced from Weber et al 2008 (86)).

Increased inflammation, oxidative stress, and endothelial dysfunction are all consequences of aging and render the artery highly susceptible to the formation of atherosclerotic plaques. While the development and progression of atherosclerosis is distinct from the stiffening of the arteries, the two pathological processes are known to be highly associated. In fact, atherosclerosis often causes increased aortic stiffness, and this has been observed in several different species (71). The Rotterdam population-based study also found that arterial stiffness is strongly associated with atherosclerosis at various sites in the vascular tree (18).

Furthermore, increased stiffness likely accelerates atherosclerosis, creating a vicious cycle between these two pathologies. Atherosclerotic plaques primarily develop in regions of disturbed flow and lower shear stress. The state of the endothelium, which essentially dictates the onset of this disease, is highly sensitive to the characteristics of the flow to which it is exposed. Thus, the altered hemodynamics that occur with vessel stiffening and the consequent widening of the pulse pressure would alter the fluid shear stress and cyclic stress imparted on the endothelium, predisposing it to the progression of atherosclerosis.

2.6.7 Other extrinsic factors

Changes in the vessel wall leading to increased stiffness can also be modulated by local hemodynamic forces, such as wall shear stress, and other extrinsic factors, including hormones, salt, and glucose regulation (23).

The rennin-angiotensin system imparts a significant influence on arterial stiffness via its known roles in blood pressure regulation, cellular proliferation, matrix production, vascular hypertrophy (90). Angiotensin II (Ang II) stimulates collagen formation, decreases nitric oxide-dependent signalling, and increases oxidative stress (23, 91, 92). It also can induce the release of various cytokines and growth factors and exerts downstream effects such as VSMC hypertrophy, fibrosis, fibronectin expression, and release of endothelin-1 (23). Studies have shown that Ang II promotes atherosclerotic plaque development (93). Collectively, this can have a significant impact on the elastic properties of the vessel walls. This is evidenced by the fact that treatment with angiotensin converting enzyme inhibitors has been shown to reduce PWV, calcification, and collagen accumulation (82, 94). Angiotensin receptor antagonists have also been shown to reduce PWV and AIx independently of blood pressure (95).

Neurogenic mechanisms may also play a direct role in modulating large artery stiffness, although this is less well-defined. Increased sympathetic activity may alter stiffness via increased heart rate, which affects PWV (96), and VSMC tone.

2.7 Endothelial function

The endothelium is comprised of a continuous monolayer of endothelial cells which lie at the interface of blood flow and the artery wall. Its many functions include moderating vascular homeostasis, inflammatory responses, vascular smooth muscle tone, processes such as coagulation and thrombosis, and maintaining permeability of the vessel wall. This involves regulating transendothelial migration of circulating nutrients, biological molecules, and various types of cells into the surrounding tissue (97). The state of the endothelium is thus a good indicator of vessel health, and plays a key role in the pathogenesis of diverse and prevalent cardiovascular diseases.

The endothelial layer is strongly influenced by the characteristics of the blood flow to which it is subjected. Hemodynamic forces are known to induce changes in endothelial cell morphology, structure, production of matrix, intercellular interaction and communication, gene expression, and function (98, 99). Through mechanotransduction, endothelial cells are able to sense hemodynamic factors in their local environment and convert these into biological, chemical, and physical changes. Important hydrodynamic forces continually acting on the endothelium include blood pressure, circumferential strain, and wall shear stress (99, 100).

The endothelium secretes various vasoactive substances in response to the local physical and chemical environment. One such substance is nitric oxide (NO), which is produced by the enzyme endothelial nitric oxide synthase (eNOS). NO has two major physiologic pathways of activity. The first is through the formation of cyclic guanosine monophosphate, which induces smooth muscle cell relaxation and subsequent vasodilatation. The second, a focus of the work presented in this thesis, is through post-translational modification of cysteine residues, a process termed S-nitrosylation. S-nitrosylation is now accepted as an important signalling mechanism regulating key processes in the vascular system (101). Both of these pathways are

regulated by the balance between NO and reactive oxygen species (ROS), the nitroso-redox balance (102, 103).

Endothelial dysfunction is characterised by a disruption in this balance, which is often seen in aging and inflammation, and results in a decreased bioavailability of NO. Evidence shows that this is due to enhanced vascular oxidative stress. Elevated ROS production, which is associated with inflammatory vascular diseases, may inactivate endothelial NO before it reaches its molecular targets. In atherosclerosis and hypertension, increased levels of superoxide anion radical react rapidly with NO to form peroxynitrate which effectively decreases NO bioactivity. Endothelial sources of superoxide anion radical include the enzyme NADPH oxidase, xanthine oxidase, uncoupled eNOS, mitochondria, and cytochrome P450. While superoxide is the major ROS which impairs NO bioavailability, there are other important forms of oxidative stress which can influence endothelial function, such as hydrogen peroxide, oxidized lipoproteins, lipid peroxidation, peroxynitrite, and myeloperoxidase (102). This impacts arterial stiffness due to the fact that NO is a regulator of vascular smooth muscle tone, which directly affects the manner in which the vessel wall transmits pressure pulses from the heart. However, there are other downstream effects stemming from endothelial dysfunction which can eventually translate into stiffer arteries.

2.7.1 S-Nitrosylation

As previously mentioned, S-nitrosylation is now recognized as an important NO-based signalling mechanism. S-nitrosylation is a reversible post-translational protein modification that involves the covalent attachment of an NO molecule to a reactive cysteine thiol (104). In fact, to date, over 100 proteins have been shown to undergo S-nitrosylation (105). Generally speaking, protein S-nitrosylation can modulate structural proteins, ion-channels, and enzymes and results in either an activation or an inhibition of activity (106). While some form of NOS is expressed ubiquitously, and many proteins contain cysteine residues, S-nitrosylation is a

process with a high substrate specificity and regulation of protein function is often brought about with the modification of only one or a few active cysteine sites. NOS expression and activity, and thus the bioavailability of NO, is an obvious regulator of S-nitrosylation; however, other NOS-independent mechanisms influencing S-nitrosylation are receiving more attention (101). For example, ions (e.g. Ca^{2+}) which can induce changes in protein structure can stimulate S-nitrosylation and de-nitrosylation (104). This appears to be the case with transglutaminase 2 (TG2) S-nitrosylation which will be discussed in the following sections. ROS, such as hydrogen peroxide, can also bind the same cysteine moieties as NO, thereby preventing S-nitrosylation from occurring. At physiological levels, this actually plays a beneficial role in regulating S-nitrosylation of proteins. However, excess levels of superoxide will not only disrupt the nitroso-redox balance, but may also react directly with NO, preventing normal signalling mechanisms and possibly forming other ROS (107). Additionally, as S-nitrosylation mechanisms are active in the heart and vasculature, a disruption in the nitroso-redox balance can have detrimental effects on cardiovascular function (107). In fact, evidence shows that hypo- or hyper-S-nitrosylation of target proteins are likely to contribute to a variety of human pathologies, including cardiovascular disease (101).

2.7.2 Nitric oxide inhibition

Many studies have attempted to elucidate the role of endothelial dysfunction, characterised by a reduced bioavailability of NO, in increased arterial stiffness. One of the most common ways to do this is by inhibition of NOS (108). It is difficult to interpret the data, as type and concentration of drug and method and duration of treatment vary vastly between studies. While it is generally accepted that NOS inhibition will increase blood pressure and arterial stiffness, this is not always the case. Additionally, it is unclear if NOS inhibition causes changes in vascular stiffness that are independent of blood pressure alterations.

There are actually three distinct NOS isoforms: inducible NOS (iNOS), neuronal NOS (nNOS) and endothelial NOS (eNOS). iNOS can be found in most vascular cells, but is only expressed after activation by cytokines or other inflammatory mediators, thereafter producing high levels of NO (109). It has often been shown to play a detrimental role in a wide variety of disease processes, such as atherosclerosis (110). The multifunctional nNOS is constitutively expressed in neurons, and skeletal, cardiac, and smooth muscle and has been implicated in a range of pathological processes, for example, cerebral ischemia (111). eNOS, as previously mentioned, produces the majority of endothelial NO, which is crucial in the maintenance of cardiovascular health and homeostasis. Impairment in this process promotes vascular inflammation and disease. In fact, $eNOS^{-/-}$ mice develop spontaneous hypertension, impaired vascular remodelling, vascular thrombosis, and atherosclerosis (102).

Some of the most common NOS inhibitors are N^G-monomethyl-L-arginine (L-NMMA) and N^G-nitro-L-arginine methyl ester (L-NAME), and asymmetric dimethylarginine (ADMA). They have been shown to cause concentration-dependent inhibition of vascular eNOS, endothelium-dependent aortic relaxation, an increase in mean arterial pressure and bradycardia (112, 113). However, it is known that these drugs are not endothelial NOS specific, therefore, care should be taken in interpreting results of inhibition studies.

Fitch et al examined pressure dependent PWV in rats, whereby pressure was altered by acute infusion of both L-NAME and phenylephrine (PE). They found that at every given level of pressure, PWV was higher with L-NAME infusion than with PE (28). However, PP was lower during L-NAME infusion than with PE. In the same study, rats were chronically treated with L-NAME, which resulted in increased blood pressure and PWV. When corrected for blood pressure, the chronically treated rats had even higher PWV than those acutely treated. Results from the acute experiment suggest that NO modulates vascular compliance by modulating vascular tone. Those from the chronic treatment indicate that the additional

increase in PWV is likely due to arterial remodelling caused by inhibition of NOS itself and also due to the sustained level of hypertension caused by L-NAME administration. Conversely, Cayette et al found that while chronic L-NAME administration in rabbits caused increased early atherosclerosis development, there were no changes in systolic or mean blood pressure after treatment (114). Local acute administration of the NOS-inhibitor L-NMMA in sheep increased iliac PWV significantly without affecting blood pressure or heart rate, supporting the idea that basal NO production does influence large artery stiffness (31). Rats treated with L-NAME for three weeks showed increased blood pressure by the third day of treatment which continued to progress over the 21 day course. PWV, even after adjusting for pressure, also increased significantly by the third day. The wall-to-lumen ratio did not significantly increase until one week had passed, indicated that changes in PWV may actually precede structural changes in the arteries. These data are in agreement with that produced by Fitch et al where the short term changes in PWV may be more associated with alterations in smooth muscle tone, whereas longer term changes may be caused by changes in vascular structure (115).

In a different study by Fitch and colleagues, mice chronically treated with L-NAME alone did not demonstrate any changes in blood pressure, PWV, *ex vivo* aortic elastic modulus and contractility, or the collagen-to-elastin ratio in the vessel wall. In combination with Ang II, there were significant increases in all of the above measures suggesting only a synergistic effect of the two drugs but no individual influences (45). On the other hand, it has also been shown that only two weeks of oral L-NAME treatment increased PWV in both WT and arginase II knockout mice, along with an impairment of the endothelium-dependent acetylcholine (ACh) relaxation response in aortic rings (43). Interestingly, a study by Joannides and colleagues found that in the human radial artery, infusion of L-NMMA decreased arterial stiffness, increased compliance, and exerted no change in diameter, wall thickness or midwall stress (116). The changes in stiffness and compliance occurred in a

dose-dependent manner. They suggest that perhaps there is a compensating vasodilatory mechanism which is active upon inhibition of NOS, such as an increase in the release of endothelium derived hyperpolarizing factor (EDHF). EDHF-mediated responses induce vasorelaxation by hyperpolarizing VSMCs. It has been suggested that EDHF provides vasodilation when there is a reduced bioavailability of NO, such as in hypertension and atherosclerosis (117). It is quite evident that the effects of NOS inhibition are varied in the context of the cardiovascular system, especially within the large conduit arteries. Further work is required to elucidate the specific or direct effects that NOS inhibition has on large artery stiffness.

Studies using $eNOS^{-/-}$ mice have provided useful data on the role of NO in hypertension and vascular stiffness. Twenty-four hour blood pressure assessed by telemetry revealed a modest increase in mean blood pressure in $eNOS^{-/-}$ mice compared to WT controls. This was accompanied by a much larger increase in pulse pressure, indicating that NOS inhibition was exerting a significant effect on large artery stiffness itself (118). Soucy et al found that $eNOS^{-/-}$ mice had significantly increased PWV compared to WT controls, although the results were not normalized for any potential differences in blood pressure (119). Jung et al also found both PWV and MAP increased in $eNOS^{-/-}$ mice relative to WT controls. To normalize for pressure, they investigated the pressure-dependent PWV and found that at MAP greater than 125 mmHg, $eNOS^{-/-}$ had significantly higher PWV. They also demonstrated that aortic *ex-vivo* stiffness, assessed by tensile testing, is increased and carotid arterial compliance decreased in eNOS knockout mice as well (120). Studies in $eNOS^{-/-}$ mice are much more conclusive in defining a role for NO in maintaining healthy arteries and reducing arterial stiffness. The mechanisms by which it exerts these beneficial effects are gradually being elucidated.

2.8 Transglutaminase 2

Transglutaminase 2 (TG2) is an enzyme belonging to the transglutaminase family, of which there are 9 known proteins (121). It is ubiquitously expressed in the vasculature, including endothelial cells, smooth muscle cells, fibroblasts, and monocytes-macrophages (122). TG2 is a highly multifunctional protein which has been shown to influence a wide variety of pathologies and processes, including Huntington disease (123), Type-1 diabetes (124), Celiac disease (125), atherosclerosis (126), small artery-remodelling (127), and apoptosis (128). TG2 mediates several Ca^{2+}- and thiol-dependent reactions which results in post-translational modification of proteins (129); however, it is its ability to catalyse the transamidation reaction which leads to the formation of an N^{ε}(γ-glutamyl)lysine isopeptide bond between a lysine residue of one protein and the glutamine residue of another that is of particular interest in the studies presented in two of the chapters in this thesis (Chapters 5 and 6). This bond creates a mechanically and chemically stable crosslink which may affect both the properties of the ECM (and thus the vessel wall itself) and the cell-matrix interactions that occur within the vessel wall (122, 129). The crosslinks are found primarily in the adventitia and sub-endothelial layer (16). Additionally, TG2's transamidation activity is important for processes such as wound healing, angiogenesis, and bone remodelling (129). There is accumulating evidence supporting the importance of the cross-linking-independent functions of TG2. The review by Chen and Mehta (130) provides an in depth description of these functions.

TG2 is generally localized in the cytosol of the cell; however, a fraction of it is found on the external surface of the cell membrane and in the ECM (121, 131). The exact mechanism of externalization and deposition into the ECM has not been fully elucidated (129), but appears to require an active site, Cysteine (Cys^{277}). Once outside the cell, TG2 can crosslink several vascular ECM proteins, including: fibronectin (132), vitronectin (133), laminin (134), and collagen (135). Aside from influencing cell-matrix interactions (such as adhesion, motility,

and spreading), an important implication of this activity is the alteration of the mechanical properties (and thus stiffness) of the vessel wall through the formulation of these strong cross-links which are highly resistant to degradation (136). Telci et al demonstrated *in vitro* in Swiss 3T3 fibroblasts that inducing TG2 activity leads to increases in collagen and fibronectin deposition and expression (137).

TG2 activity is Ca^{2+}-dependent, meaning it requires a relatively high level of intracellular Ca^{2+}; so under normal conditions, there is generally no cross-linking activity (121, 122, 136, 138). However, disruptions in homeostasis and different pathways induced by stress, injury, and inflammation may cause increased TG2 expression and activity (129, 136, 139). For example, Auld et al showed that thrombin, an inflammatory molecule, upregulated TG2 mRNA, protein, and cross-linking activity (140). Other pro-inflammatory cytokines, such as IL-6 and TNF-α also induce TG2 expression (141). TG2 cross-linking activity is further regulated by nitric oxide (NO), which has been shown to S-nitrosylate several cysteine residues, including its active site Cys^{277} (142). This results in an inhibition of TG2 activity as well as increased sensitivity to guanosine triphosphate (GTP) (142, 143). Lai and colleagues showed, however, that TG2 activity is regulated by NO in a Ca^{2+}-dependent manner, that is, levels of S-nitrosylation, denitrosylation and corresponding levels of TG2 activity are dependent on the presence or absence of calcium (142).

Another study showed that TG2 inhibition by NO S-nitrosylation not only affects its cellular distribution, but also results in a decrease in the expression and deposition of collagen and fibronectin and the activity of transforming growth factor β1 (TGFβ1) and NF-κB (137). Santhanam et al also demonstrated *in vitro* that endothelial NO S-nitrosylates TG2 thereby regulating its crosslinking activity and location in endothelial cells (16). Endothelial cell derived NO also reduces TG2 externalization from the cell via S-nitrosylation in both fibroblasts and VSMCs (17).

It is worth noting that TG2 can also bind GTP, causing it to behave as a G-protein which may interact with various G-protein-coupled-receptors (129). The binding of GTP and Ca^{2+} reciprocally regulate its G-protein and transamidating activities respectively, such that while performing the function of a G-protein, its cross-linking capabilities are inhibited and vice versa (121).

The membrane integrins, both of which are present in endothelial cells and smooth muscle cells, play an important role in vascular physiology. Integrins can sense the local environment (for example, blood pressure), and control downstream responses to this, such as vascular tone, remodelling, and endothelial permeability, through the synthesis of various ECM proteins. As such, integrins provide a cross-talk between the ECM and the cells comprising the vasculature. TG2 is involved in some of these interactions via its ability to bind to fibronectin which anchors it to the cell surface, and to activate cytokines, such as TGF-β (137). In fact, several ECM proteins are substrates for TG2. For these reasons, TG2 plays an important role in wound healing, angiogenesis, and vascular remodelling (138).

TG2 has been shown to play an important role in small artery remodelling (122). Depending on the conditions, this role may be either physiological or pathological. This is important as the small resistance arteries have a huge impact on mean blood pressure, and thus stiffness. In the spontaneously hypertensive rat (SHR), cystamine (which is a competitive inhibitor of TG2) attenuates the inward remodelling of resistance arteries induced by endothelin-1 *in vitro*. Furthermore, administration of cystamine for 3 weeks was also able to induce a mild but significant decrease in blood pressure in the SHR rats, although there were no observed functional or structural changes in the small arteries of these animals (144). A study by Bakker et al found that inward remodelling depends on both chronic vasoconstriction combined with TG2 crosslinking activity (145). First they demonstrated that inward remodelling induced by a reduction in blood flow or activation by endothelin-1 can be

reduced when TG2 activity is inhibited. Inward remodelling could also be induced in pressurized vessels by application of endogenous TG2. Results from this experiment indicated that this was due to collagen-crosslinking, as the pressure of the vessel was at a level where collagen recruitment would occur. Using inflammatory stimuli of TG2 activity (such as retinoic acid) or inhibitors (such as NO) enhanced or diminished arterial remodelling was shown respectively. And importantly, TG2 activity was dependent on pressure. In support of these studies, van den Akker and colleagues were able to show that the cross-linking activity of TG2 is required to induce inward remodelling of small arteries, and an associated decrease in distensibility, and in order to do so, TG2 must be in a reduced state (146). Further, this could be inhibited by the addition of NO. This indicates that the redox state of TG2 is an important mediator of its extracellular cross-linking activity, which can be regulated by a redox-sensitive cysteine triad consisting of Cys^{230}, Cys^{370}, and Cys^{371} (147). Interestingly, treatment with the TG2 competitive inhibitor cystamine inhibited both inward and outward remodelling of resistance arteries in rat and this occurred independently of any hemodynamic changes (148). It is important to note that cystamine inhibits TG2 activity by forming a mixed disulfide with its cysteine thiol active centre, causing TG2 to be in a reversibly inactivated form (149). Conversely, Bakker et al found that outward remodelling was similar in $TG2^{-/-}$ and WT mice (150). They also found that inward remodelling was delayed but not suppressed in $TG2^{-/-}$, indicating the presence of compensatory mechanisms, likely by monocyte/macrophage derived factor XIII (150).

Cardiovascular parameters in the $TG2^{-/-}$ mouse, such as heart rate and blood pressure, have been demonstrated to be no different than those of their wild type controls (151). It is likely there is some redundancy among the TG family, and translational and functional compensation by other TGs in $TG2^{-/-}$ mice has been demonstrated in heart and aortic tissue (152). However, some studies have shown both beneficial and detrimental effects of TG2 deletion. For example, it has been reported that $TG2^{-/-}$ mice have reduced heart rates, coronary

and aortic flow, and aortic pressure compared to control (153). On the other hand, hearts from these mice were shown to be more sensitive to ischemia/reperfusion injury with larger infarct sizes and a worse level of recovery of post-ischemic cardiac function (154). TG2 has also been linked to cardiac hypertrophy in mice, rats, and humans (129). Iwai et al found that TG2 expression was upregulated during the development of cardiac hypertrophy and the transition to heart failure in rats (155). Small and colleagues found that mice which overexpress TG2 display remodelling of the heart with mild hypertrophy and depressed resting ventricular function (156). Another study also found that mice in which TG2 was overexpressed experienced left ventricular hypertrophy, in addition to elevated heart rate and lowered blood pressure and left ventricular ejection fraction (157). Conversely, in the human heart, downregulation of TG2 activity was shown to be associated with heart failure due to both dilated and ischemic cardiomyopathy (158). While it is evident that TG2 is associated with cardiac dysfunction, it is unclear whether this is due to its transamidating activity or any of TG2's host of other functions. Furthermore, changes in TG2 expression are often reported, but levels of activity are not.

Fibrosis involves the accumulation of excess fibrous tissue, including collagen. While it is a part of the natural response to tissue injury and repair, it can become pathological if not carefully mediated. Further, fibrosis, and thereby excess collagen, in aortic tissue could lead to an increase in the local arterial stiffness. TG2 has been implicated in various forms of tissue fibrosis, including the kidneys (159), liver (160), and heart (157).

TG2 expression in the vessel wall increases with the development of atherosclerosis. It seems to play a protective role in this case by limiting the growth of atherosclerotic plaques while increasing plaque stability (140, 161). Increased deposition of collagen, a substrate of TG2 (135), is necessary for plaque stabilization (140). As such, increased TG2 activity has been shown to be characteristic of stable plaques (126, 162). This is important as it protects the

lesions from rupture due to stresses imparted by fluid shear stress and blood pressure. It has been shown that TG2 activity is increased in endothelial cells by turbulent shear stress and down regulated by high shear stress. Oscillatory shear stress also increases endothelial TG2 activity. Under oscillatory flow, TG2 activity increased expression of monocyte chemotactic protein-1 *in vitro*. $TG2^{-/-}$ mice had reduced monocyte recruitment *in vivo* in response to oscillatory shear and TG2 inhibition in apoE knockout mice showed a reduction in macrophage and fat content in distal lesions. However, lesion size was increased concomitantly with smooth muscle cell content (163).

TG2 activity is also involved in vascular calcification. *In vitro* studies by Johnson et al (164) demonstrated that in injured arteries, TG2 is required for the intra-arterial chondro-osseous differentiation and calcification of smooth muscle cells in response to increased levels of P_i and bone morphogenic protein-2. A study by Faverman et al also found that TG2 produced a 3-fold increase in matrix mineralization and an upregulation of osteoblastic markers in smooth muscle cells (165). Finally, it has been shown that TG2 plays a critical role in the β-catenin signalling pathway leading to warfarin-induced medial calcification in aortic VSMCs (166).

It is evident that TG2 does play many beneficial physiological roles, particularly in inflammatory diseases and tissue healing. However, if its expression and activity are disrupted or not properly regulated, it may then contribute to many pathologies. With age and increased inflammation and oxidative stress, given its ability to interact with several ECM proteins and cytokines, its role in small artery remodelling, calcification, cardiac hypertrophy and atherosclerosis (all of which can influence blood pressure and arterial hemodynamics), its ability to mediate cell-cell and cell-matrix interactions and matrix stability, all via its cross-linking activity, it is highly plausible that increased TG2 activity could contribute to increased arterial stiffness.

Indeed, Chabot et al used a fluorescent probe to show that TG2 activity increased over 4 weeks in a rat model of hypertension that had previously demonstrated increases in arterial stiffness over the same time frame (167). While their results suggest an association between TG2 and stiffness, it would be beneficial to measure stiffness, blood pressure, and TG2 activity in the same rats. Rats that underwent hind limb unweighting (HLU, to simulate microgravity) for 7 days showed increased aortic PWV that could be reduced under TG2 inhibition by cystamine. However, HLU also induced an increase in aortic collagen content that was not associated with TG2 activity (168). Another study by Santhanam and colleagues (16) showed that WT, but not $TG2^{-/-}$ mice, had increased aortic PWV and decreased carotid compliance when treated with the NOS inhibitor, L-NAME, compared to untreated controls. What is of specific interest is that $TG2^{-/-}$ mice treated with L-NAME had significantly higher blood pressure than their WT counterparts. Similarly, aging rats treated with cystamine, a TG2 inhibitor, showed significantly lower PWV at the end of the treatment period compared to untreated animals. It is important to note that PWV was measured non-invasively by Doppler ultrasound at baseline values and was not corrected for any changes in mean pressure. Finally, they also found higher TG activity and crosslinks in aged human aorta obtained at autopsy compared to young controls, suggesting that TG2 activity may contribute to age-related changes in the vasculature (16). In $eNOS^{-/-}$ mice which display increased arterial stiffness, matrix-associated TG2 and TG2 crosslinking were higher while TG2 S-nitrosylation was lower compared to WT controls. Cystamine treatment in the mice led to an increase in *ex vivo* carotid artery compliance without having any effects on mean arterial pressure. These data support a role for NO in regulating TG2 location and activity, and suggests that TG2 crosslinks may potentially contribute to increased arterial stiffness, although further work is required to substantiate this (120).

Important caveats should be mentioned before concluding this chapter. Care should be taken when interpreting *in vitro* findings as it has been shown that TG2 activity varies between cell

types and should be measured *in situ* in addition to *in vitro* when studying TG2-related mechanisms and functions in biological and pathological processes (139). Furthermore, several studies use cystamine as a TG2 inhibitor even though it is known that cystamine is not a specific TG2 inhibitor. It does not show any selectivity for TG2 over TG1, TG3, or factor XIIIa (169). It has also been shown to inhibit protease caspase 3 and cause increased production of glutathione in cells (170). Finally, TG2 activity is often reported to be increased with various pathologies but it does not necessarily imply causation, especially as TG2 is such a multifunctional enzyme, found virtually everywhere in the body.

Nevertheless, aside from directly affecting arterial stiffness by the formation of crosslinks in the ECM, TG2 activity may also influence arterial stiffness and hypertension indirectly via downstream mechanisms in which it is involved, such as its role in integrin signalling, calcification, arterial remodelling and fibrosis. Figure 4 summarizes some of the major biological functions of TG2, especially within the context of the cardiovascular system.

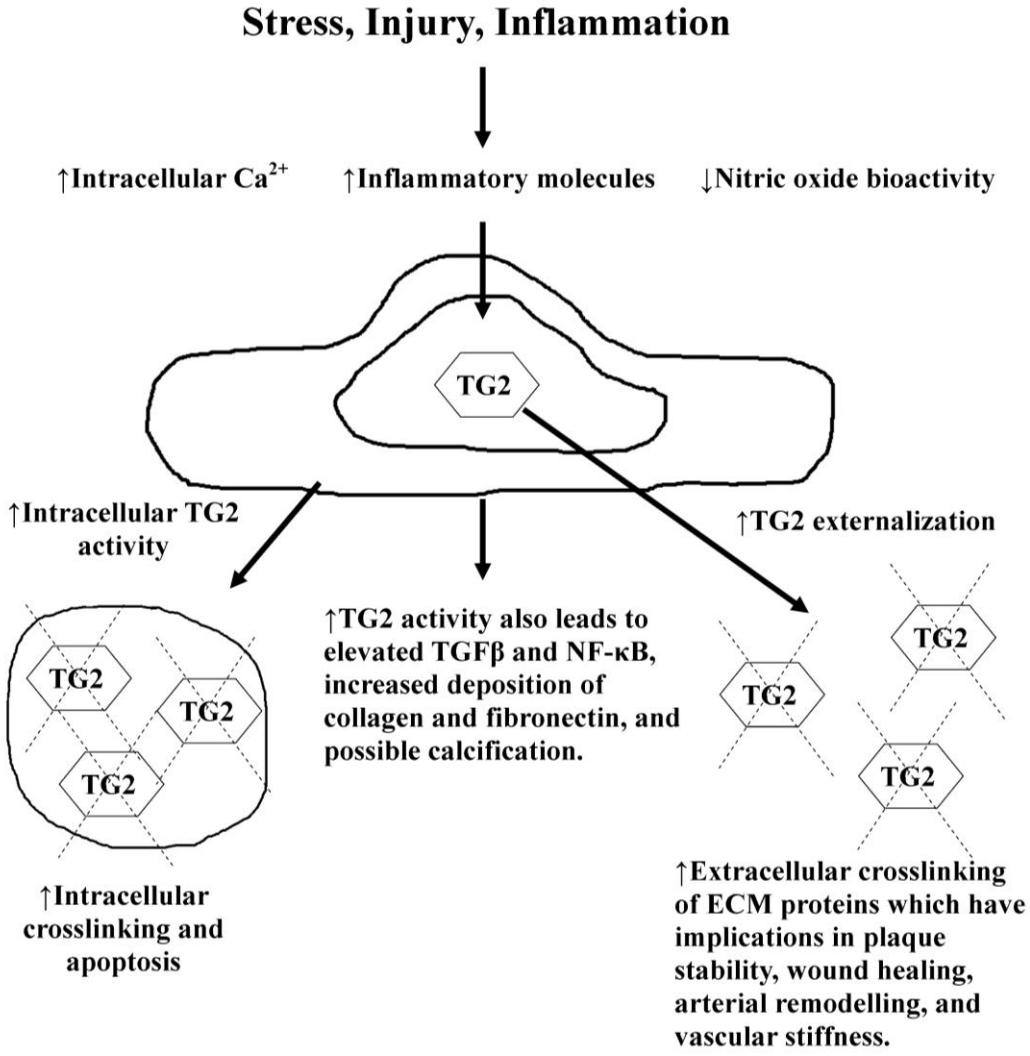

Figure 4: TG2 activity in response to tissue injury and inflammation. Under normal physiological conditions TG2 activity is latent. Environmental stress causes increased intracellular Ca^{2+}, inflammatory molecules, and reduced NO bioavailability. Collectively, this causes an upregulation of TG2 activity. This can cause massive intracellular crosslinking leading to apoptosis (crosslinking designated by dashed crossed lines). Decreased S-nitrosylation of TG2 caused by a reduction in NO leads to externalization of TG2 where it mediates the formation of crosslinks of ECM proteins. These crosslinks play a role in various physiological and pathological processes, including arterial stiffness. Other downstream effects of increased TG2 activity involve elevated TGFβ, increased deposition of collagen and fibronectin, and possible calcification.

2.9 Apolipoprotein E

Atherosclerosis is a highly prevalent disease in which plaque builds up in the arteries. This hardens and narrows the arteries which are affected over time, eventually resulting in a complete blockage of the artery or plaque rupture, both of which may have serious consequences. The development of atherosclerosis was described previously (Section 2.6.6)

along with its relationship to increased arterial stiffness, as well as the involvement of TG2 activity in plaque stability and progression (Section 2.8).

Apolipoprotein E (apoE) plays an important role in the transport and hepatic metabolic clearance of circulating cholesterol. It also has a beneficiary role against inflammation(171). In the mouse, apoE deficiency causes severe hypercholesterolemia. Under normal circumstances, mouse plasma cholesterol is in the antiatherogenic high-density lipoprotein fraction. However, in apoE$^{-/-}$ mice, the plasma cholesterol is in the atherogenic lipoprotein fractions. Specifically, very-low and intermediate density lipoprotein levels are dramatically elevated, which is essentially what drives the progression of atherosclerosis in these mice (172). Indeed, apoE knockout mice experience spontaneous hyperlipidemia and development of atherosclerotic lesions throughout the arterial tree. Lesions primarily develop at the aortic root, the lesser curvature of the aortic arch, the principal branches of the aorta, and in the pulmonary and carotid arteries; however, in older animals, they are also found in the descending thoracic, lower abdominal, proximal coronary, common iliac and femoral arteries (173). These effects are exacerbated when the mice are fed a high-fat, high-cholesterol diet (172). The distribution and size of lesions also progress with age and resemble human atherosclerotic lesion development and progression (42, 174). In fact, foam cell lesions develop as early as 8 weeks and fibrous plaques by 15 weeks of age (173). In very advanced lesions, calcium deposits have also been observed (174). This makes the apoE$^{-/-}$ mouse an efficacious tool for studying atherosclerosis; however, there are other cardiovascular phenotypes associated with this particular knockout model.

Firstly, apoE$^{-/-}$ mice have increased stiffness, as assessed by PWV. Wang et al examined PWV in 4 and 13 month old apoE$^{-/-}$ mice and WT controls and found that both age groups showed extensive atherosclerotic lesions in the aorta, while only the 13 month old apoE$^{-/-}$ had significantly increased PWV and elastic laminar fragmentation. There were no changes in

blood pressure between groups, indicating that the increase in stiffness was in fact due to changes within the vessel wall itself (51). As WT mice do not develop atherosclerosis, the observed changes can generally be attributed to the atherosclerotic changes induced by the deletion of apoE in these mice (171). Hartley and colleagues also found no differences in heart rate and blood pressure in 13 month old apoE$^{-/-}$ mice compared to control (42). They did find significant decreases in body weight and hematocrit, as well as significant increases in heart weight, aortic velocity, mitral velocity, and PWV. Abnormal blood flow waves were also observed, suggesting alterations in impedance and additional sites of wave reflection close to the heart. Using MRI, Zhao et al were able to demonstrate increased PWV in 9 month old apoE$^{-/-}$ mice compared with WT controls, as well as lower wall shear stress, which is an important mediator of atherosclerosis development (50). This was the first study to demonstrate functional impairments in the apoE mice at less than 1 year of age, suggesting that perhaps with more sensitive techniques, small changes may be detected earlier on in the disease progression. ApoE$^{-/-}$ mice treated with Ang II, a potent vasoconstrictor, for 30 days showed increased atherosclerosis, aneurysm formation, heart weight-to-body weight ratio, blood pressure, and stiffness as assessed by PWV and Young's modulus of elasticity compared with untreated mice. The mice also showed increased collagen content and a decrease in elastin content with fragmentation in the elastic lamina (41). Conversely, Maizel et al found that WT and apoE$^{-/-}$ mice present similar cardiovascular abnormalities in response to chronic renal failure (CRF), aside from serum cholesterol levels. Mice were studied at 8, 14, and 18 weeks of age, and while CRF rapidly induced changes in aortic stiffness, left ventricular hypertrophy, and endothelial function, there were no strain differences observed (53).

Endothelium-dependent relaxation of aortic rings to ACh was not different between apoE$^{-/-}$ and controls at 4 months of age; however, at 13 months, the maximal response was significantly attenuated in the knockout mouse. There were no changes in endothelium-

independent relaxation to SNP, indicating that smooth muscle cells responses to NO remain intact (51). ApoE$^{-/-}$ mice treated with Ang II do demonstrate impaired endothelial-independent relaxation in response to SNP, but not endothelium-dependent relaxation to ACh (41).

A link between endothelial NO and atherosclerotic lesion development has also been established via treatment with the NOS inhibitor L-NAME (175). ApoE$^{-/-}$ mice (4 months old) showed an impaired basal endothelial NO-dependent contraction to the NOS inhibitor N$^{\omega}$-nitro-L-arginine (L-NNA) compared to controls. However, when treated with L-NAME, there was also significant inhibition in endothelium-dependent vasorelaxation to ACh and a significant acceleration in plaque formation compared to untreated control. Neither mean arterial pressure, nor dose-response curves to SNP were different among groups. Interestingly, treatment with L-arginine, an important substrate of NOS, did not provide any beneficial effects on vasoreactivity or atherosclerotic progression. apoE/eNOS double knockout mice have elevated blood pressure and increased atherosclerosis compared to apoE$^{-/-}$ mice (176), a finding which emphasizes the importance of endothelial NO in atherosclerosis development. Kuhlencordt et al found that eNOS deficiency not only augments atherosclerosis in apoE$^{-/-}$ mice, but also induces other cardiovascular complications including distal coronary arteriosclerosis, spontaneous aortic aneurysm, and left ventricular dysfunction (177).

Collectively, these studies demonstrate a complex interplay between atherosclerosis, nitric oxide, vascular reactivity, aging and arterial stiffness. Furthermore, various genetic and environmental factors regulate the pathogenesis of this disease and its downstream effects.

2.10 Aging

It is known that arterial stiffness, as measured by PWV, increases significantly with age in humans (19), and rats (119). However, it is unclear how arterial stiffness and function are

altered in the aging mouse. Understanding of the arterial aging process is important if the mouse is to be used as a model for investigation of mechanisms of large artery stiffness.

Reddy et al reported that aortic impedance, PWV, AIx, and pulse pressure all increased significantly in mice between the ages of 8 and 29 months in a similar manner to that in humans (39). Interestingly, there were no associated increases in mean pressure or blood flow velocity. Sindler and colleagues also found that mice between 4 to 6 months and 26 to 28 months old experience age-associated endothelial dysfunction, oxidative stress, inflammation, and increased stiffness (aortic PWV). Short term nitrite therapy in these mice could reverse these age-related changes such that they were not different to the younger group studied. This indicates a significant role for endothelial dysfunction in age-related stiffness (178). Conversely, PWV measured using MRI in the ascending and abdominal aorta in 2 and 8 month old WT mice showed no differences (49). Similarly, in 13 month old WT mice PWV was not statistically different from that in 4 month old mice. ApoE$^{-/-}$ mice from the same study did, however, experience increased PWV over the same time frame. Older apoE$^{-/-}$ mice also experience impaired endothelial-dependent relaxation, increased atherosclerotic plaque formation, and fragmentation of the elastic laminae. Mean and pulse pressure did not change in any of the groups (51). Both of these studies examine aging under a significantly smaller time frame than those previously discussed which likely accounts for the discrepancy.

2.11 Hypotheses and specific aims

2.11.1 Refining measurement of PWV in the mouse

The genetically modified mouse is a powerful tool which may be used to elucidate cellular and molecular mechanisms of arterial stiffness, and lead to the identification of novel therapeutic targets. In order to achieve this goal, an accurate, reproducible method of

obtaining PWV over a range of physiological pressures in the mouse is necessary. The specific aims (SAs) necessary to achieve this are outlined below.

SA1.1: To develop a reliable, high fidelity technique of measuring aortic PWV in the mouse. Aortic PWV has been explored in the mouse using several different techniques as discussed in Section 2.4.1. However, there are several problems associated with these techniques ranging from human error (Doppler) to high cost (MRI), or highly invasive surgical procedures. To overcome these errors, we aimed to use a high-fidelity dual pressure-sensing catheter to measure aortic PWV in the mouse.

SA1.2: To characterise the pressure dependency of arterial stiffness in the adult WT mouse. To the best of current knowledge, there is no complete characterization of pressure dependent PWV over pressure ranges encompassing both a hypotensive and hypertensive state in the mouse. This is critical in order to be able to make definitive statements regarding changes in elasticity when simultaneous changes in blood pressure are observed, as is often the case in physiological measurements.

It is thus of interest to characterise pressure dependent arterial stiffness in C57BL/6 wild type mice by transferring arterial stiffness measurement techniques established in rats to the mouse model. Post-mortem functional and structural analysis of the mouse aorta will also be performed. Collectively, these experiments will enable the characterisation of the mouse aorta in terms of both functional stiffness and morphological parameters.

2.11.2 Transglutaminase 2

Based upon the current understanding that NO produced by the endothelium inhibits TG2 externalization and subsequent activity via S-nitrosylation, the **hypothesis** that will be tested is as follows: increased TG2 extracellular matrix cross-linking activity, caused by a reduction

in NO bioavailability, directly increases large artery stiffness. Figure 5 depicts this. Two specific aims have been determined in order to achieve this goal.

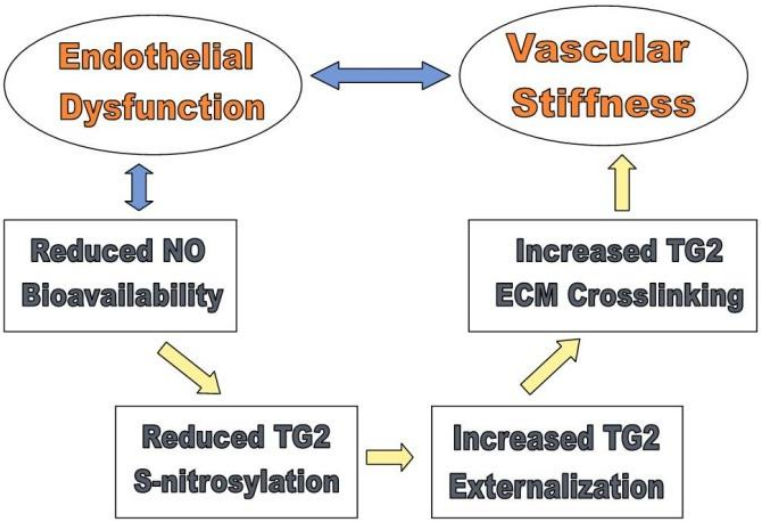

Figure 5: The hypothesized role of TG2 in regulating arterial stiffness.

SA2.1: To characterise the pressure dependency of arterial stiffness in the TG2$^{-/-}$ mouse. Based on the above hypothesis, increased TG2 activity likely contributes to increased vascular stiffness. In order to ascertain this, PWV in TG2$^{-/-}$ mice and WT littermate controls will be evaluated using the same pressure dependent arterial stiffness measurement and ex-vivo structural analysis techniques as developed to satisfy SA1.2.

SA2.2: To compare the pressure dependent arterial stiffness in WT and TG2$^{-/-}$ mice treated with a NOS inhibitor. The purpose of this aim is to clarify the pathway leading to increased TG2 activity. Inhibiting NOS has been shown to increase PWV. WT and TG2$^{-/-}$ mice will be treated with the NOS inhibitor, L-NAME. This will reduce the amount of NO derived from the endothelium of blood vessels, and establish if there is any link between NO, TG2, and arterial stiffness. It is suspected that TG2$^{-/-}$ mice treated with L-NAME will not develop increased PWV to the extent of WT mice.

2.11.3 Apolipoprotein E

The link between atherosclerosis and arterial stiffness is well documented in several species. As previously discussed, the apoE knockout mouse, which is a good model of human atherosclerosis, often demonstrates increased baseline PWV. Therefore, it is **hypothesized** that the pressure-dependent PWV curves in the apoE$^{-/-}$ mouse will be significantly higher than WT controls. Two specific aims have been defined in order to test this hypothesis.

SA3.1: To characterise the pressure dependency of arterial stiffness in the apoE$^{-/-}$ mouse. The severity of increased PWV in the apoE$^{-/-}$ varies between studies according to age and method. Results may also be skewed if concomitant increases in blood pressure are observed. In order to clarify the discrepancies that have been observed, it is necessary to obtain PWV over a range of physiological blood pressures.

SA3.2: To compare the pressure dependent arterial stiffness in WT and apoE$^{-/-}$ mice treated with a NOS inhibitor. While a correlation between atherosclerosis progression and endothelial dysfunction has been made in L-NAME treated apoE$^{-/-}$ mice, the pressure-dependent PWV has never been examined. Endothelial dysfunction, characterised by a reduced bioavilability of NO, is known to play a role in the development of atherosclerosis. Therefore it would be advantageous to investigate how NOS inhibition would potentially accelerate the hypothesized arterial stiffening in these mice.

2.11.4 Aging

The development of vascular stiffening in mice with age is not well defined. Since PWV generally increases with age in other species, it is **hypothesized** that the same trend in mice will be present. Since atherosclerosis exacerbates increased vascular stiffness, it was also hypothesized that apoE$^{-/-}$ mice would have significantly higher PWV than age matched controls with age.

SA4.1: To analyse pressure-dependent PWV in mice from 8-weeks to almost 50-weeks of age. While developing the invasive measurement technique in mice, PWV data was acquired in mice ranging from 8 weeks of age to 46 weeks of age. Analysis of this data will provide observations, for the first time, of the possible effects of early aging in the mouse. Few studies have explored how age affects vascular stiffness in the mouse, and none have provided pressure-dependent data. As age and blood pressure are the two most significant factors in determining PWV, it is critical to understand how they impact vascular function.

SA4.2: To compare the pressure dependent arterial stiffness in WT and apoE$^{-/-}$ mice at 12 and 36 weeks of age. It is still unclear as to when age-induced vascular stiffening occurs in the apoE$^{-/-}$ model, especially as the PWV-MAP relationship has never been explored using a high-fidelity technique. As atherosclerosis progression often occurs alongside arterial stiffening, it is important to understand when these changes begin to take place.

Chapter 3

Aortic pulse wave velocity measurement in the mouse: method development

Studies in rats conducted by our group and others have shown that the blood pressure dependent characteristics of arterial stiffness are useful in elucidating the arterial properties contributing to high blood pressure in different disease models (28, 29, 94, 179, 180). Aortic PWV, a measure of large arterial stiffness, offers an indication of the structural and functional characteristics of large arteries *in vivo*. A review of the literature shows that there is no complete characterization of pressure dependent PWV over pressure ranges encompassing both a hypotensive and hypertensive state in the mouse. The aim of this study was to develop a reliable, high fidelity method to characterise pressure dependent arterial stiffness in male WT mice using the knowledge gained in past studies of arterial stiffness measurement techniques in rats. This chapter outlines and assesses relevant PWV measurement techniques, stating the benefits and shortcomings, with the aim of proposing a standard, reliable technique for measuring pressure dependent PWV in the mouse aorta. It also investigates methods of acutely altering blood pressure, and the impact of those methods on mouse aortic PWV.

3.1 Housing and anaesthesia

In all procedures, mice were housed in the animal facility of Macquarie University with controlled light (12 hours light/dark cycle), temperature (21±2^{o} C) and standard chow and water *ad libitum*. All procedures and handling of animals were approved by the Animal Ethics Committee of Macquarie University, Sydney, Australia (ARA 2011/002, 2011/036). Hemodynamic measurements were made in anaesthetized mice. Anaesthesia was induced by placing mice in an induction chamber with 4.5% isoflurane. Once induced, mice were transferred to a thermoregulated heating pad and anaesthesia was maintained using between 1-2% isoflurane in 100% oxygen via a nose cone. Depth of anaesthesia was monitored throughout the surgery and levels of isoflurane were adjusted accordingly. Temperature was monitored and maintained at 37± 1 ^{o}C with a rectal probe and thermoregulated heating pad. Three electrodes were placed subcutaneously to provide the electrocardiogram (ECG) for calculation of heart rate (HR).

3.2 Calculation of PWV

PWV is calculated using the pulse transit time (TT) between two pressure, diameter, or flow waveforms at locations a known distance apart (Figure 6, Equation 3.1). TT can be calculated using a variety of techniques (181). The most robust technique is dependent upon the waveform shape. However, for short pulse durations with an acute waveform foot, such as in rodents, the peak of the second derivative provides a good marker of the waveform foot (29). Beat-to-beat TT can be determined from the foot of the proximal and distal pressure pulse using the peak of the second derivative.

$$PWV = distance / transit\ time \tag{3.1}$$

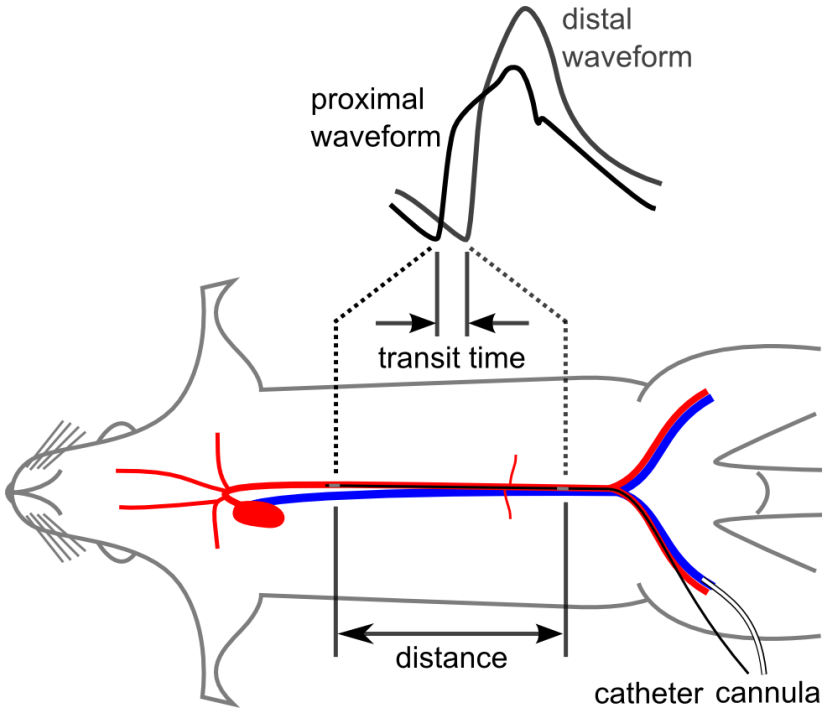

Figure 6: Surgical preparation to measure PWV in the rat. A dual pressure sensor catheter is positioned in the aorta via the femoral artery. Two simultaneously recorded pressure waveforms are measured by the two pressure transducers located a known distance apart. PWV is calculated by dividing this distance by the time it takes for the pressure wave to propagate down the aorta (Equation 3.1).

3.3 Assessment of PWV measurement techniques

Published studies investigating PWV in mice have used non-invasive techniques such as Doppler (41, 42, 45) or MRI (49, 50) and invasive techniques such as fluid filled pressure sensors (54), or extravascular techniques (51). With the exception of MRI measurement of PWV, these techniques were trialled, with the addition of the use of high-fidelity, solid state intravascular catheters.

At the onset of the initial experiments, the plan was simply to transfer the well-established surgical techniques used in rats (94, 179, 180) to mice, in exactly the same way, but on a much smaller scale. However, due to the small size and fragility of the vessels and the low blood volume in the mouse this was not a straightforward task. Following is a detailed description of the development of the method for measuring pressure-dependent aortic PWV.

3.3.1 PWV measurement using Doppler flow

Non-invasive Doppler measurements were made using a 10 MHz Doppler probe. It was placed right of the sternum at an angle which allowed recording of blood flow velocity in the aortic arch. A mark was made on the chest to indicate the measurement site. A second measurement was made by insonating the abdominal aorta at a distance of between 3 and 4 cm. PWV could then be calculated by dividing the distance between these two measurement locations by the difference in arrival times of the velocity pulse timed with respect to the ECG (Figure 7). The inaccuracies and error associated with Doppler measurements have been previously discussed in Section 2.4.1. Additionally, Doppler measurement still required catheterization of another artery in order to measure pressure, to obtain a pressure dependent measurement of PWV. Given the shortcomings of the technique, especially in inaccuracies in distance measurement, and given the need to record intravascular pressure, pressure based methods of PWV measurement were also investigated.

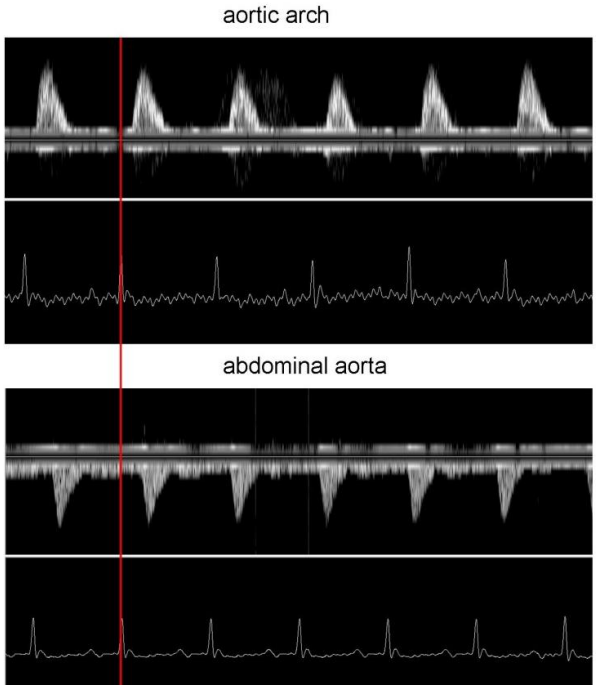

Figure 7: Doppler velocity signals from the aortic arch and the abdominal aorta in an anaesthetized mouse using a 2 mm diameter 20 MHz probe. The vertical red line corresponds to the R wave of the ECG and is used to measure velocity pulse arrival times for determination of PWV. The abdominal aortic flow waveform is inverted due to the direction that the vessel was insonated.

3.3.2 Use of fluid filled pressure catheters

The use of fluid filled pressure catheters was investigated briefly. A short, polyethylene fluid filled tube was introduced into the aortic arch via the carotid artery, and connected to a high-fidelity pressure transducer (SP 844, Memscap, Norway). A signal was obtained, but was highly damped and contained a large respiratory component. It may be that small adjustments, such as heating the saline fluid, and other methods to reduce gas in the fluid filled line, may improve the signal. However, any degree of damping is of a major concern in PWV measurement, where the transit time between sites 3 to 4 cm apart requires resolution in the millisecond range. Therefore, pressure measurement techniques not requiring fluid filled lines were investigated.

3.3.3 PWV measurement using an intravascular catheter and applanation tonometry

The method of Wang et al. (51) describes the use of applanation tonometry to measure a pressure signal, and thus PWV. The concept relies on an intravascular measure of mean arterial pressure (MAP) in the aortic arch, with an extravascular measurement of pressure in the abdominal aorta (Figure 8). The extravascular measurement is via applanation of the external surface of the aorta using a pressure transducer. It is important to note that a calibrated pressure reading from the distal site is not actually necessary as it is only a clearly defined foot that is required for PWV measurement. Consequently, pressure-dependent PWV can in fact be obtained using pressure from the proximal, intravascular catheter.

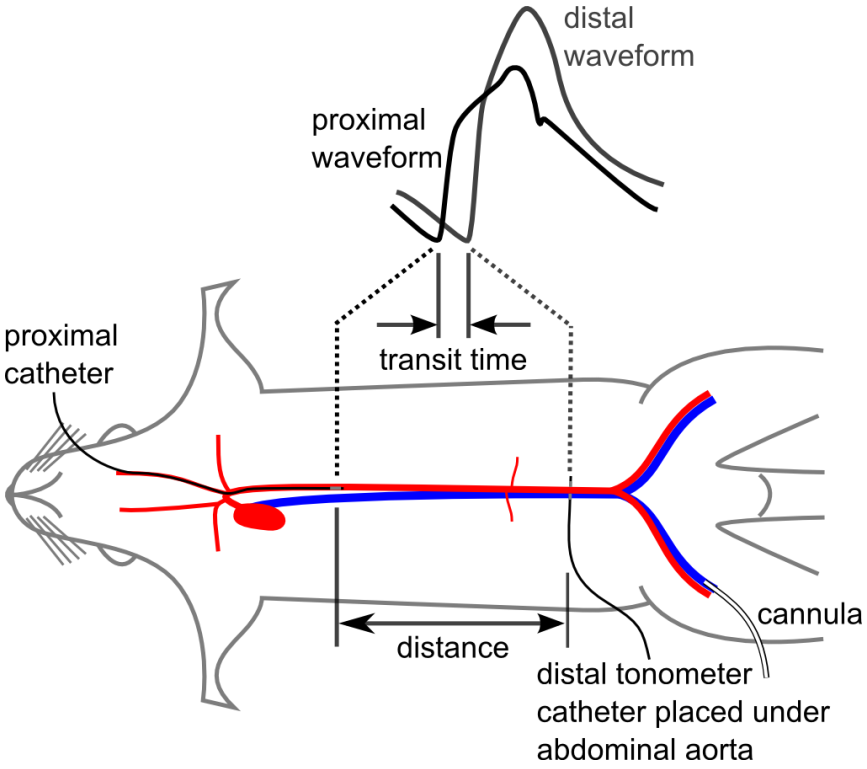

Figure 8: Schematic of the method employed by Wang et al (51) where the proximal sensor is placed in the aortic arch via the carotid artery. Applanation of the abdominal aorta to obtain the distal signal was via a pressure sensor placed either beneath, or held upon the abdominal aorta.

Two tonometry based techniques were investigated. In both cases, the proximal, aortic arch pressure was obtained using an intravascular high-fidelity pressure sensor introduced via the carotid artery. The abdominal aorta was exposed by surgical cut down through the abdomen, and applanated via either *(i)* the ventral surface using a tonometer built into a pen-like body or *(ii)* the dorsal surface using a catheter (Figure 9).

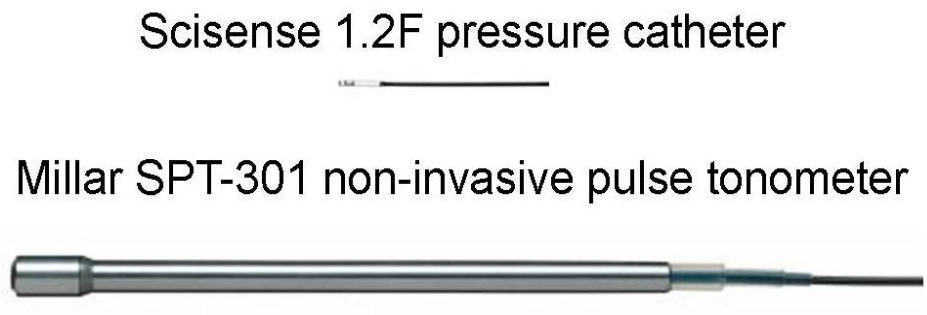

Figure 9: Devices used to record distal tonometric pressure. Although not exactly to scale, the image offers the reader an indication of the relative sizes of the two measuring devices.

The first method involved the positioning of a tonometer (SPT-301, Millar, Figure 9) on the ventral surface of the abdominal aorta using a micromanipulator arm to permit more precise control of the applanation pressure. Figure 10 provides a sample of the acquired data. There was a relatively large degree of noise in the tonometer's signal. The peaks of the second derivative were not highly distinguished and therefore may introduce error in the calculation of PWV. Additionally, due to the physical size of the housing of the tonometer, positioning (and maintaining the position) of it was troublesome.

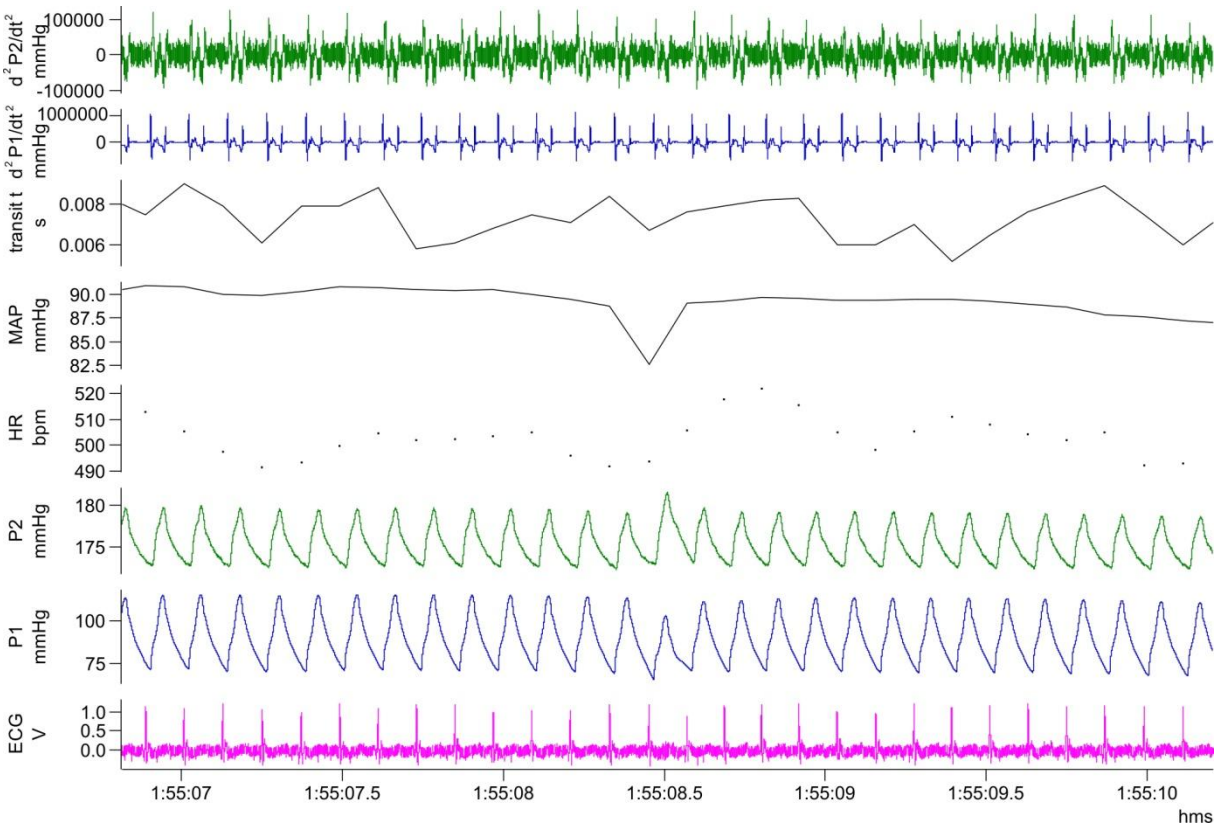

Figure 10: Spike trace showing (from bottom to top) the ECG, proximal pressure P1 (intravascular pressure), distal pressure P2 (extravascular pressure), HR, MAP, TT, 2nd derivative of proximal pressure, and 2nd derivative of distal pressure. The second derivative of distal pressure does not yield well-defined peaks which may introduce errors into TT determination.

The method of Wang et al (51) was replicated by placing a 1.2F pressure catheter (Scisense, Canada, Figure 9) under and against the dorsal surface of the abdominal aorta. The applanation pressure was reliant on the surrounding tissue holding the catheter in place. A waveform was obtained (Figure 11); however, the sensor was prone to movement with

respiration and peristaltic motion of the gut upon which it rested. Respiration especially gave an artefact that interfered with pressure waveform foot.

The two tonometry methods required highly invasive surgery, including a large displacement of the gastrointestinal tract. In such a small animal, a more minimally invasive approach would be optimal. In addition, applanation of the artery may affect the local geometry and therefore hemodynamics in the aorta.

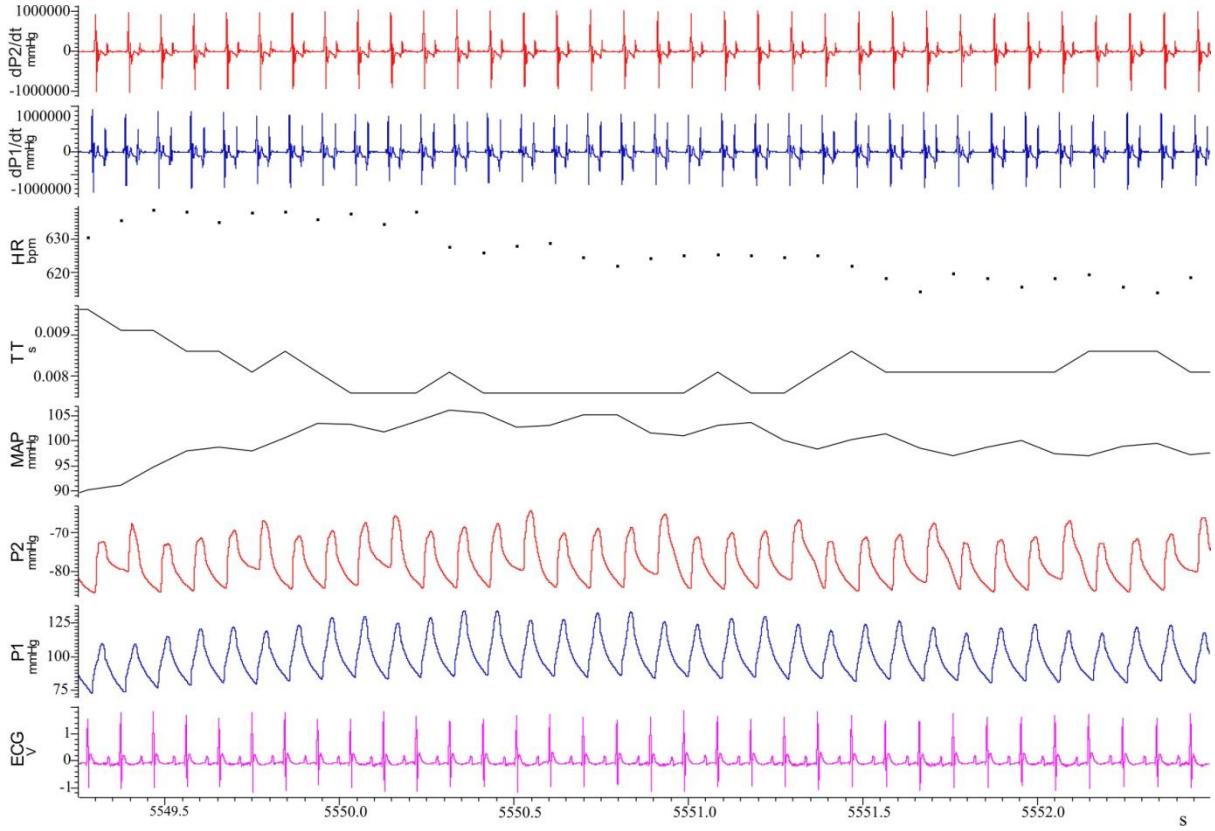

Figure 11: Spike trace of data acquired using an intravascular and an extravascular catheter. From the bottom up: ECG signal, proximal pressure, distal pressure, MAP, TT, HR, second derivative of P1, and second derivative of P2. Clearly defined feet can be determined from the peaks of the second derivatives.

Nevertheless, this method actually produced results that were not significantly different to the final method outlined below. A detailed description of this surgical technique, as well as a comparison of the pressure-dependent PWV obtained using this technique versus the final technique can be found in Appendix A1.

3.3.4 Intra-vascular pressure measurement of PWV

With a high degree of surgical experience in the mouse, cannulation of the femoral artery was possible. The method described in this section was the most accurate method of PWV measurement due to the high fidelity acquisition of pressure waves and precise setting of the distance. It was used to obtain all *in vivo* PWV data presented in the thesis hereafter.

A 1.2 F dual sensor catheter with 2 high fidelity pressure sensors set 3cm apart was introduced into the descending aorta via the right femoral artery such that one sensor was positioned in the descending portion of the aortic arch, resulting in the other sensor being 3 cm distal in the abdominal aorta. Signals were sampled at 2 kHz using a CED 1401 data acquisition unit with Spike2 analysis software (CED, Cambridge). A photograph of the surgical preparation is shown in Figure 12. Figure 13 shows a small segment of the data collected with this method and how TT and ultimately PWV are determined.

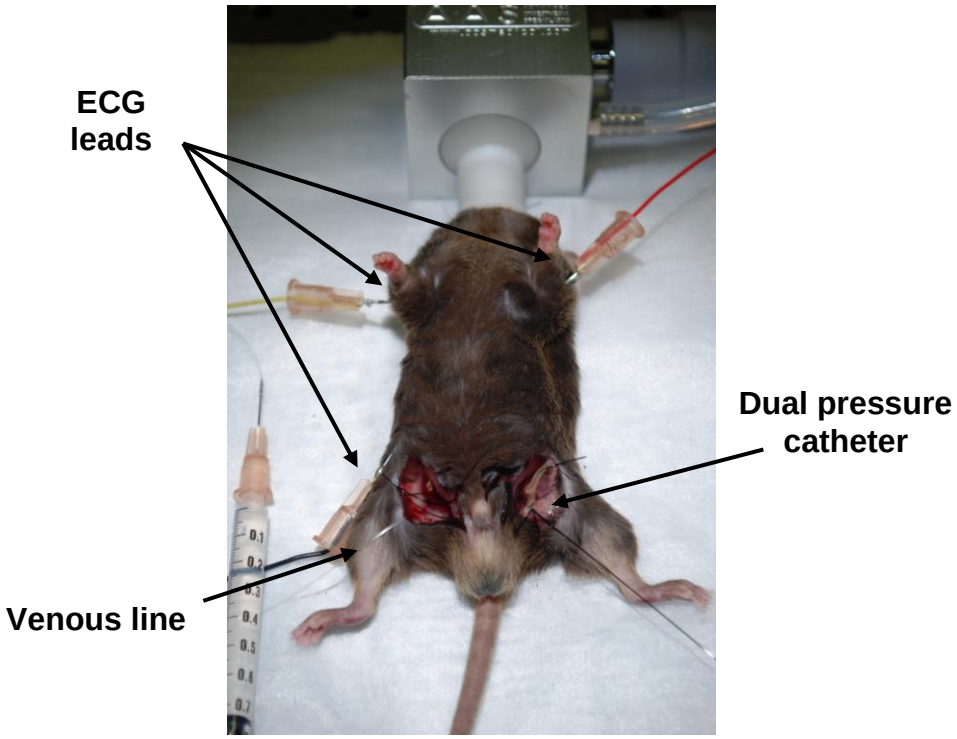

Figure 12: Photograph showing the surgical preparation for measurement of PWV in the mouse. The face is completely covered by a nose cone delivering a continuous flow of isoflurane anaesthesia. The 3 ECG leads are positioned subcutaneously at the two forelimbs and one rear hind limb. The dual pressure catheter is inserted into the aorta via the right femoral artery. A polyethylene cannula is positioned in the left femoral vein for fluids administration.

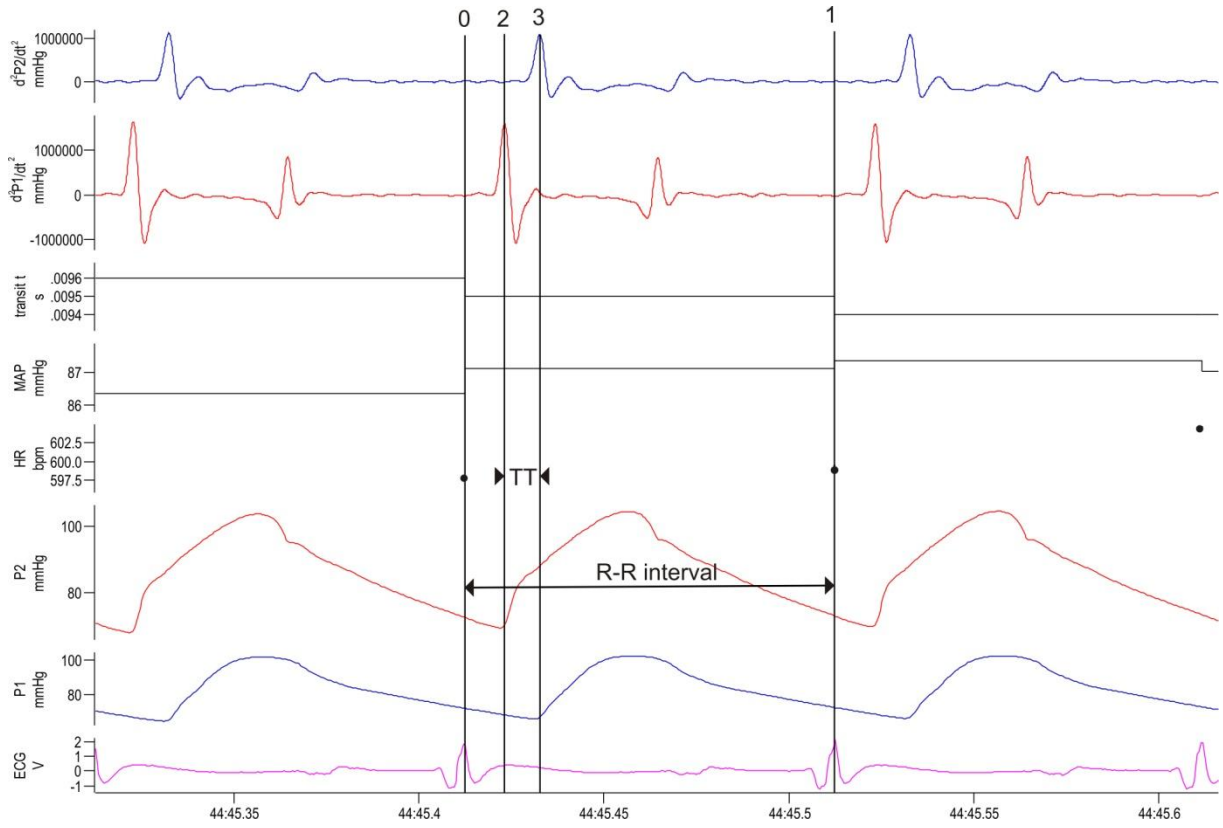

Figure 13: Example recording demonstrating how TT was obtained on a beat-to-beat basis within the Spike software using custom scripts. Cursors '0' and '1' are set up to detect the R-wave of the ECG signal. Within this boundary, cursors '2' and '3' detect the feet of the proximal and distal pressure waves by locating the peak of their second derivative. TT is then calculated as the time difference between cursors '3' and '2' and PWV calculated using Equation 3.1 (distance = 3 cm). Shown on this trace from bottom to top is the ECG, distal blood pressure, proximal blood pressure, HR derived from the ECG, MAP from the proximal signal, TT, the second derivative of the proximal pressure, and the second derivative of the distal pressure.

3.4 Vasoactive control of blood pressure

The left femoral vein was exposed and a polyethylene cannula (0.20 mm/0.50 mm, inner/outer diameter) was inserted to allow intravenous administration of fluids or blood-pressure-altering drugs. Sometimes, due to the small size and thin nature of the venous walls, the femoral vein could not be cannulated. In these cases, the left jugular vein was used instead.

Arterial blood pressure was allowed to stabilize and then phenylephrine (PE, 100 μg/mL) was infused at a rate of 0.1 ml/min to increase blood pressure until it reached a plateau. The infusion was then stopped and pressure was allowed to return to baseline (Figure 14). Once

blood pressure was again stable, sodium nitroprusside (SNP, 100 µg/mL) was infused to decrease blood pressure and pressure was allowed to return to normal in the same manner (Figure 15).

At the end of each experiment, mice were euthanized with an infusion of potassium chloride. Immediately following this, the hearts were excised and the left ventricles (LVs) were isolated and weighed.

Figure 16 depicts a sample PWV-MAP curve obtained from a single mouse. It includes data collected during infusions as well as the return to baseline once infusions were stopped. It also demonstrates that both values of blood pressure and PWV are the same at baseline as well as during saline infusion.

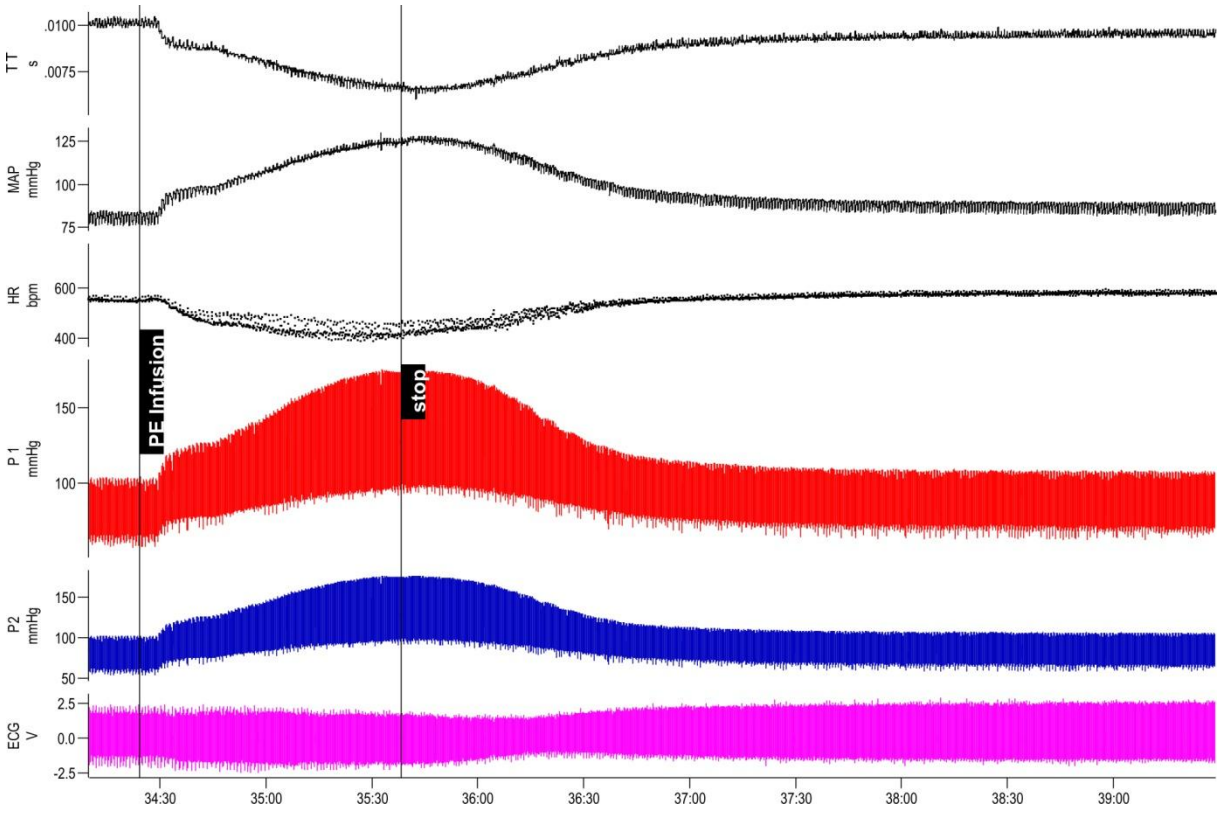

Figure 14: Spike trace during a PE infusion and the following return to baseline values. From bottom to top: ECG, distal pressure (P1), proximal pressure (P2), HR, MAP, and TT. As pressure increases, HR and TT both drop, and slowly rise to baseline as pressure decreases.

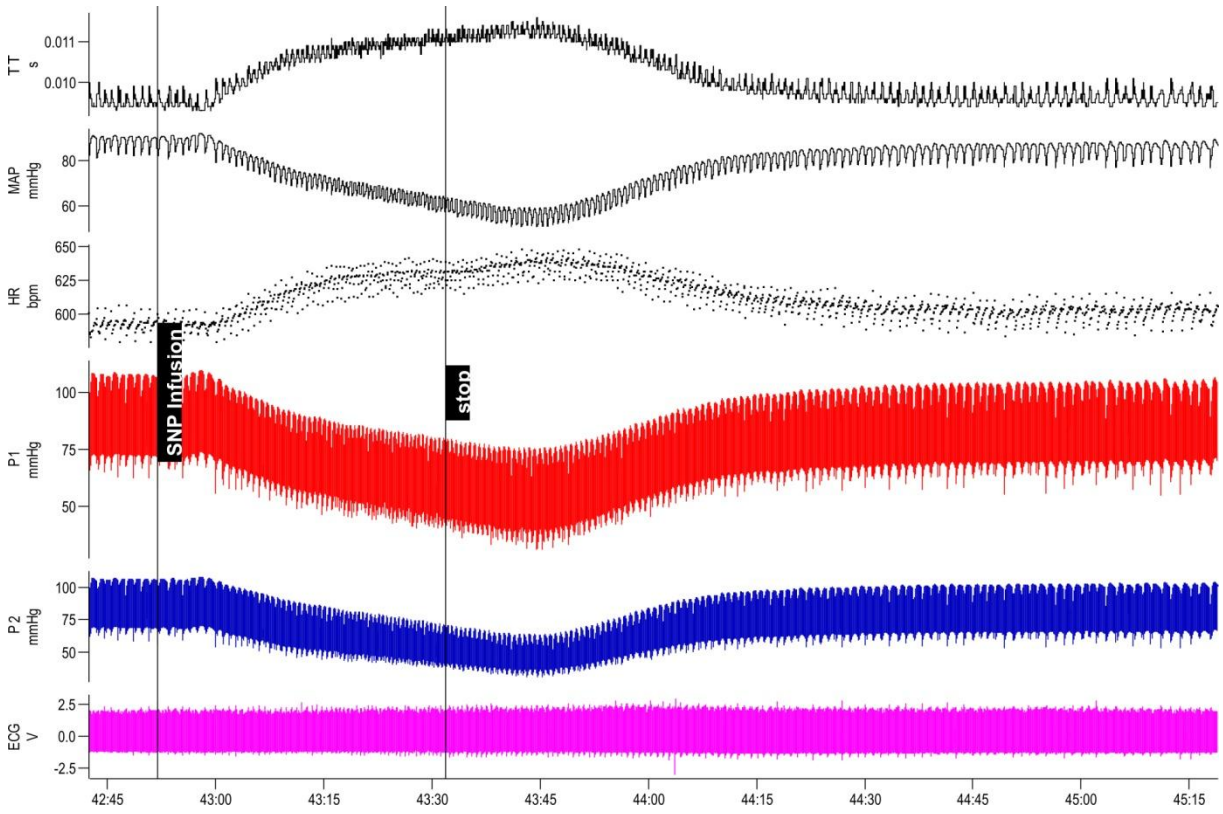

Figure 15: Spike trace during an SNP infusion and the following return to baseline values. From bottom to top: ECG, distal pressure (P1), proximal pressure (P2), HR, MAP, and TT. In this case, as pressure decreases, HR and TT increase.

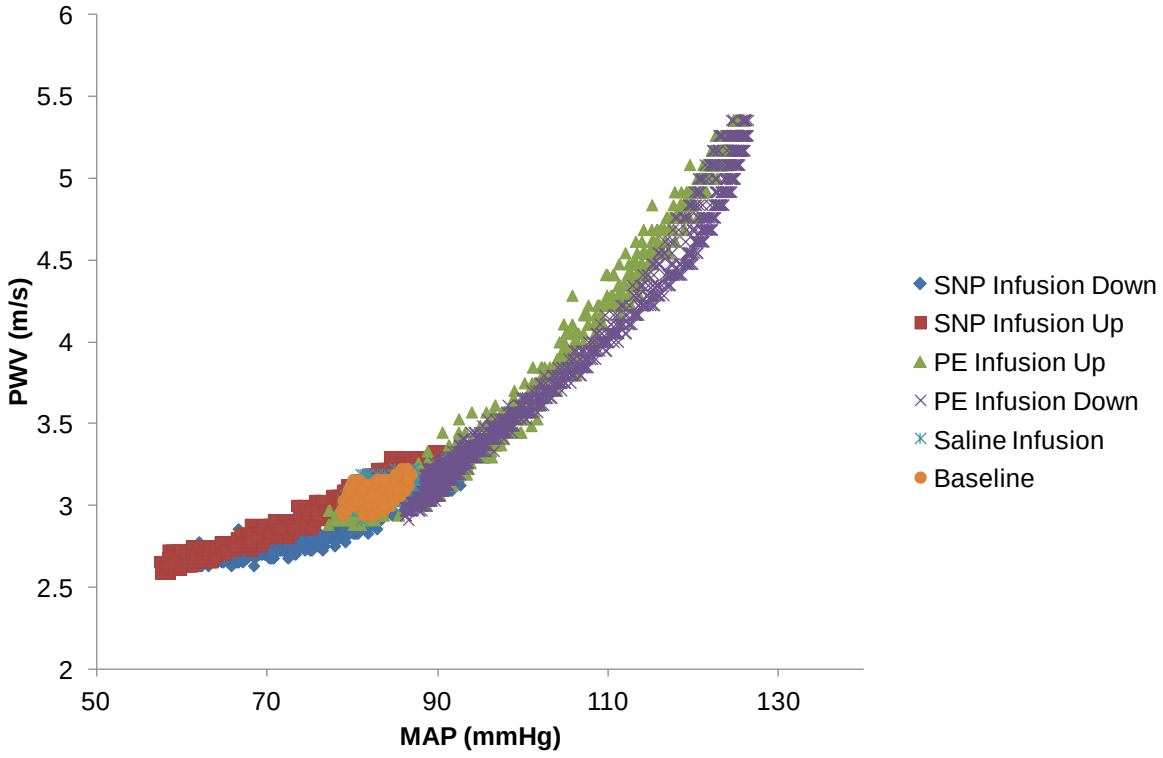

Figure 16: Sample plot of the PWV-MAP relationship from a single mouse.

3.5 Altering blood pressure: Effect of SNP on the mouse aortic PWV

PE is an adrenergic α_1-receptor agonist that causes vasoconstriction, and an increase in blood pressure. SNP is an exogenous nitric oxide donor, causing smooth muscle cell relaxation and a decrease in blood pressure. Both of these drugs therefore have the potential to act upon the cells in the aorta causing intrinsic effects on the local arterial stiffness, aside from those induced by the change in mean arterial pressure. While it is assumed that the blood pressure-altering effects of these drugs are mediated primarily through the periphery, the aim of this experiment was to provide data to support this assumption, by comparing PWV obtained over a range of blood pressures induced passively (by occluding the vena cava) and actively (by infusion of SNP). Our group has generated data to support this assumption previously in the rat model (29, 182) as discussed in Appendix A2, but it has not been done thus far in the mouse.

3.5.1 Methods

3.5.1.1 Animals

Female SJL mice aged 12 to 16 weeks (n=4) were subject to housing, ethics and anaesthesia as described in Section 3.2. Aortic pulse wave velocity was measured using a dual pressure sensor catheter introduced into the descending aorta via the femoral artery, as outlined in Section 3.3.4.

3.5.1.2 Infusion rates and venous return

To determine whether venous infusion at a rate of 0.1 mL/min significantly affects venous return and thereby cardiac output and MAP, saline was infused at the same rate and signals were acquired during this infusion.

3.5.1.3 Active and passive lowering of blood pressure

The abdomen was opened and a section of the vena cava was isolated. A suture was placed around it which was then used to partially occlude the vena cava in order to lower blood pressure passively through reduction of venous return. The suture was released and pressure was allowed to return back to baseline. Following this, pressure was reduced actively via infusion of SNP as previously described. Signals were continuously recorded across all pressure ranges.

3.5.1.4 Data and statistical analysis

Using the R-R interval from the ECG signal, each parameter (heart rate (HR), mean arterial pressure (MAP), systolic blood pressure (SBP), diastolic blood pressure (DBP), pulse pressure (PP), maximum of the first time derivative of pressure (Max dP/dt), TT, PWV, and pulse pressure amplification (PPA)) were measured and analysed for each heart beat.

Data are presented as mean ± standard error, except where otherwise indicated. Data were analysed offline using a combination of Microsoft Excel, IBM SPSS Statistics 19, and GraphPad Prism 6.

Data recorded across all pressure ranges were divided into 5 mmHg pressure bins. Statistical differences between groups were determined using either: paired Student's t-tests for each pressure bin, 2-way ANOVA (with repeated measures where data allowed) followed by various post-hoc tests. This is detailed in the results sections. P-values less than 0.05 were considered to be statistically significant.

3.5.2 Results

3.5.2.1 Infusion rates and venous return

For each mouse, HR, MAP, PP and PWV were compared using a paired t-test between baseline values and during a saline infusion. No significant difference was detected between

the two states (Table 2). This indicates that the rate of infusion used (0.1 mL/min) does not significantly affect cardiac output to an extent that induces MAP changes.

Table 2: Comparison between baseline values for HR, MAP, PP, and PWV between baseline and during saline infusion at 0.1 ml/min. Data are shown as mean ± SD.

	Baseline	**Saline Infusion**	**p-value**
HR (bpm)	500 ± 32	518 ± 24	0.19
MAP (mmHg)	93 ± 8	89 ± 4	0.24
PP (mmHg)	33 ± 4	31 ± 3	0.31
PWV (ms)	2.99 ± 0.13	3.08 ± 0.21	0.34

3.5.2.2 Vasoactive control of blood pressure: Directional dependence in the PWV-MAP relationship

It has been anecdotally observed that the PWV-MAP relationship demonstrates a directional dependence; i.e., PWV is higher at the same MAP when pressure is rising than when it is falling. In order to investigate this, the pressure-dependent PWV was compared between values acquired while pressure was increasing and decreasing. This was done for pressure changes induced by both PE and SNP (Figure 17 and Figure 18). A directional dependence was confirmed for both PE and SNP.

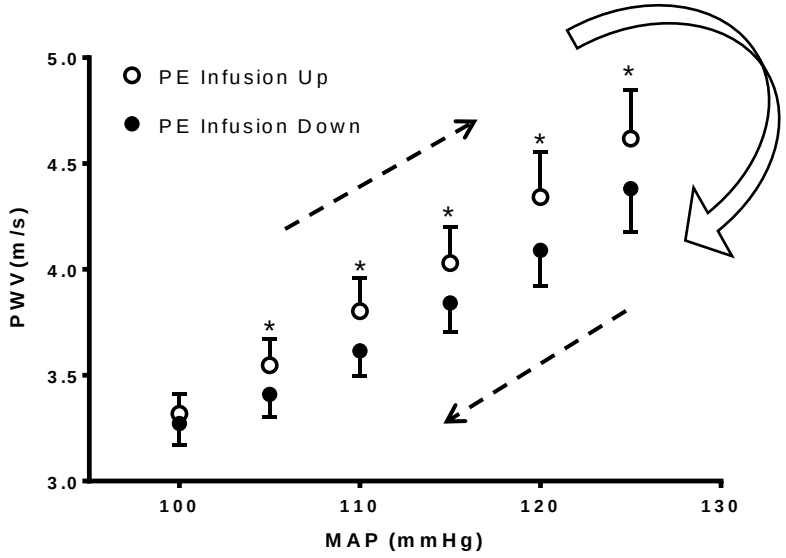

Figure 17: The directional dependence of PWV on MAP for a pressure range of 100 – 125 mmHg. This pressure range was achieved by PE infusion. Data was analysed using two-way ANOVA with repeated measures in both directions followed by Sidak's multiple comparisons test. The two factors were pressure and direction of pressure change (i.e. up or down). The analysis showed that pressure, direction of pressure change, and the interaction between the two factors was significant. *p<0.05.

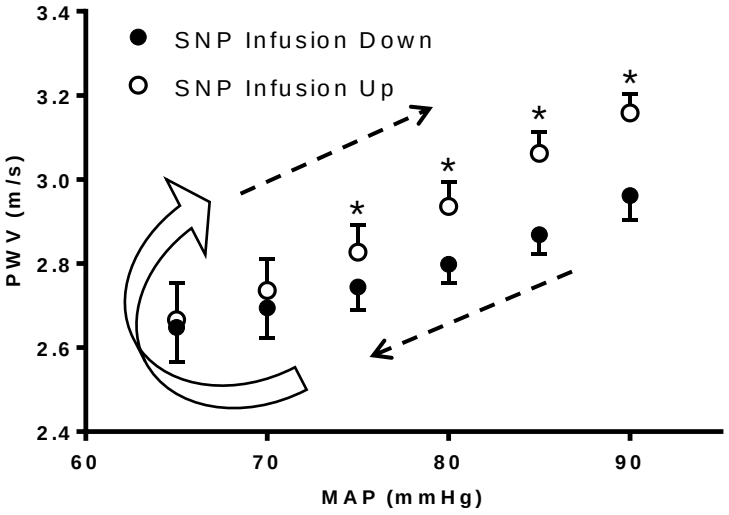

Figure 18: The directional dependence of PWV on MAP for a pressure range of 65 – 90 mmHg. This pressure range was achieved by SNP infusion. Data were analysed using two-way ANOVA with repeated measures in both directions followed by Sidak's multiple comparisons test. The two factors were pressure and direction of pressure change (i.e. up or down). The analysis showed that pressure, direction of pressure change, and the interaction between the two factors was significant. *p<0.05.

The directional dependence was also investigated using an area under the curve (AUC) approach. For each mouse, the AUC of the PWV-MAP relationship was calculated for the pressure range of 100 – 125 mmHg while pressure was increasing during a PE infusion and compared to the AUC while pressure was decreasing back to baseline using a paired t-test. The AUC was significantly greater for the "up" part of the infusion than the "down" part ($p<0.05$, Table 3). The same analysis was also performed for the pressure range of 65 – 90mmHg while pressure was decreasing during an SNP infusion and compared to the AUC while pressure was returning back to baseline. The AUC was also significantly greater for the "up" part of the infusion than the "down" part ($p<0.001$, Table 3).

Table 3: AUC of the PWV-MAP relationship. It can be seen that the AUC is significantly greater while pressure is increasing as compared to decreasing for both PE and SNP infusions. Units are m·s-1·mmHg.

	Up	**Down**	**p-value**
PE	98 ± 4	94 ± 3	0.03
SNP	72 ± 2	70 ± 1	<0.001

3.5.2.3 Comparison of passive and active pressure changes

The average body weight (BW) and age of the 4 SJL mice was 21 g and 10 weeks old. The resting parameters for these mice are shown in Table 4.

Table 4: Baseline cardiovascular parameters for the SJL mice.

	Mean ± SD
HR (bpm)	390 ± 50
MAP (mmHg)	76 ± 5
SBP (mmHg)	93 ± 8
DBP (mmHg)	60 ± 7
PP (mmHg)	33 ± 3
Max dP/dt (mmHg·s^{-1})	728 ± 181
PWV (m/s)	2.74 ± 0.17

Figure 19 shows the PWV-MAP relationship during both active and passive blood pressure lowering. Data points are obtained while pressure is returning back to baseline post-venous occlusion or SNP Infusion. Given that there was no statistical difference in PWV at any MAP between the two methods, it can be stated that the method of lowering blood pressure did not affect the PWV measurements.

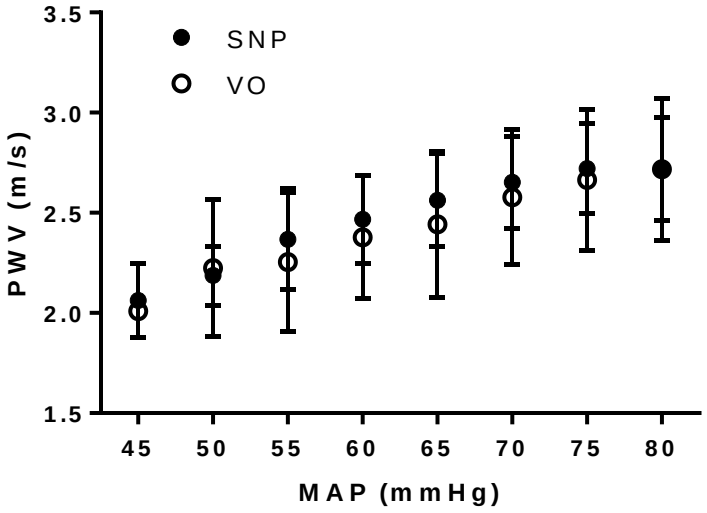

Figure 19: PWV-MAP relationship measured for both SNP infusion (SNP) and reduced venous return via occlusion of the vena cava (VO). While PWV changes with pressure induced by both reduced venous return and SNP infusion, there were no significant differences between the two methods of lowering MAP.

3.6 Discussion

Although measurement of PWV is not an overly complex surgical procedure, there are many challenges that arise when attempting to perform these measurements in mice due to their small size. They have a very small blood volume, which means that there is little room for error or blood loss during surgery. There is a smaller window of anaesthetic dosage than for larger animals. Micro-particles or small air bubbles during venous infusions can pose significant problems, and small animals are quite sensitive to temperature changes. Most importantly for this work, the vessels are much smaller, which make them extremely difficult to cannulate. The thin vessel walls tear easily. These challenges can be overcome with

experience; however, even with this experience, more invasive approaches provide a greater physiological challenge to the animal and could confound hemodynamic results. Therefore, a method for PWV measurement should ideally be both highly accurate, but also minimally invasive.

A range of methods of PWV measurement, both non-invasive and invasive, were trialled. Doppler measurements have the advantage of being non-invasive and simple to perform; however, there are significant inaccuracies associated with measuring the distance between the two measurement points. And in order to obtain pressure-dependent PWV, one of the arteries would require cannulation. Using fluid filled sensors did not provide very high-fidelity signals, requires two separate cannulations, and there is also error associated with measuring the distance between the two measurement sites. The use of extravascular tonometry to provide a distal pressure foot provided fairly reasonable results; however, it was highly invasive and it was quite difficult to obtain consistent, clear signals. There were also challenges with obtaining an accurate measure of distance as the tonometer must be removed in order to access the aorta for measurement and the pressure sensor is subject to movement as the gut is being moved aside in order to access the aorta. As a result, the use of a high-fidelity dual pressure catheter provided solutions to these problems. It is minimally invasive as the access point is the femoral artery. It provides high-quality signals with a high resolution. Finally, the distance between the two sensors is fixed, which eliminates any distance measurement error.

The overall aim of this chapter was to establish a robust technique for measuring pressure-dependent PWV in the mouse aorta. This was accomplished by placing a 1.2F high fidelity dual pressure transducer into the descending aorta via the femoral artery. Blood pressure-altering drugs (PE and SNP) were then used to acquire PWV over a range of physiological blood pressures.

In order to determine if the rate of infusion affected venous return, and thereby PWV, various parameters were compared at baseline values and during saline infusion. No significant differences between these two conditions were detected, indicating that the infusion itself did not significantly affect the hemodynamics in the aorta.

As previously mentioned, a directional dependence of PWV has been observed in rats (183). This study also confirms the presence of this phenomenon in the mouse. Whether pressure was being altered by PE or SNP, PWV was higher when rising compared to falling. It is uncertain as to why this occurs; however, there is likely an interaction between the mechanical and viscoelastic properties of the arteries which determine the level of directional dependence observed in the PWV-MAP relationship. There may also be a direct action of PE and SNP on the aorta itself, causing vasoconstriction at higher concentrations of PE (upward direction) and vasodilation at higher concentrations of SNP (downward direction).

Hysteresis has been observed in the pressure-diameter relationships of barosensory vessels in various species (184-187). Lenard et al observed that within a pulse interval, carotid artery diameters are larger at any given pressure when pressure is falling than when pressure is rising (188). This type of pattern is also observed in the baroreflex, such that heart rate responses to alterations in blood pressure depend on the direction of the pressure change. Specifically, HR is lower while BP is decreasing and higher which it is increasing (189).

It is generally thought that the baroreflex hysteresis is derived primarily from the viscoelastic nature of vessels (185, 190). However, it has been demonstrated that in addition to the mechanics of the vascular wall, neural aspects related to the transduction of stretch leading to a change in heart rate also contribute to baroreflex hysteresis. It has been demonstrated by our group that increases in HR are associated with increases in PWV (179). Further, due to the viscoelastic nature of the vessel wall, its mechanical properties, and thus its ability to stretch

and recoil, are frequency dependent. Therefore, perhaps the differences in HR that are seen when pressure is rising versus falling contribute to the differences observed in PWV.

Another possible factor may be the role of sympathetic regulation of smooth muscle tone in the aorta. Information relayed to the brain as pressure is raised or lowered may result in changes that differentially affect the mechanical properties of the vessel wall such as diameter or distensibility. On this note, it is also important to consider the possibility of smooth muscle cell activation during the infusions.

In this study, while hysteresis in the PWV-MAP relationship was always observed, the extent was highly variable between animals. Studinger et al also noted inconsistencies in baroreflex hysteresis patterns and suggested that other factors may affect hysteresis, such as changes in sympathetic activity or stroke volume during drug infusion (191).

Further work is needed to elucidate the components contributing to the observed hysteresis in the PWV-MAP curves. Observations suggest that there is a dynamic and complex interplay between the baroreflex, the mechanical properties of the arteries, and both sympathetic and vagal neural components. This information may be useful in understanding altered vascular responses in hypertension and cardiovascular disease.

A limitation to the study is that vasoactive drugs are used to alter the blood pressure and this could potentially influence the local arterial stiffness aside from its effect on pressure through modulation of aortic smooth muscle tone. In an attempt to mitigate this, the data used to measure pressure-dependent PWV is taken after the infusions are completed and pressure is returning back to baseline. To further address this issue, a reduction in blood pressure similar to that achieved using SNP was caused by lowering stroke volume with venous occlusion, and no significant difference was found in stiffness between the two circumstances. As such, it can be assumed that the pressure changes produced by SNP infusions are due to peripheral or cardiac effects, and not due to local changes in aortic stiffness. Passively increasing blood

pressure in order to confirm these results during PE infusion could not be achieved. Although it is highly likely that PE is primarily acting in the periphery and not the large arteries, it would be very advantageous to design an experiment which could achieve this in the future. As shown in Appendix A2, results from rats indicate that both PE and SNP infusions do not significantly affect aortic smooth muscle tone, supporting the assumption that the pressure-dependent changes in PWV are mediated primarily through effects on total peripheral resistance (182). However, it is important to note that it has been suggested previously that in elastic arteries, during the rise in BP due to PE infusion, drug-induced passive wall stretch likely dominates over any possible drug-induced smooth muscle contraction (185).

In conclusion, a reliable and repeatable method for accurately measuring pressure-dependent PWV in the mouse aorta was developed and trialled successfully.

Chapter 4

Characterisation of pressure dependency of aortic PWV in the mouse

4.1 Introduction

Due to the structure and composition of the arterial wall, PWV depends on the location and pressure at which it is measured. Aortic stiffness sensitivity to changes in MAP can be assessed in the mouse with high-fidelity pressure sensors to measure PWV, and inducing changes in MAP using intravenous infusions of blood-pressure altering drugs. However, it is also known that there are other factors which may influence PWV. This chapter describes the characterization of these factors in the mouse aorta.

4.2 Methods

4.2.1 Animals

Male C57Bl6 mice (n=6, Animal Resource Centre, Perth), 12 weeks of age were kept in a temperature controlled environment (21 ± 2^{o}C) with 12 hour light/dark cycles. Animals had *ad libitum* access to standard laboratory mouse feed and water. The animal protocol was approved by the Macquarie University Animal Ethics Committee (ARA 2011/002).

4.2.2 Incremental stiffness along the length of the mouse aorta

Mice were anaesthetized and surgically prepared as described in Sections 3.1 and 3.3.4. The dual pressure catheter was introduced into the abdominal aorta via the femoral artery and advanced until the pressure waveform was typical of the aortic arch (Figure 20). The catheter was withdrawn 0.5 cm and pressure was recorded. The catheter was withdrawn in 0.5 cm increments until the signal from the proximal sensor was lost, indicating that it was no longer in the aorta.

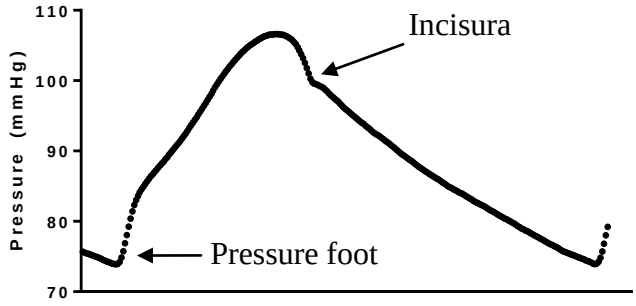

Figure 20: An example of a pressure waveform recorded from the aortic arch using a high-fidelity pressure catheter. Catheters are capable of measuring high frequency components, such as the incisura, which is shown in this figure. High frequency components are important in TT measurement.

The TT was calculated between the R-peak of the ECG and the foot of the pressure waveform at each of the recording sites along the length of the aorta. PWV was then calculated by dividing the change in distance between the initial placement of the catheter and the amount by which it was withdrawn, by the change in TT (measured from the ECG) between those two points.

4.2.3 Pressure dependent PWV relationship

Pressure was allowed to stabilize and then PE (100 μg/mL) was infused at a rate of 0.1 mL per/min to increase blood pressure until it reached a plateau. The infusion was then stopped

and pressure was allowed to return to baseline. Once stable, SNP (100 μg/mL) was infused to decrease blood pressure and pressure allowed to return to normal in the same manner.

4.2.4 Cardiovascular parameters predictive of dynamic changes in PWV

It is known that there are other factors besides MAP which influence PWV. To further elucidate some of these factors in the mouse model, PWV, MAP, PP, form factor (4.1), maximum slope of pressure, and R to R interval from the ECG were calculated for each individual pulse. These variables, along with the direction of pressure change (up=1, down=0) were entered into a stepwise linear regression model (dependent variable: PWV).

$$form\ factor = \frac{MAP - DP}{PP} \tag{4.1}$$

4.2.5 Data and statistical analysis

Data are presented as mean ± standard error, except where indicated. Data were analysed offline using a combination of Microsoft Excel, IBM SPSS Statistics 19, and GraphPad Prism 6.

Data recorded across all pressure ranges were divided into 5 mmHg pressure bins. Statistical differences between groups were determined using either: paired Student's t-tests or 1-way ANOVA followed by various post-hoc tests. This is detailed in the results sections. P-values less than 0.05 were considered to be statistically significant.

4.3 Results

The dual pressure sensor was successfully positioned in the aorta via the femoral artery. Both proximal and distal waveforms could be recorded with feet that could accurately be detected

to give PWV. The 6 male C57Bl6 mice had an average weight of 26 ± 2g. The other baseline parameters, measured under isoflurane anaesthesia are outlined in Table 5.

Table 5: Baseline cardiovascular characteristics

	Mean ± SD
HR (bpm)	500 ± 13
MAP (mmHg)	93 ± 3
SBP (mmHg)	111 ± 4
DBP (mmHg)	77 ± 3
PP (mmHg)	33 ± 2
Max dP/dt (mmHg·s^{-1})	862 ± 48
PWV (m/s)	3.08 ± 0.09
LV/BW (mg/g)	351 ± 8

4.3.1 Incremental stiffness along the length of the mouse aorta

Figure 21 shows representative waveforms at each location along the mouse aorta. MAP was not significantly different at any distance along the aorta (Figure 22), although there was a slight decreasing trend. Interestingly, PWV also did not significantly differ at any point along the length of the aorta; however, a similar trend in this data to the MAP can be observed (Figure 23).

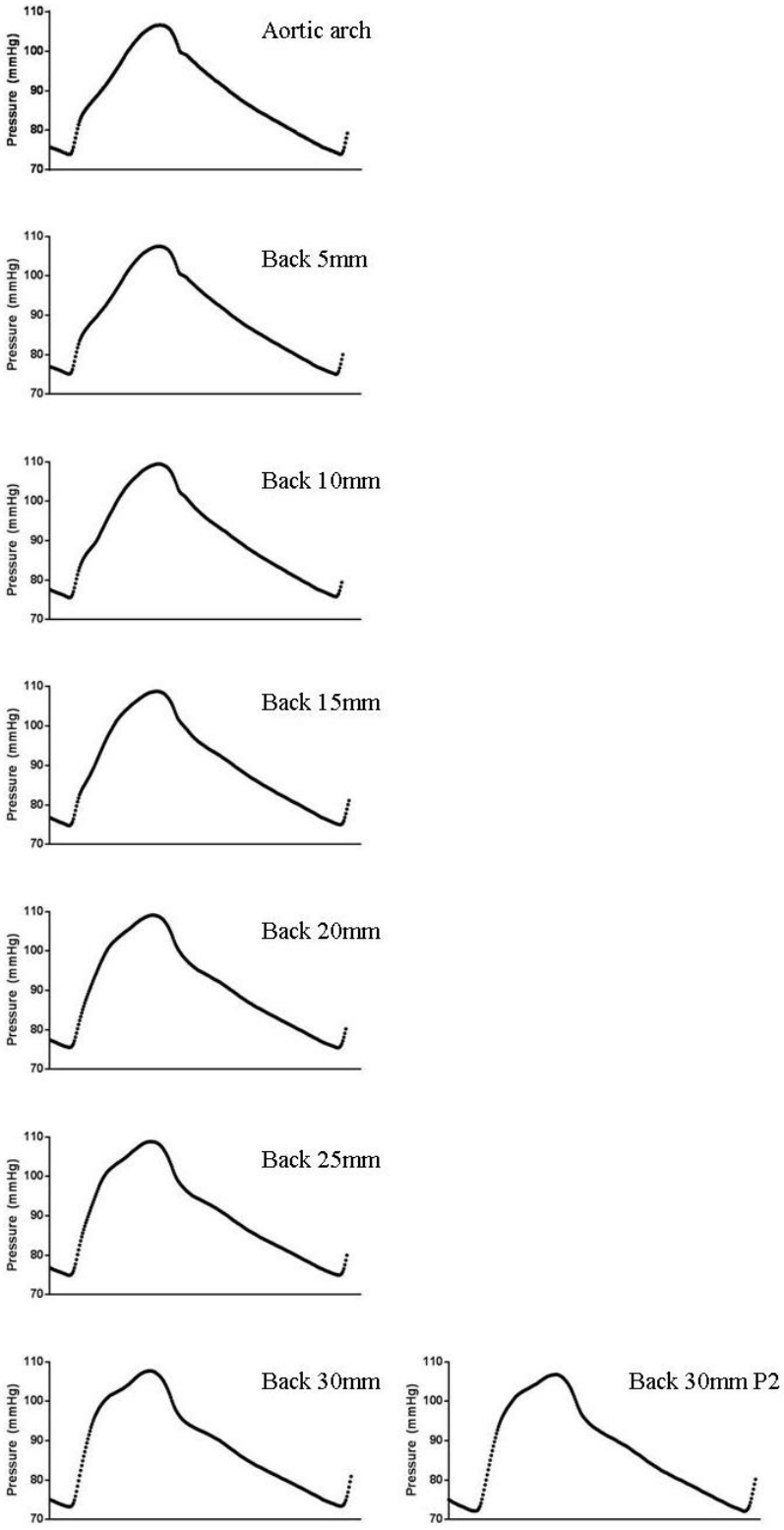

Figure 21: The shape of the pressure waveform changes as it travels down the length of the aorta. The distance from the aortic arch is indicated on the diagram. The waveform on the right (P2) was detected by the distal pressure sensor located 3cm away from the proximal sensor. The waveforms measured by the two sensors at a position of 30mm from the aortic arch are very similar, indicating that the presence of the catheter itself is not significantly interfering with the pressure waveforms. All waveforms are aligned at the pressure waveform foot (that is, the delay of the distal waveform is not indicated).

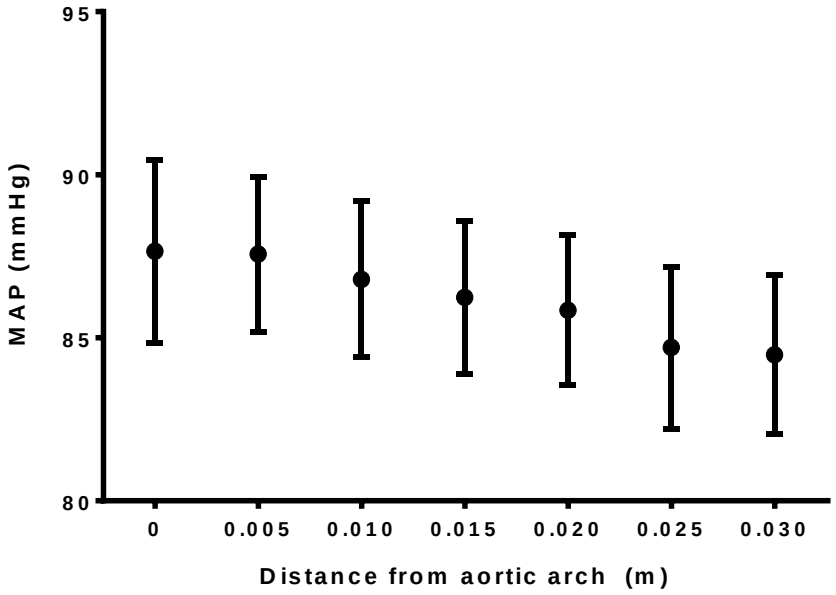

Figure 22: Relationship between MAP and distance of the proximal pressure sensor from the aortic arch. MAP did not differ significantly between any of the locations along the aorta. Data were analysed using one-way ANOVA and Tukey's multiple comparisons test.

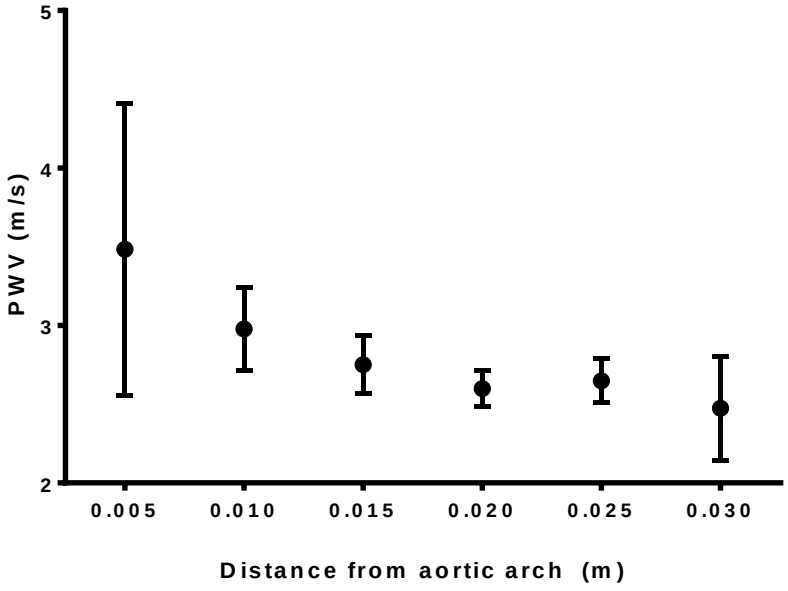

Figure 23: Relationship between PWV and distance from the aortic arch. PWV was not significantly different between any of the locations in the aorta as determined using one-way ANOVA followed by Tukey's multiple comparisons test.

4.3.2 Pressure dependent PWV relationship

The graph shown in Figure 24 depicts the relationship between pulse pressure amplification (PPA) and MAP. PPA can be determined as the ratio between distal and proximal PP:

$$PPA = PP_{distal}/PP_{proximal} \tag{4.2}$$

Above 80 mmHg PPA is approximately 3%. Below this value of MAP, PPA steadily drops.

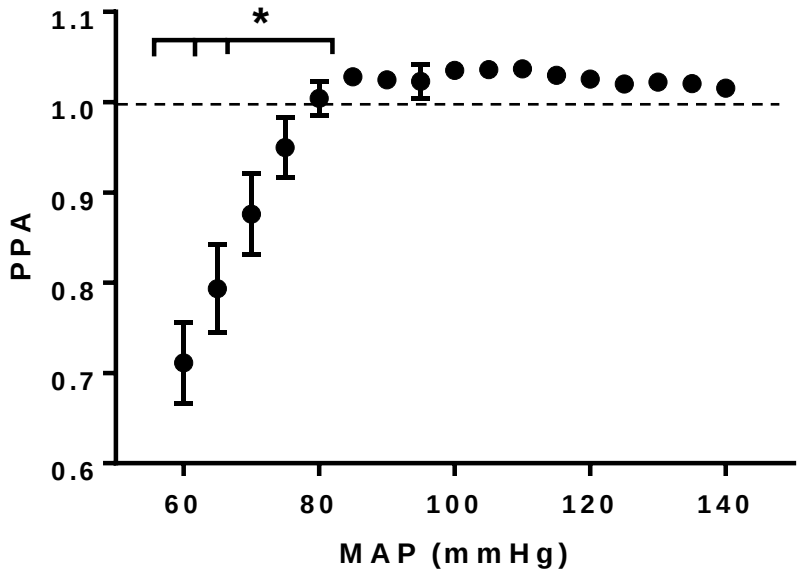

Figure 24: Graph of the PPA-MAP relationship. PPA remains approximately constant around 1.03 for pressures of 85 mmHg and above. PPA drops steadily as pressure decreases below this value. Using one-way ANOVA followed by Dunnett's multiple comparisons test, PPA becomes significantly different from the value of 1.028 at 85 mmHg at pressures of 70, 65, and 60 mmHg. *$p<0.05$.

The PWV-MAP relationship is well described by a second order polynomial (Figure 25). The data used to determine this was acquired while pressure was returning to baseline after an infusion was completed. It does not include data acquired during infusion.

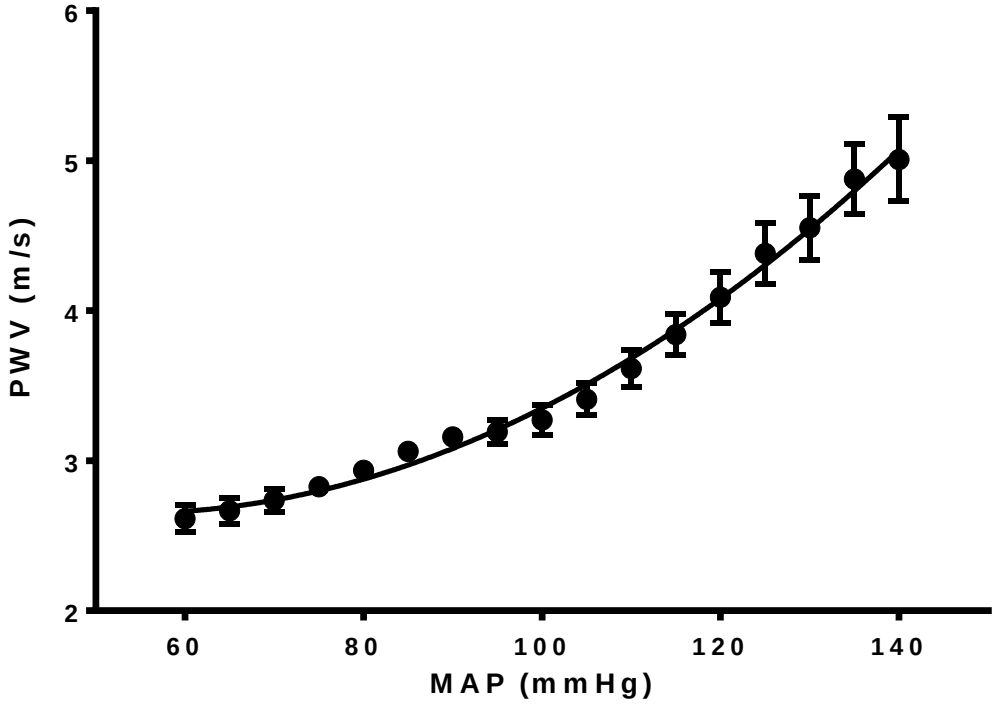

Figure 25: PWV-MAP curve fitted with a second order polynomial: PWV=0.0003228(MAP)^2 – 0.03447(MAP) + 3.569. R^2=0.9939. This indicates that the sensitivity of PWV to changes in MAP increases linearly with pressure. Regression was fitted to average data points.

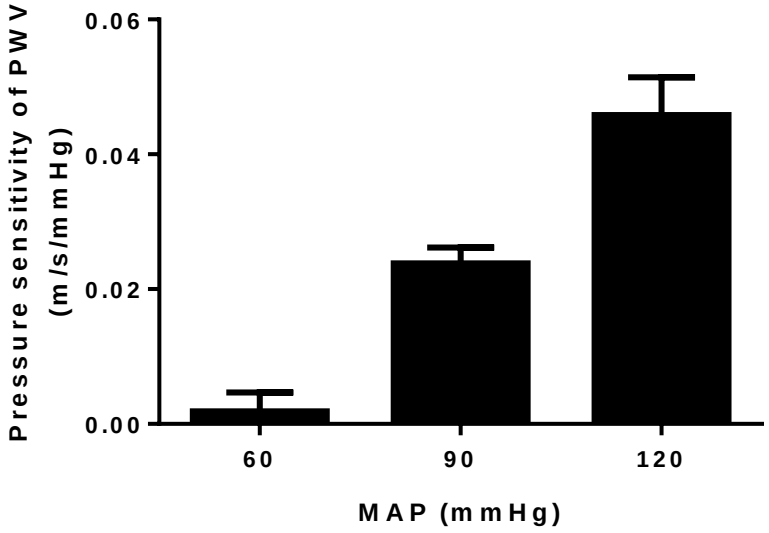

Figure 26: The sensitivity of PWV to changes in MAP increases linearly with MAP.

4.3.3 Cardiovascular parameters predictive of dynamic changes in PWV

MAP, R to R interval, pulse pressure, maximum dP/dt, and pressure change direction all remained in the model (Table 6 and Figure 27), with MAP having the greatest weighting and the other factors contributing to a lesser extent.

Table 6: Cardiovascular parameters that significantly affected PWV.

	coefficient	standardized coefficient	p-value	partial R-value
MAP	0.034 ± 0.014 m·s^{-1}/mmHg	0.95	<0.001	0.37
maximum dP/dt	0.00025 ± 0.00003 m·s^{-1}/mmHg/s	0.17	<0.001	0.053
ΔMAP direction	0.20 ± 0.02 m·s^{-1}/direction change	0.12	<0.001	0.060
pulse pressure	0.076 ± 0.031 m·s^{-1}/mmHg	0.091	0.013	0.0057
R-R interval	-4.2 ± 1.3 m·s^{-1}/s	-0.069	0.0011	0.0098

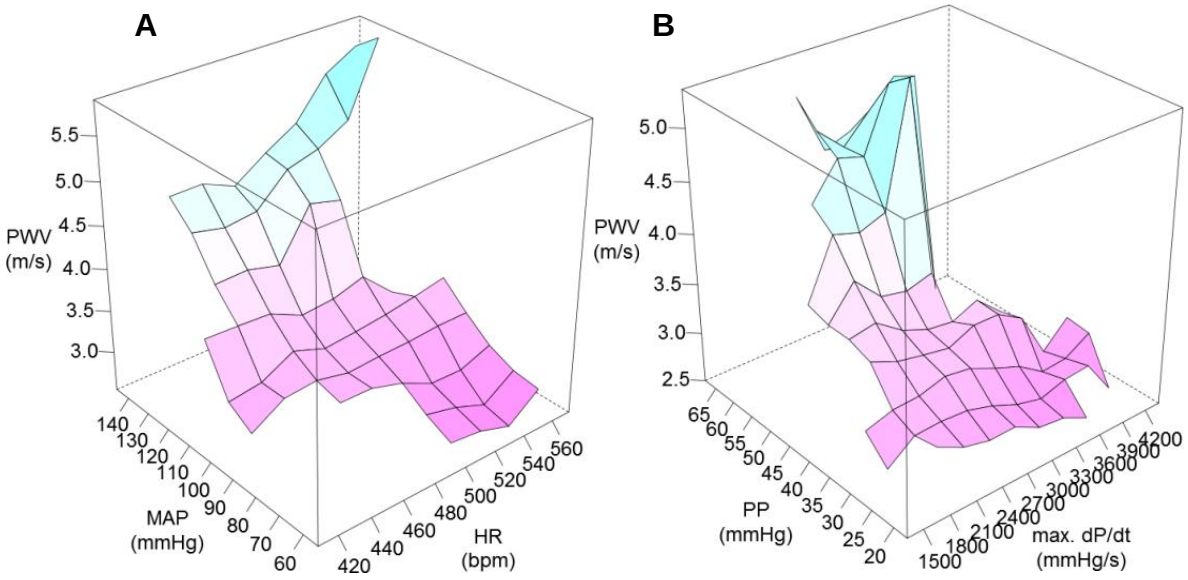

Figure 27: Relationship between PWV and (A) MAP and HR, (B) PP and max dP/dt. These plots indicate an interaction between terms (e.g. HR sensitivity of PWV is greater at higher MAP).

4.4 Discussion

Arterial stiffness increases along the length of the aorta (3); thus, it was expected that there would be a trend of increasing stiffness as measurements were taken which encompassed larger amounts of the abdominal aorta. However, PWV remained relatively constant along the entire length of the aorta with a slight, insignificant, decrease which appeared to follow a similar trend in MAP. This was different to what has been observed in the rat, where regional increases in PWV from the thoracic to the abdominal aorta have been shown (29). The trend for increased PWV towards the aortic arch may be due in part to the curvature of the aorta not being taken into account when considering the distance travelled by the pulse wave. The 0.5 cm which the catheter is withdrawn underestimates the distance travelled in the arch because it is a straight line. This results in a higher apparent velocity. The increased MAP towards the arch may also contribute to this. It is possible that the presence of the catheter provides enough resistance to increase pressure. As it is withdrawn from the aorta, full capacitance is restored and MAP drops. However, this potential effect is likely small as there were no statistically significant changes in MAP with distance from the arch.

There are some other errors associated with this technique. The first is the inability to precisely measure the amount with which the catheter is withdrawn. This means that the distance between the two points used to calculate each incremental PWV value is less precisely determined. As the measurements are taken at 0.5 cm increments, small errors in catheter placement could actually be relatively significant. Additionally, the measurements are timed with respect to the ECG and PWV is calculated based on sequential, not simultaneous, measurements. This means that small fluctuations in HR or MAP may affect the TT. These errors are not present when measuring PWV with the dual pressure catheter as the separation distance between the sensors is precisely fixed and the PWV measurement is simultaneous (not sequential). However, the small length of the mouse aorta does not allow

for incremental PWV measurements to be made otherwise as the 3 cm separation distance spans across most of the aorta.

There was no PPA between the two sites of pressure measurement in the aorta. Moreover, PPA actually dropped significantly as pressure decreased below 80 mmHg. In the normal vasculature, due to vessel stiffness and wave reflection, there is an amplification of the pressure pulse between distal and proximal sites (3). PPA can be influenced by different factors such as age, posture, exercise, transmission length, HR, and BP (3, 192-195). Changes in BP may alter wave reflection and increased early wave reflection may reduce PPA (196). Yet this is more often seen as pressure is increased, whereas results of these experiments indicate a relatively constant PPA for higher pressures and a severe reduction at lower pressures.

The placement of the catheter in the aorta may also both increase early wave reflection and alter the transmission characteristics of the aorta, thereby significantly affecting PPA. However, in Figure 10, it can be seen that as the pressure sensors are withdrawn from the aorta, the pulse pressure does not change. As such, it is difficult to determine to what extent the presence of the catheter influences these various factors, though the pressure patterns suggest minimal effect. In addition, inspection of the aortic waves obtained from the same position with both the proximal and distal pressure sensors shows that there does not appear to be any significant change to the waveform shape. This would indicate that the presence of the catheter is not significantly affecting the local hemodynamics. The significant drop in PPA at MAP of 70 mmHg and below might indicate an interaction with the catheter itself as pressure (and diameter) is at the lower physiological extreme. However, for MAP above 70 mmHg, this dependency does not appear, and it can be assumed to represent the hemodynamics without significant interaction with the catheter itself.

The multiple linear regression analysis provided an interesting first glimpse into some other factors that may influence PWV aside from blood pressure. The results indicate that maximum dP/dt, PP, and R to R interval all have an additional effect on PWV, beyond MAP. MAP direction remained in the model, indicating that other factors are also significant, or that the aorta displays a short term viscoelastic memory as previously discussed in Chapter 3. From the surface plots shown in Figure 27, it can be seen that PWV has a positive association with HR, with a greater effect seen at higher pressures. As expected, PP is also positively associated with PWV.

Further studies are required to investigate the isolated effect of maximum dP/dt (and possibly effects of cardiac contractility), PP, and R to R interval upon PWV. Care must also be exercised in interpreting these results, as multiple linear regression analysis assumes that each parameter is independent of one another, which is not entirely the case in this experimental preparation. Studies by our group have started to tease apart these parameters, for example by pacing heart rate (179) while maintaining a constant blood pressure, and acutely blocking sympathetic activity (unpublished data). These studies were performed in rats. The multiple linear regression technique provided in this Chapter provides a preliminary outlook into the various parameters affecting PWV, in addition to blood pressure, in the mouse model.

This study provides the pressure-dependent relationship of PWV in the murine aorta using high fidelity pressure recordings. It also lays the groundwork for future experiments in knockout mice which will enable investigations of both altered vascular responses in hypertension and pressure dependent and independent mechanisms of arterial stiffness.

Chapter 5

Effect of transglutaminase 2 on arterial stiffness

Structural changes of the arterial wall are associated with increased arterial stiffness and hypertension (Section 2.6). TG2, an enzyme ubiquitously expressed in the vasculature, forms stable crosslinks between extracellular matrix proteins, including collagen, which may lead to increased arterial stiffness (Section 2.8). Santhanam et al showed that inhibition of TG2 by cystamine prevented age-related increased arterial stiffness in the rat. They also demonstrated, using Doppler ultrasound measurements, that $TG2^{-/-}$ mice were protected against increases in arterial stiffness caused by NOS-inhibition when compared to controls (16). Additionally, TG2 has been implicated in cardiovascular disease due to its role in small artery remodelling (127, 145), calcification (164, 197) and atherosclerosis (163). The aim of this study was to compare parameters of large artery function between $TG2^{-/-}$ mice and WT littermates, with a focus on pressure-dependent PWV measurements.

In vitro studies have also demonstrated that TG2 crosslinking activity is inhibited by endothelial NO (17, 142, 143, 198). Therefore, the second aim of this investigation was to determine if reducing the bioavailability of NO translates to functional cardiovascular changes mediated by TG2 activity and to possibly establish a link between NO, TG2, and aortic stiffness.

5.1 Methods

5.1.1 Animals

Male $TG2^{-/-}$ and WT mice, aged 16 weeks were studied. Animals were kept in a temperature controlled environment (21 ± 2^{o}C) with 12 hour light/dark cycles. Animals had *ad libitum* access to standard laboratory mouse feed and water. The animal protocol was approved by the Macquarie University Animal Ethics Committee and the Garvan/St. Vincent's Animal Ethics Committee (ARA 2011/017, 12_29).

From Chapter 4, the estimated standard deviation for PWV measurements using a dual pressure sensor catheter was 0.09 m/s for the mean value of 3.08 m/s measured in WT mice. For a detectable difference of 0.15 m/s (a 5% change) with a confidence of 95% and a power of 80%, the minimum sample size for mice groups is n=6.

5.1.2 L-NAME administration

Four groups of mice were studied. Groups 1 and 2 ($TG2^{-/-}$, n=6 and WT, n=6) were given standard tap water. Groups 3 ($TG2^{-/-}$, n=8) and 4 (WT, n=6) received N_{ω}-Nitro-L-arginine methyl ester hydrochloride (L-NAME: Sigma, Australia) via drinking water (0.5 g/L). L-NAME was administered for two weeks prior to surgery. The concentration and duration of L-NAME used in the drinking water was based on published reports that have shown impaired endothelial function, hypertension, or increased PWV in the mouse aorta (43, 199, 200).

5.1.3 PWV measurement

PWV was measured as described in Section 3.3.4. Briefly, mice were anaesthetised (induced at 4.5%, maintained at 1.5% isoflurane in oxygen) and spontaneously breathing through a nose cone during surgery and measurements. Temperature was maintained at 37^{o}C. ECG

leads were placed subcutaneously to determine heart rate. A high fidelity, dual pressure sensor catheter was inserted into the aorta via the femoral artery to MAP and beat-to-beat PWV. The jugular or femoral vein was cannulated for drug administration. MAP was increased by infusion of PE (10 μg/min) until pressure reached a plateau. Once MAP returned to baseline SNP was then used to lower blood pressure in the same manner.

5.1.4 Baroreflex sensitivity

Drug-induced baroreflex sensitivity (BRS) was determined from the sigmoid response of the pulse interval to changes in MAP after an intravenous injection of PE to evoke peripheral vasoconstriction. The increase in MAP was then plotted against the corresponding increase in pulse interval (60/HR), and the slope (in ms/mmHg) obtained by regression analysis of the linear component of the curve was taken as an indicator of baroreflex sensitivity.

5.1.5 Tissue dissection and preparation

After the PWV measurements, the heart and entire length of the aorta were rapidly excised and placed in cold physiological salt solution (PSS) of the following composition (in mM): 130 NaCl, 4.7 KCl, 1.18 KH_2PO_4, 1.17 $MgSO_4 \cdot 7H_2O$, 14.9 $NaHCO_3$, 5.5 glucose, 0.026 EDTA, 1.6 $CaCl_2$. The left ventricle was isolated and weighed. The aorta was cleaned of all connective tissue. Two sections 2-3 mm in length were cut and mounted as ring preparations in a wire myograph (620M, DMT) for isometric tension measurements: one section from the descending aorta, just proximal to the first intercostal branches, and the second from the abdominal aorta between the renal branches and the iliac bifurcation.

For selected cases, the remaining aorta was preserved for a calcium quantification assay. The aorta was washed three times with saline, dried, and stored at -80^{o}C. In the others, the aortas were placed in 10% phosphate-buffered formalin in order to be fixed for histological examination.

5.1.6 Wire Myography

The aortic rings were mounted on 200 µm posts in 5 mL of PSS bubbled with 95% O_2/5% CO_2. Vessels were allowed to sit for approximately 20 minutes while the chambers slowly heated up to 37^{o}C. Following this period, the vessels underwent a normalization procedure. The normalization was performed by stretching the segment stepwise to a normalized internal circumference (IC1) defined as a set fraction of the internal circumference (IC100) that a fully relaxed segment would have at a specified transmural pressure. The target transmural pressure used was 100mmHg and the set fraction used to determine the IC1 was 0.9. Vessels were then allowed to rest for approximately 20 minutes. Potassium chloride (KCl, 120mM final concentration) was then added to the bath and left until the vessels maximally constricted. The vessels were then washed 3 times until they returned to baseline tensions and dose-response curves were performed.

A cumulative dose-response curve ($1x10^{-9}$ – $3x10^{-4}$ M) was performed with PE. Following this, vessels were preconstricted with 1 µm PE (to give about 80% maximal constriction) and a cumulative dose-response curve was performed with ACh ($1x10^{-10}$ – $3x10^{-4}$ M) to evaluate endothelium-dependent relaxation. Vessels were washed out, allowed to return to resting tension, again preconstricted with PE (1µM), and their response to SNP ($1x10^{-10}$ – $3x10^{-5}$ M) to evaluate endothelium-independent relaxation was determined. Relaxation responses were calculated as a percentage of tension following pre-constriction. Constriction responses were calculated as a percentage of maximum constriction induced by KCl. Maximum constriction was also determined. Sigmoidal dose-response curves were fitted to the data.

5.1.6.1 Tensile testing

A tensile test provides useful information about the mechanical properties of the specimen being tested, including its material stiffness (the elastic modulus). Generally, this involves stretching a specimen of known initial dimensions uniaxially. Changes in length are recorded

as increasing force is applied. As PWV depends on the material stiffness of the arterial wall, subjecting aortic rings to tensile tests provides *ex vivo* observations that can support the *in vivo* PWV measurements and indicate whether changes have occurred in the arterial wall which have modified its inherent stiffness.

The myograph normalization procedure returns values of force and distension as the vessel is being stretched stepwise. This is similar to the output a tensile testing apparatus would return, with the exception that these are discrete values recorded once per minute as opposed to continuous data. For thoracic aortic sections, these values were then converted to stress (σ) and strain (ε) according to the following equations:

$$\sigma = \frac{F}{A_0} \tag{5.1}$$

$$\varepsilon = \frac{l - l_0}{l_0} \tag{5.2}$$

where F is force, A_0 is the initial cross-sectional area, l is the distension and l_0 is the initial length of the sample. The stress-strain relationship was then plotted, fit with a quadratic equation and the incremental elastic modulus (E_{inc}) was calculated as the slope of the curve for a strain of 0.1.

5.1.7 Calcium quantification assay

The aorta was stored at -80^{o}C until use. To measure calcium content, each aortic section was dried at 60^{o}C. Dry tissue weight was recorded and the aortas were then placed in 1M HCl (20 µL / mg dry tissue) at 4^{o}C for 72 hours for calcium extraction.

Calorimetric quantification of calcium was achieved through a reaction with ortho-cresophthalein complexone (CPC). In brief, a volume of 20 µL of sample was placed into a clean absorbance cuvette and 0.5 mL of working solution was added. The working solution is comprised of CPC (0.1mM) which forms a purple-coloured complex with calcium, 8

hydroxy-quinoline (8HQ, 5.2mM) which chelates magnesium or iron which may interfere with calcium absorbance, and 2-amino-2-methyl-1-propanol (26.4mM) which provides the proper alkalinity necessary for the colour reaction to occur. The absorbance, or intensity of the colour, was then read at a wavelength of 575nm using a Beckman Coulter analyser AU 800 spectrophotometer.

A standard curve of absorbance versus calcium content was generated in the same manner using known quantities of calcium chloride dehydrate ($CaCl_2 \cdot 2H_2O$). This curve was then used to calculate the quantity of calcium in each tissue sample based on its absorbance reading.

5.1.8 Histological analysis

Aortas were fixed overnight in 10% phosphate-buffered formalin. The thoracic aorta was dehydrated through a graded ethanol series, cleared with xylene, infiltrated with warm paraffin, and embedded in paraffin blocks (Leica Paraffin Tissue processor). The embedded aorta was cut into 5µm cross-sections which were mounted on glass slides. Sections were stained with haematoxylin and eosin (H&E) and studied to evaluate thickening of the aortic wall. The cross-sectional area of the aortic lumen and media were measured (ImageJ, NIH, USA) and the media-lumen ratio was then calculated. The media was defined as the space between the internal and external elastic lamina. Medial thickness was calculated as the average distance measured at 8 locations around the circumference of the aorta.

5.1.9 Statistical Analysis

Data are presented as mean ± standard error, except where indicated otherwise. Data were analysed offline using a combination of Microsoft Excel, IBM SPSS Statistics 19, and GraphPad Prism 6.

Data recorded across all pressure ranges were divided into 2 mmHg pressure bins. Statistical differences between groups were determined using either: paired Student's t-tests for each pressure bin, 1-way ANOVA followed by Tukey's multiple comparisons test, or 2-way ANOVA followed by Sidak's multiple comparisons test (unless otherwise stated). P-values less than 0.05 were considered to be statistically significant.

Dose-response curves were fitted with a sigmoidal dose-response function through non-linear regression in Prism, returning EC_{50} and maximum response parameters. Two-way ANOVA with Bonferroni post-hoc test was employed to compare responses at each concentration. EC_{50}s and maximum responses were compared using one-way ANOVA followed by Tukey's multiple comparisons test. Again, P-values less than 0.05 were considered to be statistically significant.

5.2 Results

5.2.1 Baseline Characteristics

TG2 knockout mice had baseline parameters similar to their WT controls. They did not show an abnormal cardiovascular phenotype with no statistical differences between any of the cardiovascular parameters as shown in Table 7. Furthermore, animals administered with L-NAME showed no differences between strains or from the untreated groups.

Table 7: Baseline cardiovascular characteristics. Data are presented as mean ± SD. No statistical differences between groups were observed.

	WT	**TG2$^{-/-}$**	**WT L-NAME**	**TG2$^{-/-}$ L-NAME**
BW (g)	30 ± 4	28 ± 2	29 ± 2	30 ± 2
HR (bpm)	519 ± 60	527 ± 59	578 ± 46	565 ± 35
MAP (mmHg)	90 ± 8	87 ± 10	90 ± 4	88 ± 6
SBP (mmHg)	110 ± 9	105 ± 12	110 ± 3	106 ± 7
DBP (mmHg)	73 ± 8	70 ± 9	71 ± 6	70 ± 6
PP (mmHg)	37 ± 2	34 ± 5	39 ± 3	36 ± 3
Max dP/dt (mmHg·s^{-1})	1074 ± 209	939 ± 294	1238 ± 245	1012 ± 145
PWV (m/s)	3.17 ± 0.19	3.24 ± 0.57	3.26 ± 0.23	3.19 ± 0.10
LV/BW (mg/g)	320 ± 9	308 ± 14	314 ± 24	312 ± 10

5.2.2 Pulse Wave Velocity

While there was no difference in PWV at baseline values between TG2-/- mice and WT controls, at pressures greater than and equal to 126 mmHg, WT mice had significantly higher PWV (Figure 28; at 126mmHg: PWV = 4.92 ± 0.18 versus 4.49 ±0.05m/s; at 128mmHg: PWV = 5.06 ± 0.19 versus 4.62 ± 0.05m/s; at 130mmHg: PWV = 5.22 ± 0.23 versus 4.75 ± 0.05m/s; $p<0.05$).

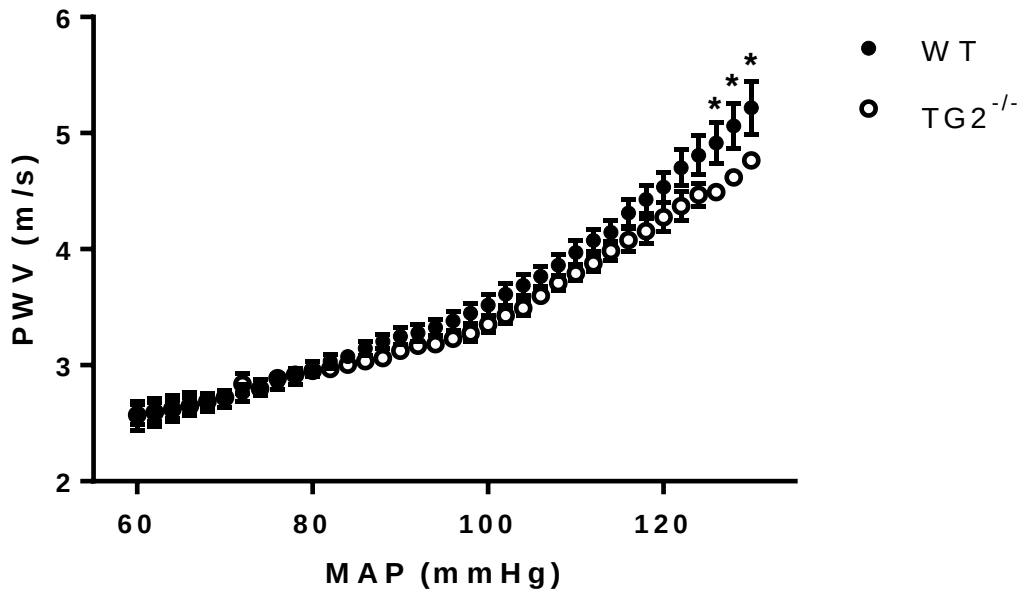

Figure 28: PWV-MAP relationship in WT and TG2$^{-/-}$ mice. PWV was higher in WT mice at pressures of 126 mmHg and higher. *p<0.05

Figures 29-31 present the effect of L-NAME on the pressure-dependent PWV curves in WT and TG2$^{-/-}$ animals. After L-NAME administration, PWV was slightly reduced at pressures greater than 120 mmHg in the WT animal (Figure 29), though this was not statistically significant. There were no statistically significant differences with L-NAME administration in TG2$^{-/-}$ animals (Figure 30); however, in the middle pressure ranges, the L-NAME treated animals had a slightly higher PWV and this effect is diminished at higher pressures (non-significant). Figure 31 shows the PWV-MAP relationship for L-NAME treated WT and TG2$^{-/-}$ mice. There was no difference in PWV at any of the pressures investigated.

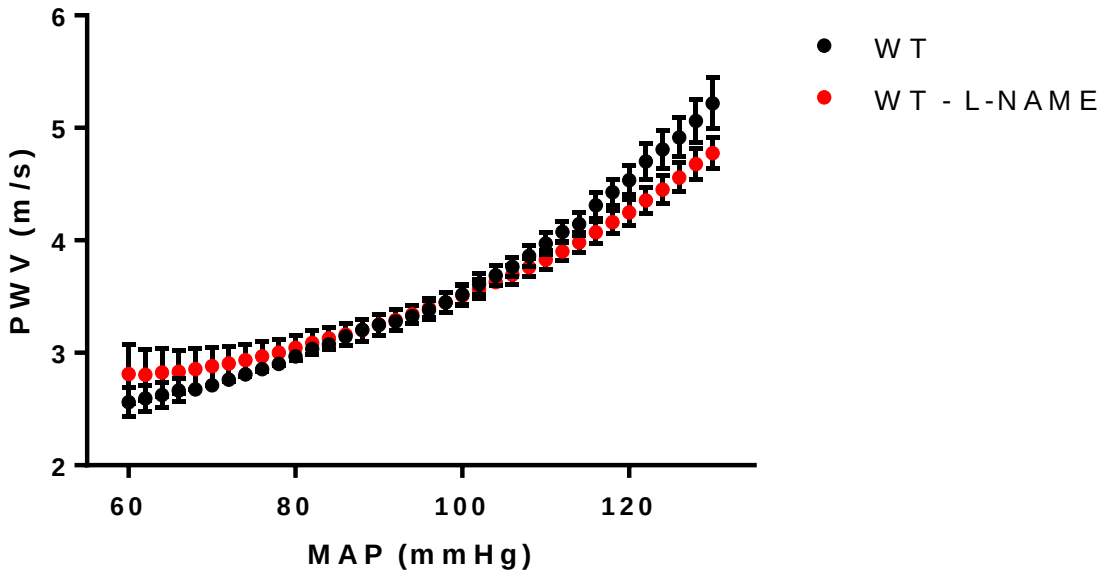

Figure 29: PWV-MAP relationship for L-NAME treated and control WT animals. No statistical difference between L-NAME and control animals was observed.

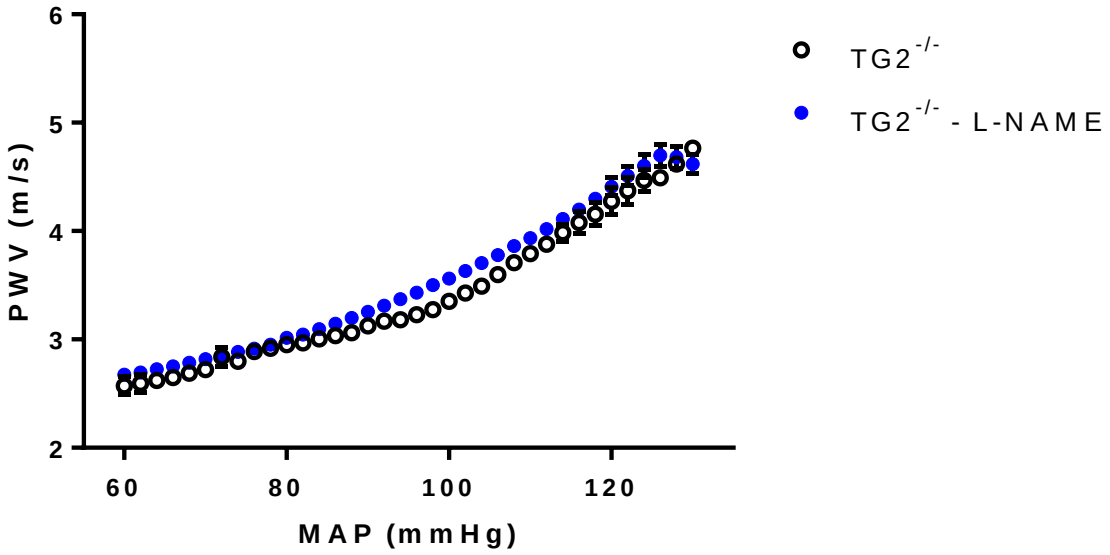

Figure 30: PWV-MAP relationship for L-NAME treated and control $TG2^{-/-}$ animals. No statistical difference between L-NAME and control animals was observed.

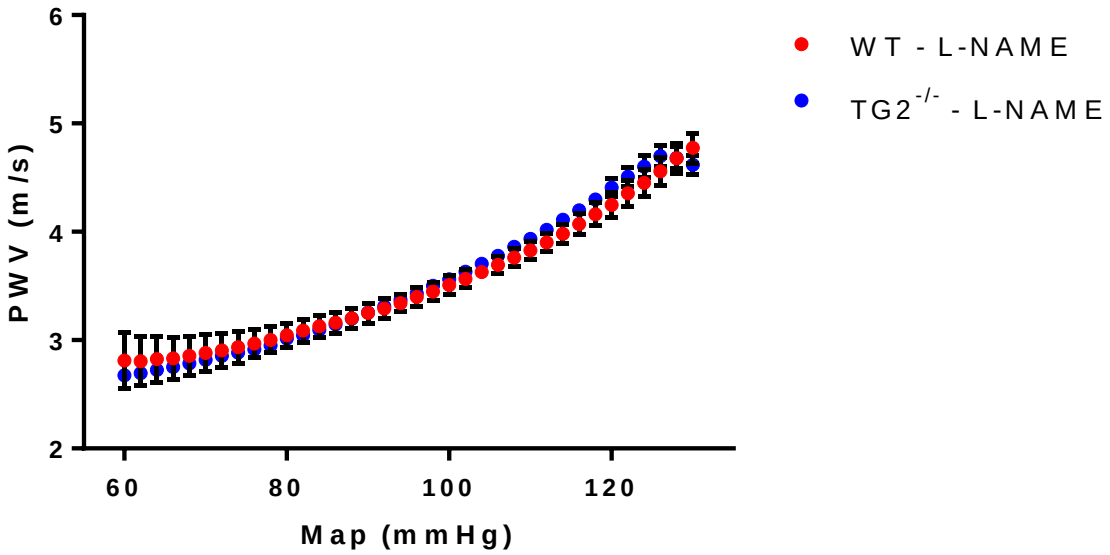

Figure 31: PWV-MAP relationship for L-NAME treated WT and $TG2^{-/-}$ mice. No statistical difference between L-NAME and control animals was observed.

Each PWV-MAP curve was fitted with a quadratic equation (Table 8). This indicates that for each group, the pressure sensitivity of PWV increases linearly with pressure (Figure 32). The values for pressure sensitivity were not significantly different among groups.

Table 8: PWV-MAP relationships are described by a quadratic equation.

	Quadratic equation	**R^2**
WT	$PWV = 3.733 - 0.04401(MAP) + 0.0004230(MAP)^2$	0.9974
$TG2^{-/-}$	$PWV = 3.567 - 0.03674(MAP) + 0.0003524(MAP)^2$	0.9953
WT – L-NAME	$PWV = 3.803 - 0.03684(MAP) + 0.0003391(MAP)^2$	0.9992
$TG2^{-/-}$ – L-NAME	$PWV = 2.900 - 0.01997(MAP) + 0.0002672(MAP)^2$	0.9958

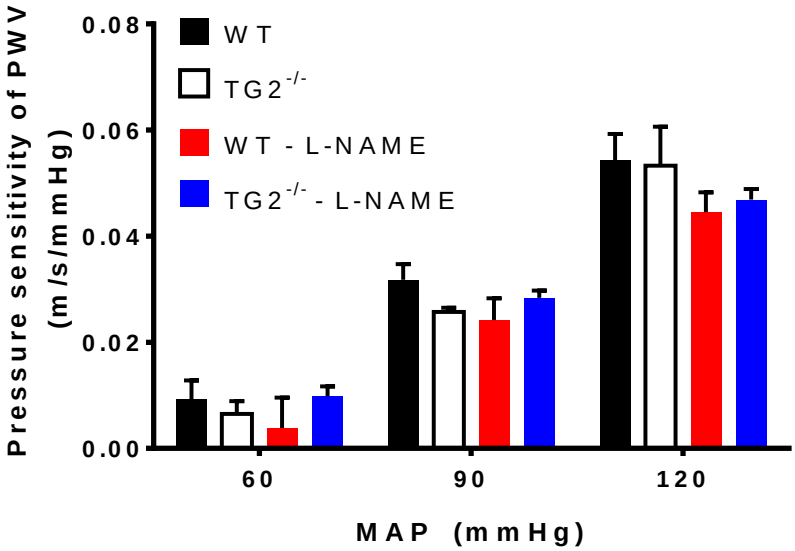

Figure 32: Sensitivity of PWV to changes in MAP increases linearly with pressure. The sensitivity at low (60 mmHg) medium (90mm Hg) and high (120 mmHg) MAP was not different between strain or treatment groups (2-way ANOVA followed by Tukey's multiple comparisons test).

Figures 33 to 36 show the relationships between PPA and MAP for each of the groups of mice. As described in Chapter 4, PPA is around 1 at pressures of 80mmHg and greater. PPA steadily dropped as pressures fell below 80 mmHg. There were no differences between WT and $TG2^{-/-}$ mice although there was a slight trend towards increased PPA in untreated $TG2^{-/-}$ mice compared to WT controls (Figure 33). This trend was diminished in L-NAME treated animals (Figure 36). While not statistically significant, L-NAME treated animals also demonstrate a trend towards increased PPA compared to untreated controls (Figure 34 and Figure 35). These slight differences are apparent at pressures of approximately 80 mmHg and higher.

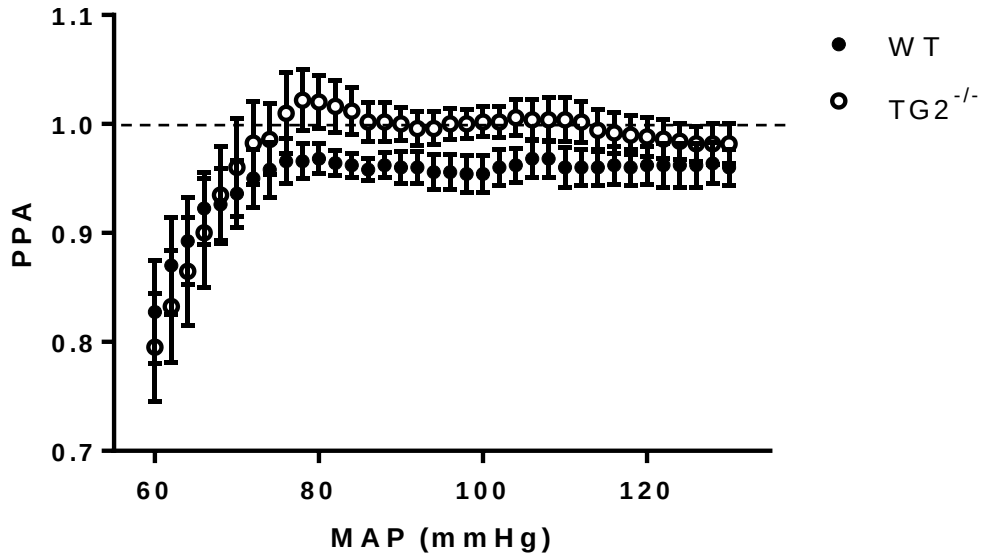

Figure 33: PPA-MAP relationship for WT and TG2$^{-/-}$ mice. While both strain and pressure were detected as significant sources of variation in PPA, the post-hoc test did not reveal any statistically significant pressure bins. There is a trend of increased PPA in the TG2 mice between pressures of 80 and 100mmHg.

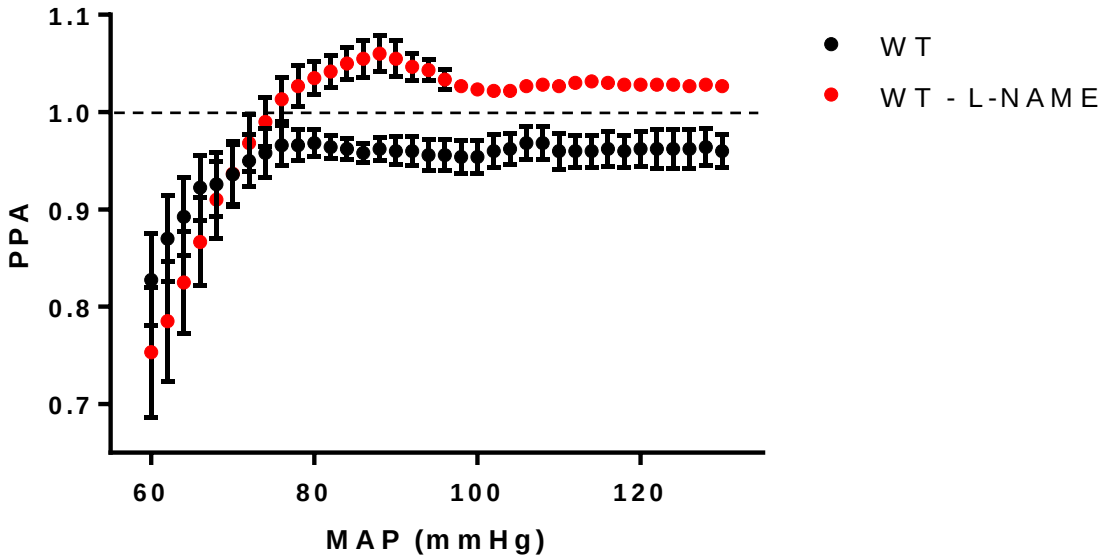

Figure 34: PPA-MAP relationship for L-NAME administered and control WT mice. The L-NAME administered animals appear to have a higher PPA compared to controls. Similar to the data presented in Figure 6, both treatment and pressure were detected as significant sources of variation in PPA; however, post-hoc tests did not detect any statistically significant pressure bins.

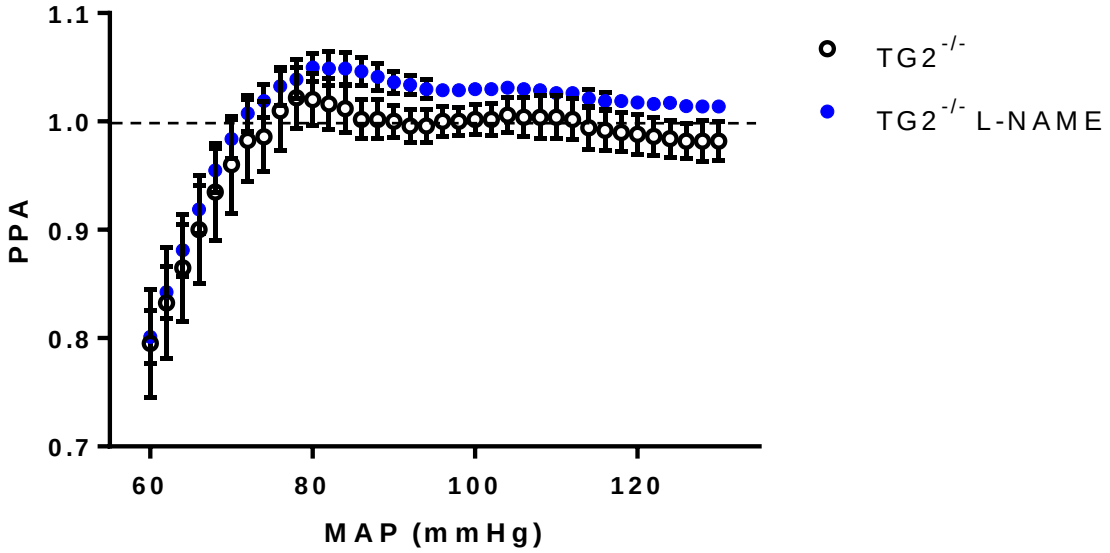

Figure 35: PPA-MAP relationship for L-NAME administered and control TG2$^{-/-}$ mice. L-NAME administered mice show a trend towards higher PPA compared to control. There were no statistically significant differences detected.

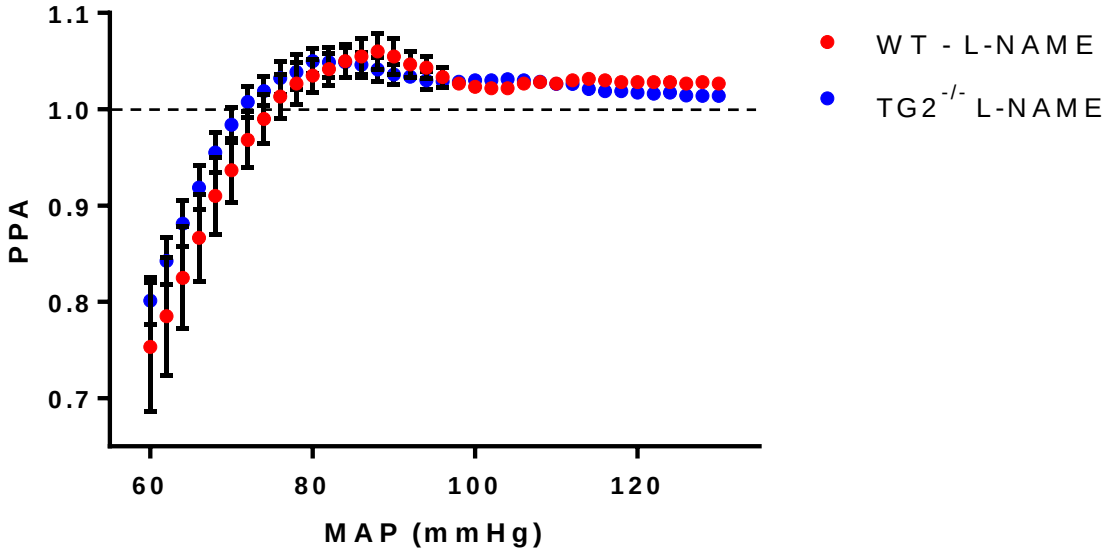

Figure 36: PPA-MAP relationship for L-NAME administered WT and TG2$^{-/-}$ mice. There were no significant differences detected between strains.

5.2.3 Baroreflex sensitivity

There was no significant difference in drug-induced BRS between strains or treatment groups; although, there was a trend towards decreasing sensitivity in the L-NAME treated animals (Figure 37).

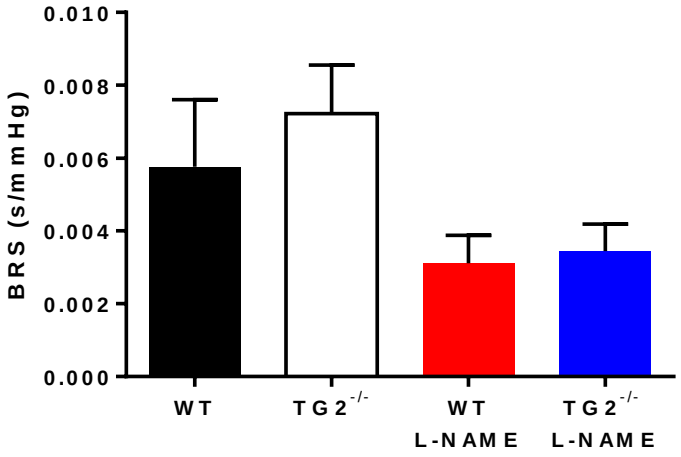

Figure 37: BRS in response to PE administration in WT, $TG2^{-/-}$ and L-NAME treated mice.

5.2.4 Tensile testing

The passive mechanical properties of the intact thoracic aorta were explored by calculating the stress-strain relationship from force-distension information provided by the wire myograph experiments (Figure 38A). The E_{inc} at a strain of 0.1 was not different between groups (Figure 38B); however, there was a trend of increased E_{inc} in WT mice compared to $TG2^{-/-}$ and a further tendency of reduced E_{inc} in L-NAME treated animals compared to untreated controls.

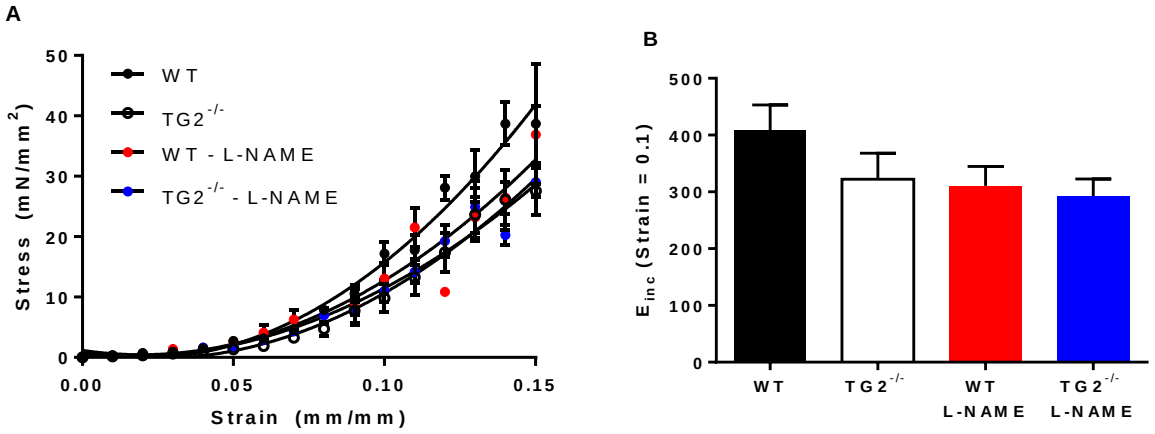

Figure 38: The stress-strain curves (A) and E_{inc} at a strain of 0.1 (B) for control and L-NAME treated WT and $TG2^{-/-}$ mice. No significant differences were observed.

5.2.5 Vascular Studies

To examine vascular function, *ex vivo* myograph experiments using mouse aortic rings were performed. Vascular dose-response curves to PE, SNP, and ACh to evaluate VSMC and endothelial cell function were performed. Rings were taking from both the thoracic aorta, immediately proximal to the first intercostals branch, and the abdominal aorta, proximal to the iliac bifurcation.

5.2.5.1 Smooth muscle contraction

Vasoconstrictor responses to PE were examined. There was no attenuation of the maximum contractile response to PE between untreated and L-NAME-treated WT and $TG2^{-/-}$ mice in rings from the thoracic aorta (10.93 ± 2.48 vs. 8.85 ± 2.20 mN and 2.58 ± 0.55 vs. 4.47 ± 0.72 mN respectively). However, L-NAME treatment significantly impaired the contraction in the thoracic aortas of WT mice compared to untreated controls (2.58 ± 0.55 vs. 10.93± 2.48 mN; $p<0.05$; Figure 39A). There were no statistically significant differences observed in the abdominal aortic segments between any of the groups studied (WT: 7.48 ± 1.47, $TG2^{-/-}$: 6.98 ± 0.62, WT – L-NAME: 3.95 ± 0.89, and $TG2^{-/-}$ - L-NAME: 6.09 ± 1.71 mN; Figure 39B). There was a trend towards decreased maximal responses in the L-NAME treated animals.

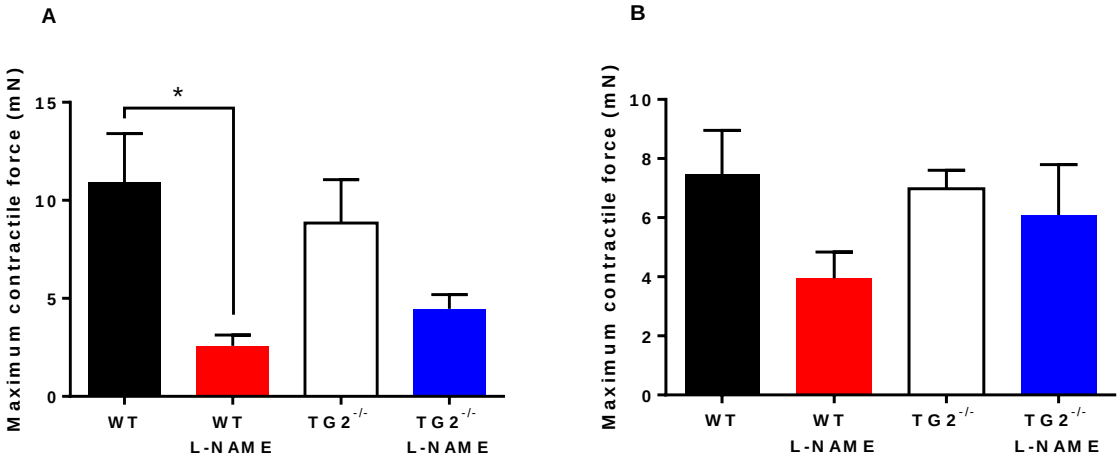

Figure 39: Maximal contraction to PE in thoracic (A) and abdominal (B) segments isolated from the four different mice groups. Treatment with L-NAME impaired vascular smooth muscle contractile response significantly only in the thoracic sections from the WT mice; however, there was a similar trend in all groups studied. *P<0.05.

There were no strain-related differences in the dose-response curve to PE in the thoracic aorta (Figure 40). There was a shift to the right in the L-NAME treated mice, indicating a decrease in sensitivity to PE. While not statistically significant, this is reflected by the EC_{50} values which are slightly reduced in the groups given L-NAME.

There were also no observed strain-related differences in the PE dose-response curve in rings isolated from the abdominal aorta (Figure 41). Again, there was a shift to the right in the L-NAME treated mice, indicating a decrease in sensitivity to PE. The EC_{50} values were also lower in the L-NAME treated animals, although this only reached statistical significance in the $TG2^{-/-}$ animals.

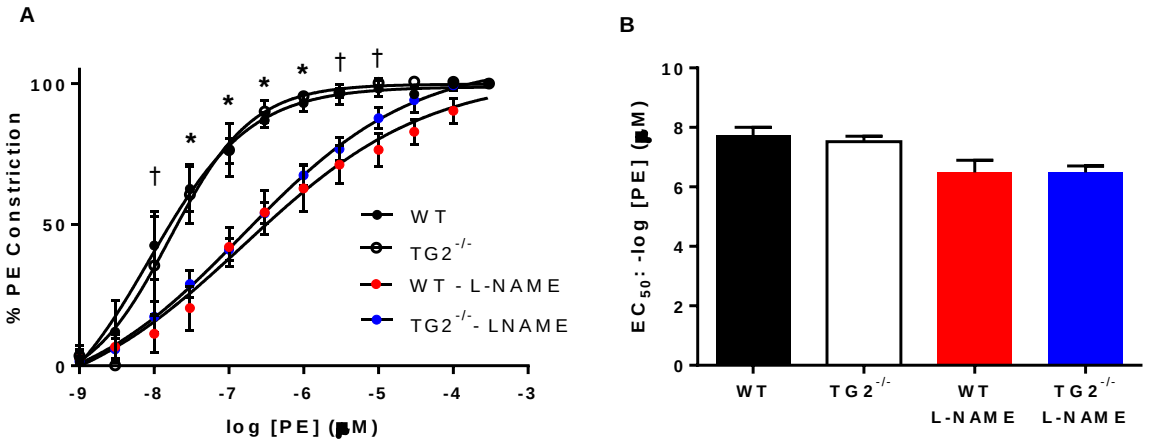

Figure 40: Contractile response to PE (A) and EC_{50} values (B) in the thoracic aorta of L-NAME administered and control $TG2^{-/-}$ and WT mice. *P<0.05 for untreated versus L-NAME administered mice, †P<0.05 for untreated versus L-NAME treated WT mice only.

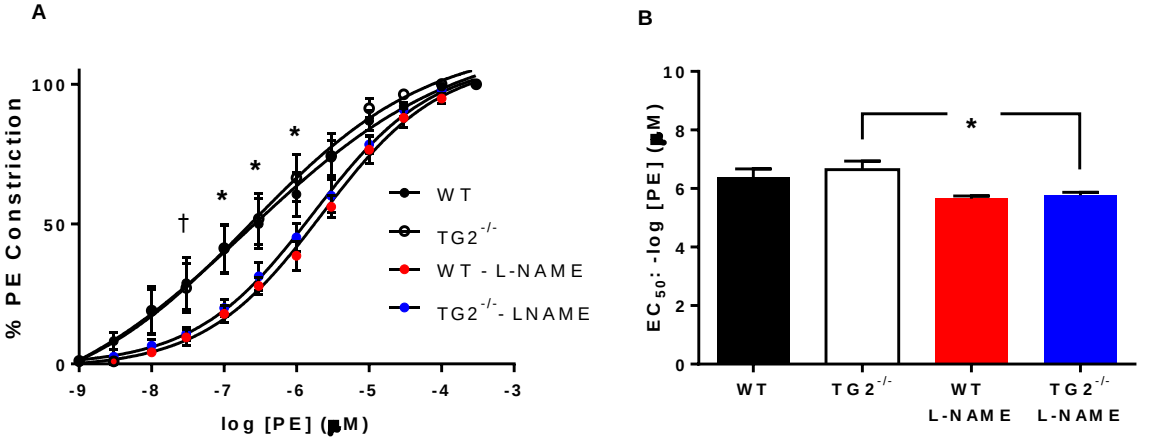

Figure 41: Contractile response to PE (A) and EC_{50} values (B) in the abdominal aorta of L-NAME administered and control $TG2^{-/-}$ and WT mice. *P<0.05 for untreated versus L-NAME treated mice, †P<0.05 for untreated versus L-NAME treated WT mice only.

There were almost no differences detected between aortic rings from the thoracic aorta versus those taken from the abdominal aorta regarding responses to PE. There was a trend of decreased sensitivity (indicated by reduced EC_{50}) in the abdominal sections; however, this only reached significance in the control WT mice. The maximum contractile force to PE was not statistically different between thoracic and abdominal sections, although it appeared to

slightly decrease in untreated animals and increase in L-NAME treated animals in the abdominal sections compared to thoracic (Figure 42).

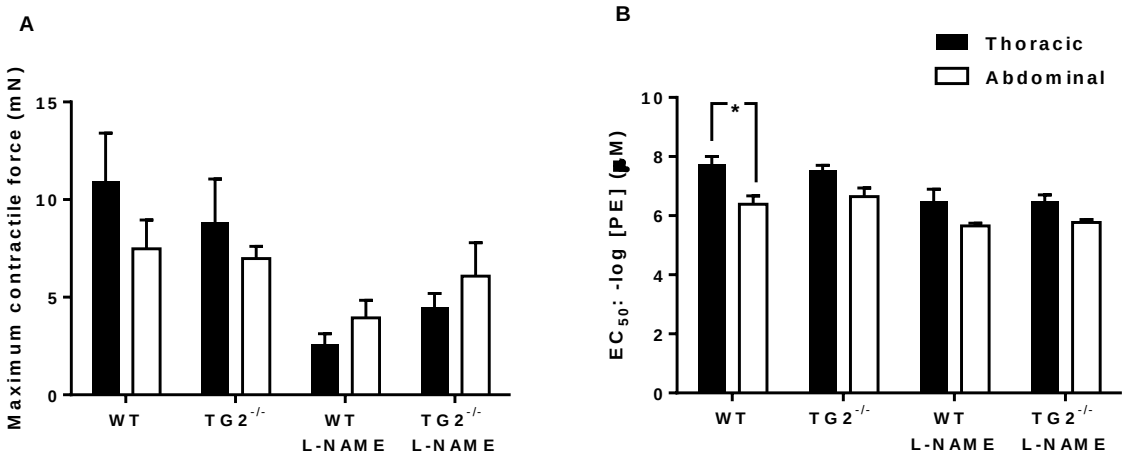

Figure 42: Maximum force of contraction to PE (A) and EC_{50} values (B) for rings taken from the thoracic and abdominal aortas. *p<0.05

5.2.5.2 Smooth muscle cell relaxation

There were no impairments in endothelium-independent relaxation to SNP in any of the four groups studied whether rings were isolated from the thoracic (Figure 43) or abdominal aorta (Figure 44). There was a small but significant reduction in the EC_{50} values of the L-NAME administered animals indicating slightly reduced sensitivity. This is also reflected by the small shift to the right of the dose-response curves from the L-NAME administered animals compared to untreated controls.

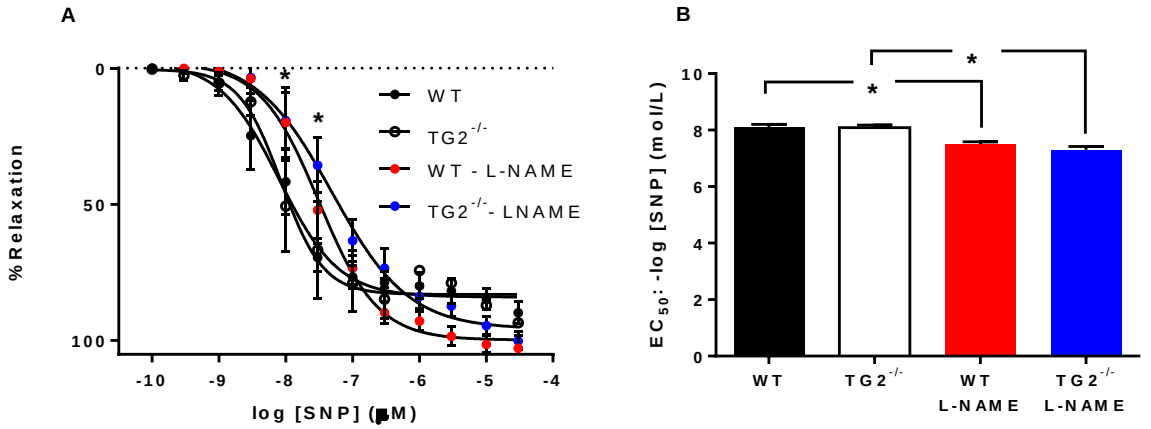

Figure 43: Relaxation response to SNP (A) and EC50 values (B) in the thoracic aorta of L-NAME treated and untreated TG2-/- and WT mice. The curves from the L-NAME treated animals were slightly shifted to the right; however, there were no differences in maximal response to SNP, *P<0.05 for untreated versus L-NAME treated TG2-/- mice only in graph A. The EC50 values were reduced in L-NAME treated animals compared to control *P<0.05 as indicated in graph B. In both graphs no strain differences were observed.

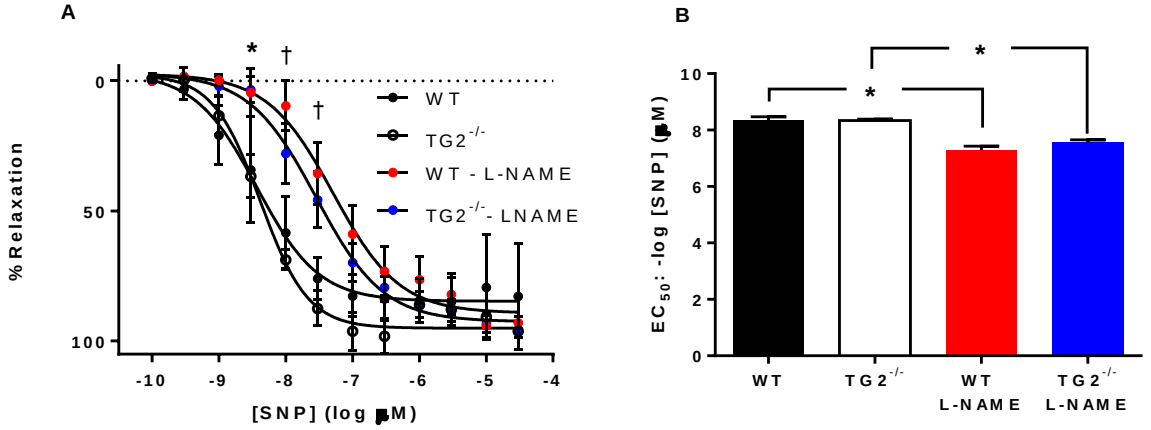

Figure 44: Relaxation response to SNP (A) and EC50 values (B) in the abdominal aorta of L-NAME treated and untreated TG2-/- and WT mice. The curves from the L-NAME treated animals were slightly shifted to the right; however, there were no differences in maximal response to SNP, *P<0.05 for untreated versus L-NAME treated TG2-/- mice only, †P<0.05 for both WT and TG2-/- treated versus untreated mice in graph A. The EC50 values were reduced in L-NAME treated animals compared to control *P<0.05 as indicated in graph B. There were no differences observed between WT and TG2-/- mice (both control and L-NAME treated).

There were no differences observed between the thoracic and abdominal aortic rings regarding responses to SNP (Figure 45).

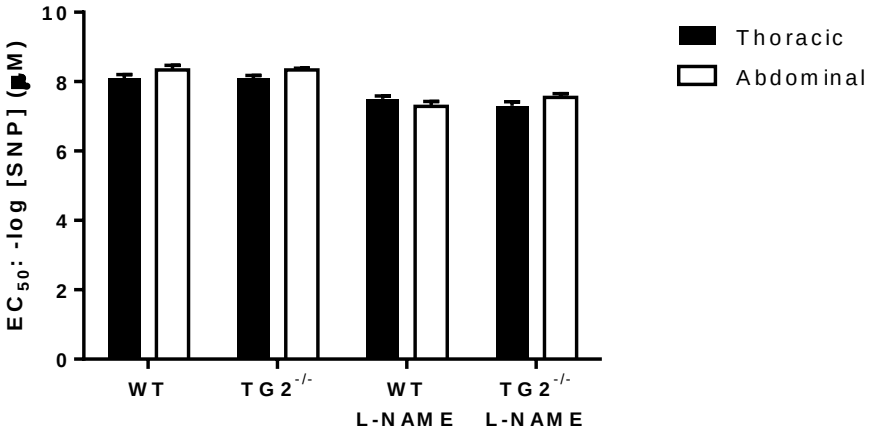

Figure 45: EC50 values from the thoracic and abdominal aortas. No differences were observed.

5.2.5.3 Endothelium-dependent relaxation

Relaxation responses to ACh were examined. There was no attenuation of the maximum relaxation response between untreated and L-NAME-treated WT and $TG2^{-/-}$ mice in both the thoracic and abdominal aortic rings. However, L-NAME treatment significantly impaired the relaxation in the thoracic aortas of WT mice compared to untreated controls (-13.45 ± 30.69 vs. 51.39 ± 7.13 %) and in the abdominal aortas of WT and $TG2^{-/-}$ mice compared to untreated controls (-10.98 ± 6.73 vs. 62.25 ± 16.96 and -12.11 ± 10.23 vs. 52.24 ± 18.02 % respectively; Figure 46).

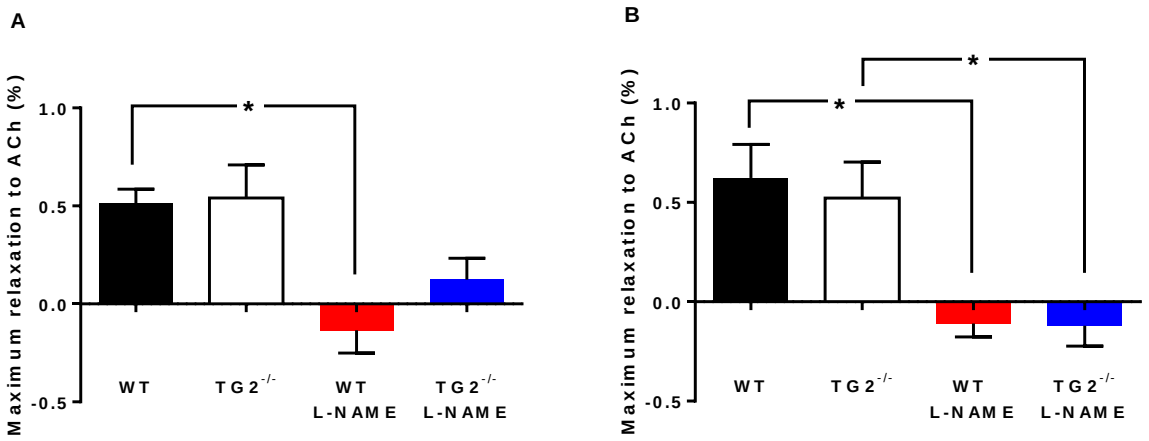

Figure 46: Maximum relaxation to ACh in thoracic (A) and abdominal (B) segments isolated from the four different mice groups. Treatment with L-NAME impaired the endothelium-dependent response significantly only in the thoracic sections from the WT mice, and in the abdominal sections from both WT and $TG2^{-/-}$ mice; however, there was a similar trend in untreated $TG2^{-/-}$ mice as well. *P<0.05.

The relaxation-response curves to ACh in thoracic aortic rings were not different between WT and $TG2^{-/-}$ mice (Figure 47A). L-NAME treatment severely impaired endothelium dependent relaxation in both strains of mice. The only difference observed between WT and $TG2^{-/-}$ mice treated with L-NAME was at the highest dose of ACh. While there was a significant difference observed in the EC_{50} of WT and $TG2^{-/-}$ given L-NAME, the WT animals in this case showed constriction as opposed to relaxation, therefore, this comparison cannot actually be made (Figure 47B).

In abdominal aortic rings, no strain differences were observed in the dose-response curve for control or L-NAME treated mice (Figure 48A). L-NAME treatment completely abolished endothelium-dependent relaxation in both mice strains. The EC_{50} values were not different between strains and cannot be compared between L-NAME treated and untreated animals as the L-NAME treated rings constricted where as control rings relaxed (Figure 48B).

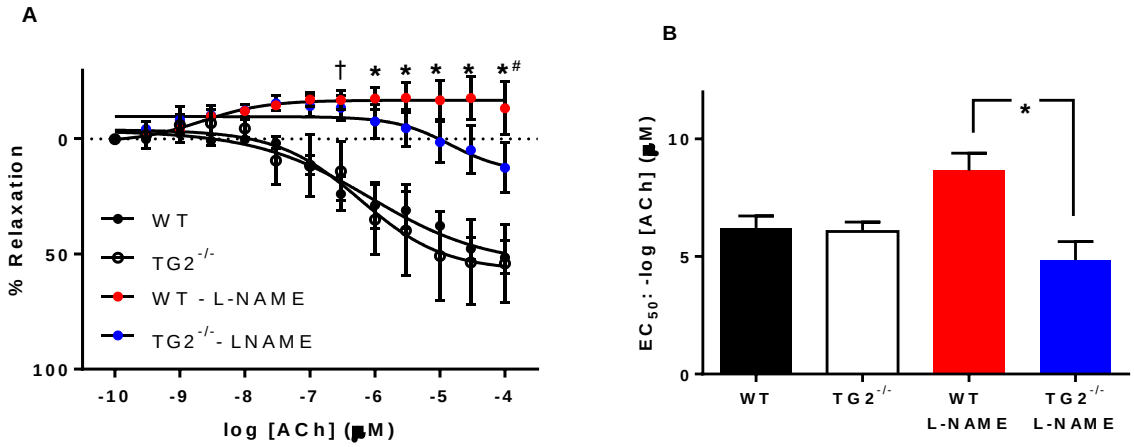

Figure 47: Relaxation response to ACh (A) and EC50 values (B) in the thoracic aorta of L-NAME treated and untreated TG2$^{-/-}$ and WT mice. There were no differences observed between control WT and TG2$^{-/-}$ animals. The curves from the L-NAME treated animals were shifted to the right and in both strains of mice, the relaxation response was severely impaired, †P<0.05 for untreated versus L-NAME treated WT mice only, *P<0.05 for untreated versus L-NAME treated WT and TG2$^{-/-}$ mice, #P<0.05 for L-NAME-treated WT versus TG2-/- mice in graph A. The EC_{50} values were significantly different between L-NAME treated WT and TG2$^{-/-}$ mice *P<0.05 as indicated in graph B.

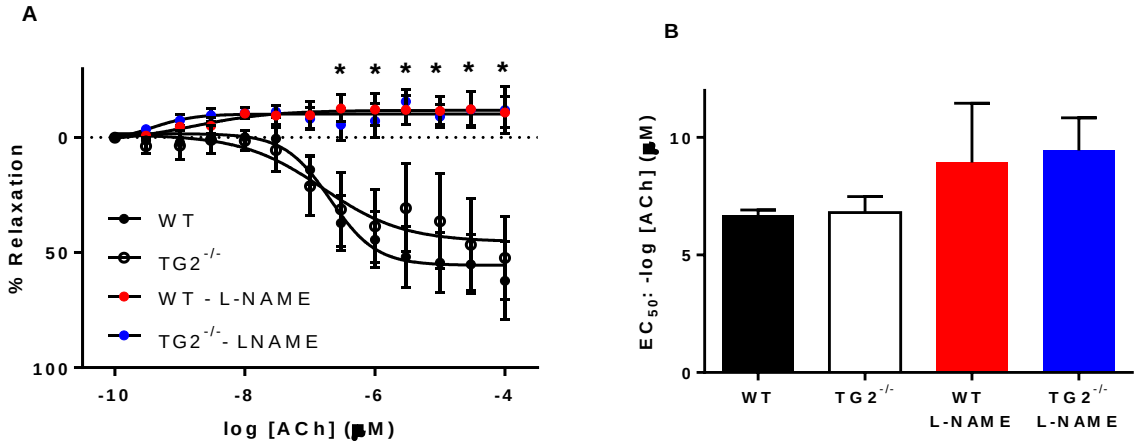

Figure 48: Relaxation response to ACh (A) and EC50 values (B) in the thoracic aorta of L-NAME treated and untreated TG2$^{-/-}$ and WT mice. There were no differences observed between control WT and TG2$^{-/-}$ animals. In both strains of mice, the relaxation response was severely impaired in L-NAME treated animals, *P<0.05 for untreated versus L-NAME treated WT and TG2$^{-/-}$ mice in graph A. The EC_{50} values were not significantly different between any of the 4 groups.

There were almost no differences detected between aortic rings from the thoracic aorta versus those taken from the abdominal aorta regarding responses to ACh. The maximum relaxation to ACh was not statistically different between thoracic and abdominal sections. The only

difference observed was in the EC_{50} values for $TG2^{-/-}$ mice treated with L-NAME, which are not comparable as previously mentioned (Figure 49).

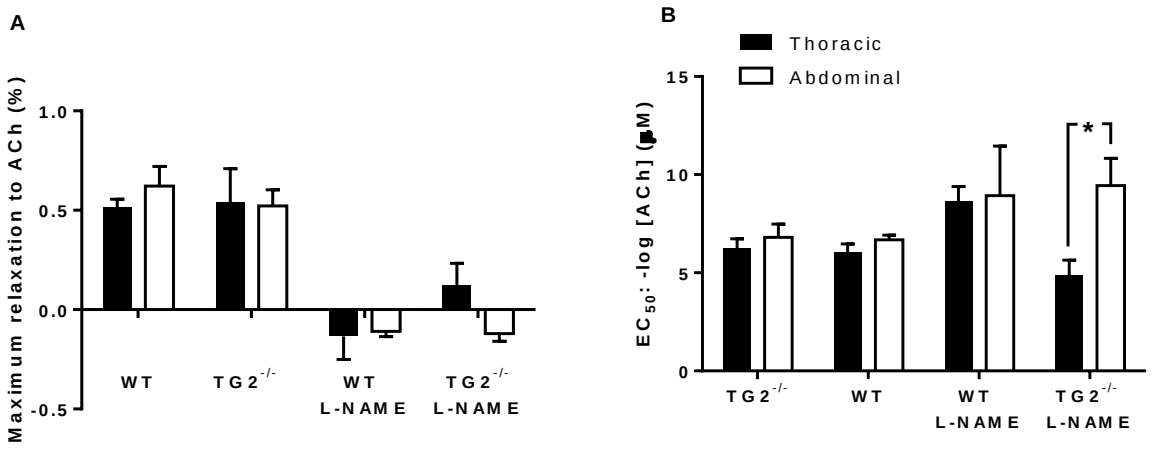

Figure 49: Maximum relaxation to ACh (expressed as a percentage of complete relaxation) (A) and EC50 values (B) for rings taken from the thoracic and abdominal aortas. *p<0.05.

5.2.6 Calcification Assay

There were no statistically significant differences between calcium levels in the aortas of any of the four groups studied (Figure 50), although there was a slight trend towards decreased levels of calcium in the L-NAME treated groups.

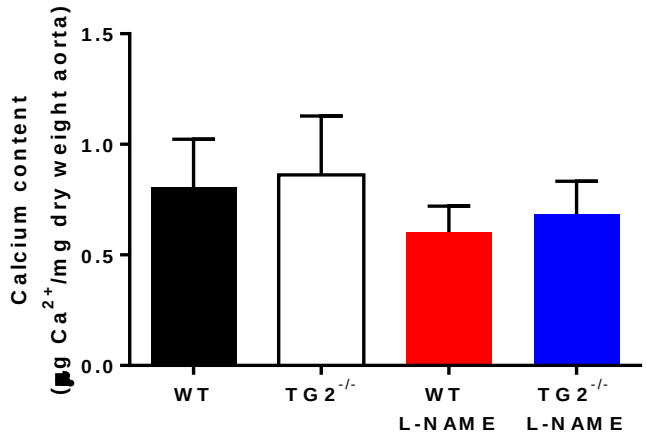

Figure 50: Aortic calcium content. There were no significant differences between any groups examined.

5.2.7 Histology

Neither the media-to-lumen ratio nor the medial thickness of the thoracic aorta were different between any of the 4 groups examined (Figure 51 and Figure 52).

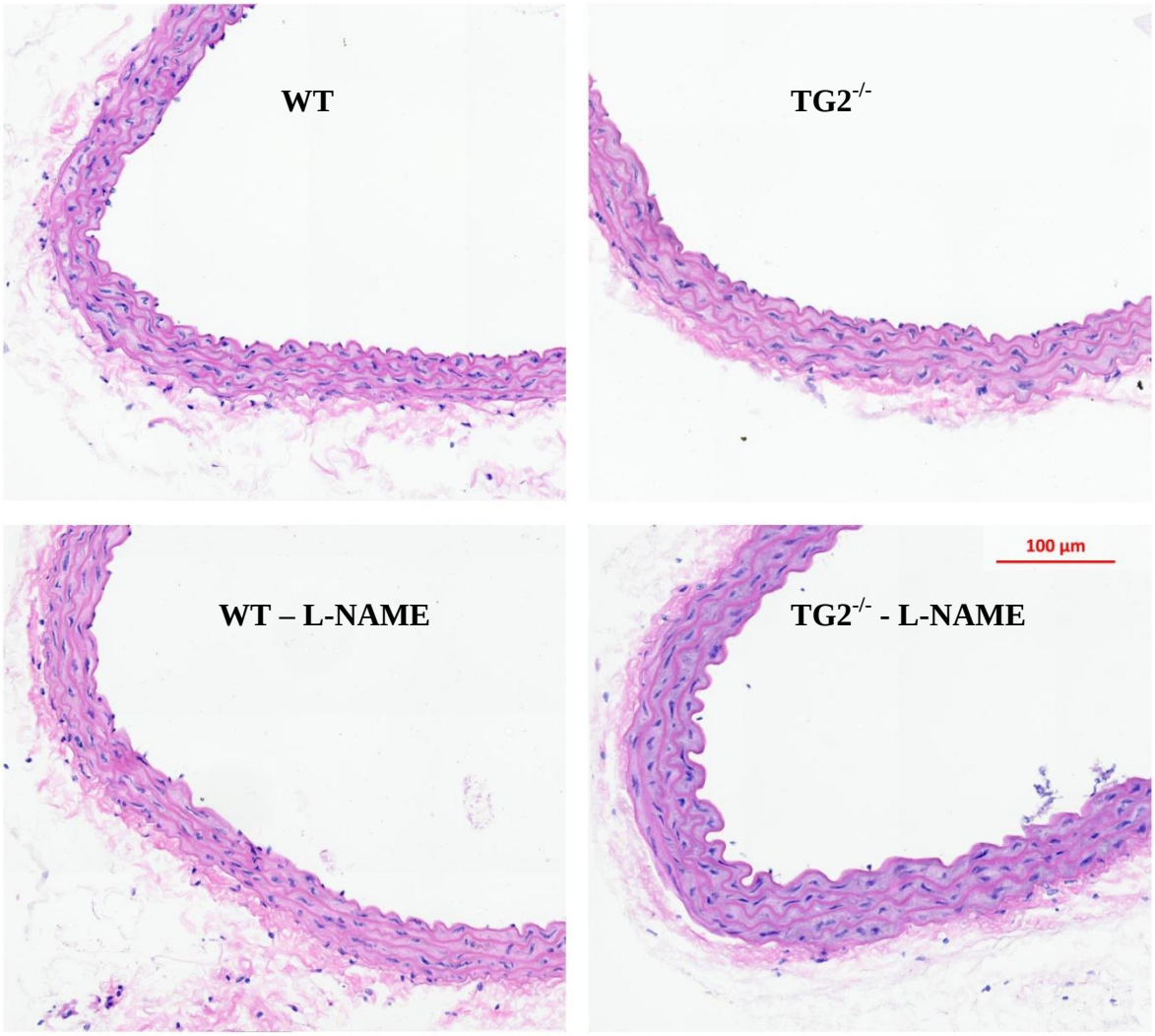

Figure 51: Representative images of histological cross-sections of thoracic aorta stained with H&E from control and L-NAME treated WT and $TG2^{-/-}$ mice. Bar: 100µm.

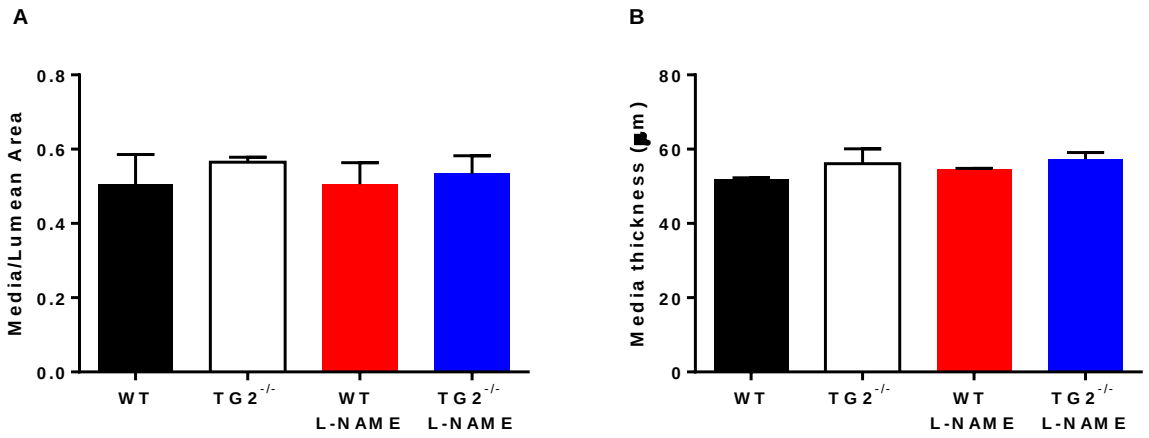

Figure 52: The media-to-lumen ratio (A) and the medial thickness (B) of the thoracic aortas from control and L-NAME treated WT and $TG2^{-/-}$ mice. No significant differences were detected.

5.3 Discussion

TG2 knockout mice did not show any abnormal cardiovascular phenotype when compared to WT controls at baseline values. This is consistent with previous studies showing no obvious abnormal phenotype in the $TG2^{-/-}$ mouse (129). It has been specifically demonstrated that TG2 knockout animals show no difference in blood pressure or heart rate when compared to WT controls (151). Baseline values of PWV as measured by Doppler ultrasound have also shown no differences in PWV between WT and $TG2^{-/-}$ animals (16). Furthermore, under normal conditions, levels of TG2 activity remain low as it is a tissue injury response molecule. In fact, a characteristic of many inflammatory diseases is an increase in TG2 expression (129). When challenged, knockout mice have shown delayed vascular remodelling responses to hypertension and reduced blood flow (122). This suggests that $TG2^{-/-}$ animals may demonstrate a different cardiovascular phenotype under stressed conditions.

In addition, it is hypothesized that there is a degree of redundancy among the TG family. Johnson et al demonstrated TG2-independent TG activity in both the aorta and vena cava. They were also able to show the expression of both TG1 and TG4 in these tissues. Using biotin-pentylamide incorporation assay, TG activity was found to be similar in WT and $TG2^{-/-}$

mice (201). Compensation by the other TGs could partly explain the similarity in cardiovascular parameters in $TG2^{-/-}$ and WT mice. Plasma factor XIII is highly expressed in $TG2^{-/-}$ mice and presents a potential mechanism accounting for the loss of TG2 activity (150).

However, when considering PWV-MAP relationship, the WT mice begin to have significantly higher PWV compared to $TG2^{-/-}$ at MAPs above 126 mmHg. At higher pressures, the stress imparted on the vessel wall is taken up by the collagen fibres. As collagen is a substrate for TG2, then it is fitting that differences between the two strains are apparent in pressure ranges where collagen is being recruited.

L-NAME treatment did not affect any of the baseline cardiovascular parameters measured. Treatment with L-NAME appeared to slightly lower pressure-dependent PWV in both the $TG2^{-/-}$ and WT mice, although there was no significant differences between treated and untreated groups or between treated WT and TG2 knockout animals. This was not entirely expected as reduced NO bioavailability, induced by NOS inhibition, is generally associated with increased MAP and large artery stiffness (28, 31, 43, 115). It has also been found that $TG2^{-/-}$ mice treated with L-NAME have significantly lower PWV, measured noninvasively with Doppler methods, than treated WT controls (16). However, while a study by Pistea and colleagues did show that L-NAME treatment increased blood pressure within one week of treatment, there were no differences found between WT and $TG2^{-/-}$ mice (127). Additionally, Fitch et al found that L-NAME treatment given in the drinking water (0.5g/L) for 28 days did not affect aortic stiffness measured both *in vivo* and *ex vivo*, blood pressure, collagen-to-elastin ratio, or lumen cross-sectional area in the WT mouse aorta (45). NOS-inhibition has also been shown to significantly increase arterial compliance without any changes in blood pressure or arterial geometry (116). From the present results and those of other investigators, it is postulated that there is a compensatory mechanism at play over short term NOS-inhibition that could account for the observed effects.

Prostacyclin is another potent hypotensive agent and vasodilator produced by the endothelium (202). It is possible that prostacyclin activity may be enhanced in the absence of NO. Indeed, an *in vitro* study by Osanai and colleagues demonstrated an inhibitory effect of NO on prostacyclin production under shear stress and an increase in prostacyclin production when NO production is inhibited (203). Inhibition of NOS in swine results in increased vasodilation due to prostacyclin in systemic vascular beds (204). Puybasset et al have shown that in the coronary circulation in dogs, prostacyclin production via the cyclooxygenase pathway is increased in response to NOS inhibition by L-NNA (205). Increased release of prostacyclin has also been shown to maintain a nearly normal flow-induced dilation in the arterioles of $eNOS^{-/-}$ mice (206). Collectively, these studies indicate that prostacyclin is likely to play a backup role when NO bioavailability is reduced. This may explain partially why L-NAME did not produce increases in blood pressure and aortic PWV.

EDHF provides an alternative pathway to vascular relaxation via VSMC hyperpolarization (207). Various substances can act as EDHF. Epoxyeicostrienoic acids (EETs) are an important class of EDHF that are produced by cytochrome P_{450}, an enzyme expressed in endothelial cells which have been shown to produce NO- and prostacyclin-independent relaxation in various arterial beds. Studies have shown that hydrogen peroxide can also act as an EDHF in certain vessels *in vivo*, although it is unclear whether this is physiologically significant (102). Studies in isolated vessel segments have found that endothelium-dependent relaxation can often be resistant to NOS inhibitors, likely due to increased EDHF responses (208-210). This suggests that EDHF may compensate when there is a reduced bioavailability of NO. The *in vivo* importance of EDHF is still highly unknown and the precise mechanisms regulating its activity still have yet to be elucidated, and can vary between vascular beds (117); however, it has been demonstrated *ex vivo* that EDHF plays a greater role in vasodilatation as vessel diameter decreases (211). This may explain in part why L-NAME treatment did not induce an increase in mean blood pressure. The smaller resistance arteries

where EDHF assumes greater importance are the vessels which determine MAP. The lack of increased pressure may also account for the lack of changes in large artery stiffness when mice were treated with L-NAME. The hyperpolarization induced by EDHF may also spread along the artery wall. So while EDHF may be produced in smaller arteries, it's relaxing effects may be realised in distant locations (212). Furthermore, the fact that the postulated role of EDHF is minimal in the large arteries may explain why the aortic rings did not show resistance to NOS inhibition in vascular reactivity experiments. This explanation is supported by findings from Waldron et al in which relaxation of aortas to ACh from $eNOS^{-/-}$ mice was completely abolished (213). Conversely, in femoral and mesenteric arteries of $eNOS^{-/-}$ mice, vasorelaxation occurred, mediated by EDHF. Regarding the vascular reactivity results, when arteries are maximally constricted, the influence of EDHF may be blocked (212). While the endothelium-dependent relaxation-response experiments were theoretically performed under submaximal constriction (~80%), each vessel is different and the level of pre-constriction may have been great enough to diminish the potential effects of EDHF.

There are also limitations to the L-NAME treatment method used. First, it is difficult to know how much of the L-NAME is absorbed by the animal when given in the drinking water. It would be better to administer a dosage of L-NAME based on the weight of the mouse and daily intake of water. As they are housed in groups of 4, this is very difficult to accurately measure. Secondly, it is not clear if the duration of the treatment is long enough. Although studies have reported changes in PWV with NOS-inhibition as early as 3 days post treatment (115), two weeks of treatment has been shown not to be sufficiently long to induce high levels of vascular remodelling (43). As TG2 is known to play a role in arterial remodelling (122), the effects of L-NAME might become more apparent over a longer treatment period. L-NAME may have other non-specific effects which could render it a poor choice for NOS-inhibition (214), although this seems unlikely in this case, as several aforementioned studies have used L-NAME to induce changes in PWV. Finally, it is known that anaesthesia can have

depressive effects on the cardiovascular system (215). As all measurements were made in the anaesthetized mouse, some of the effects of L-NAME on the measured parameters may have been masked. However, isoflurane was used at a modest level which has been shown to have fewer systemic hemodynamic effects, including MAP and HR, compared to other forms of anaesthesia (47, 216).

Tensile testing of thoracic aortic rings showed a non-significant increase in the incremental modulus of elasticity in WT mice compared to $TG2^{-/-}$ and a non-significant decrease in L-NAME treated mice compared to controls. This *ex vivo* measure of passive stiffness agrees well with the *in vivo* functional stiffness measured by PWV. The rings were only stretched to a force equivalent to 100 mmHg, which may account for the lack of significance. Future experiments should stretch the rings to equivalent pressures where differences in PWV were observed (~126mm Hg) to see whether changes in the material stiffness of the vessel wall are translated to functional alterations in PWV.

The PWV-MAP relationships for all four groups could be described by a second order polynomial (R^2>0.99), indicating that pressure sensitivity of PWV increases linearly with pressure. However, the pressure sensitivity was not significantly different between any of the groups. This means that the changes in PWV per mmHg rise in MAP is similar in all four groups of mice.

There are possibilities for changes in baroreflex sensitivity when changes occur in the mechanical properties, such as distensibility, of barosensitive regions, as this may alter the level of stretch the baroreceptors undergo with changes in pressure. Baroreflex sensitivity was not different between any of the groups examined, although there was a trend towards decreased sensitivity in the L-NAME treated groups.

In healthy arteries, there is an amplification of pulse pressure between proximal and distal sites along the aorta. In this study, the relationship between PPA and MAP was very similar

as that described in Chapter 4. At mean pressures above 80 mmHg, there was essentially no PPA (~ 1) and it fell quite rapidly with mean pressure below 80 mmHg. There were no significant differences in this relationship between any of the groups observed. However, there was a slight trend towards increased PPA for $TG2^{-/-}$ mice compared to WT that was diminished when both groups were treated with L-NAME. Again, L-NAME treatment, while not significant, seemed to have a positive effect of increasing PPA.

TG2 has many functions aside from its cross-linking activity; for example, it is involved in G protein signalling via α_{1B}/ α_{1D} adrenergic receptors (129). In addition to modulating its cross-linking activity, evidence in the literature has also suggested the interaction between NO and TG2 may regulate its ability to activate TGFβ-1, which is a cytokine involved in fibrosis, tissue scarring, and many cellular functions, including apoptosis (137). Furthermore, the cells comprising the vasculature are very responsive to their local hemodynamic environment, which in turn is influenced by the mechanical properties of the arteries. This led to investigations of potential differences in both smooth muscle and endothelial cell function between aortic rings taken from WT and $TG2^{-/-}$ mice by assessing vascular responses to PE, SNP, and ACh.

The maximum force of contraction in response to PE tended towards being reduced in L-NAME treated animals, although this only reached statistical significance in rings taken from the thoracic aortas of WT mice. Fitch et al also observed similar reductions in maximum contractile response to PE in L-NAME treated animals (45). L-NAME treatment also slightly shifted the dose-response curves to the right in both WT and $TG2^{-/-}$ mice, indicating a reduced sensitivity to PE. This is further demonstrated by the reduced EC_{50} values calculated from the dose-response curves in L-NAME treated animals, although this was only significant in the abdominal aortic rings of $TG2^{-/-}$. Taken together, these results show that the presence or

absence of TG2 does not affect the contractile response to PE, even after L-NAME treatment, which slightly impaired PE responses in both mouse strains.

Similarly, no differences were observed in the dose-response curves or EC_{50}s between WT and $TG2^{-/-}$ mice. L-NAME treatment slightly shifted the dose-response curves to the right and reduced EC_{50} values, lowering sensitivity to SNP in both strains. However, both thoracic and abdominal aortic rings from all four groups were able to achieve complete endothelium-independent relaxation, indicating that TG2 does not influence smooth muscle cell relaxation responses to SNP.

Endothelium-dependent responses to ACh were severely impaired in all four groups of mice. It is uncertain why this is the case. It is likely related to the fact that these aortic rings were removed post-surgery, which involved both the insertion of a catheter fully into the aorta and the infusion of blood-pressure altering drugs, in addition to being under anaesthetic for approximately one hour. The entire procedure may disturb the endothelial layer. This would be a useful investigation to undertake in the future. Regardless, from the data presented in this chapter, it also appears that TG2 does not affect the relaxation response to ACh. In untreated mice, there were no differences in the maximum relaxation, the dose-response curves, or the EC_{50} values between WT and $TG2^{-/-}$ in both the thoracic and abdominal aortas. L-NAME treatment completely abolished the relaxation response in all animals. In some cases, the vessels even underwent constriction. The only difference observed between WT and $TG2^{-/-}$ animals was a greater reduction in the maximum relaxation in WT mice treated with L-NAME compared to control than in the L-NAME treated $TG2^{-/-}$ mice. However, this only occurred in the thoracic aorta, and in both cases, there was no relaxation response. Consequently, based on these observations, $TG2^{-/-}$ does not affect endothelium-dependent relaxation. Given the similar level of endothelial dysfunction in all groups, it is not possible to

make definitive conclusions regarding the downstream effects of TG2 on arterial stiffness under a range of factors affecting endothelial function.

Taken together, the *ex-vivo* myography studies show that there were no strain differences in the responses to PE, SNP, or ACh. This was not surprising as $TG2^{-/-}$ has not been previously reported to affect vascular reactivity. Furthermore, as both WT and $TG2^{-/-}$ mice were young and healthy and there were no very strong differences in any of the other parameters that were studied, it seemed unlikely that there would be strong strain differences in the myograph experiments.

The amount of calcium in the aorta was also not different between any of the groups studied. While it has been shown that TG2 has a potential role in arterial calcification (164), it has not yet been demonstrated *in vivo* that TG2 activity causes increased aortic calcification. The mice used in this study were quite young and healthy which could account for the lack of differences seen between the strains. On the other hand, this observation also highlights the importance of validating findings from *in vitro* studies in *ex vivo* experiments and in quantifying if there are any functional consequences in *in vivo* parameters. TG2 activity is increased in inflammation and aging. While it was attempted to induce inflammation by L-NAME treatment, this evidently did not have the hypothesized effect on cardiovascular function. Therefore, it would be of interest to examine calcification in aged $TG2^{-/-}$ mice or under a stronger inflammatory influence.

Staining with H&E yielded no gross morphological changes, and no statistical differences in the media-to-lumen ratio or the medial thickness between any of the groups examined. As $TG2^{-/-}$ has been shown to play an important role in small artery remodelling (122), it was thought that there may be changes in these parameters in the aorta. However, the process of arterial remodelling requires a sustained stimulus, such as increased blood pressure. This did not occur in any of the groups examined, which may explain the lack of changes in the aorta.

From the evidence presented in this Chapter, it can be concluded that $TG2^{-/-}$ does not strongly influence vascular function in young, healthy mice, even when treated with a NOS inhibitor. There was a small but significant decrease in PWV in $TG2^{-/-}$ mice compared to WT control at pressure above 126 mmHg. As no differences in baseline parameters were observed, vascular reactivity or calcification, it is likely that this difference is due to increased TG2 crosslinking of collagen which only becomes apparent at high pressures, as it has previously been shown that there are increased TG2 crosslinks in WT animals compared to control (16). It is known that NO regulates TG2 activity *in vitro* in vascular cells, such that improved vascular function was expected in $TG2^{-/-}$ mice compared to WT control after NOS inhibition. However, this was not the case. This lack of effect of NOS inhibition may be due to inadequate treatment dose or duration, compensatory mechanisms which account for the loss of NO bioavailability, or perhaps, NO does not mediate its noted detrimental vascular effects primarily through TG2. Or, if it does, the effect may be overshadowed by the multitude of other downstream effects that NOS inhibition produces. TG2 is a tissue injury response molecule, with latent activity that is only likely apparent under extreme conditions. It is a possibility that the effects, if any, that deletion of TG2 has on the cardiovascular system in these mice are simply not pronounced enough to have induced functional changes in large artery pressure or stiffness as is sensed using the high fidelity method developed in Chapter 3. Another possibility is that TG2 activity only affects cardiovascular functions in pathological conditions more severe than what have been investigated in this set of experiments.

Chapter 6

Transglutaminase 2 and arterial stiffness: effect of increased duration of NOS inhibition

Chapter 5 presented data regarding cardiovascular function in $TG2^{-/-}$ mice compared to WT controls with and without L-NAME treatment administered in the drinking water. As TG2 is an inflammatory molecule, its activity is likely held latent under normal conditions. This was supported by the observation that only minor differences were found between the two strains of mice. NOS inhibition using L-NAME produced essentially no effect on many of the parameters examined. In fact, it appeared that L-NAME was tending to produce beneficial effects in many cases, which was opposite to the hypothesized result. In order to confirm and investigate this finding, the study was repeated with a longer duration and a more direct route of L-NAME administration.

6.1 Methods

6.1.1 Animals

Male $TG2^{-/-}$ and WT mice, aged 16 weeks were studied. Animals were kept in a temperature controlled environment (21 ± 2^{o}C) with 12 hour light/dark cycles. Animals had *ad libitum* access to standard laboratory mouse feed and water. The animal protocol was approved by the

Macquarie University Animal Ethics Committee and the Johns Hopkins University Animal Care and Use Committee (ARA 2011/017, MO13M258).

6.1.2 L-NAME treatment

Mice were divided into four study groups. Each mouse was implanted with an osmotic pump (1004, Alzet, Durect Corp, Cupertino, CA). Groups 1 and 2 ($TG2^{-/-}$ and WT, n=4) received pumps filled with vehicle control and groups 3 and 4 ($TG2^{-/-}$ and WT, n=6) received pumps filled with a 4-week dose of L-NAME (20mg/kg/day). At the end of the treatment period, conscious blood pressure was measured using an XBP1000 non-invasive tail blood pressure system (Kent Scientific Corporation).

6.1.3 Cardiac Function – Transthoracic echocardiography

Transthoracic echocardiography was performed in conscious mice using an ultrasound machine (Sequoia Acuson C256, Malvern, PA) equipped with a probe of frequency of 15 MHz. Two-dimensional (2-D), M-Mode echocardiograms were obtained in the parasternal short and long axis view of the left ventricle (LV) at the level of the papillary muscles and sweep speed of 200 mm/s.

From the images, four parameters were measured: *(i)* left ventricular posterior wall thickness at end diastole (LVPWD), *(ii)* interventricular septal thickness at end diastole (IVSD), *(iii)* left ventricle chamber diameter at end diastole (LVEDD), and *(iv)* left ventricle chamber diameter at end systole (LVESD). These measurements were performed according to the guidelines set by the American Echocardiography Society. Three to five values of each measurement were taken and averaged for each mouse. Fractional shortening (FS) was derived from the LVEDD and LVESD. This represents the percent change in LV chamber dimension with systolic contraction. FS provides an estimation of the LV wall contractility or systolic function (Equation 6.1).

$$FS(\%) = [\frac{LVEDD - LVESD}{LVEDD}] \times 100 \quad (6.1)$$

LV mass was estimated and used to indicate LV hypertrophy and enlargement (Equation 6.2, (217)).

$$LV\ mass(mg) = 1.055[(IVSD + LVEDD + PWTED)^3 - (LVEDD)^3] \quad (6.2)$$

where 1.055 is the specific gravity of the myocardium.

6.1.4 PWV Measurement

PWV was measured as described in Chapter 3. Briefly, mice were anaesthetised (induced at 4.5%, maintained at 1.5% isoflurane in oxygen) and spontaneously breathing through a nose cone during surgery and measurements. Temperature was maintained at 37^{o}C. ECG leads were placed subcutaneously to determine heart rate. A high fidelity, dual pressure sensor catheter was inserted into the aorta via the femoral artery MAP and beat-to-beat PWV. The jugular or femoral vein was cannulated for drug administration. MAP was increased by infusion of PE (10 μg/min) until pressure reached a plateau. Once MAP returned to baseline SNP was then used to lower blood pressure in the same manner. Baroreflex sensitivity and LV mass was also determined in the same manner as described in Chapter 5.

6.1.5 Histological analysis

Thoracic aortas from each mouse were isolated, fixed, processed, and stained with H&E as described in Section 5.1.8. Media-to-lumen ratio and medial thickness were then evaluated.

6.1.6 Statistical Analysis

Data are presented as mean ± standard error, except where indicated otherwise. Data were analysed offline using a combination of Microsoft Excel, IBM SPSS Statistics 19, and GraphPad Prism 6.

Data recorded across all pressure ranges were divided into 5 mmHg pressure bins. Statistical differences between groups were determined using either: paired Student's t-tests for each pressure bin or 2-way ANOVA followed by Sidak's multiple comparisons test (unless otherwise stated). Echocardiography results were analysed by 1-way ANOVA followed by Tukey's multiple comparisons test. P-values less than 0.05 were considered to be statistically significant.

6.2 Results

6.2.1 Baseline Characteristics

Conscious baseline values of blood pressure and HR measured using a tail cuff apparatus are shown in Table 9. $TG2^{-/-}$ mice had higher values of HR and lower values of MAP, SBP, DBP, and PP compared to WT mice. L-NAME treated $TG2^{-/-}$ mice had lower HR and higher MAP, SBP, DBP, and PP compared to untreated $TG2^{-/-}$ mice. They also had significantly lower PP compared to WT mice treated with L-NAME.

Table 9: Blood pressure and heart rate obtained from a tail-cuff apparatus. Data are presented as mean ± SD. *$p<0.05$ $TG2^{-/-}$ versus WT, †$p<0.05$ $TG2^{-/-}$ versus $TG2^{-/-}$ + L-NAME, #$p<0.05$ WT + L-NAME versus $TG2^{-/-}$ + L-NAME.

	WT	**$TG2^{-/-}$**	**WT – L-NAME**	**$TG2^{-/-}$ – L-NAME**
HR (bpm)	656 ± 46	704 ± 38*	675 ± 94	641 ± 56†
MAP (mmHg)	92 ± 6	82 ± 3*	91 ± 7	94 ± 4†
SBP (mmHg)	114 ± 8	98 ± 4*	113 ± 8	112 ± 5†
DBP (mmHg)	82 ± 6	75 ± 3*	81 ± 8	85 ± 4†
PP (mmHg)	31 ± 6	23 ± 2*	32 ± 6	26 ± 2†#

Invasive measurements showed that TG2 knockout mice had baseline parameters similar to their WT controls. They did not show an abnormal cardiovascular phenotype with no statistical differences between any of the *in vivo* cardiovascular parameters as shown in Table

10. Furthermore, animals treated with L-NAME showed no differences between strains or from the untreated groups. However, $TG2^{-/-}$ mice had lower body weight than WT. $TG2^{-/-}$ mice given vehicle and L-NAME had lower LV mass (normalized by BW) compared to untreated WT mice. WT mice given L-NAME also had smaller LV mass compared to untreated controls (this would therefore seem to be a contrary observation to the accepted notion that NOS inhibition presents a cardiovascular challenge).

Table 10: Baseline cardiovascular characteristics. Data are presented as mean ± SD. *p<0.05 with respect to WT animals. #p<0.05 with respect to $TG2^{-/-}$ animals. †p<0.05 with respect to WT – L-NAME treated animals.

	WT	**$TG2^{-/-}$**	**WT – L-NAME**	**$TG2^{-/-}$- LNAME**
BW (g)	34 ± 2	29 ± 2*†	35 ± 1	30 ± 2#†
HR (bpm)	477 ± 21	512 ± 36	465 ± 47	487 ± 43
MAP (mmHg)	88 ± 8	84 ± 7	91 ± 8	92 ± 4
SBP (mmHg)	107 ± 9	100 ± 8	110 ± 10	109 ± 5
DBP (mmHg)	70 ± 5	68 ± 6	76 ± 7	77 ± 3
PP (mmHg)	37 ± 5	31 ± 2	34 ± 3	32 ± 3
Max dP/dt ($mmHg \cdot s^{-1}$)	1221 ± 403	789 ± 57	1115 ± 273	776 ± 52
PWV (m/s)	3.22 ± 0.51	2.87 ± 0.07	3.03 ± 0.46	3.03 ± 0.12
LV/BW (mg/g)	440 ± 46	350 ± 23*	371 ± 31*	344 ± 38*

6.2.2 Cardiac function

Cardiac echocardiography demonstrated no differences in LVEDD, LVESD, EF, IVSD/LVPWD, or FS between any of the groups examined (Figure 53). In contrast, LV mass normalized to body mass was significantly greater in both untreated and L-NAME treated WT mice compared to $TG2^{-/-}$ mice (148.2 ± 11.1 versus 95.1 ± 6.7 and 142.0 ± 9.5 versus 97.5 ± 4.5 respectively). There was no treatment effect of L-NAME on this measurement (Figure 53). Representative echocardiography images from all four groups are shown in Figure 54.

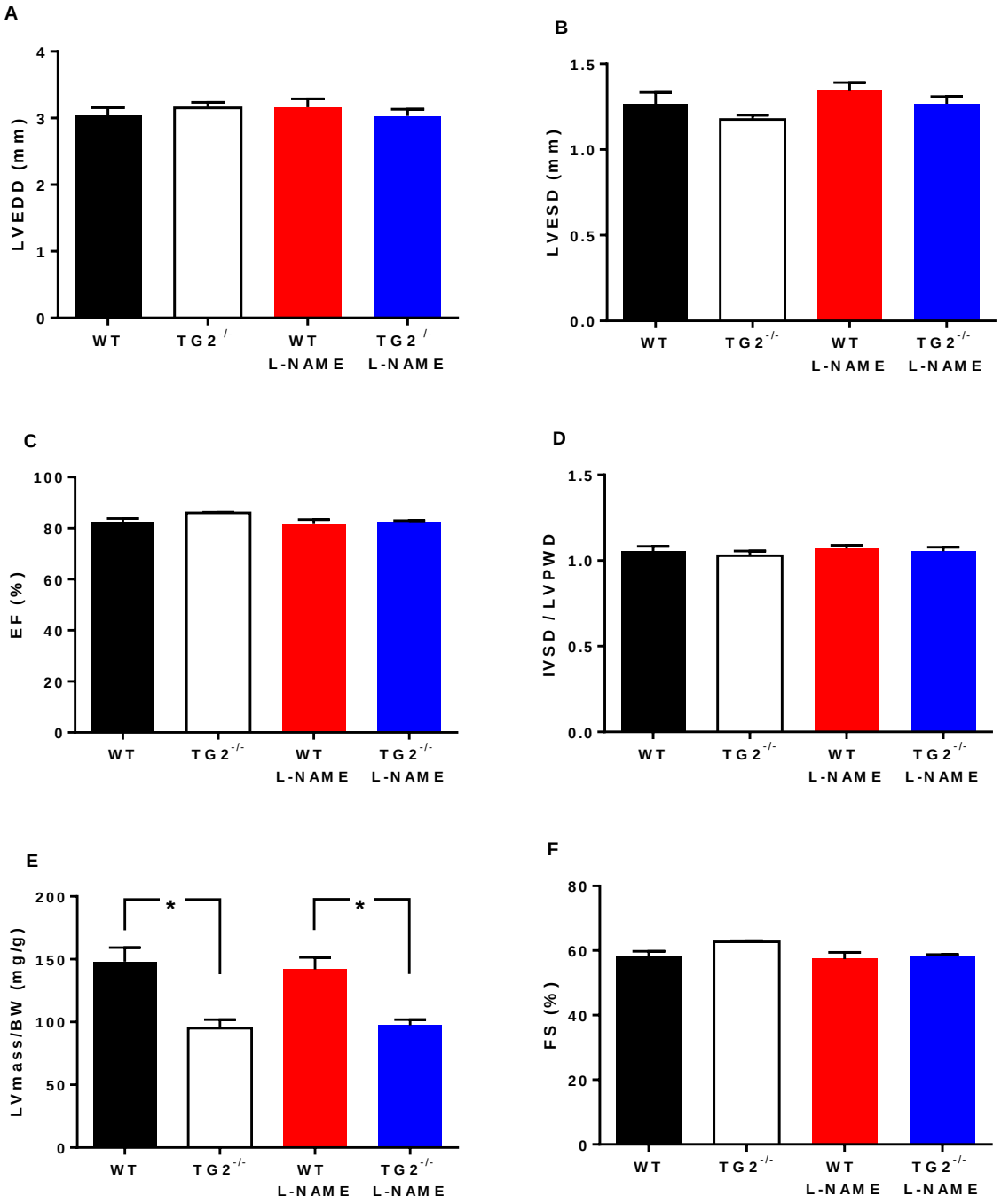

Figure 53: Graphical representation of parameters from echocardiography studies showing (A) left ventricle end diastolic diameter (LVEDD), (B) left ventricle end systolic diameter (LVESD), (C) ejection fraction (EF), (D) ratio of septal thickness (IVSD) and wall thickness (LVPWD), (E) left ventricular mass (LV mass), and fractional shortening (FS) in WT, $TG2^{-/-}$, WT + L-NAME, $TG2^{-/-}$+ L-NAME mice. *$p<0.05$.

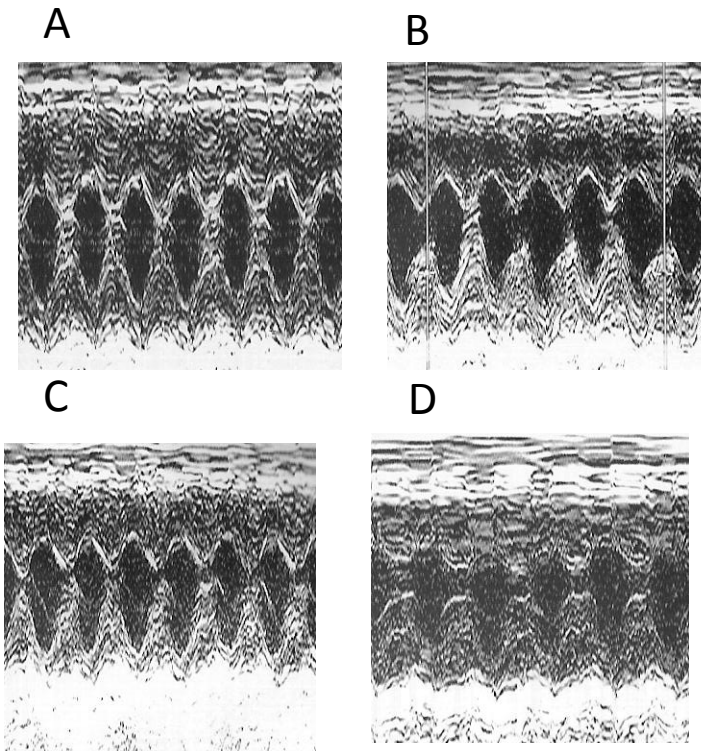

Figure 54: Representative m-mode echocardiography images from WT (A), WT + L-NAME (B), $TG2^{-/-}$ (C), and $TG2^{-/-}$ + L-NAME (D).

6.2.3 Pulse Wave Velocity

There were no statistically significant differences in PWV at any of the MAPs examined between $TG2^{-/-}$ mice and WT controls (Figure 55). This is at variance with data presented in Chapter 5 which showed that at higher MAP, $TG2^{-/-}$ mice have lower PWV. It is important to note that there were almost no significant differences in PWV between the measurements obtained at Johns Hopkins University (presented in this Chapter) and those from Macquarie University (shown in Chapter 5). A comparison can be seen in Appendix A3.

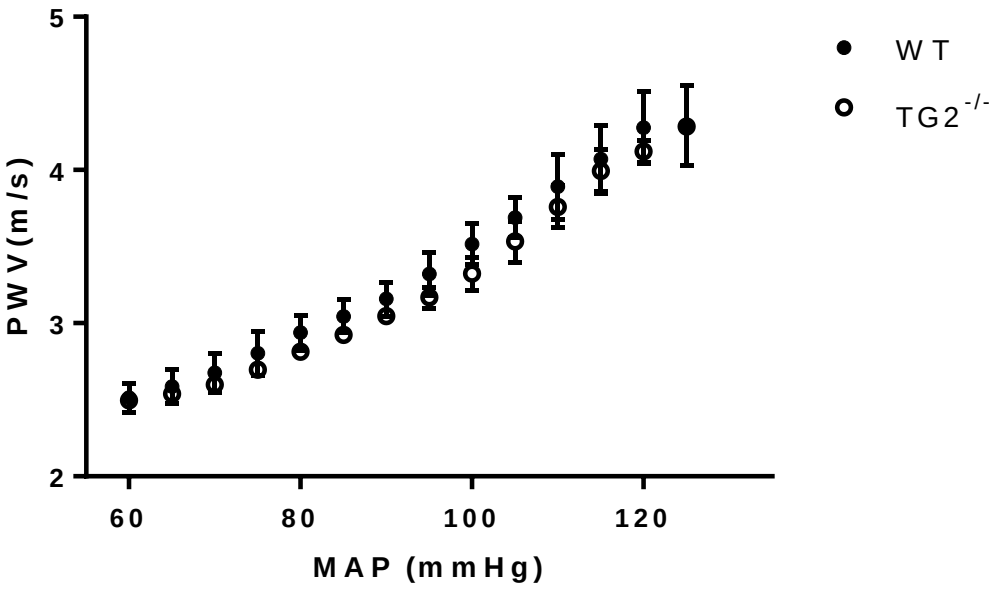

Figure 55: PWV is not different between WT and $TG2^{-/-}$ mice at any given MAP.

Figures 56 to 58 present the effect of L-NAME on the pressure-dependent PWV curves in WT and $TG2^{-/-}$ animals. There were no significant differences between treated and untreated animals and no strain differences in the PWV-MAP curves.

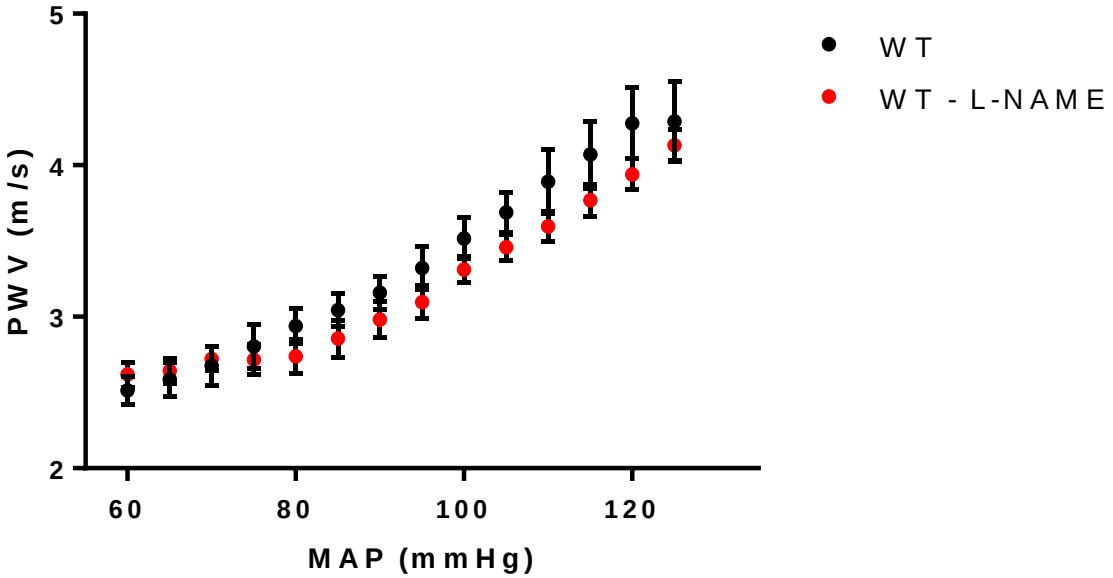

Figure 56: PWV-MAP relationship between L-NAME treated and untreated WT mice. There were no statistically significant differences between groups.

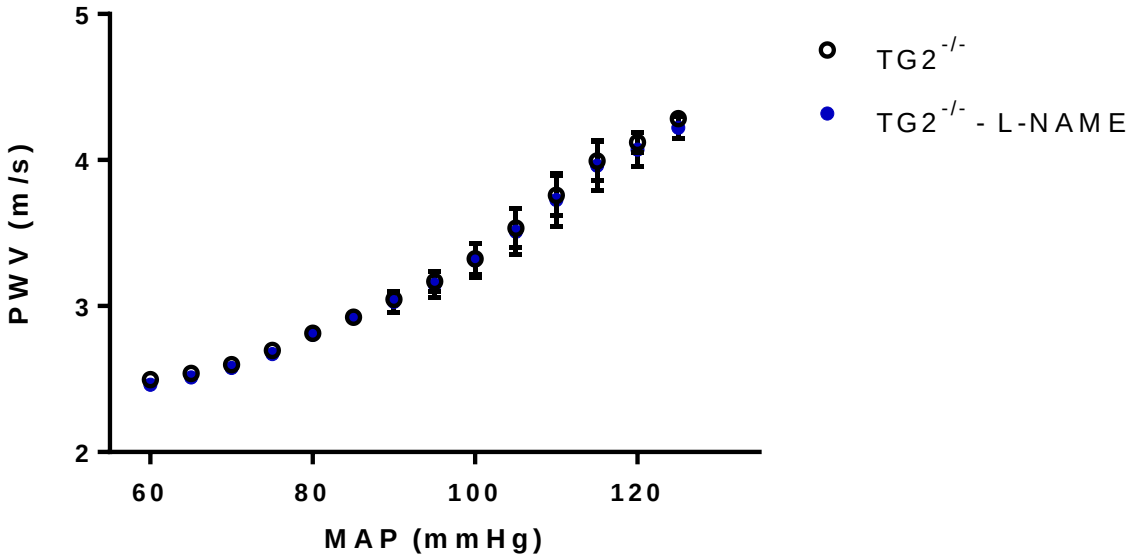

Figure 57: PWV-MAP relationship for TG2$^{-/-}$ mice. L-NAME had no effect on the pressure-dependent PWV.

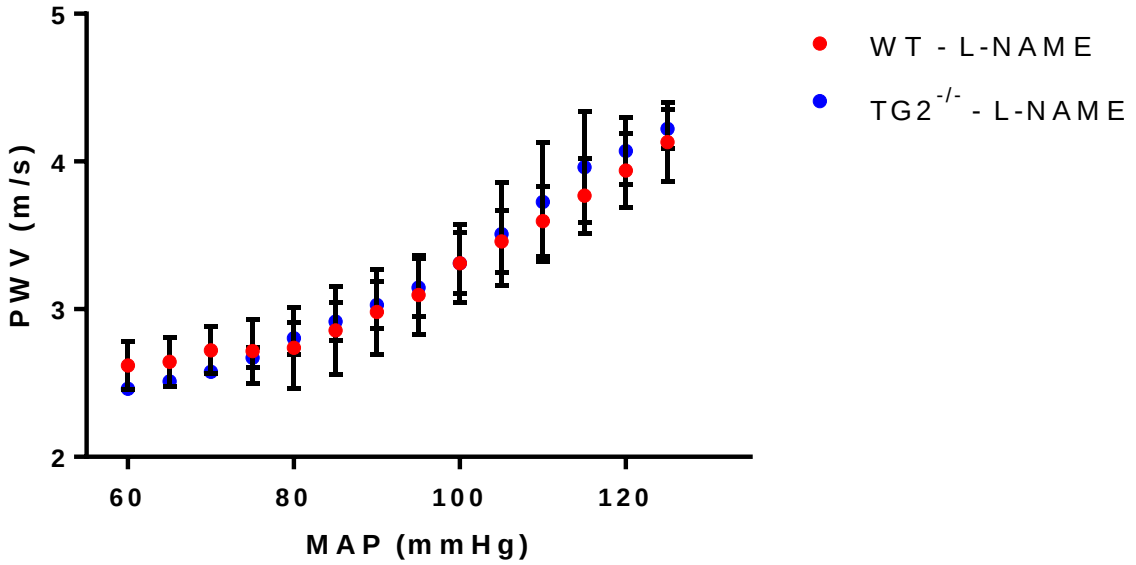

Figure 58: There were no differences in the PWV-MAP relationship between WT and TG2$^{-/-}$ mice treated with L-NAME.

Quadratic equations could be used to describe the PWV-MAP relationship for all strains (Table 11), indicating that the pressure sensitivity of PWV increased linearly with MAP. As can be seen in Figure 59, pressure sensitivity was not different between any of the strains at low (60 mmHg) and medium (90 mmHg). However, at high (120 mmHg) MAP, WT mice

treated with L-NAME had significantly lower pressure sensitivity compared to treated and untreated TG2$^{-/-}$ mice (0.037 ± 0.003 versus 0.052 ± 0.005 and 0.053 ± 0.005 m/s/mmHg respectively).

Table 11: PWV-MAP relationships are described by a quadratic equation.

	Quadratic equation	R^2
WT	$PWV = 1.889 + 0.00050(MAP) + 0.0001569(MAP)^2$	0.9946
TG2$^{-/-}$	$PWV = 2.794 - 0.02167(MAP) + 0.0002729(MAP)^2$	0.9966
WT – L-NAME	$PWV = 3.521 - 0.03405(MAP) + 0.0003138(MAP)^2$	0.9948
TG2$^{-/-}$ – LNAME	$PWV = 2.520 - 0.01567(MAP) + 0.0002385(MAP)^2$	0.9963

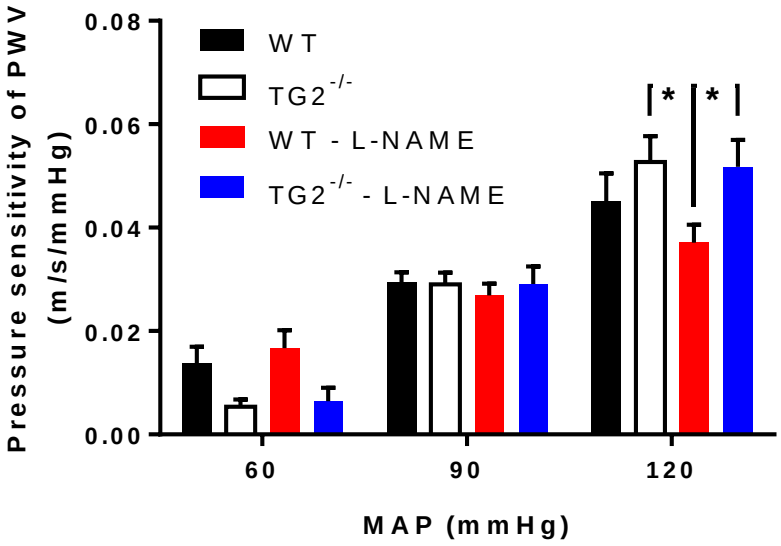

Figure 59: Sensitivity of PWV to changes in MAP increases linearly with pressure. The sensitivity at low (60 mmHg) and medium (90 mmHg) MAP was not different between strain or treatment groups. At high (120 mmHg) MAP, WT-L-NAME animals had decreased pressure-sensitivity compared to treated and untreated TG2$^{-/-}$ mice (2-way ANOVA followed by Tukey's multiple comparisons test). *p<0.05

The pull-back technique described in chapter 5 was used to measure the incremental stiffness along the length of the aorta. PWV did not significantly differ at any distance from the arch and no differences in strain were detected either (Figure 60). MAP also did not vary with location along the aorta for any of the groups studied.

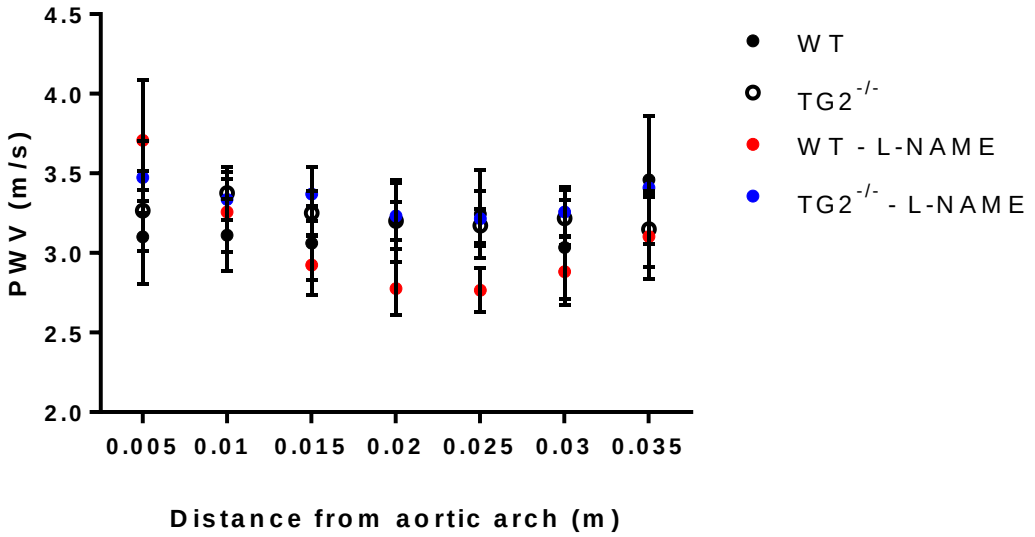

Figure 60: Relationship between PWV and distance from the aortic arch. PWV was not significantly different between any of the locations in the aorta or between strains as determined using two-way ANOVA followed by Tukey's multiple comparisons test.

Figures 61 to 64 show the relationship between PPA and MAP for each of the groups of mice. As described in Chapter 5, PPA is around 1 at pressures of 80 mmHg and greater. PPA steadily drops as pressures fall below 80 mmHg. From Figure 61, it can be seen that at pressures between 65 and 70 mmHg, WT mice have higher PPA compared to $TG2^{-/-}$(at 65mmHg: PPA = 0.93 ± 0.05 versus 0.78 ± 0.05; at 70mmHg: PPA = 1.04 ± 0.05 versus 0.86 ± 0.05). L-NAME treatment did not have any effect on this relationship. WT mice given L-NAME had higher PPA at pressures between 60 and 70mmHg compare to $TG2^{-/-}$ (Figure 64; at 60 mmHg: PPA = 0.94 ± 0.07 versus 0.75 ± 0.07; at 65mmHg: PPA = 1.00 ± 0.07 versus 0.85 ± 0.07; at 70mmHg: PPA = 1.06 ± 0.06 versus 0.91 ± 0.06). There were no differences observed between treated and untreated groups (Figure 62 and Figure 63).

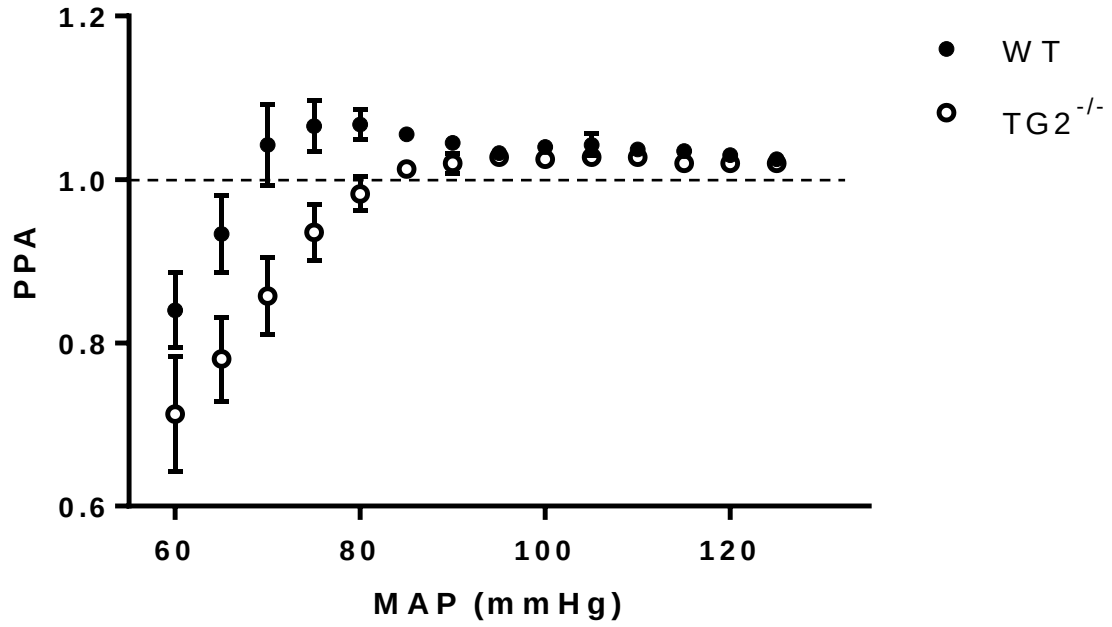

Figure 61: PPA-MAP relationship for WT and TG2$^{-/-}$ mice. As previously demonstrated, PPA remains around 1 at MAP above 80 mmHg and begins to steadily decline as pressure is reduced. WT mice have significantly higher PPA at pressures between 65 and 70 mmHg; however, this trend is apparent at pressures less than 85mmHg. *p<0.05.

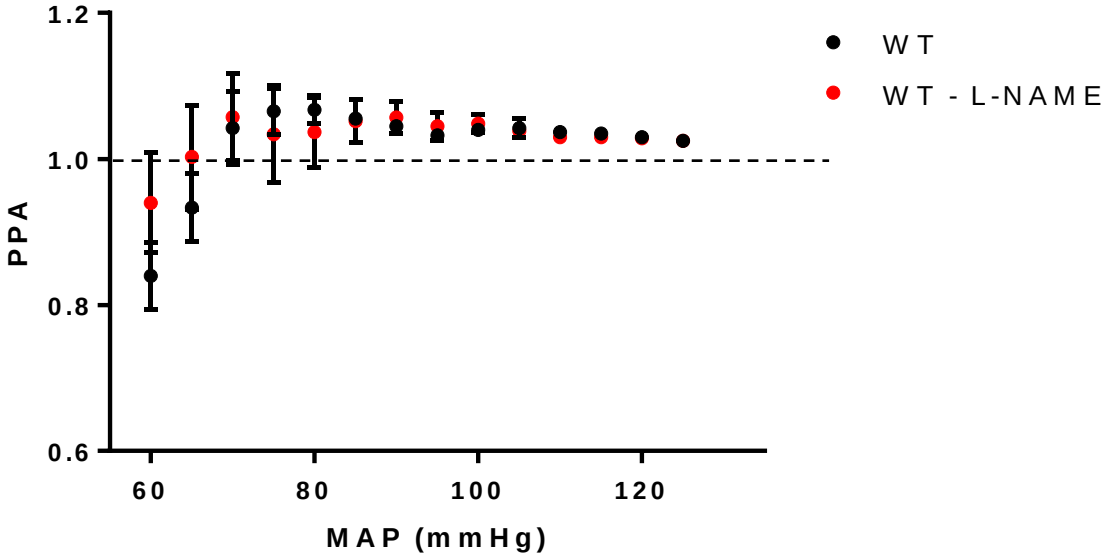

Figure 62: PPA-MAP relationship between L-NAME treated and untreated WT mice. There were no differences detected at any level of MAP.

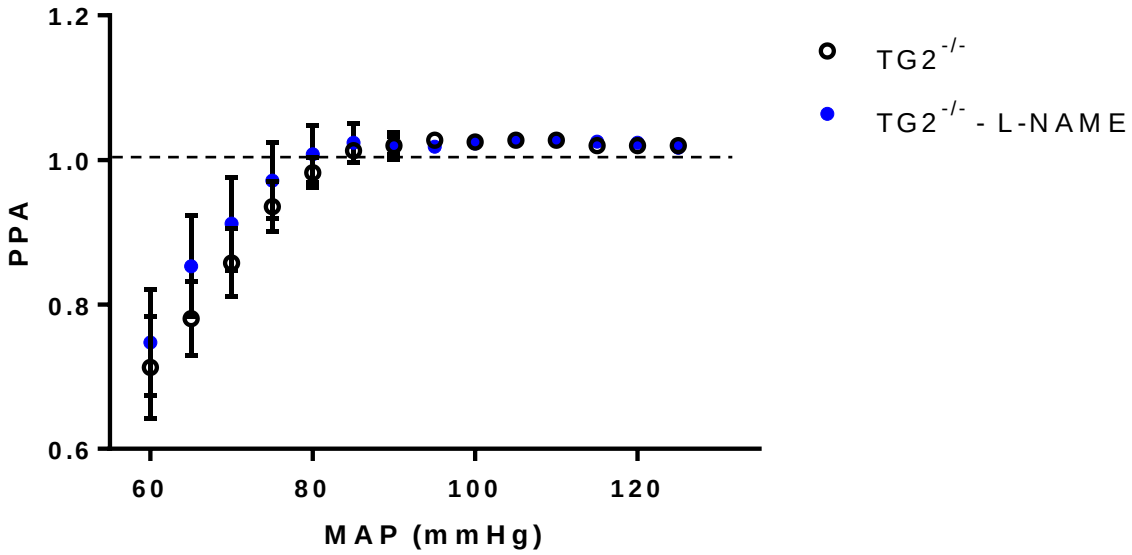

Figure 63: PPA-MAP relationship between L-NAME treated and untreated $TG2^{-/-}$ mice. There were no differences detected at any level of MAP.

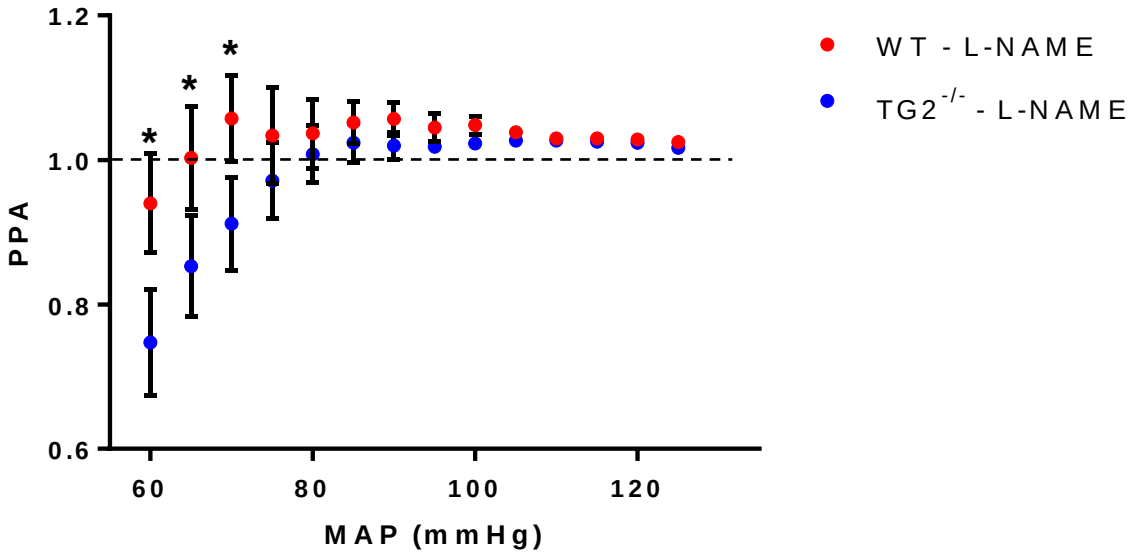

Figure 64: PPA-MAP relationship for WT and $TG2^{-/-}$ mice given L-NAME. WT mice have significantly higher PPA at pressures between 60and 70 mmHg. *p<0.05

6.2.4 Baroreflex Sensitivity

There was no significant difference in drug-induced BRS between strains or treatment groups; although, there did appear to be a trend towards decreasing sensitivity in the $TG2^{-/-}$ animals (Figure 65).

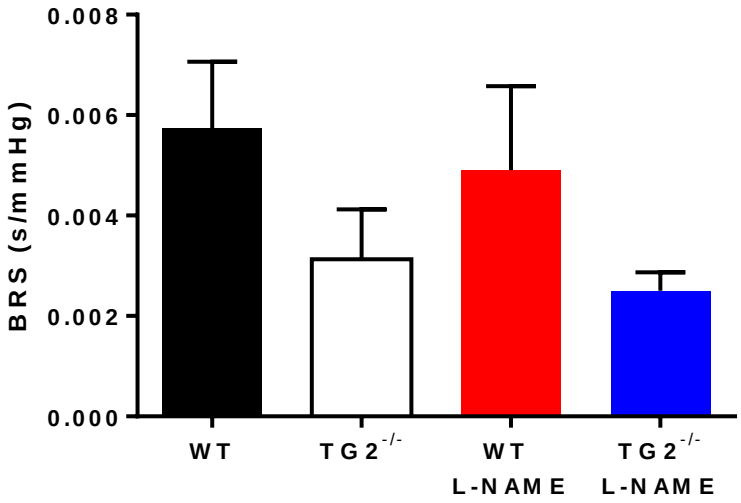

Figure 65: BRS in response to PE administration in anaesthetized mice.

6.2.5 Histology

The media-to-lumen ratio of the thoracic aorta was not different between WT and $TG2^{-/-}$ mice regardless of L-NAME administration. After 4 weeks of L-NAME administration, the wall-to-lumen ratio was significantly larger in WT mice compared to control (0.67 ± 0.08 versus 0.40 ± 0.02). Medial thickness was not significantly different between any groups examined (Figure 66 and Figure 67).

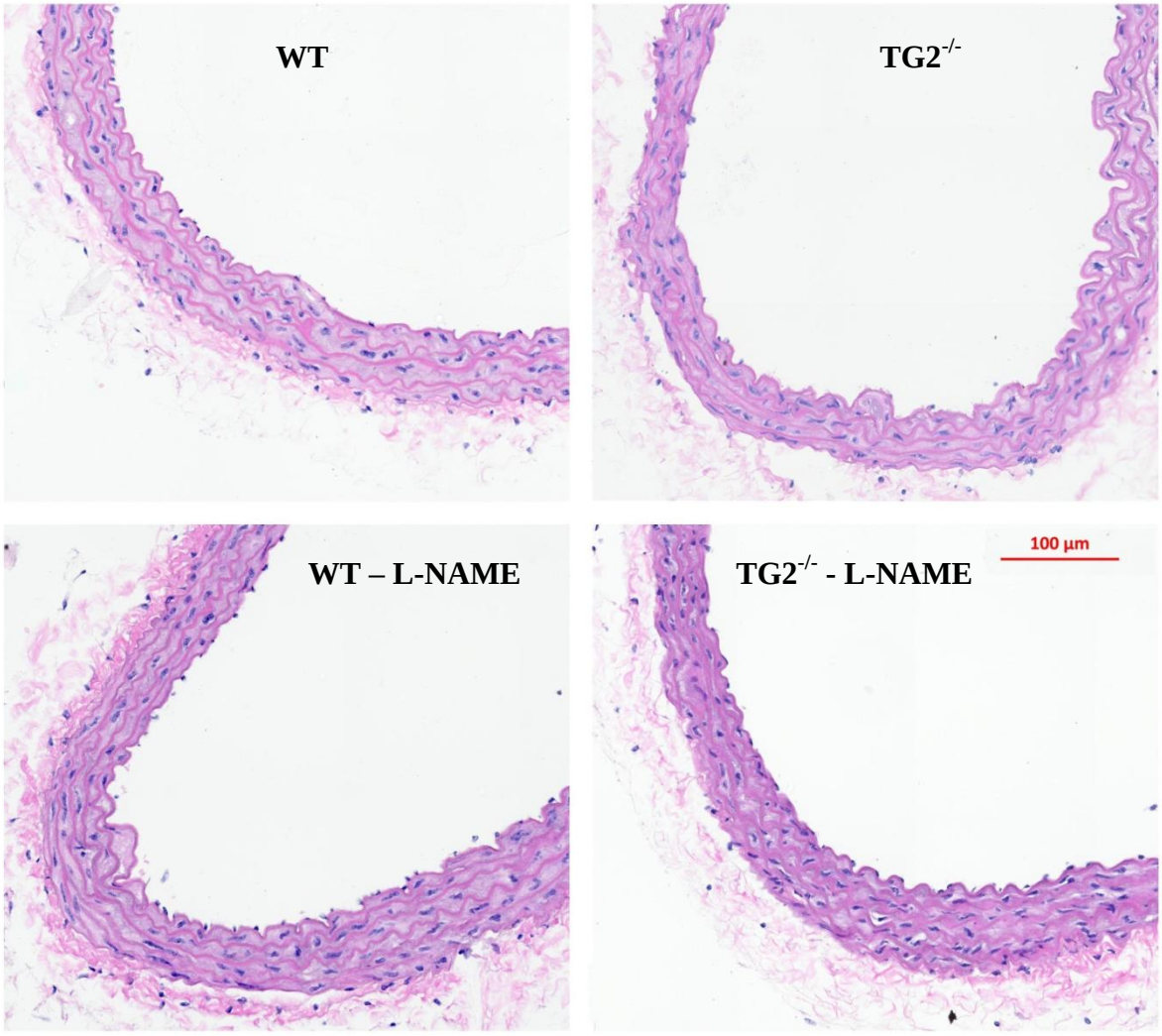

Figure 66: Representative images of histological sections of thoracic aorta stained with H&E in WT, $TG2^{-/-}$ control mice and mice given L-NAME for 4 weeks. Bar: 100µm.

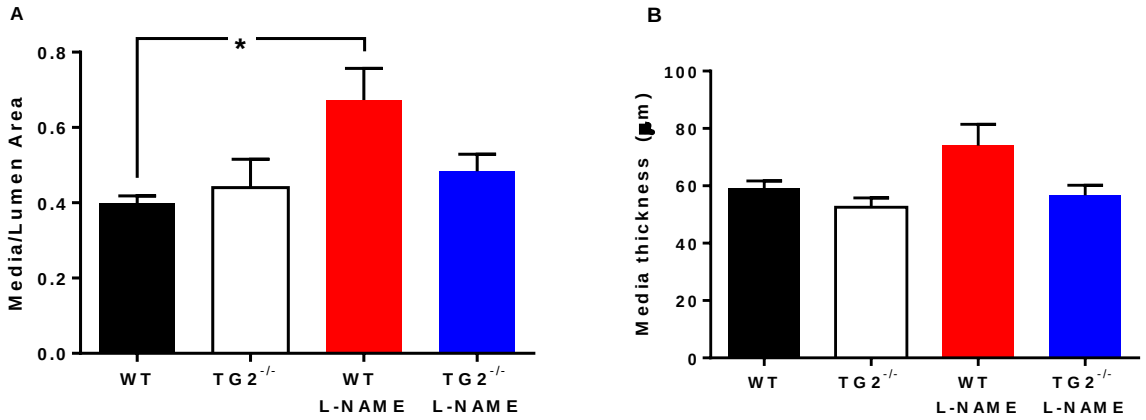

Figure 67: Thoracic aorta media-to-lumen ratio (A) and medial thickness (B) in control and L-NAME treated WT and TG2$^{-/-}$ mice. The wall-to-lumen ratio was significantly greater in WT mice given L-NAME compared to WT controls. No other significant differences were found. *p<0.05.

6.3 Discussion

Results of this study extended experimental findings described in Chapter 5. The blood pressure and heart rate measurements taken with the tail-cuff system at the end of the 4 week treatment period demonstrated that L-NAME had no effect on these parameters in WT mice. Untreated TG2$^{-/-}$ mice had higher HR and lower MAP, SBP, DBP, and PP compared to WT controls. This contrasts with the study presented in Chapter 5 and published data demonstrating that there are no differences in these baseline values (129, 151). L-NAME treatment did increase blood pressure in TG2$^{-/-}$ mice such that their tail-cuff pressure measurements were not different to those of treated or untreated WT mice, with the exception that PP was significantly higher in WT mice given L-NAME compared to TG2-/- given L-NAME. As PP is an indirect measure of arterial stiffness, this would suggest that WT mice have stiffer arteries than TG2$^{-/-}$ mice after L-NAME administration (assuming similar stroke volume). Indeed, this finding has been reported in previous studies (16). While it was expected that 4 week L-NAME treatment via osmotic minipumps would increase blood pressure, this effect was only observed in TG2$^{-/-}$ mice and not in WT mice.

One possible explanation is the use of the tail-cuff apparatus to determine blood pressure and heart rate. The mice are under a significant amount of stress during the measurements which could cause erroneous readings. This stress is still present even after the animal has been trained. Readings can also be quite variable and are subject to movement artefacts (218).

The invasive measurements yielded no differences in any of the groups studied which is in agreement with our previous data (Chapter 5.2) and that published by others (129). Isoflurane anaesthesia may have depressive cardiac effects; however, as discussed in Chapter 5, it has been demonstrated to be the anaesthetic of choice when measuring cardiovascular parameters. Further, the invasive blood pressures are within the same range as the tail-cuff pressures. The heart rate is certainly lower but it is likely higher than normal during the tail-cuff measurements (due to stress), so the effects of isoflurane may not be significant. The apparent lack of effect from the L-NAME treatment persisted even with the increased duration and the more effective route of administration. As opposed to the results presented in Chapter 5 where L-NAME showed a trend towards beneficial effects, in this study no effects were detected with invasive measurements. While L-NAME treatment at this concentration and duration has been shown to increase blood pressure (16), the study by Fitch et al (45) also did not report any effects of 28 days of L-NAME treatment on any cardiovascular parameters. Additionally, there could be compensation for the lack of NO by other endothelium-modulated relaxant pathways, such as prostacyclin or EDHF, as discussed in Section 5.3.

$TG2^{-/-}$ mice had smaller body weight and LV mass compared to WT controls in both L-NAME treated and untreated groups. This finding is in contrast with our previous work (Chapter 5.2) in which there were no differences in body weight or heart weight in TG2 knockout or WT animals. This discrepancy between $TG2^{-/-}$ animals and their littermate controls in Australia and the USA may be due to slight genetic variation (though the strains are nominally identical) or differences in environmental conditions (though quite similar).

Elucidating the genetic and environmental subtleties between the two strains/housing conditions is beyond the scope of this thesis, but highlights the importance of these factors.

TG2 has been linked to cardiac hypertrophy in mice, rats, and humans (129). Mice which overexpress TG2 have demonstrated left ventricular hypertrophy, depressed resting ventricular function, elevated heart rate and lowered blood pressure and left ventricular ejection fraction (156, 157). Additionally, in rats TG2 expression was upregulated during the development of cardiac hypertrophy and the transition to heart failure (155). The exact mechanisms for reported associations between TG2 and cardiac hypertrophy have yet to be elucidated; however, the observational findings presented in the literature are in accordance with the finding in this study that LV mass is decreased in $TG2^{-/-}$ mice.

Echocardiography results demonstrated no differences in systolic and diastolic function amongst the four animal groups studied. However, it did detect that the WT mice had larger left ventricles compared to $TG2^{-/-}$ mice in both L-NAME treated and untreated animals, which corresponds well with the manually weighed LV masses. It is not immediately apparent why these knockout animals would have lower LV masses when the rest of their cardiovascular parameters are not different to WT controls. Cardiac hypertrophy is often a consequence of increased stiffness and blood pressure. However, invasive measurements did not yield any differences in these two values. Although tail-cuff measurements showed that WT mice had higher blood pressure than $TG2^{-/-}$, SBPs were still modest, hence it is not evident that this would cause the differences in heart size. Furthermore, L-NAME treated animals had similar blood pressures measured by tail cuff and invasively, and still there was a differences in LV mass. TG2 is generally not active unless there are some injurious or inflammatory stimuli present, which is also unlikely in the untreated young animals. A possible explanation is that it corresponds to the lower body weight of the $TG2^{-/-}$ mice. Further work is required to

elucidate the cause of decreased LV mass in the knockout animals, including precise measures of cardiac function, including left ventricular pressures, and pressure-volume loops.

The PWV-MAP curves indicated no difference in stiffness between treated or untreated WT and $TG2^{-/-}$ mice at any of the pressures investigated. Generally, this corresponds to the data presented in Chapter 5. However, whereas it was previously found that WT mice had stiffer aortas at PWV above 126 mmHg (Chapter 5.2.2) the data shown here indicate no differences across all pressure ranges. Similarly, L-NAME treated animals showed no differences compared to vehicle control across the pressure ranges studied. It is known that L-NAME treatment of this duration is enough to induce vascular remodelling (115). Therefore, it was expected that changes in the stiffness would be apparent. These findings indicate that structural and functional correlates may not have a simple association. The extent to which vascular remodelling influences stiffness independently of its effects on blood pressure is currently unknown. Findings from the present experiments suggest that the structural changes induced by the L-NAME treatment are not sufficient to manifest as significant functional stiffness and hemodynamic changes to be detected by PWV measurements. These observations suggest the possibility of adaptive changes (as described in Section 5.3) that could be explored in further studies.

At low and medium MAP, the sensitivity to changes in pressure of PWV was similar for all groups of mice. At high pressures, WT mice given L-NAME had significantly lower pressure sensitivity compared to both treated and untreated $TG2^{-/-}$ mice. Notwithstanding these results, no differences in the pressure sensitivity of PWV are apparent.

No differences in stiffness along the length of the aorta were observed for any of the groups studied. Normally, the stiffness of the aorta increases with distance from the heart. The lack of this effect in the WT mouse was discussed in Chapter 4. It was originally hypothesized that there would be strain differences detected in incremental PWV due to increased collagen

cross-linking in the control mice or the L-NAME treated mice. Additionally, there may be localised changes in stiffness that are lost when PWV is measured across the whole aorta and which are only able to be detected when stiffness is measured in small increments. However, this was not observed with segmental PWV measurements. There are limitations of the pull-back method to measure incremental stiffness that were previously discussed (Chapter 4). Given the small distances, the incremental stiffness changes in the mouse aorta may not be large enough to be detected by this method. Future studies could include *ex vivo* tensile tests on sequential rings along the length of the aorta to quantify structural stiffness (free of any active smooth muscle effect) in a regional fashion.

The PPA-MAP curves follow the trend discussed in Chapters 4 and 5 where PPA is approximately 1 at pressures around 80mmHg and above. Below this pressure, PPA begins to drop with MAP. $TG2^{-/-}$ mice had significantly lower PPA at pressures between 65 and 70 in untreated animals and between 60 and 70 in L-NAME treated animals compared to WT mice. The reason for this may be related to the fact that the TG2 mice are smaller than their WT controls. Due to the smaller size they would have smaller diameter aortas which could affect the pressure wave transmission characteristics, especially with the presence of the intravascular catheter.

Similarly to Chapter 5, histological sections stained with H&E showed no gross morphological differences between the aortas of all four groups. No changes in medial thickness were observed either. The media-to-lumen ratio significantly increased in WT mice after four weeks of L-NAME treatment compared to control, while in $TG2^{-/-}$ mice, L-NAME treatment did not induce any changes. This suggests that TG2 may play a protective role in arterial remodelling in response to NO inhibition. It has previously been shown that inward remodelling depends on TG2 crosslinking activity, which supports this finding. Yet when comparing WT and $TG2^{-/-}$ mice, there were no differences in the media-to-lumen ratio,

regardless of L-NAME administration. From the Moens-Korteweg equation (2.1), PWV is influenced by both the vessel wall thickness, and the internal radius, thus it was expected that an increase in the media-to-lumen ratio would translate into increased stiffness. As there was no increase in PWV in L-NAME treated WT mice, there did not appear to be any functional consequences of the geometrical changes that were measured. A longer treatment period may induce more pronounced changes, such as those reported by Kameyama et al where L-NAME administration increased both PWV and the media-to-lumen ratio in rats after just one week of treatment. It would also be beneficial to examine the geometry of the aortas once they have been fixed under a perfusion pressure of 100mmHg. This would give a better idea of the geometry of the vessel under *in vivo* conditions.

Though the aim of this study was to obtain supporting evidence for the previous work with $TG2^{-/-}$ mice and to clarify results that opposed hypotheses, the findings have suggested a much more complex role of TG2. Indeed, this is reflective of the current state of the literature with respect to TG2. Its ubiquitous expression and its upregulation in concordance with many cardiovascular pathologies have linked TG2 to many pathophysiological processes, sometimes playing a beneficial role and other times a detrimental role. This thesis provides evidence that TG2 may be involved in large artery stiffness at high blood pressures, and left ventricular hypertrophy. Future studies investigating the role of TG2 in large artery stiffness could consider a stronger inflammatory stimulus over a longer time period to investigate TG2 activity in more severe, chronic scenarios.

While *in vitro* data support the notion that increased TG2 activity contributes to large artery stiffness, it may not readily translate to functional changes measured *in vivo*. TG2 activity is held latent under normal conditions and requires supraphysiological levels of intracellular Ca^{2+} to be activated in addition to reduced bioavailability of NO. This suggests that only in very extreme cases TG2 activity is increased to an extent that it directly causes increased

vascular stiffness. Under such circumstances, there are likely other pathological processes occurring simultaneously which may overpower the potential effects of TG2. Further work is required to investigate arterial stiffness in different disease models using more specific NOS inhibitors and under differing disease conditions.

Chapter 7

Arterial stiffness in apolipoprotein E knockout mice

Atherosclerosis is often considered synonymous with arteriosclerosis, or increased arterial stiffness. However, while they are two entirely different processes, aortic atherosclerotic plaques are often present in patients with increased arterial stiffness and often these two pathologies exacerbate one another (18, 23, 71). This can make it difficult to understand the contribution of each to overall cardiovascular function. The apoE$^{-/-}$ mouse is an accepted model for atherosclerosis (219, 220) as it develops plaques similar to those seen in humans with age (173). C57Bl6 mice are used as WT controls because they develop essentially no plaques with age (221). While there is a large body of work surrounding the apoE$^{-/-}$ mouse, to the best of our knowledge, there are no studies with comprehensive characterisation of pressure-dependent arterial stiffness in the aortic trunk. Since apoE$^{-/-}$ mice develop hypertension with age, it is critically important to be able to account for these changes in blood pressure when examining their PWV. The progression of atherosclerosis is accelerated in the presence of inflammation, in particular, endothelial dysfunction characterised by reduced bioavailability of NO. Therefore, mice were treated with the NOS-inhibitor L-NAME for investigation of cardiovascular effects. It was also of interest to determine if L-NAME treatment would produce similar effects in the apoE$^{-/-}$ mice as those produced in the TG2$^{-/-}$ mice and their WT littermates. The aim of this study was to invasively measure the PWV-

MAP relationship in apoE$^{-/-}$ mice compared to WT controls and to apoE$^{-/-}$ mice treated with L-NAME.

7.1 Methods

7.1.1 Animals

Male apoE$^{-/-}$ and C57Bl6 (WT) mice (ARC, Perth), aged 12 weeks were studied. Animals were kept in a temperature controlled environment (21 ± 2^{o}C) with 12 hour light/dark cycles. Animals had *ad libitum* access to standard laboratory mouse feed and water. The animal protocol was approved by the Macquarie University Animal Ethics Committee (ARA 2011/017).

7.2.2 L-NAME treatment

Three groups of mice were studied. Groups 1 and 2 (apoE$^{-/-}$ and WT, n=6) were given standard tap water. Group 3 (apoE$^{-/-}$, n=8) received L-NAME (Sigma, Australia) via drinking water (0.5 g/L). L-NAME was administered for two weeks prior to surgery.

7.2.3 Experimental procedures

Mice were anaesthetized and aortic stiffness was measured across a full range of physiological arterial pressures as previously outlined (Section 5.1.3). Baroreflex sensitivity, tissue dissection and preparation, wire myography, tensile testing, calcium quantification, and histological evaluation of the aorta were also performed as described in Chapter 5.

7.2.4 Statistics and data analysis

Data are presented as mean ± standard error, except where otherwise indicated. Data were analysed offline using a combination of Microsoft Excel, IBM SPSS Statistics 19, and GraphPad Prism 6.

Data recorded across all pressure ranges were divided into 5 mmHg pressure bins. Statistical differences between groups were determined using either: paired Student's t-tests for each pressure bin, 1-way ANOVA or 2-way ANOVA followed by Tukey's multiple comparisons test. This is detailed in the results sections. P-values less than 0.05 were considered to be statistically significant.

Dose-response curves were fitted with a sigmoidal dose-response function through non-linear regression in Prism, returning EC_{50} and maximum response parameters. Two-way ANOVA with Bonferroni post-hoc test was employed to compare responses at each concentration. EC_{50}s and maximum responses were compared using one-way ANOVA followed by Tukey's multiple comparisons test. Again, P-values less than 0.05 were considered to be statistically significant.

7.2 Results

7.2.1 Baseline characteristics

$ApoE^{-/-}$ mice had baseline parameters similar to WT control mice (Table 12). They were slightly heavier and their HR was also higher. L-NAME treatment did not affect any of these measures. Their baseline HR of apoE mice given L-NAME was still higher than WT control, but not higher than untreated $apoE^{-/-}$ mice. However, the treated group no longer had significantly higher body weight.

Table 12: Baseline cardiovascular characteristics. Data are presented as mean ± SD. *p<0.05 apoE$^{-/-}$ vs. WT, †p<0.05 apoE$^{-/-}$ - L-NAME vs. WT.

	WT	**apoE$^{-/-}$**	**apoE$^{-/-}$ – L-NAME**
BW (g)	26 ± 2	30 ± 1*	27 ± 1
HR (bpm)	500 ± 32	582 ± 23*	562 ± 57†
MAP (mmHg)	93 ± 8	89 ± 9	92 ± 5
SBP (mmHg)	111 ± 9	107 ± 11	108 ± 6
DBP (mmHg)	78 ± 6	73 ± 8	76 ± 5
PP (mmHg)	33 ± 4	34 ± 3	33 ± 3
Max dP/dt (mmHg·s^{-1})	859 ± 142	976 ± 224	844 ± 216
PWV (m/s)	2.99 ± 0.13	3.11 ± 0.34	2.80 ± 0.40
LV/BW (mg/g)	351 ± 20	372 ± 37	371 ± 28

7.2.2 Pulse wave velocity

At pressures greater than or equal to 95 mmHg, apoE$^{-/-}$ mice had significantly higher PWV compared to WT control animals. When treated with L-NAME, PWV was reduced in apoE$^{-/-}$ mice such that there was no difference between them and control mice. At MAPs of 60 and 65 mmHg, WT mice had significantly higher PWV than apoE$^{-/-}$ + L-NAME mice (Figure 68).

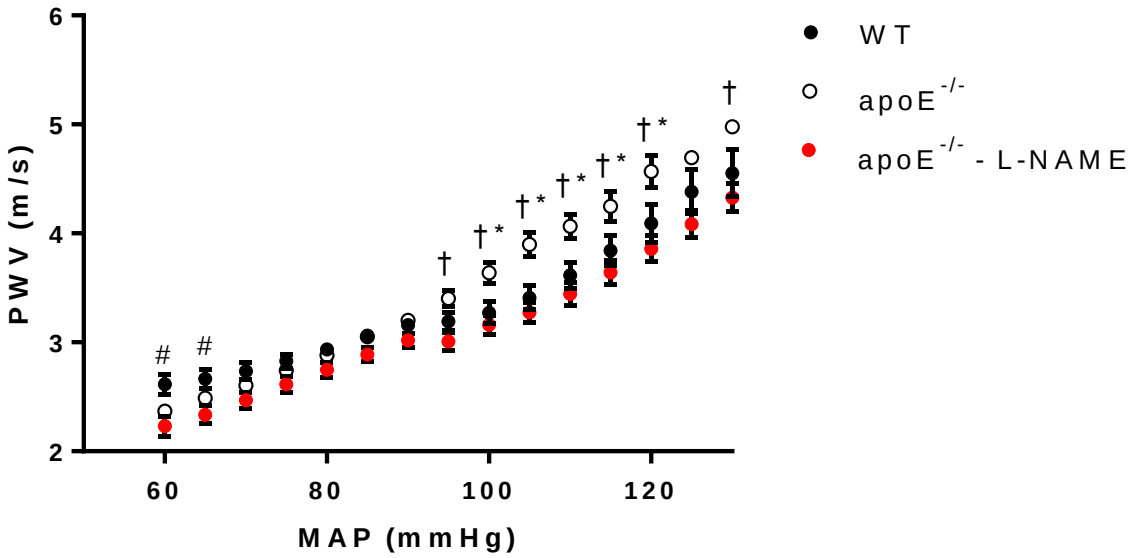

Figure 68: PWV-MAP relationships for WT, apoE$^{-/-}$ and apoE$^{-/-}$ treated with L-NAME. ApoE$^{-/-}$ mice had significantly higher PWV at pressures of 95 mmHg and above. L-NAME treatment lowered PWV in apoE$^{-/-}$ mice to that of controls, and significantly reduced it at pressures of 60-65 mmHg. *P<0.05, WT vs. apoE-/-, #P<0.05, WT vs. apoE$^{-/-}$ + L-NAME; †P<0.05, apoE$^{-/-}$ vs. apoE$^{-/-}$ + L-NAME.

Each PWV-MAP curve could be well described by a quadratic equation (Table 13). This indicated that for each group, the pressure sensitivity of PWV increased linearly with pressure (Figure 69). At low pressures, apoE$^{-/-}$ mice had increased sensitivity compared to WT controls. At medium and high pressures, apoE$^{-/-}$ mice had increased pressure sensitivity compared to both WT controls and L-NAME treated apoE$^{-/-}$ mice.

Table 13: PWV-MAP relationships are described by a quadratic equation.

	Quadratic equation	R^2
WT	$PWV = 3.596 - 0.03504(MAP) + 0.0003255(MAP)^2$	0.9908
apoE$^{-/-}$	$PWV = 1.654 - 0.00054(MAP) + 0.0002022(MAP)^2$	0.9983
apoE$^{-/-}$ – LNAME	$PWV = 1.970 - 0.00509(MAP) + 0.0001744(MAP)^2$	0.9902

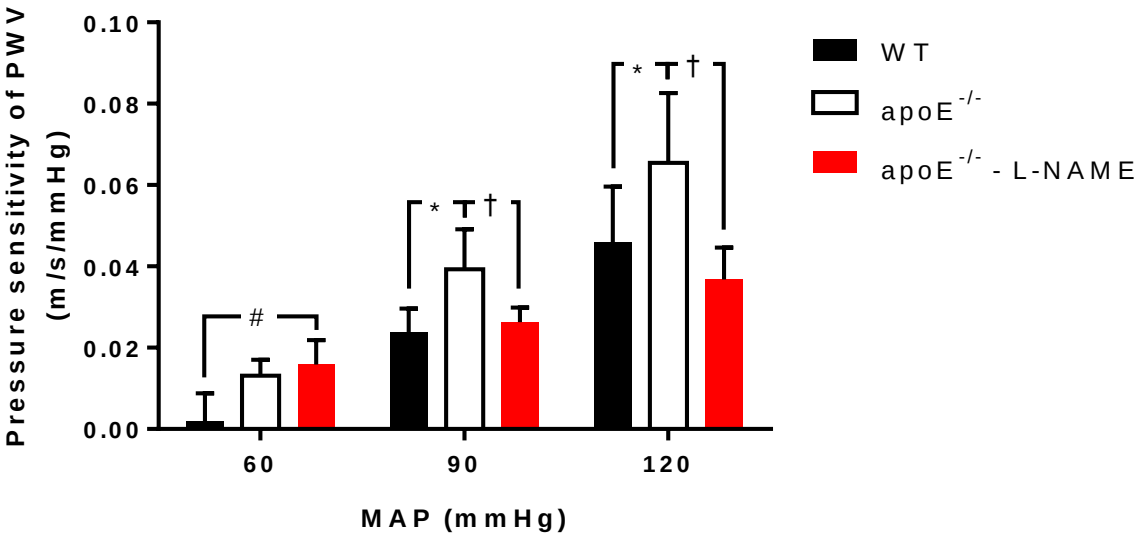

Figure 69: Sensitivity of PWV to changes in MAP increases linearly with pressure. At low MAP (60 mmHg), apoE$^{-/-}$ mice + L-NAME had significantly increased pressure sensitivity compared to WT mice. At medium (90 mmHg) and high (120 mmHg) MAP pressure sensitivity was significantly higher in the apoE$^{-/-}$ mice. *P<0.05, WT vs. apoE$^{-/-}$, #P<0.05, WT vs. apoE$^{-/-}$ + L-NAME; †P<0.05, apoE$^{-/-}$ vs. apoE$^{-/-}$ + L-NAME.

The pull-back technique described in chapter 4 was used to measure the incremental stiffness along the length of the aorta. PWV did not significantly differ at any distance from the arch and no differences in strain were detected (Figure 70). There were no differences in MAP with location along the aorta.

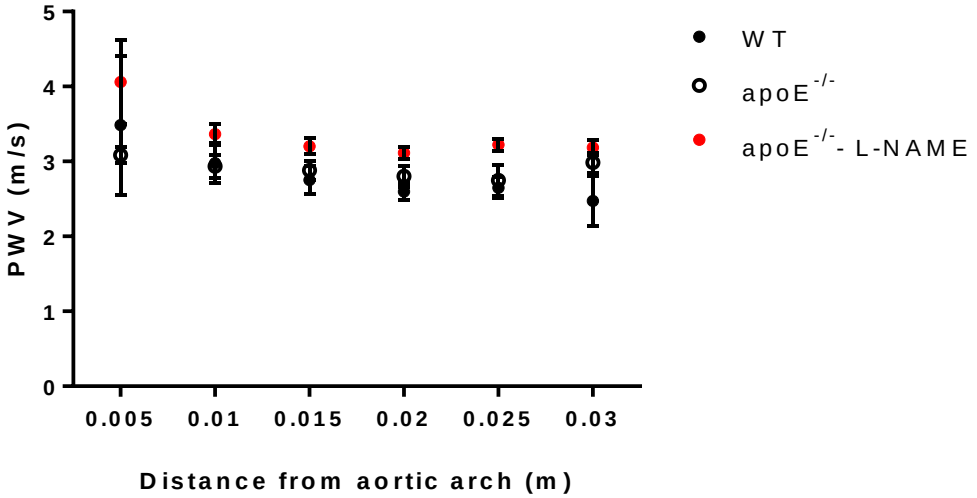

Figure 70: Relationship between PWV and distance from the aortic arch. PWV was not significantly different between any of the locations in the aorta or between strains.

As described in previous chapters, PPA was around 1 at pressures of 80 mmHg and greater. PPA steadily dropped as pressures fall below 80 mmHg. At all values of MAP, there were no significant differences in PPA between the three groups of mice studied (Figure 71).

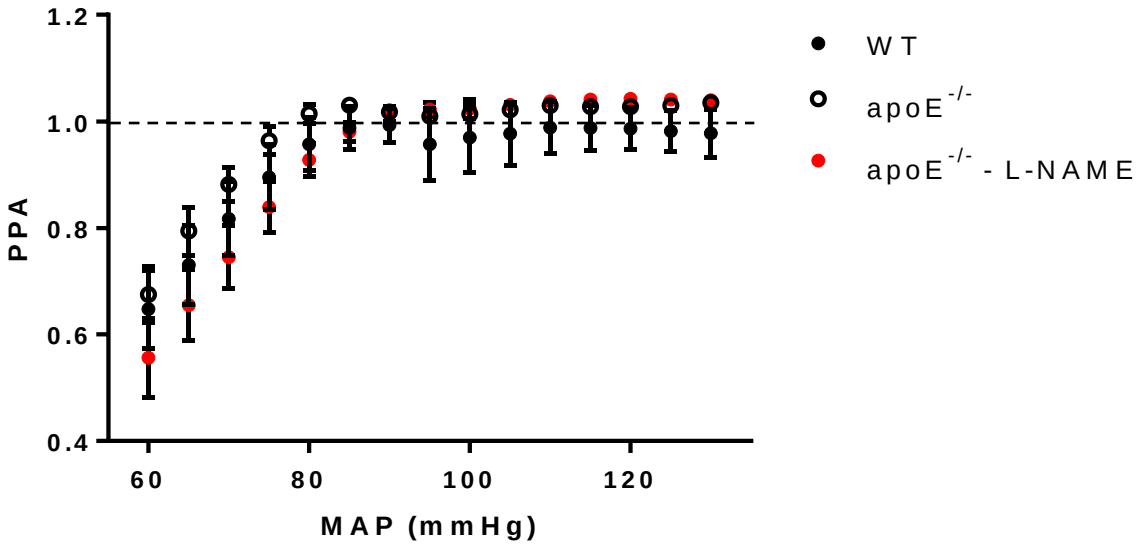

Figure 71: PPA-MAP relationship for C57, apoE-/- , and apoE-/- given L-NAME mice. No differences were detected at any of the MAPs. Data was analysed using two-way ANOVA followed by Tukey's multiple comparisons test.

7.2.3 Baroreflex sensitivity

There was no significant difference in drug-induced BRS between strains or treatment groups; although, there was a trend towards decreasing sensitivity in the apoE$^{-/-}$ and L-NAME treated animals (Figure 72).

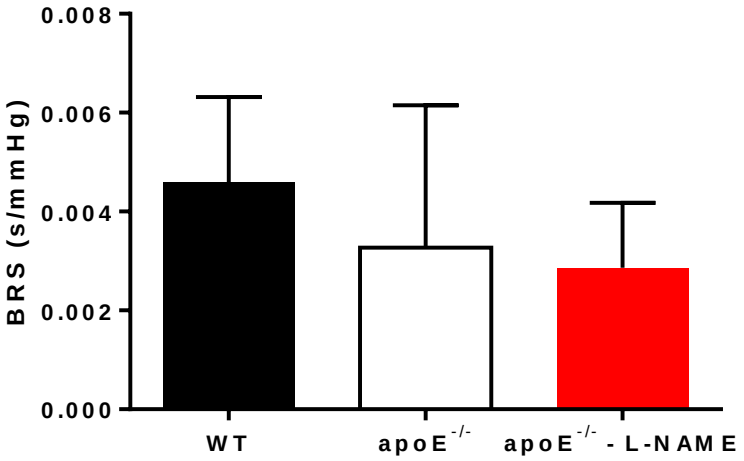

Figure 72: BRS in response to PE administration in anaesthetized mice.

7.2.4 Tensile testing

Tensile testing revealed that the intact aorta of apoE$^{-/-}$ mice is stiffer than in WT mice and in apoE$^{-/-}$ mice treated with L-NAME, as the E_{inc} at a strain of 0.1 is significantly greater (Figure 73).

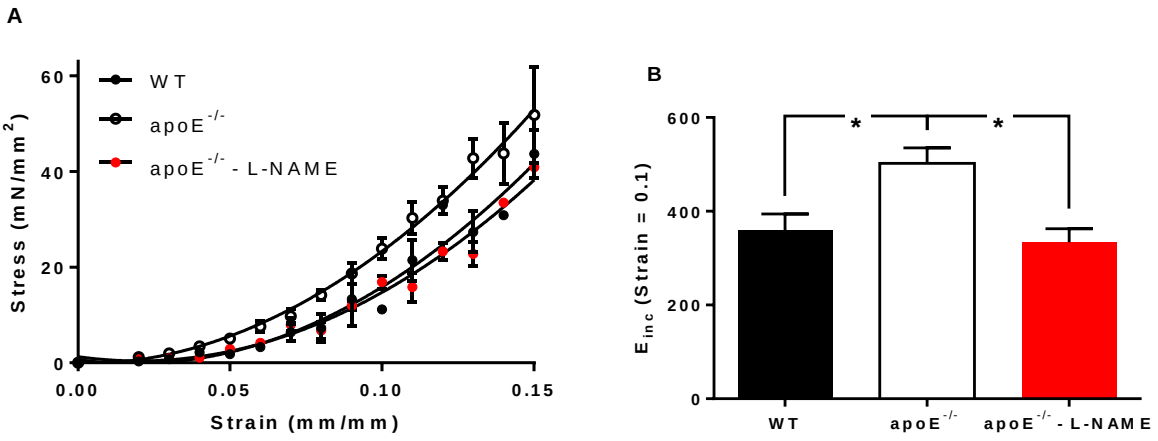

Figure 73: The stress-strain curves (A) and E_{inc} at a strain of 0.1 (B) for WT, apoE$^{-/-}$, and apoE$^{-/-}$ given L-NAME. ApoE$^{-/-}$ mice had a significantly higher incremental elastic modulus at a strain of 0.1 compared to WT and L-NAME treated apoE$^{-/-}$ mice. *p<0.05.

7.2.5 Vascular reactivity

Vascular responses to PE, SNP, and ACh to evaluate vascular smooth muscle cell and endothelial cell function were studied by performing cumulative dose response curves with aortic rings mounted on a wire myograph. Rings were taken from the thoracic aorta, proximal to the first intercostals branch, and the abdominal aorta, proximal to the iliac bifurcation.

7.2.5.1 Smooth muscle cell contraction

Vasoconstrictor responses to PE were examined. There was no attenuation of the maximum contractile response to PE between WT and apoE$^{-/-}$ mice in the thoracic aorta; however, this response was significantly diminished in the L-NAME treated mice (WT: 12.31 ± 1.28, apoE$^{-/-}$: 12.20 ± 1.88, and apoE$^{-/-}$ - L-NAME: 5.83 ± 0.99 mN; Figure 74A). There were no statistically significant differences observed in the abdominal aortic segments between any of the groups studied (WT: 7.37 ± 1.55, apoE$^{-/-}$: 5.57 ± 1.19, and apoE$^{-/-}$ – L-NAME: 1.02 ± 0.04 mN; Figure 74B). There was a trend towards decreased maximal responses in the L-NAME treated animals.

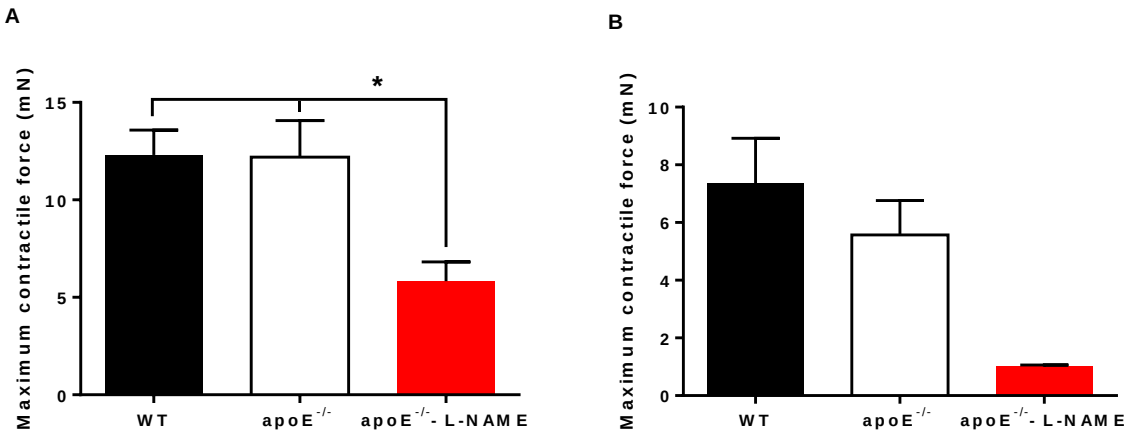

Figure 74: Maximal contraction to PE in thoracic (A) and abdominal (B) segments isolated from the three different mice groups ex vivo. Treatment with L-NAME impaired vascular smooth muscle contractile response significantly only in the thoracic sections from the apoE$^{-/-}$ mice; however, there was a similar trend in the abdominal sections as well: *P<0.05.

There were no strain-related differences in the dose-response curve to PE or the EC_{50} values in the thoracic aorta (Figure 75), or the abdominal aorta (Figure 76) indicating no changes in sensitivity to PE.

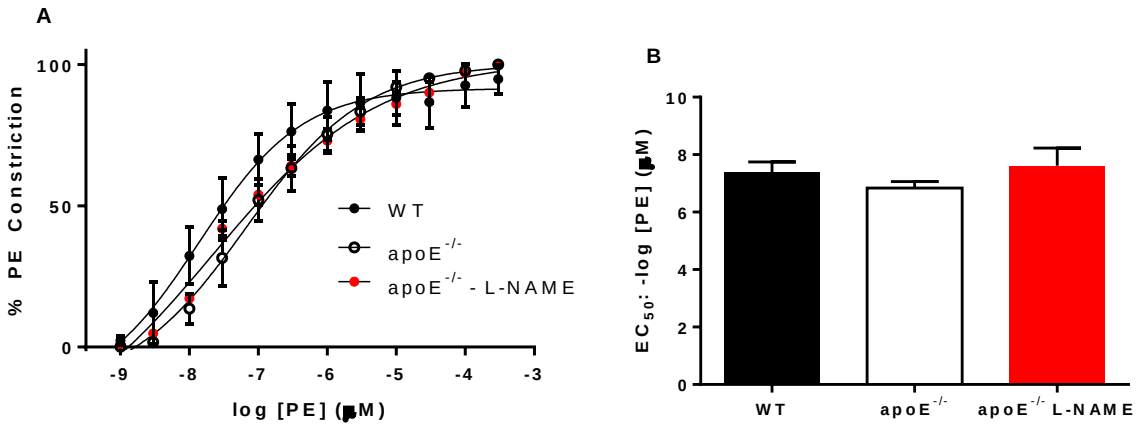

Figure 75: Contractile response to PE (A) and EC_{50} values (B) in the thoracic aorta. No differences in the dose-response curve or EC_{50} values were noted between groups.

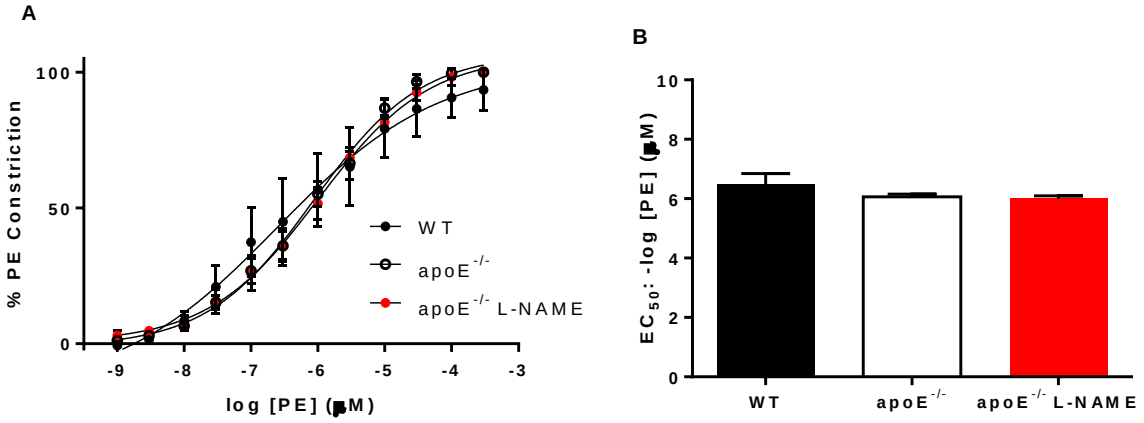

Figure 76: Contractile response to PE (A) and EC_{50} values (B) in the abdominal aorta. No differences in the dose-response curve or EC_{50} values were noted between groups.

There were almost no differences detected between aortic rings from the thoracic aorta versus those taken from the abdominal aorta regarding responses to PE. There was a trend of decreased maximum contractile force in the abdominal sections; however, this only reached significance in the $apoE^{-/-}$ mice treated with L-NAME. The EC_{50} values tended also to be

lower in abdominal rings compared to thoracic, only reaching significance in the apoE$^{-/-}$ mice given L-NAME (Figure 77).

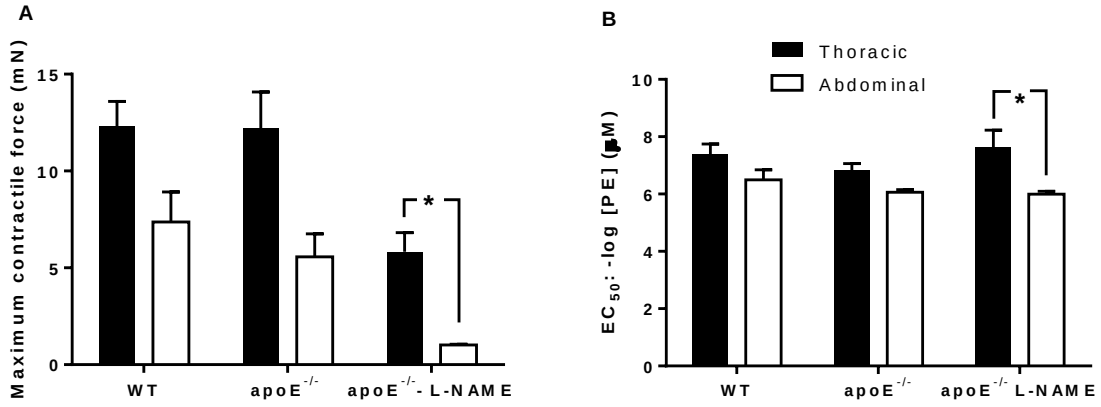

Figure 77: Maximum force of contraction to PE (A) and EC50 values (B) for rings taken from the thoracic and abdominal aortas. *p<0.5

7.2.5.2 Smooth muscle cell relaxation

Endothelium-independent relaxation to SNP was not impaired in any of the groups studied whether rings were isolated from the thoracic (Figure 78) or abdominal aorta (Figure 79). There was a small but significant reduction in the EC_{50} values of the apoE$^{-/-}$ (both control and L-NAME treated) animals in the thoracic rings, indicating reduced sensitivity. This is also reflected by the shift to the right of the dose-response curves from the L-NAME treated animals compared to untreated controls.

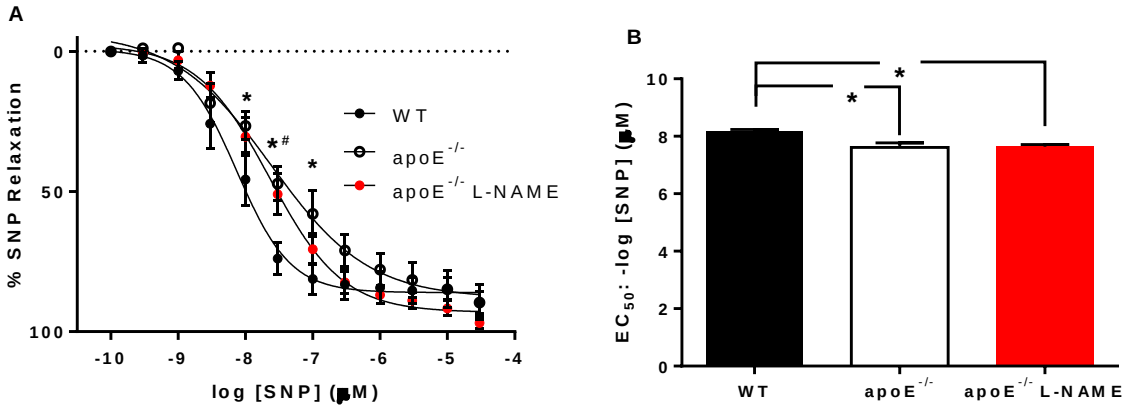

Figure 78: Relaxation response to SNP (A) and EC_{50} values (B) in the thoracic aorta. The curves from the control and L-NAME treated $apoE^{-/-}$ mice were slightly shifted to the right; however, there were no differences in maximal response to SNP, *P<0.05 WT versus apoE, # P<0.05 WT versus $apoE^{-/-}$ + L-NAME in graph A. The EC_{50} values were reduced in control and L-NAME treated $apoE^{-/-}$ mice compared to control *P<0.05 as indicated in graph B.

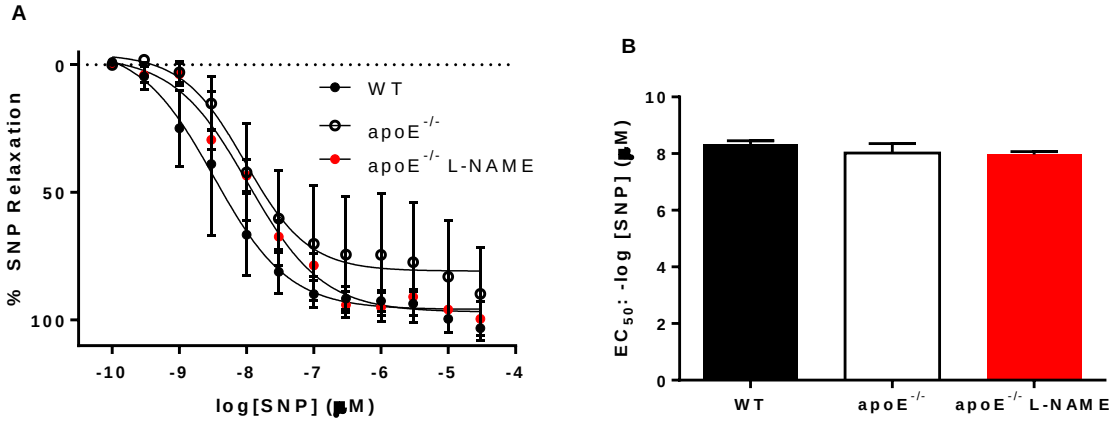

Figure 79: Relaxation response to SNP (A) and EC50 values (B) in the abdominal aorta. No significant differences were observed.

There were no differences observed between the thoracic and abdominal aortic rings (Figure 80).

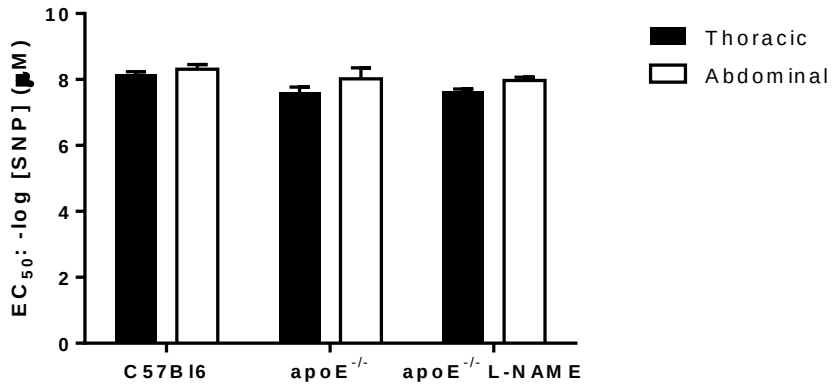

Figure 80: EC50 values from the thoracic and abdominal aortas. No differences were observed.

7.2.5.3 Endothelium-dependent relaxation

The relaxation to ACh was significantly impaired in all of the groups. However, while maximum relaxation in WT mice was approximately 50%, there was no relaxation at all in the apoE$^{-/-}$ mice (regardless of L-NAME administration). In fact, ACh induced constriction in the apoE$^{-/-}$ abdominal aortic rings (Figure 81).

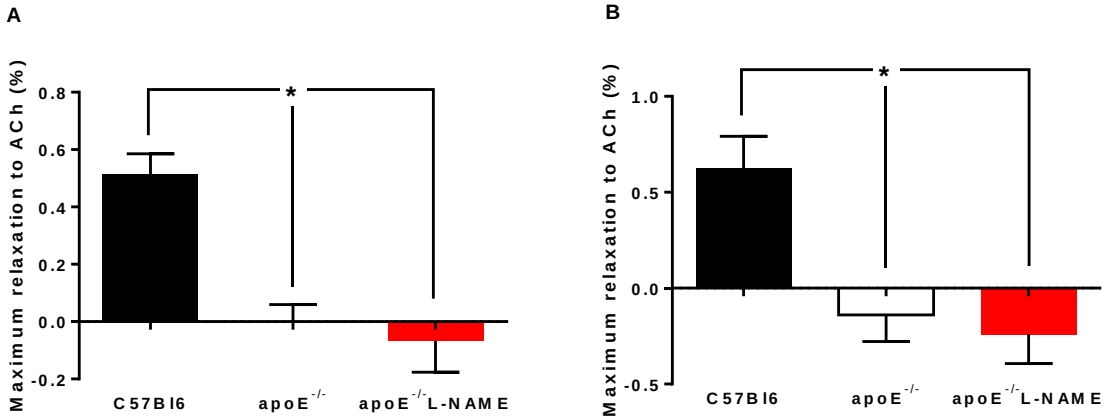

Figure 81: Maximum relaxation to ACh in thoracic (A) and abdominal (B) aortic segments. Relaxation to ACh was completely abolished in both L-NAME treated and untreated apoE$^{-/-}$ mice. Animals administered with L-NAME had aortic rings that displayed constriction instead of relaxation. *P<0.05.

The relaxation-response curves to ACh in thoracic aortic rings were severely impaired in apoE$^{-/-}$ compared to WT (Figure 82A). L-NAME treatment did not change this effect. While there were no significant differences observed in the EC_{50} of WT and apoE$^{-/-}$, both control and those given L-NAME, these animals showed a tendency for constriction as opposed to relaxation, therefore, this comparison cannot actually be made (Figure 82B).

In abdominal aortic rings, the dose-response curves demonstrated a similar trend as in the thoracic rings (Figure 83A). The EC_{50} values cannot be compared between L-NAME treated and untreated apoE$^{-/-}$ as these rings constricted and could not be fit with a sigmoidal curve, whereas WT rings relaxed (Figure 83B).

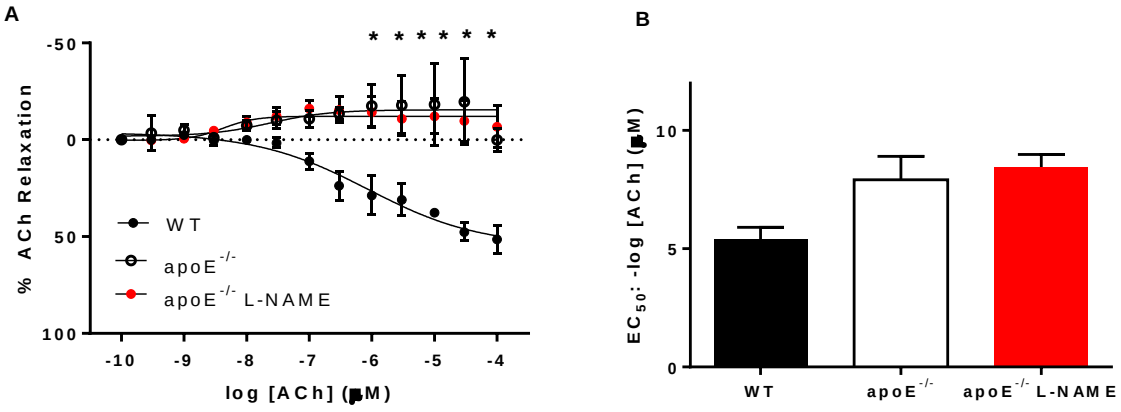

Figure 82: Relaxation response to ACh (A) and EC_{50} values (B) in the thoracic aorta of L-NAME treated and untreated apoE$^{-/-}$ and WT mice. The relaxation response from the apoE$^{-/-}$ mice (both L-NAME treated and untreated) were completely abolished, *P<0.05 for untreated and L-NAME treated apoE$^{-/-}$ versus WT mice in graph A. The EC_{50} values were not significantly different; however, as previously mentioned the EC_{50} values from the apoE/- mice reflect a value for the constriction, not relaxation, curve.

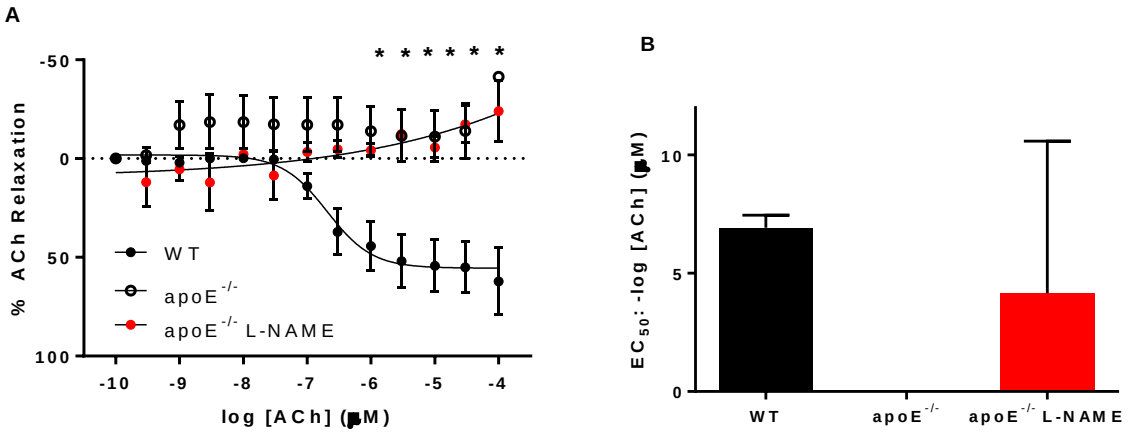

Figure 83: Relaxation response to ACh (A) and EC_{50} values (B) in the abdominal aorta of L-NAME treated and untreated apoE$^{-/-}$ and WT mice. The relaxation response from the apoE$^{-/-}$ mice (both L-NAME treated and untreated) were completely abolished, *P<0.05 for untreated and L-NAME treated apoE$^{-/-}$ versus WT mice in graph A. The EC_{50} values were not significantly different; however, as previously mentioned the EC_{50} values from the apoE$^{-/-}$ mice reflect a value for the constriction, not relaxation, curve.

There were virtually no differences detected between aortic rings from the thoracic aorta versus those taken from the abdominal aorta regarding responses to ACh. The maximum relaxation to ACh was not statistically different between thoracic and abdominal sections. The EC_{50} values for apoE$^{-/-}$ mice could not be calculated or compared as previously mentioned (Figure 84).

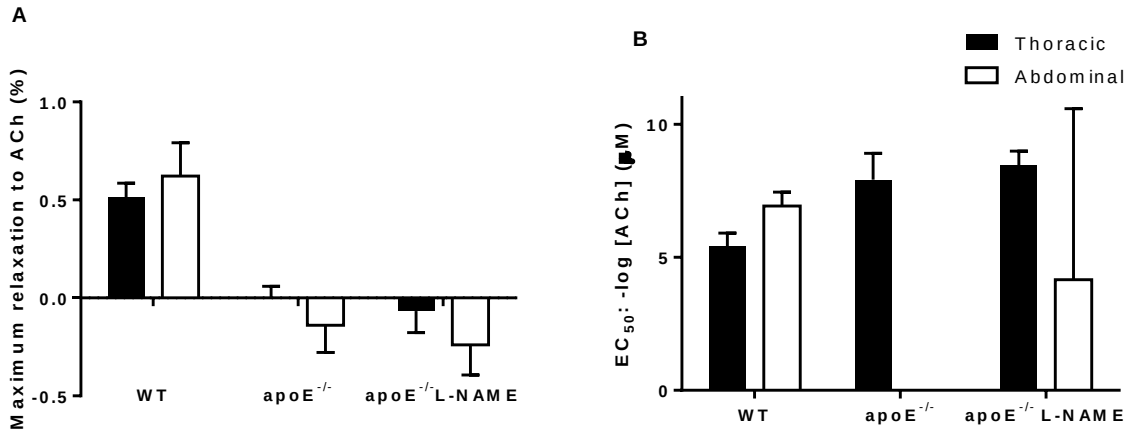

Figure 84: Maximum relaxation to ACh (expressed as a percentage of complete relaxation) (A) and EC_{50} values (B) for rings taken from the thoracic and abdominal aortas. No location-related differences were detected.

7.2.6 Calcification assay

There were no statistically significant differences between calcium levels in the aortas of any of the three groups studied (Figure 85).

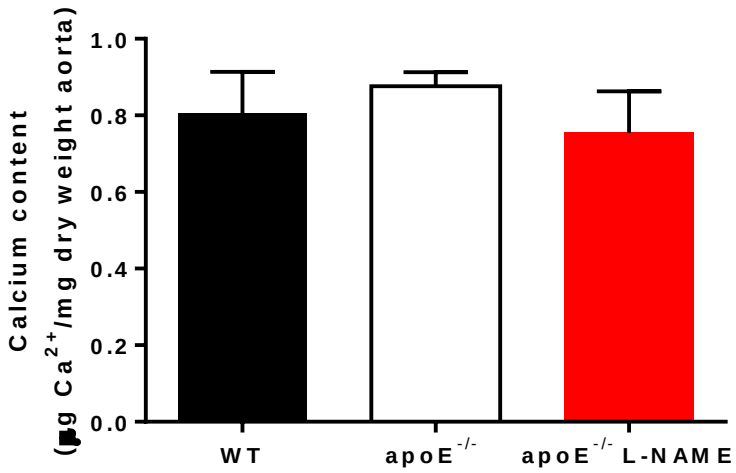

Figure 85: Aortic calcium content. There were no significant differences detected between any groups examined.

7.2.7 Histology

There were no differences in the media-to-lumen ratio or the medial thickness between any of the three groups examined (Figure 86 and Figure 87).

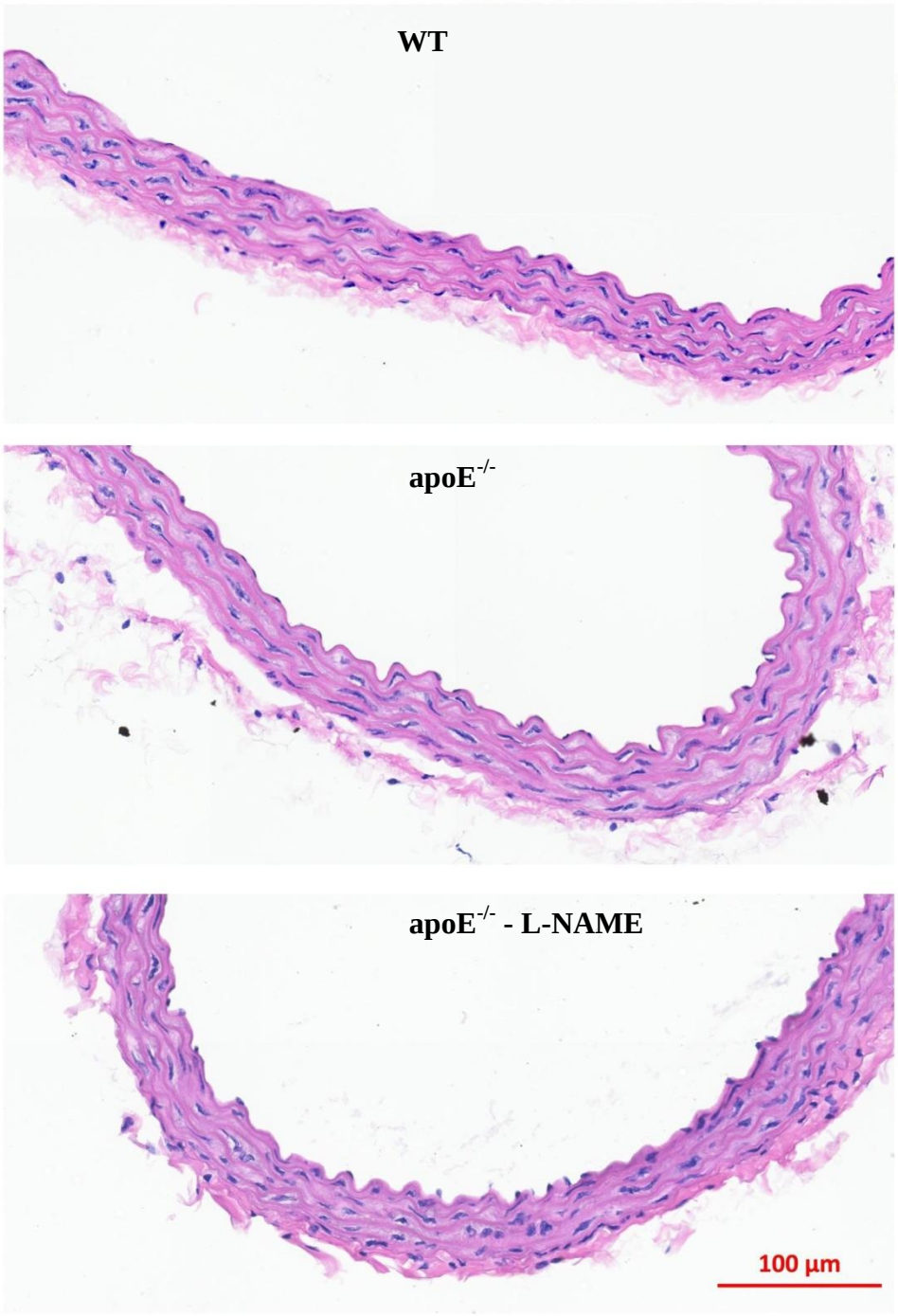

Figure 86: Representative images off histological cross sections of thoracic aortas from WT, apoE$^{-/-}$, and apoE$^{-/-}$ - L-NAME mice. Bar: 100µm.

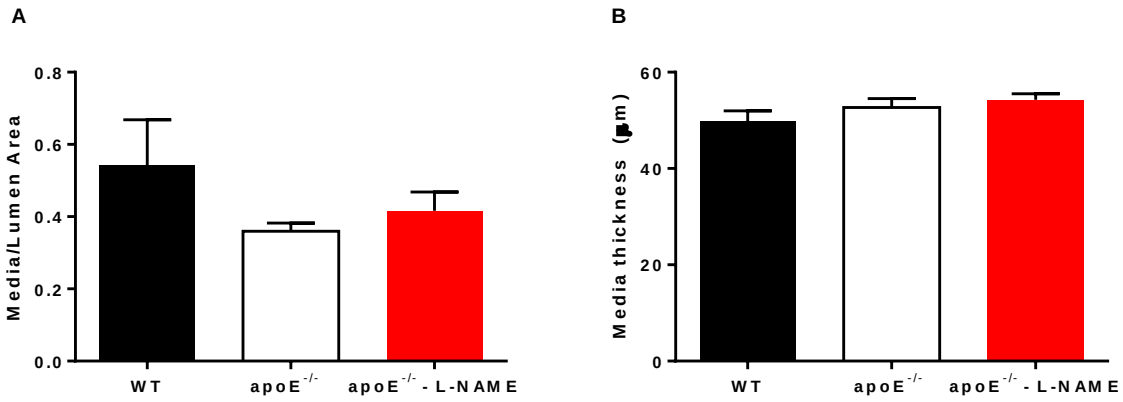

Figure 87: The media-to-lumen ratio (A) and the medial thickness (B) of WT, apoE$^{-/-}$, and apoE$^{-/-}$ -L-NAME mice. No significant differences were detected.

7.3 Discussion

The apoE$^{-/-}$ mouse has proven to be a useful tool for studying atherosclerosis development and progression. As development of atherosclerotic plaques often is associated with increased arterial stiffness, several studies have begun to investigate changes in arterial stiffness in the apoE$^{-/-}$ mouse (41, 42, 48, 50, 51, 53). However, depending on the age and technique used, different results have been attained, and, a survey of the literature revealed that no studies have assessed pressure-dependent PWV in the apoE$^{-/-}$ mouse. As the general scope of this thesis encompassed using genetically modified mouse models to investigate potential mechanisms of arterial stiffness, the study the apoE$^{-/-}$ mouse was consistent with this aim.

Baseline measurements were very similar between all three study groups. Blood pressure and HR in young apoE knockout mice are not usually reported to be different to control, even when treated with L-NAME (171, 175). While results reported in this thesis indicate similar pressures, HR was significantly higher in apoE$^{-/-}$, both untreated and L-NAME treated. The deviation in HR values is quite high and, while anaesthesia was administered in an optimal way for cardiovascular measurements, there is still some effect of isoflurane which could impact the measurements. It would be beneficial to acquire HR measurements in conscious

mice to ascertain whether or not this was a real effect. Cardiac hypertrophy was expected in the apoE$^{-/-}$ mice, not only as a consequence of increased aortic stiffness, but also because this is a documented phenotype of apoE$^{-/-}$ mice as young as 4 months of age (171, 222). However, this was not the case. While the untreated apoE$^{-/-}$ had a trend towards increased LV mass, it is plausible that they were still too young for significant changes to be present. Body weight in the untreated apoE$^{-/-}$ mice was greater than WT control and L-NAME treated mice. This does not agree with the reported body weight of apoE$^{-/-}$ mice which is often lower (42, 51) or the same (223) as WT control. L-NAME treatment, especially over such a short time frame, has been previously shown to have no effect body weight either (175).

While the baseline cardiovascular parameters, aside from HR and body weight, were not different between any of the groups under anaesthetized conditions, the pressure-dependent PWV was significantly higher in the apoE$^{-/-}$ mouse compared to WT controls at pressures of 95 mmHg and greater. These differences are novel findings and have never been shown before in such young apoE$^{-/-}$ mice. This confirms the sensitivity and applicability of the method of *in vivo* large artery stiffness measurement developed, as reported in Chapter 3. Table 14 contrasts these present PWV results to those reported in the literature. It can be seen that significant differences between WT and apoE$^{-/-}$ mice have only been observed in mice nine months and older. This may be due to the fact that PWV has only been measured at baseline MAP. As shown in the table below, no significant differences in PWV at baseline pressures were found by this present study. This demonstrates the crucial importance of measuring pressure-dependent PWV: vessel wall abnormalities may not be apparent at anaesthetized baseline MAP.

Table 14: Comparison of our PWV measurement in apoE$^{-/-}$ to those taken from the literature.

Age (months)	PWV – WT (m/s)	PWV – apoE$^{-/-}$ (m/s)	Measurement method	Source
4	2.5 ± 0.4	2.9 ± 0.5 (NS)	Two intravascular catheters	Maizel, 2009 (53)
8	2.6 ± 0.1	3.6 ± 0.2*	MRI	Herold, 2009 (49)
8	2.4 ± 0.4	3.0 ± 0.6 (NS)	MRI	Parczyk, 2010 (48)
4	~ 2.5	~2.9 (NS)	Intravascular P1,	Wang, 2000 (51)
13	2.9 ± 0.2	3.8 ± 0.2 *	tonometer P2	
6	N/A	~3.6	Doppler	Tham, 2002 (41)
9	3.55 ± 0.97	5.84 ± 2.15 *	MRI	Zhao, 2009 (50)
13	3.79 ± 1.01	4.28 ± 1.45 *	Doppler	Hartley, 2000 (42)
3	2.99 ± 0.13	3.11 ± 0.34	Invasive	This study

ApoE$^{-/-}$ mice were also treated with L-NAME in an attempt to exacerbate the progression of atherosclerosis, as it has previously been demonstrated that L-NAME treatment significantly accelerates plaque formation in the aortas of apoE$^{-/-}$ mice (175). L-NAME treatment tended to reduce the pressure dependent PWV such that it was not different to the WT control animals. Although the treatment duration was relatively short (2 weeks) this limitation does not explain why aortic stiffness was actually decreased in L-NAME-treated apoE$^{-/-}$ mice. In Chapter 5, L-NAME also seemed to produce a beneficial effect, although it was not significant, and in Chapter 6, L-NAME treatment did not produce any effect at all. However, in this study, L-NAME administration significantly lowered PWV, suggesting that perhaps there is a compensatory mechanism preventing the expected increase in arterial stiffness from occurring, in addition to prostacyclin or EDHF as previously suggested.

Wilcox et al found that there was a loss of eNOS expression over advanced atherosclerotic lesions while there was an increase in inducible NOS (iNOS) and neuronal NOS (nNOS), both of which are not detected in the normal vessel wall (224). iNOS produces very high quantities of NO (225) which may actually have adverse effects on the vasculature. Excess NO may also interact with superoxide, yielding potent ROSs which induce significant cellular

damage, or toxic cytolytic effects that may induce cell death and tissue necrosis in advanced plaques (224, 226). In fact, Kuhlencordt et al used an apoE/iNOS double knockout mouse model to demonstrate that genetic deficiency of iNOS decreases diet-induced atherosclerosis and reduces markers for oxidative stress, in apoE$^{-/-}$ mice (227). Furthermore, neuronal NO has also been shown to exacerbate acute ischemic injury and cause necrosis in brain vessels (228). Therefore, it is proposed that L-NAME administration in apoE$^{-/-}$ mice, which are prone to atherosclerosis, produced beneficial effects due to the inhibition of iNOS and nNOS.

Another possible mechanism arises from a feature of vascular dysfunction and disease: the electron flow through the eNOS enzyme becomes uncoupled, resulting in the production of superoxide anion radical rather than NO, which augments vascular dysfunction. Treatment with L-NAME may have then inhibited the production of superoxide anion radical due to uncoupled eNOS activity that may be present in the apoE$^{-/-}$ mice.

At low pressures (60-65 mmHg), both treated and untreated apoE$^{-/-}$ mice had lower PWV than WT mice. It is uncertain why this is the case. The differences are quite small and the differences occur at pressures which are lower than physiological MAP, so it may not be extremely beneficial to investigate this further, although perhaps larger group sizes would eliminate this difference.

Sensitivity of PWV to changes in MAP was higher in the apoE$^{-/-}$ mouse compared to WT control and L-NAME treated apoE$^{-/-}$ mice at medium (90 mmHg) and high (120 mmHg) pressures. This is important because it suggests that for every mmHg increase in MAP, the associated increase in PWV is significantly higher in apoE$^{-/-}$ mice compared to the other two groups.

The stress-strain relationships agreed quite well with the PWV-MAP relationships in that both measures indicated that apoE$^{-/-}$ mice had stiffer arteries compared to WT control and apoE$^{-/-}$ mice given L-NAME for two weeks. From the Moens-Korteweg equation (2.1), PWV is

directly proportion to the elastic modulus. The data suggests that changes may have occurred in the material properties of the aorta in the apoE$^{-/-}$ mouse that have caused it to become functionally stiffer compared to WT control. Furthermore, treatment with L-NAME may have reversed these changes.

There were no differences observed in the incremental stiffness in any of the groups studied. While this observation was discussed in Chapter 4 for control mice, due to the preferential distribution of atherosclerotic plaques around sites of disturbed flow along the aorta, it was thought there may be differences in PWV occurring with location in the apoE$^{-/-}$ mice. However, as these mice were quite young, the development of plaques was not severe enough to induce detectable changes in the incremental arterial stiffness. Because these measurements were taken at baseline pressures, the apoE$^{-/-}$ mice did not have increased incremental PWV compared to the other two groups.

As previously observed, there was virtually no PPA at pressures of 85 mmHg and greater (PPA ~ 1), and this value falls with MAP below this value. There were no differences observed between strains.

No significant differences were observed in BRS, although there was a trend towards slightly decreased BRS in the apoE knockout animals.

No differences were observed in the maximum contractile response to PE, dose-response curves, or EC_{50} between WT and apoE$^{-/-}$ mice. L-NAME treatment severely impaired the maximum force of contraction to PE; however, it did not alter the sensitivity of the aortic rings as evidenced by similar dose-response curves and EC_{50} values. Additionally, in L-NAME treated mice, there was a reduction in the maximum contractile response to PE and EC_{50} values in the abdominal rings compared to the thoracic. As the mice used in this study are still quite young, impairment in smooth muscle contractility was not expected.

Smooth muscle cell relaxation was not very different between any of the groups studied. There was a slight shift to the right in dose-response curves and EC_{50} values in apoE$^{-/-}$ mice (control and L-NAME treated) in the thoracic aortas only. Further, all rings were able to achieve full relaxation in both thoracic and abdominal aortas from all three groups.

Endothelium dependent relaxation, much like that discussed in Chapter 6, was severely impaired in the WT mice, and it was non-existent in apoE$^{-/-}$ mice, whether or not they were given L-NAME in the drinking water. Due to the development of atherosclerotic plaques in the apoE$^{-/-}$ animals, exacerbated by the inhibition of NOS, a reduction in the response to ACh in these mice was expected. However, a complete abolishment, or even constriction, has not previously been reported in the literature. Nevertheless, the results from this study indicate that both untreated and L-NAME treated apoE$^{-/-}$ mice have strongly diminished endothelium-dependent relaxation responses compared to control.

Vascular reactivity experiments therefore yielded the following results: *(i)* while apoE$^{-/-}$ mice have a normal response to PE, L-NAME treatment reduced this; *(ii)* there were generally no differences observed in the response to SNP; *(iii)* endothelium-dependent relaxation to ACh was abolished in control and L-NAME treated apoE$^{-/-}$ mice; and *(iv)* there were generally no differences between rings taken from the thoracic and abdominal aorta.

Results concerning the effect of apoE on vascular reactivity are quite varied from one study to the next being influenced by many factors such as age, diet or various treatments. However, impairments in vascular reactivity have not been reported in young apoE$^{-/-}$ compared to controls without a treatment that accelerates atherosclerosis progression, such as a Western diet (229). For example, Kauser et al found that contractile responses to U-46619 were no different between 4 month old WT and apoE$^{-/-}$ mice. They also did not find any differences in relaxation responses induced by ACh or SNP. They did show that L-NAME significantly inhibited ACh-induced relaxation with no changes in SNP-mediated relaxation (175). Wang

et al also found no difference in responses to ACh or SNP in 4 month old apoE$^{-/-}$ mice compared to control, but at 13 months, the response to ACh was severely diminished (51). A significant reduction in ACh-mediated relaxation has been noted at 18 weeks of age in apoE$^{-/-}$ relative to controls, but not in 14 weeks of age (53). Chen et al also found that apoE$^{-/-}$ mice had impaired vasorelaxation to ACh relative to control at 18 weeks of age and incubation of the aortic rings with L-NAME for 20 min completely abolished this response. However, these mice had been fed a Western-type diet instead of standard chow (223). Therefore, while smooth muscle cell responses to PE and SNP presented here fit well with previously reported findings, the endothelium-mediated responses to ACh do not. The accelerated endothelial dysfunction observed here may be a real effect of the deletion of the apoE$^{-/-}$ gene that has not been noted previously. Environmental factors, experimental setup, or slight genetic variation in strains may account for the discrepancies between our results and those from the literature. On the other hand, as previously discussed, the fact that these experiments were done post-surgery may be the cause of the excessive endothelial dysfunction observed.

There were no changes observed in calcium content in the aortas between the three groups of mice studied. However, it is known that calcification often occurs in conjunction with progression of atherosclerosis, although it may be located specifically in intimal plaques. An explanation may be that the mice were too young to demonstrate detectable changes in levels of calcification. However, Maizel et al detected increased levels of both intimal and medial calcification in apoE$^{-/-}$ mice compared to WT control in mice as young as 8 weeks old (53). In this study by Maizel et al, when challenged with chronic renal failure, the apoE$^{-/-}$ had even greater levels of aortic calcification compared to WT. Interestingly, they saw no differences in blood pressure, LV mass, or PWV between apoE$^{-/-}$ and WT mice, suggesting that increased calcification may not be necessarily associated with increased PWV.

H&E staining showed no gross morphological changes in the apoE$^{-/-}$ mice compared to WT controls regardless of L-NAME administration. There were also no geometrical differences in the media-to-lumen ratio or the medial thickness. This was not surprising as these mice are still in the early phase of atherosclerosis progression. At 12 weeks of age, there are likely small foam cell deposits within specific regions of the aorta, but no fibrous cap lesions or excess calcification (174). It has been previously reported that H&E stained sections of thoracic aorta from apoE$^{-/-}$ appear completely normal when compared to WT controls at 4 months of age (51). Buday and colleagues also found no change in aortic wall thickness between 8 month old C57Bl6 and apoE$^{-/-}$ mice (222). Similarly, a study by Bentzon et al demonstrated no differences in the vessel area, as quantified by the area circumscribed by the internal elastic lamina, between WT and apoE$^{-/-}$ mice at 11 weeks and 6 months of age (230). Therefore, the changes observed in PWV cannot be explained by changes in the vessel geometry. Total plaque area, although likely insignificant, and elastin fragmentation, which may occur underneath atherosclerotic lesions in apoE$^{-/-}$ mice (51), were not assessed in this study, and could possibly provide some insights regarding the increased stiffness in the young apoE$^{-/-}$ mice when compared to controls. Future experiments should include a more in depth histological assessment, including these, and other potential factors which may affect vessel wall properties, such as collagen content.

While the measured baseline parameters were approximately the same in all three groups, PWV was significantly higher at pressures of 95 mmHg and above in apoE$^{-/-}$ mice compared to WT controls. At the age of 12 weeks, it has been shown that there is no atherosclerosis development in WT mice (171). Therefore, the vascular stiffening and endothelial dysfunction observed in the apoE$^{-/-}$ mice in this study is likely due to the effects of the ongoing progression of atherosclerotic plaques that occurs in these animals. The endothelial dysfunction itself also may contribute to the increased aortic stiffness. L-NAME treatment lowered the PWV in apoE$^{-/-}$ mice back to control values. This suggests the existence of

compensatory mechanisms at play here. Firstly, as previously described (Section 5.3) EDHF or prostacyclin may be upregulated in the absence of NO. Second, the increased iNOS and nNOS activity that occurs with atherosclerosis and has detrimental effects on the vasculature is also inhibited by L-NAME, thereby benefitting vessel wall health. The apoE$^{-/-}$ mice treated with L-NAME would be expected to have at least the same levels of atherosclerosis as their untreated counterparts, and these studies have demonstrated similar levels of endothelial dysfunction. Future studies could concentrate on what this potential mechanism may be. This was an important study as it is the first to show a significantly increased PWV in apoE$^{-/-}$ mice compared to WT control at this age. Further, it demonstrates that the technique developed in this thesis for measuring PWV in the mouse is in fact capable of detecting differences in pressure-dependent PWV.

Chapter 8

Effect of age on pressure-dependent PWV in the mouse

Age is the major risk factor of increased arterial stiffness (63). Therefore, it is of interest (and also important) to understand how age affects stiffness in mouse models, especially if they are being used to mimic human pathological processes. There are few data concerning PWV and age in mice, due in part to the past difficulties faced with obtaining these measurements. Over the course of developing the technique used throughout this thesis, a substantial amount of data was acquired across a range of different types of mice and under varied techniques. This includes differences in strain, gender, and age. This prompted a preliminary investigation into the effects of aging on pressure-dependent PWV in these animals. Following the significant changes observed for the first time in the PWV-MAP relationship of apoE$^{-/-}$ mice compared to WT controls at 12 weeks of age, a study was performed in 36-week old mice of the same strains. In addition to providing more substantial results to the preliminary analysis, this study was conducted as a first attempt to assess the possible confounding effects of age and atherosclerosis on the progression of increased vascular stiffness.

8.1 Methods

8.1.1 Animals

A description of the various mice used in the first part of this chapter can be found in Appendix A4. For the second part of this chapter, male apoE$^{-/-}$ and C57Bl6 (WT) mice (ARC, Perth), aged 36 weeks (old) and 12 weeks (young) were studied. Animals were kept in a temperature controlled environment (21 ± 2^{o}C) with 12 hour light/dark cycles. Animals had ad libitum access to standard laboratory mouse feed and water. The animal protocol was approved by the Macquarie University Animal Ethics Committee (ARA 2011/002, ARA, 2011/017).

8.1.2 Experimental procedures

Mice were anaesthetized and aortic stiffness was measured across a full range of physiological arterial pressures as previously outlined in Section 5.1.3 (except in some cases for the first part of this study, descriptions of other techniques can be found in Appendix A4). Baroreflex sensitivity, tissue dissection and preparation, wire myography, tensile testing, and histological evaluation of the aorta were also performed as described in Chapter 5.

8.1.3 Statistical Analysis

Data are presented as mean ± standard error, except where otherwise indicated. Data were analysed offline using a combination of Microsoft Excel, IBM SPSS Statistics 19, and GraphPad Prism 6.

Data recorded across all pressure ranges were divided into 5 mmHg pressure bins. Statistical differences between groups were determined using either: paired Student's t-tests for each pressure bin, 1-way ANOVA followed by Tukey's multiple comparison test, or 2-way ANOVA followed by Sidak's multiple comparisons test (unless otherwise indicated). This is

detailed in the results sections. P-values less than 0.05 were considered to be statistically significant.

Dose-response curves were fitted with a sigmoidal dose-response function through non-linear regression in Prism, returning EC_{50} and maximum response parameters. Two-way ANOVA with Bonferroni post-hoc test was employed to compare responses at each concentration. EC_{50}s and maximum responses were compared using one-way ANOVA followed by Tukey's multiple comparisons test. Again, P-values less than 0.05 were considered to be statistically significant.

8.2 *Results*: preliminary analysis of the dependence of PWV on age

A description of the characteristics for each mouse included in this analysis can be found in Appendix A4. PWV measurements were examined according to pressure (60, 100, and 120mmHg) and age (8-46 weeks old). For each pressure, the PWV-age relationship was fit with a linear relationship (Figure 88).

PWV does not appear to increase markedly over this age span (Figure 88). Interestingly, the dependence of PWV on age (indicated by the slope of the line) slightly decreases with increasing pressure (Table 15). While the slopes of each line were not significantly different, the slope of the PWV-age relationship was the only slope to be significantly non-zero as determined by linear-regression analysis.

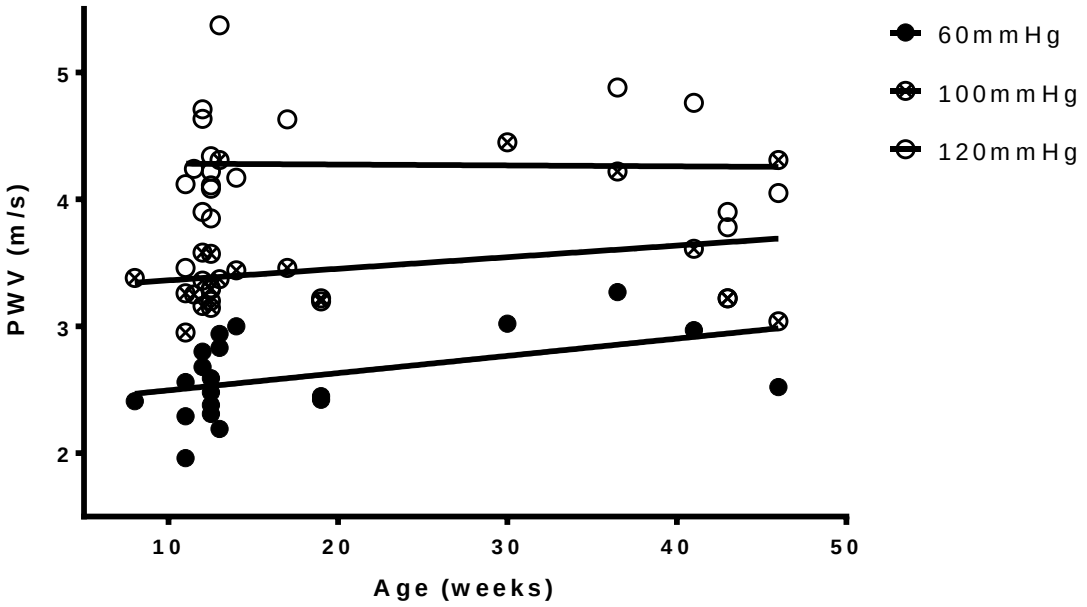

Figure 88: Relationship between age and PWV for three different values of MAP. Each data point represents values from an individual mouse. For each MAP group, data was fitted with a line. The equations for each of the lines can be found in Table 15.

Table 15: Equations of the linear regression for the PWV-age relationship for each of the three MAPs.

MAP (mmHg)	Equation of the line
60	*y = 0.0136x + 2.360*
100	*y = 0.0091x + 3.270*
120	*y = -0.0007x + 4.289*

8.3 *Results*: effect of age on WT and apoE$^{-/-}$ mice

The results presented below contain data from Chapter 7 regarding WT and apoE$^{-/-}$ mice aged 12 weeks. It is presented together with new data in this chapter in order to examine the effects of aging in both mouse strains. Consequently, the differences between WT and apoE$^{-/-}$ mice at an age of 12 weeks will not be highlighted in the following sections. The focus will be upon the differential effects of aging in the two strains.

8.3.1 Baseline characteristics

Baseline cardiovascular parameters did not differ between strains other than LV mass (normalized to body weight) at 36 weeks (Table 15). Young WT mice had lower body weight than all other groups. Old apoE$^{-/-}$ mice had higher body weight compared to young apoE$^{-/-}$ but not to age matched controls. Young apoE$^{-/-}$ mice had higher heart rates than all other groups. Old WT mice had lower baseline MAP compared to young mice. They also had lower LV weights (normalized to body weight) compared to young WT and old apoE$^{-/-}$ mice.

Table 16: Baseline cardiovascular characteristics (one-way ANOVA followed by Tukey's multiple comparisons test). *$p<0.05$ with respect to WT mice 12 weeks old; †$p<0.05$ with respect to apoE$^{-/-}$ mice 12 weeks old. $^{\#}p<0.05$ with respect to WT$^{-/-}$ mice 36 weeks old.

	WT - 12 weeks	**WT - 36 weeks**	**apoE$^{-/-}$ - 12 weeks**	**apoE$^{-/-}$ - 36 weeks**
BW (g)	26 ± 2	35 ± 3*	30 ± 1*	35 ± 2*†
HR (bpm)	500 ± 32	526 ± 51	582 ± 23*	521 ± 15†
MAP (mmHg)	93 ± 8	79 ± 5*	89 ± 9	88 ± 9
SBP (mmHg)	111 ± 9	96 ± 5*	107 ± 11	109 ± 13
DBP (mmHg)	78 ± 6	64 ± 6*	73 ± 8	72 ± 7
PP (mmHg)	33 ± 4	31± 3	34 ± 3	37 ± 7
Max dP/dt (mmHg·s^{-1})	859 ± 142	1029 ± 215	976 ± 224	1175 ± 466
PWV (m/s)	2.99 ± 0.13	3.12 ± 0.23	3.11 ± 0.34	3.27 ± 0.45
LV/BW (mg/g)	351 ± 20	297 ± 15*	372 ± 37	377 ± 40#

8.3.2 Pulse wave velocity

Old WT mice had significantly greater PWV at MAP of 100 mmHg and higher compared to young WT mice (Figure 89). There was a small but insignificant increase in PWV at pressures of approximately 115 mmHg and above in apoE$^{-/-}$ mice. There were no differences in PWV at any pressure between old WT and apoE$^{-/-}$ mice.

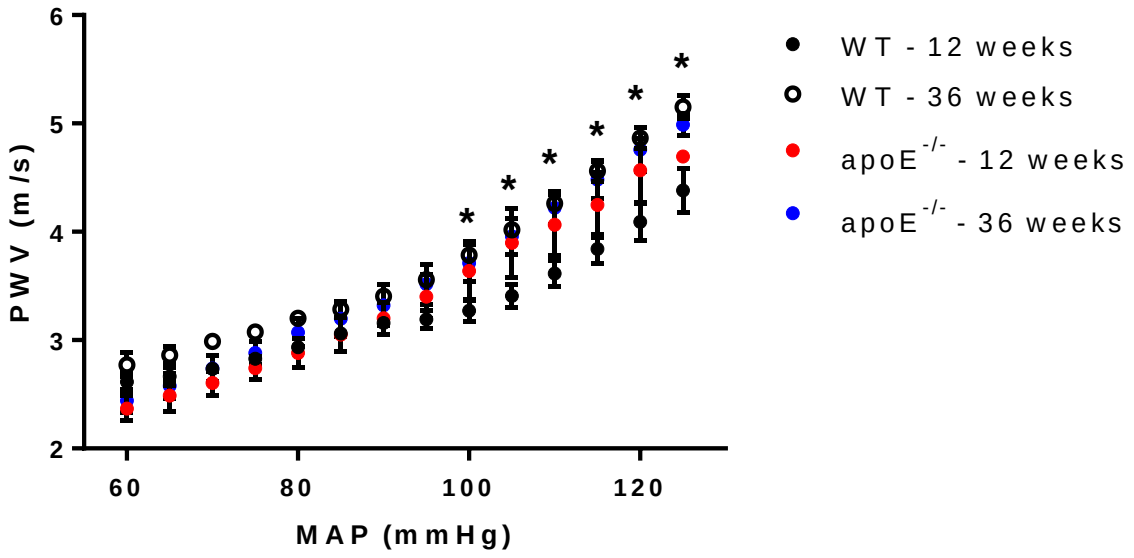

Figure 89: PWV-MAP relationship for WT and apoE$^{-/-}$ mice at ages 12 and 36 weeks. WT mice aged 36 weeks have higher PWV at 100 mmHg compared to WT control. ApoE$^{-/-}$ mice aged 36 weeks do not have significantly higher PWV than apoE$^{-/-}$ mice aged 12 weeks or WT mice aged 36 weeks. *p<0.05 for WT mice 36 weeks vs. 12 weeks.

Each PWV-MAP curve could be well described by a quadratic equation (Table 17). This indicates that for each group, the pressure sensitivity of PWV increases linearly with pressure (Figure 90). At pressures of 60 and 90 mmHg, apoE$^{-/-}$ mice trend towards increased sensitivity compared to WT controls. At all pressures, there is also a trend for increased sensitivity to pressure with age in WT mice. However, in the apoE$^{-/-}$ mice there is a tendency towards increased sensitivity at low pressures but which is diminished as pressure is increased.

Table 17: The PWV-MAP relationships in all four groups are well described by a quadratic equation. This indicates that sensitivity of PWV to changes in MAP increases linearly with pressure.

	Quadratic equation	**R^2**
WT – 12 weeks	$PWV = 3.553 - 0.03401(MAP) + 0.0003196(MAP)^2$	0.9871
WT – 36 weeks	$PWV = 4.042 - 0.04704(MAP) + 0.0004472(MAP)^2$	0.9978
apoE$^{-/-}$ - 12 weeks	$PWV = 1.742 - 0.002671MAP) + 0.0002145(MAP)^2$	0.9978
apoE$^{-/-}$ - 36 weeks	$PWV = 2.202 - 0.01185(MAP) + 0.0002740(MAP)^2$	0.9985

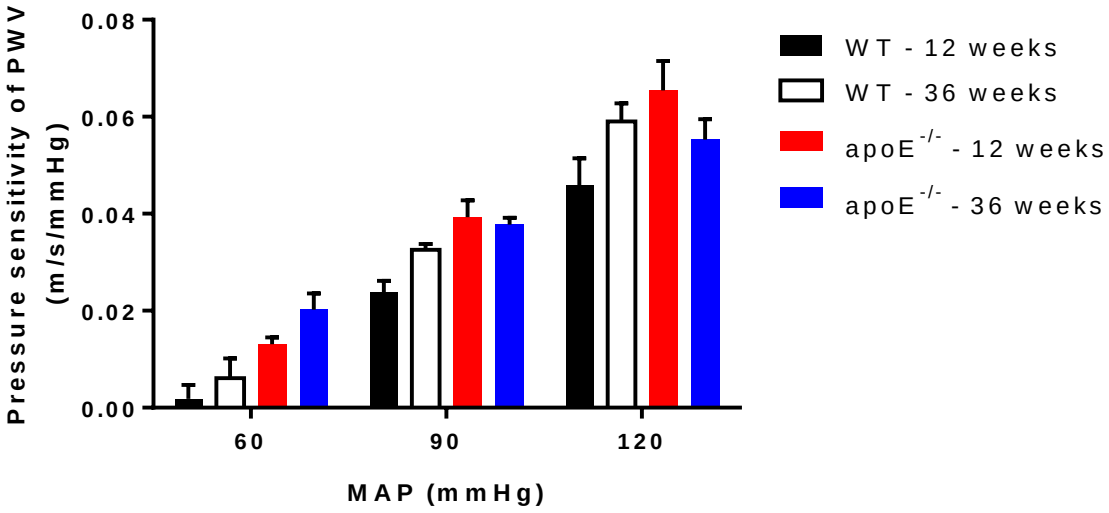

Figure 90: The pressure sensitivity of PWV increases with pressure. **N**o significant changes with age were observed in WT and apoE$^{-/-}$ mice. In addition, there were no significant differences between WT and apoE$^{-/-}$ at 36 weeks of age.

The pull-back technique described in Chapter 5 was used to measure the incremental stiffness along the length of the aorta. At distances greater than 0.005m from the aortic arch, PWV did not significantly differ with decreasing proximity or strain (Figure 91). At 0.005m from the arch, the PWV was significantly higher in the aorta of old WT mice compared to all other groups studied. It is important to note that there were no differences in MAP with location or strain along the aorta.

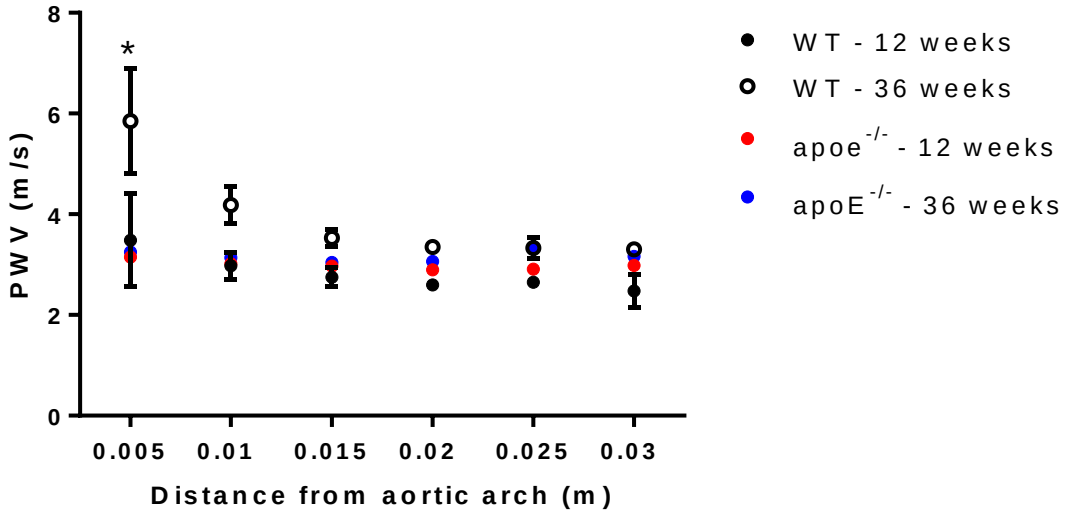

Figure 91: Relationship between PWV and distance from the aortic arch. PWV was significantly higher in old WT mice compared to all other groups at the most proximal location to the heart. *p<0.05.

As described in previous chapters, PPA is around 1 at pressures of 80mmHg and greater. PPA steadily drops as pressures fall below 80mmHg. At all values of MAP, there were no significant differences in PPA between the four groups of mice studied (Figure 92).

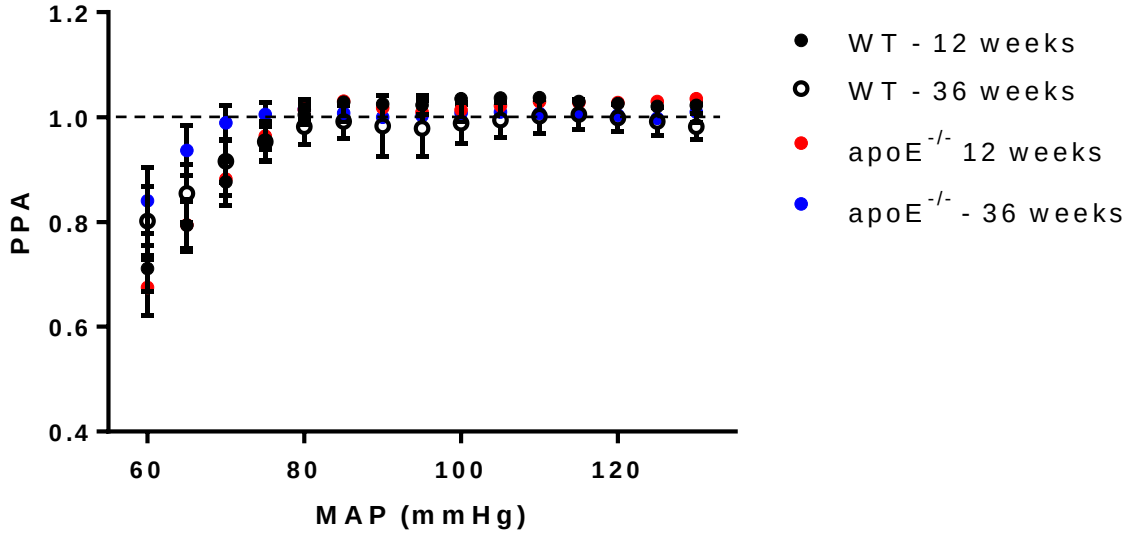

Figure 92: PPA-MAP relationship for WT mice and apoE$^{-/-}$ mice at ages 12 and 36 weeks. There were no significant differences detected between any of the groups studied.

8.3.3 Baroreflex sensitivity

There was no significant difference in drug-induced BRS with strain or age (Figure 93).

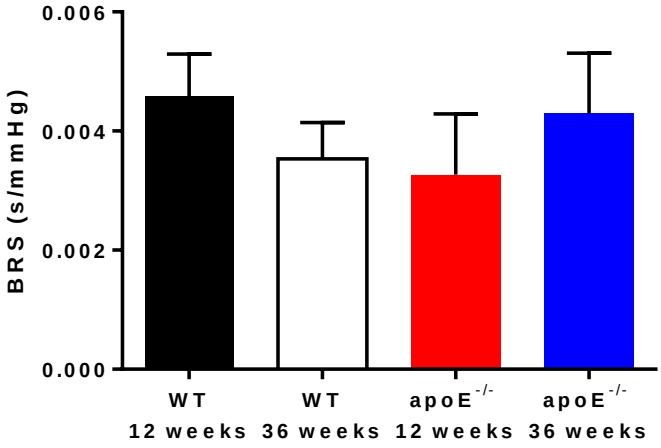

Figure 93: Drug-induced BRS was not different between groups.

8.3.4 Tensile testing

The tensile testing data showed that the incremental elastic modulus (strain = 0.1) increased significantly in WT mice from the age of 12 weeks to 36 weeks. There was a slight though non-significant increase in the E_{inc} in apoE$^{-/-}$ mice over the same time period (Figure 94).

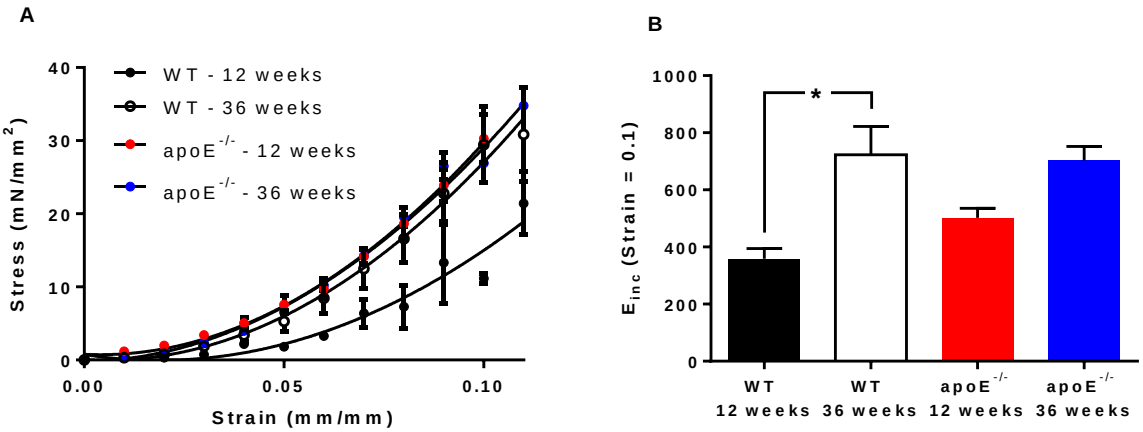

Figure 94: The stress-strain curves (A) and E_{inc} at a strain of 0.1 (B) for old and young WT apoE$^{-/-}$ mice. The incremental elastic modulus increased significantly in old WT mice compared to young WT mice. *p<0.05

8.3.4 Vascular reactivity

8.3.4.1 Smooth muscle cell contraction

Vasoconstrictor responses to PE were examined. There was no attenuation of the maximum contractile response to PE in apoE$^{-/-}$ mice compared to WT mice in the thoracic or abdominal aorta. In the thoracic aorta there was a trend towards decreased maximal responses in the old compared to the young mice which was significant only in the apoE$^{-/-}$ mice (Figure 95A). This was not seen in the abdominal sections (Figure 95B).

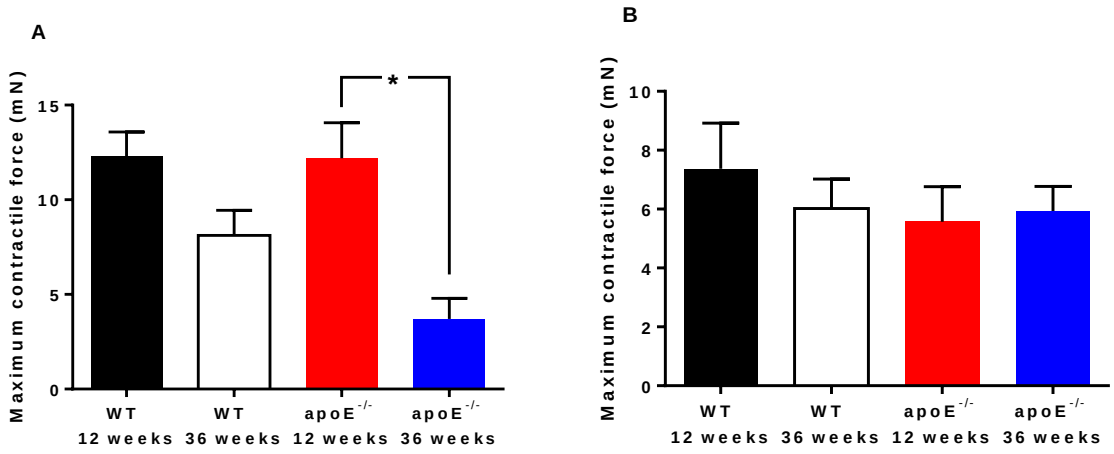

Figure 95: Maximal contraction to PE in thoracic (A) and abdominal (B) segments isolated from the three different mice groups *ex vivo*. Old apoE$^{-/-}$ mice aged had an impaired vascular smooth muscle contractile response significantly only in the thoracic sections compared to young apoE$^{-/-}$ mice. No changes were observed in the abdominal rings *P<0.05.

There were no strain-related differences in the dose-response curves to PE or the EC_{50} values in the thoracic aorta, indicating no changes in sensitivity to PE (Figure 96). Aside from two points on the dose-response curve that indicate a slight shift to the right of the 12 week old WT mice, there were no age-related differences in the thoracic aorta either.

There were also no observed strain-related differences in the PE dose-response curve or EC_{50} values in rings isolated from the abdominal aorta (Figure 97). However, in apoE$^{-/-}$ mice and

WT controls, there was a shift to the right of the dose-response curve with age and a decreased EC_{50} value indicating reduced sensitivity to PE in the old mice.

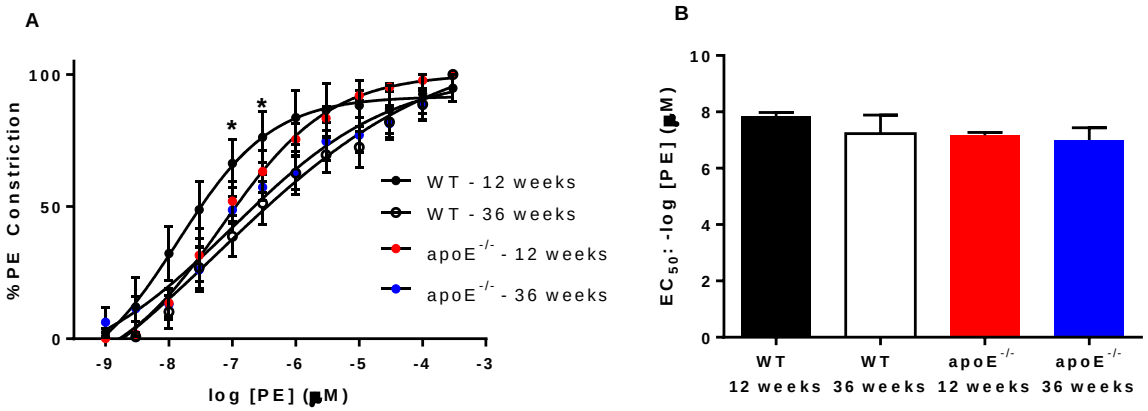

Figure 96: Contractile response to PE (A) and EC_{50} values (B) in the thoracic aorta. With the exception of a slight shift to the left in the dose-response curve from the old WT mice, no differences were observed in the dose-response curves of EC_{50} values. *p<0.05 for old versus young WT mice.

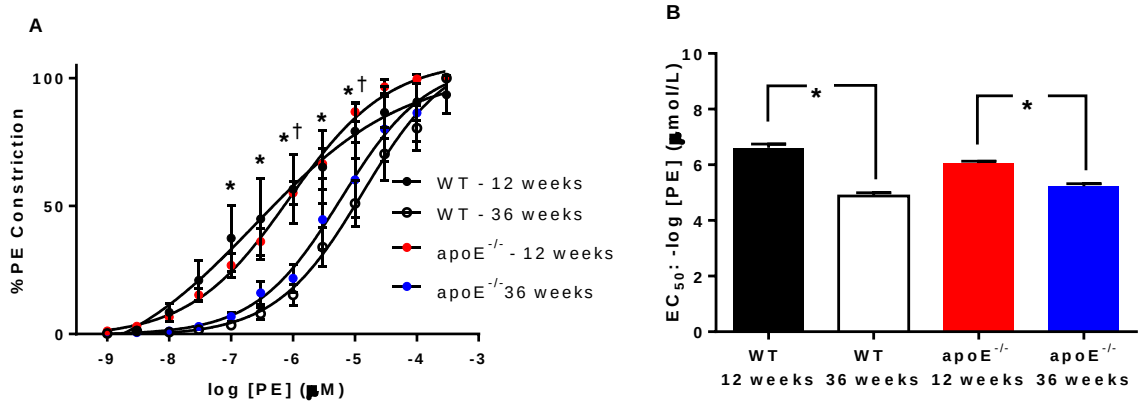

Figure 97: Contractile response to PE (A) and EC_{50} values (B) in the abdominal aorta. There is a shift to the right in the dose-response curve and reduced EC_{50} values between 36 week old animals and 12 week old animals. (A) *p<0.05 WT – 12 weeks versus WT – 36 weeks; †p<0.05 $apoE^{-/-}$ - 12 weeks versus $apoE^{-/-}$ - 36 weeks. (B) *p<0.05

There were no differences between thoracic and abdominal rings regarding the maximum contractile force (Figure 98A). The EC_{50} values were lower in the abdominal rings compared to the thoracic rings in all groups (Figure 98B).

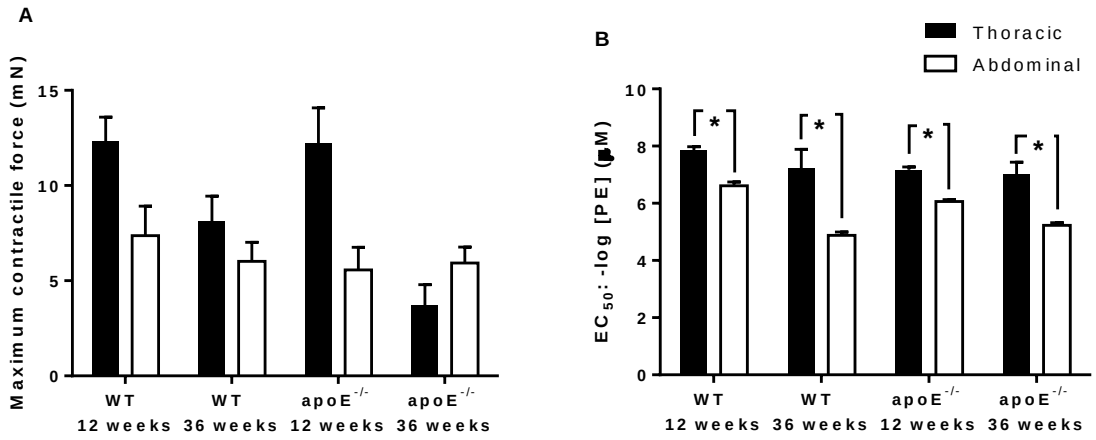

Figure 98: Maximum force of contraction to PE (A) and EC_{50} values (B) for rings taken from the thoracic and abdominal aortas. There were no differences in maximum contractile forces between thoracic and abdominal sections. The EC_{50} values were significantly lower in all groups.

8.3.4.2 Smooth muscle cell relaxation

There was no impairment in endothelium-independent relaxation to SNP in any of the groups studied whether rings were isolated from the thoracic (Figure 99) or abdominal aorta (Figure 100), as full relaxation was achieved in all groups consistently. In the thoracic aorta, there was slightly increased sensitivity in older apoE$^{-/-}$ mice compared to younger ones. No age-related differences were detected in the WT mice. There was also a small but significant shift to the right in the apoE$^{-/-}$ mice compared to WT control at 36 weeks.

The abdominal aortas of older mice had reduced sensitivity to SNP. In both WT and apoE$^{-/-}$ mice the dose-response curves of the older age group were right shifted compared to the younger group and EC_{50} values were lower (Figure 100).

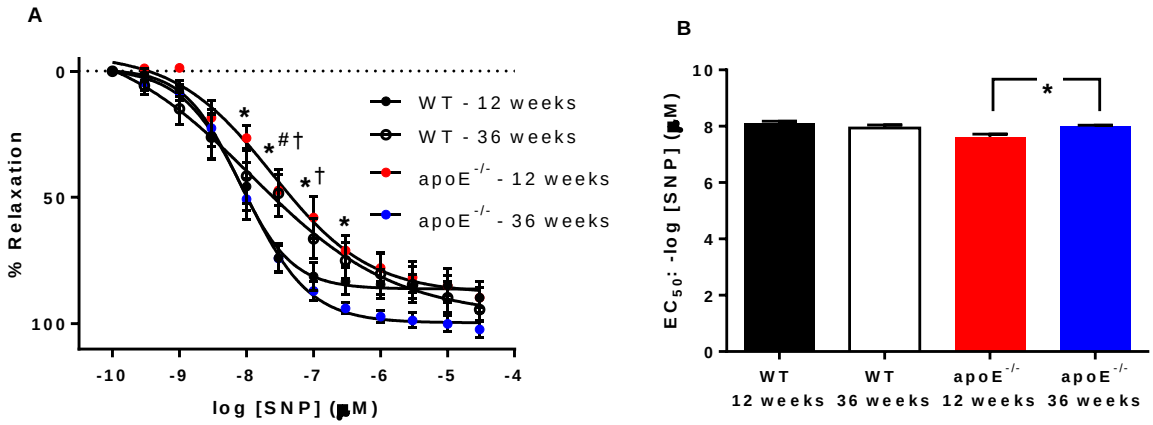

Figure 99: Relaxation response to SNP (A) and EC_{50} values (B) in the thoracic aorta. While there was a slight shift to the right of the old WT and young apoE$^{-/-}$ mice, none of the groups had any impairment in their smooth muscle relaxation responses. Old apoE$^{-/-}$ mice had a slightly higher EC_{50} value compared to young apoE$^{-/-}$ mice. (A) *p<0.05 between young and old apoE$^{-/-}$ mice; †p<0.05 between 36 week old WT and apoE$^{-/-}$ mice; $^{\#}$p<0.05 between young and old WT mice. (B) *p<0.05.

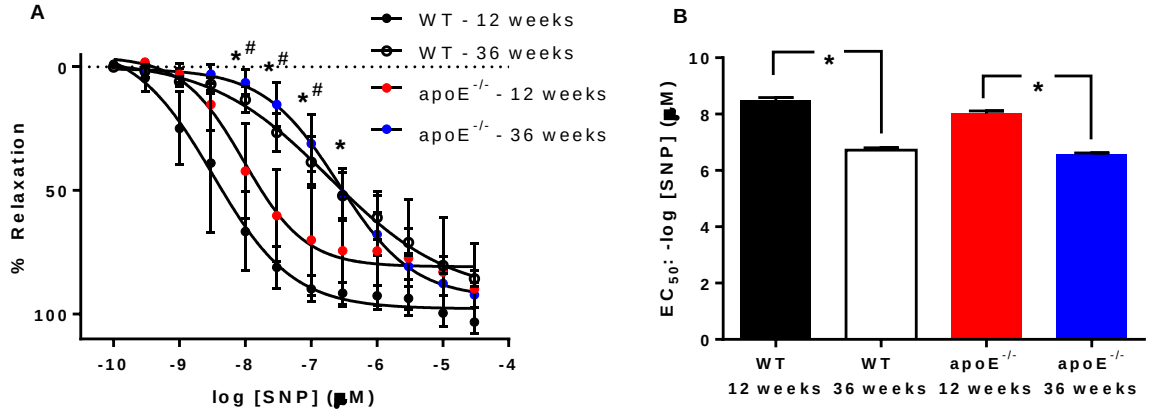

Figure 100: Relaxation response to SNP (A) and EC_{50} values (B) in the abdominal aorta. While the relaxation response was not impaired in any of the four groups examined, mice that were 36 weeks old had reduced sensitivity to SNP as indicated by a right-ward shift in the dose-response curves and reduced EC_{50} values. (A) *p<0.05 between young and old apoE$^{-/-}$ mice; $^{\#}$p<0.05 between young and old WT mice. (B) *p<0.05.

In younger mice, abdominal aortas had higher EC_{50}s than thoracic while in older mice abdominal aortas had lower EC_{50}s (Figure 101). This suggests that age impacts the sensitivity in the abdominal aortic regions rather than the thoracic ones.

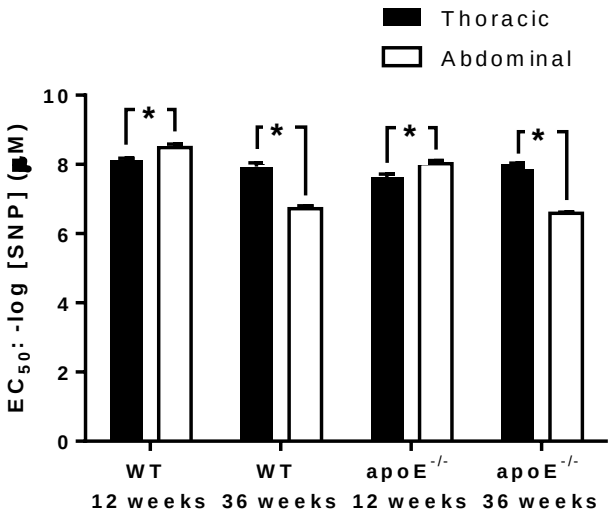

Figure 101: EC_{50} values from the thoracic and abdominal aortas. At 12 weeks of age, thoracic sections had reduced sensitivity to SNP compared to abdominal sections. At 36 weeks of age, abdominal sections have reduced sensitivity to SNP compared to thoracic sections. *p<0.05.

8.3.4.3 Endothelium-dependent relaxation

The relaxation to ACh was significantly impaired in all of the groups. There were no significant age-related changes observed; however, from Figure 102, it can be seen that the maximum relaxation is reduced in the old WT animals compared to their young counterparts. In both groups of $apoE^{-/-}$ mice the response to ACh was completely abolished. This was the case in both thoracic and abdominal aortas.

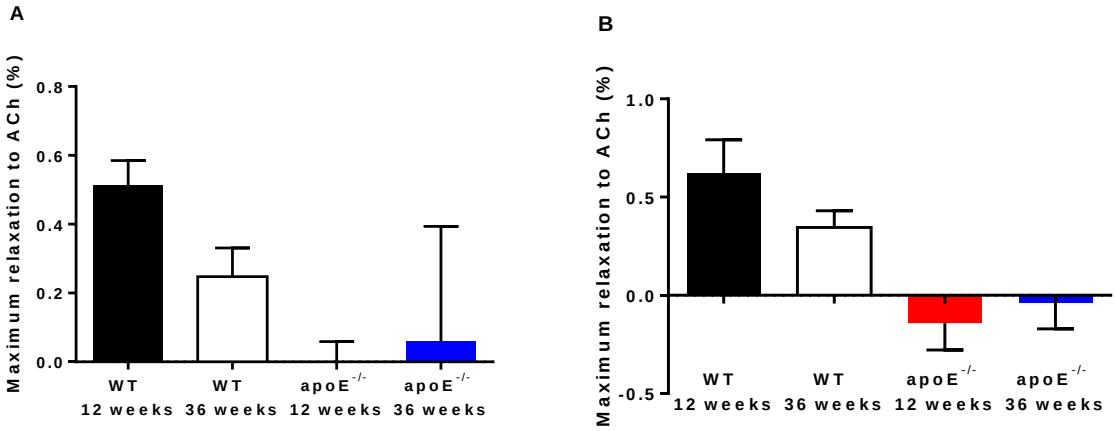

Figure 102: Maximum relaxation to ACh in thoracic (A) and abdominal (B) aortic segments. Relaxation to ACh was completely abolished in apoE$^{-/-}$ mice. No significant differences were observed between old and young mice or between old WT and apoE$^{-/-}$ mice.

The relaxation-response curves to ACh were severely impaired in the thoracic aorta of all groups. No relaxation at all was observed in apoE$^{-/-}$ mice regardless of age. In WT mice, there were no statistically significant differences at 12 versus 36 weeks of age. It can be seen in Figure 103A that the dose-response curve from the old WT mice was shifted to the right compared to young WT mice. This is supported by the slightly reduced EC_{50} values (Figure 103B). EC_{50} values are not shown for the apoE$^{-/-}$ mice as a sigmoid curve could not accurately be fit to the data points as there was no dose response.

In abdominal aortic rings, the dose-response curves demonstrated a similar trend as in the thoracic rings (Figure 104A). There was a shift to the right of the dose-response curve in old compared to young WT mice. This was accompanied by a significant reduction in the EC_{50} values indicating a reduced sensitivity to ACh with age in WT mice. The EC_{50} values cannot be evaluated in apoE$^{-/-}$ mice as these rings constricted and could not be fit with a sigmoidal curve, whereas WT rings relaxed (Figure 104B).

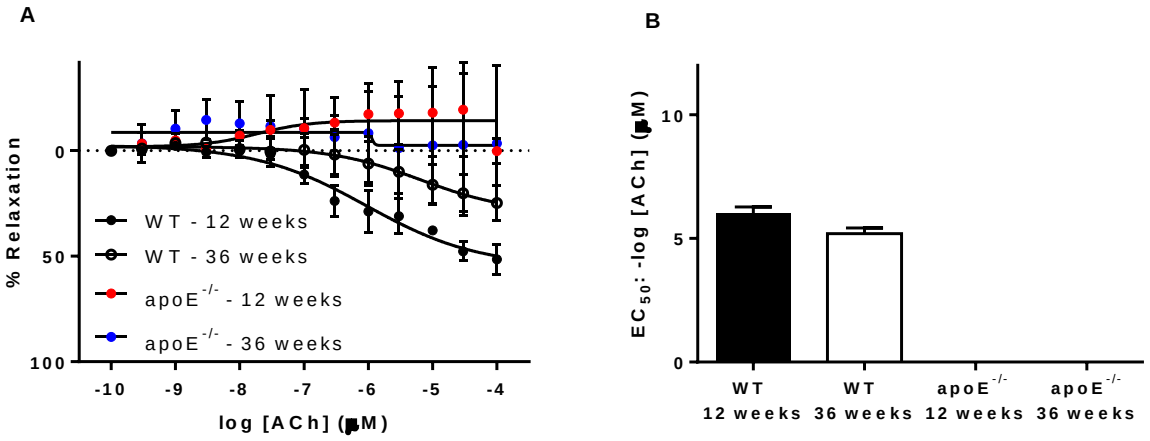

Figure 103: Relaxation response to ACh (A) and EC50 values (B) in the thoracic aorta of 12 and 36 week old apoE$^{-/-}$ and WT mice. The relaxation response from the apoE-/- mice was completely abolished. Though not statically significant, the relaxation to ACh was reduced in the old WT mice compared to young WT mice. The EC50 values were not significantly different; however, as previously mentioned the EC_{50} values from the apoE$^{-/-}$ mice do not exist as there was no dose response.

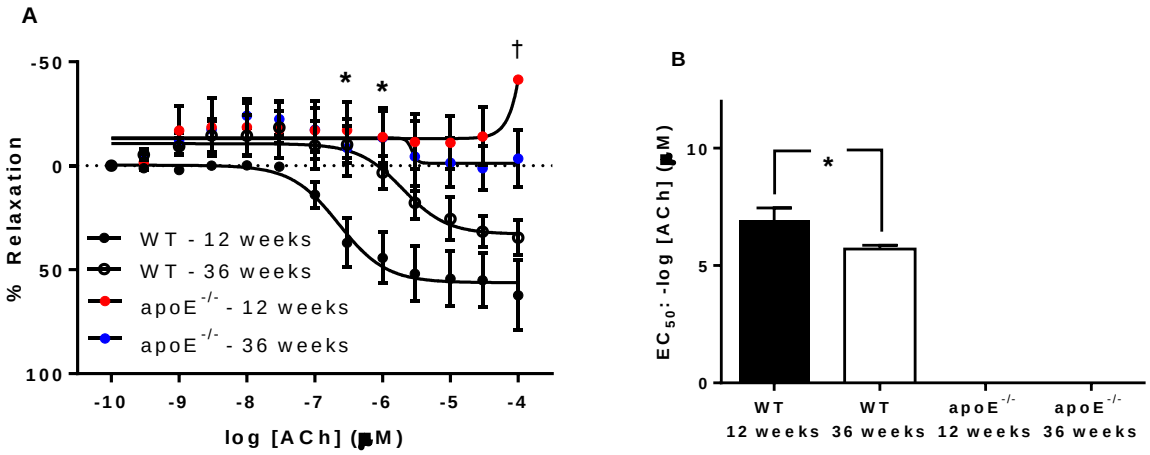

Figure 104: Relaxation response to ACh (A) and EC50 values (B) in the abdominal aorta of 12 and 36 week old apoE$^{-/-}$ and WT mice. The relaxation response from the apoE$^{-/-}$ mice was completely abolished. The old WT mice had reduced endothelium dependent responses, although this was not significant. The EC_{50} values were significantly lower in the old WT mice compared to the young WT mice; however, as previously mentioned the EC_{50} values from the apoE$^{-/-}$ mice are invalid. (A) *$p<0.05$ for young versus old WT mice; †$p<0.05$ for old apoE$^{-/-}$ versus WT mice. (B) *$p<0.05$.

There were no differences detected between aortic rings from the thoracic aorta versus those taken from the abdominal aorta regarding responses to ACh. Neither the maximum relaxation to ACh, nor the EC_{50} values were statistically different between thoracic and abdominal sections. The EC_{50} values for $apoE^{-/-}$ mice could not be compared as previously mentioned (Figure 105).

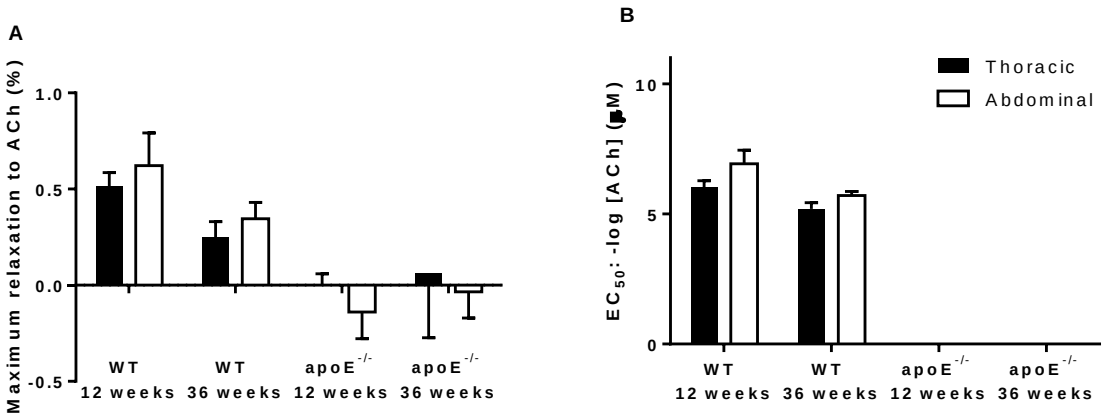

Figure 105: Maximum relaxation to ACh (expressed as a percentage of complete relaxation) (A) and EC50 values (B) for rings taken from the thoracic and abdominal aortas. No location-related differences were detected.

8.3.5 Histology

Although the aortas were not specifically stained for quantification of atherosclerotic lesions, in the old $apoE^{-/-}$mice, lesions were visible to the naked eye as can be seen in the following photograph and in some histological sections stained with H&E (Figure 106).

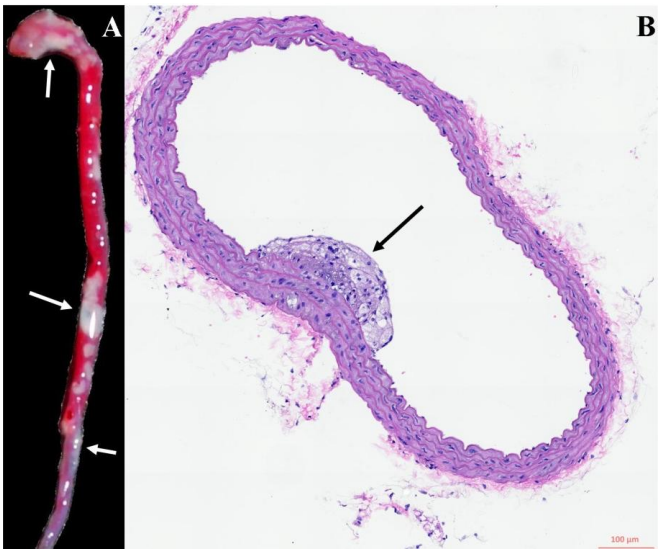

Figure 106: Photograph of an aorta from an old apoE$^{-/-}$ where lesions are clearly visible (A) and an aortic cross-section stained with H&E from an old apoE$^{-/-}$ mouse with an obvious lesion (B). Lesions are indicated with arrows.

The media-to-lumen ratio was not different between groups. The wall thickness in WT mice significantly increased between 12 and 36 weeks of age (50 ± 2 and 60 ±3 μm respectively, $p<0.05$). There was a trend of increased wall-to-lumen ratio and wall thickness with age in the apoE$^{-/-}$mice. However, no significant changes were observed in the apoE$^{-/-}$ mice with age or compared to age matched WT controls (Figure 107 and Figure 108).

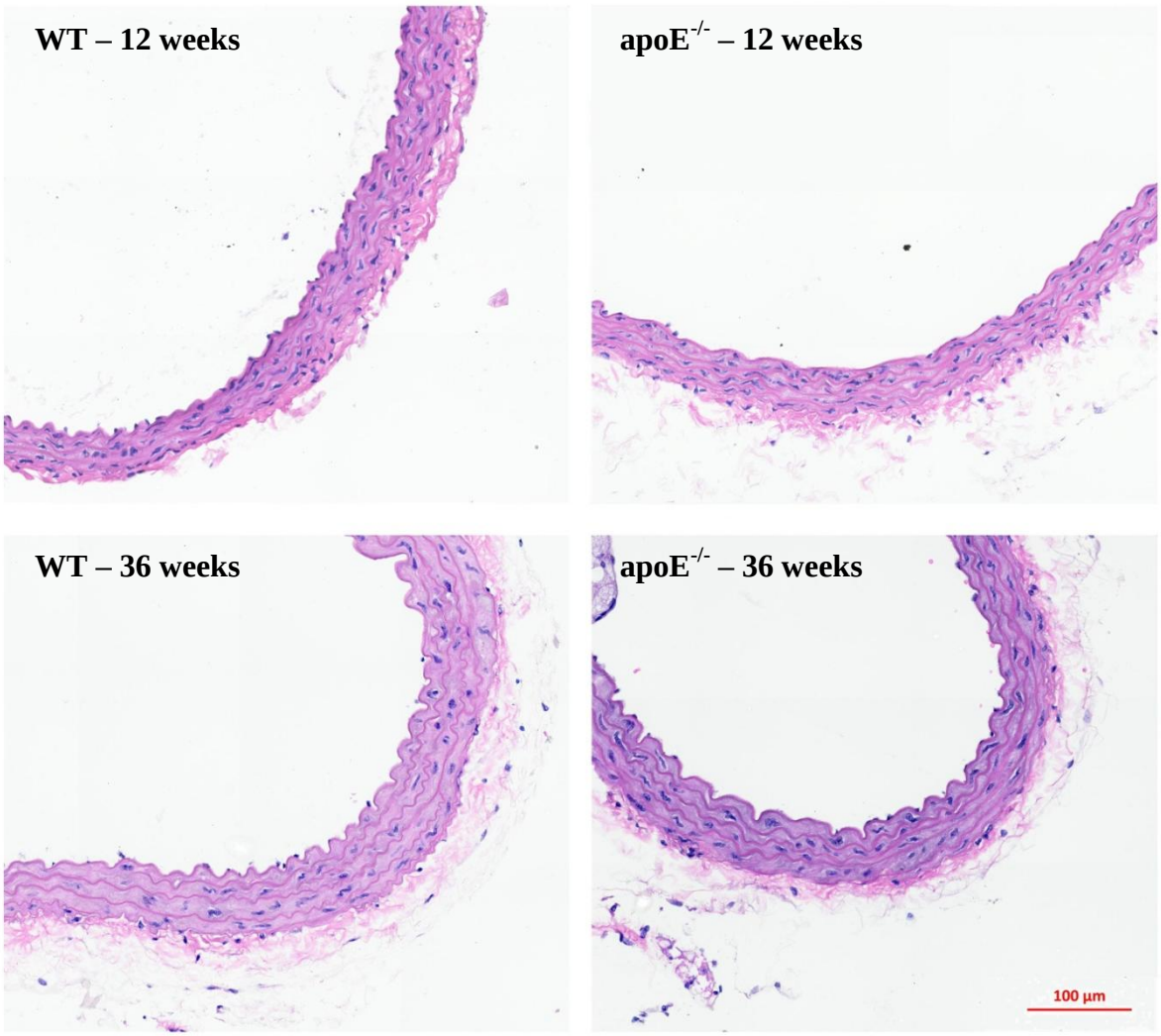

Figure 107: Representative images of histological cross sections of thoracic aortas from 12 and 36 week old WT and apoE$^{-/-}$ mice. Bar: 100 µm.

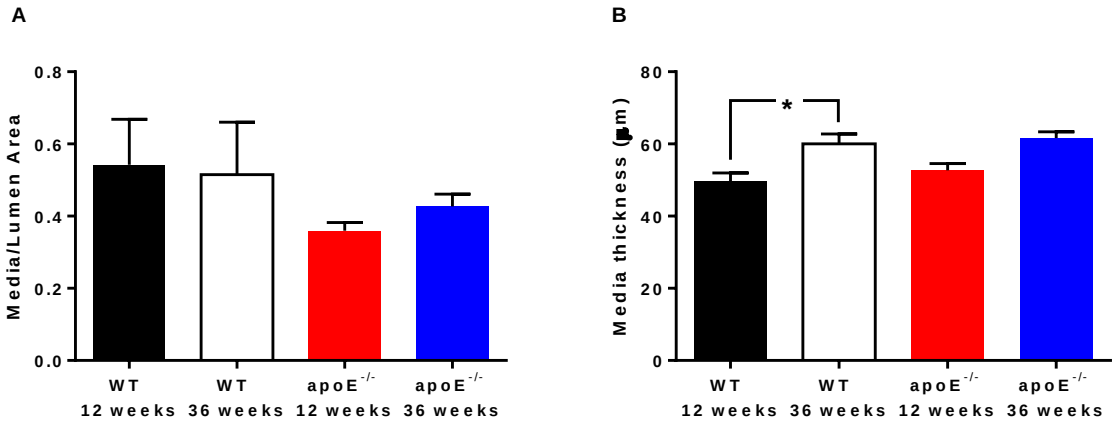

Figure 108: The media-to-lumen ratio (A) and the media thickness (B) of young and old WT and apoE$^{-/-}$ mice. No differences were detected in the media-to-lumen ratio between groups. Old WT mice had significantly greater medial thickness compared to young WT mice. No other significant differences were observed. *p<0.05.

8.4 Discussion

8.4.1 Preliminary analysis of the dependence of PWV on age

There are a number of possible factors that are at play in the preliminary analysis section of this study, with further work required to uncover their inter-relationships. Yet, the data provide informative initial insight into the effect of age on PWV in the mouse model. Aging studies in mice often involve mice that are around 24 months old or more (39, 178, 231), which is roughly double the age of the oldest mice used in this study. It is therefore possible that the mice may not be old enough to manifest marked changes in PWV. However, the relationship between PWV and age is stronger at lower pressures and gradually diminishes as pressure is increased. This may reflect the structural changes in the arteries that occur with age. At normal blood pressures, the majority of the pulsatile load is borne by the elastic components of the arteries and this load is increasingly transferred to the stiffer components (collagen) as pressure is increased (3, 23). So at high pressures, which depend less on elastin, there would be less of an age-related effect on PWV, while at lower pressures which are influenced more by the presence of elastin, there would be more of an age-related effect on

PWV as elastin is fragmented and broken down with age. Further work is required to support these suggestions, such as the quantification of elastin and collagen content in the aortas of these mice.

8.4.2 The effect of age on WT and apoE$^{-/-}$ mice

The finding that PWV is increased in WT mice with age is consistent with previous reports that demonstrate an age-related increase in arterial stiffness in mice (39, 178, 231). However, these studies have investigated vascular stiffness in later stages of aging (from approximately 6 to 29 months) and none of them have investigated pressure-dependent PWV or corrected reported PWV values for concomitant changes in MAP. The importance of investigating the pressure-dependency of PWV is highlighted here by the fact that differences were not detected under baseline anaesthetized blood pressures, but only when pressure was raised to 100 mmHg. A few studies have examined PWV in early aging. Herold et al found no differences in PWV as measured by MRI in WT mice aged 2 and 8 months (49). However, no values for MAP were reported in this study. Wang et al also found no changes in PWV between the ages of 4 and 13 months (51). While MAP was recorded in this study, the values were quite low (~ 70 mmHg) which may have masked potential changes in stiffness that are more apparent at higher mean pressures.

There were no statistically significant increases in PWV with age at any level of MAP in the apoE$^{-/-}$ mice. Furthermore, the 36 week old apoE$^{-/-}$ mice had similar PWV values compared to age-matched WT controls. This was unexpected as 12 week old apoE$^{-/-}$ mice were demonstrated to have significantly increased PWV compared to WT controls at pressures of 95 mmHg and greater in Chapter 7. It is also known that by 36 weeks of age there are more advanced fibrous-cap lesions and aortic calcification (174) which would suggest that PWV should be increased compared to both 12 week old apoE$^{-/-}$ mice and age matched controls. Indeed, several published studies have provided data demonstrating these kinds of changes

(summarized in Chapter 7 Table 14). Often reported changes in PWV in apoE$^{-/-}$ compared to WT mice are difficult to interpret because MAP was not measured (50), only tail-cuff systolic pressures were measured non-simultaneously with PWV (42), or mice were fed a high fat or high cholesterol diet (49). However, Wang et al demonstrated an age-related increase in PWV between 4 and 13 months in apoE$^{-/-}$ mice as well as increased PWV in 13 month old apoE$^{-/-}$ compared to age-matched controls with no statistical differences in MAP, SBP, DBP, or PP measured invasively in any of the groups examined (51). Some of the errors associated with their method of PWV measurement were discussed in Section 2.4 and they did not measure pressure dependent PWV. Importantly, the two ages they used in this study (4 and 13 months) were different to the two ages used in the study reported in this thesis (12 weeks ~ 3 months and 36 week ~ 9 months). It is plausible that the atherosclerotic progression between the ages of 9 and 13 months is significant enough to induce changes in vascular stiffness over this time period.

In this (pilot) study, specific atherosclerotic plaque quantification was not performed. As a result, it remains unknown whether the increase in PWV seen in the 12 week old apoE$^{-/-}$ mice compared to WT controls was a result of plaque initiation and progression in the aorta or other factors, such as endothelial dysfunction, that are associated with the apoE knockout phenotype. Hence, although it is known that there is increased plaque development in the aorta with age in apoE$^{-/-}$ mice, this may not have directly translated into increased PWV with age over this particular time course. This notion can be exemplified by a previous study from our group in which PWV was not significantly different in Brown Norway rats with marked elastic tissue lesions in the aorta compared to controls (29).

There is also the possibility that the *rate* of change in PWV with age is different between WT and apoE$^{-/-}$ mice whereby within the age ranges that were assessed in this study, apoE$^{-/-}$ mice had an accelerated age-related increase in pressure-dependent PWV compared to WT control.

This is further emphasized when considering the data presented in the preliminary analysis in the first part of this Chapter. PWV data collected across different strains, genders, and experimental techniques yielded no differences with age across a range of 8 to 46 weeks; however, it could be that each of these groups has a unique rate of change of PWV which is masked when analysed together as a whole. This initial PWV-age analysis provided an interesting first glimpse into age-related changes in vascular stiffness and some key questions and points arose from it, but it does highlight the importance of ensuring that all experimental variations are accounted for.

Future experiments should include measurements obtained at both intermediate and later time points in order to elucidate the dynamics of age-associated changes in aortic stiffness in the WT and apoE$^{-/-}$ mouse. Thus far, studies have focused on measuring PWV at two time points: an "old" and "young" age, which are often dissimilar between reports. If the rates of change in PWV vary with strain or disease model, it is important to create a more complete picture regarding the stiffness-age relationship, especially in widely used models of human diseases which progress with age, such as the apoE$^{-/-}$ mouse.

There were no differences in the pressure sensitivity of PWV, PPA-MAP relationship, or BRS between groups. In the WT mice there was a non-significant trend of increased pressure sensitivity with age at each pressure range, while in apoE$^{-/-}$ mice, this trend was *reversed* at medium to high pressures.

The incremental stiffness measured using the pull-back technique showed an increase in stiffness with age in WT mice only in the most proximal location of the aorta. This generally corresponds with the PWV data acquired across the entire length of the aorta. However, PWV measured at baseline MAP (which is the MAP that incremental stiffness is measured at) was not different in old versus young WT mice. Furthermore, if the incremental stiffness is higher with age in WT mice, it would be expected to be consistently higher at each increment along

the length of the aorta. As previously discussed, there is some error inherent in the most proximal measurement as the curvature of the aorta is not taken into account in the distance travelled by the pressure wave in the PWV calculation. Other sources of error arise from the inability to very precisely withdraw the catheter, and the sequential collection of TT data gated to the R-wave of the ECG which may be susceptible to any changes in cardiac function over the course of these measurements.

The stress-strain relationships obtained from the wire myography normalization procedure correspond well to the PWV-MAP data indicating that the material stiffness of the aortic wall is altered with age in the WT mice, causing increased functional stiffness as measured by PWV. There was a slight though insignificant increase in the incremental elastic modulus at a strain of 0.1 in apoE$^{-/-}$ with age. It was hypothesized that the increase in atherosclerotic plaques that occurs with age in these mice would increase the elastic modulus. There are two primary explanations for why this may not have occurred: *(i)* the vessels were not stretched to a sufficient length, and *(ii)* the sections of aorta used may not have had sufficient plaque build up to cause significant differences to appear.

Maximal contractions to PE were reduced with age in the thoracic aortas, with this being significant only in the apoE$^{-/-}$ mice. There was also a significant reduction in sensitivity to PE with age in the abdominal aortas of WT and apoE$^{-/-}$ mice as indicated by right shifts in the dose-response curves and reduced EC_{50} values. This suggests that effects of aging may be different with location in the aorta. It also eliminates the possible contribution of increased active smooth muscle contraction to the observed rises in PWV with aging.

There was no impairment in smooth muscle cell relaxation as all groups were able to fully relax in response to SNP. There was a significant decrease in sensitivity with age in the abdominal aortas only. This again indicates possible differential effects of aging with location in the aorta.

A non-significant reduction in the maximum relaxation response to ACh with age was observed in WT mice. Furthermore there was a trend towards decreased sensitivity to ACh with age which was significant only in the abdominal aortic rings. These results are consistent with other reports which demonstrate endothelial dysfunction with aging in mice (178, 231). A characteristic of the apoE$^{-/-}$ mouse is endothelial dysfunction and this progresses with age (171). The results presented here show that there was no endothelium-dependent relaxation response at all to ACh in young and old apoE$^{-/-}$ mice. Due to this abolishment of endothelium-mediated vascular relaxation it is then not possible to evaluate the impacts of aging on ACh-mediated responses in these rings. However, the increased endothelial dysfunction may contribute to the increased arterial stiffness observed in young and old apoE$^{-/-}$ mice compared to young WT controls.

The aorta thickens and dilates with age. Goyal also observed a progressive increase in the thickness of the WT mouse aorta with age (232). Vessel wall area has also been shown to increase progressively with age in apoE$^{-/-}$ mice (230). Although no changes in wall-to-lumen ratio were observed, there was a significant increase in medial thickness in WT mice with age. A similar trend in the aortic geometry was found in apoE$^{-/-}$ mice with age although this was not statistically significant. As PWV is proportional to vessel wall thickness, the observed medial thickening may have contributed to the observed increase in aortic PWV. Morphological data concerning assessing the plaque area, elastin content and integrity, and collagen content in these mice should be the focus of future experiments in order to ascertain what changes might be occurring in the vessel wall that alter the passive mechanical stiffness and contribute to increased PWV.

Chapter 9

Conclusion

The clinical significance of arterial stiffness is evident. A stiffer aorta directly leads to increased systolic blood pressure, which places a greater workload on the heart resulting in cardiac hypertrophy and decreased coronary perfusion, eventually leading to serious cardiac events. Furthermore, increased stiffness impairs the cushioning function of the aorta. Pulsatile flow is then transmitted to sensitive vascular beds which are conditioned for more steady flow, resulting in end organ damage, especially in the brain and kidneys (3).

This is a highly relevant issue as cardiovascular disease remains the number one cause of death worldwide (1) and it has been demonstrated in various disease groups and in the general population that arterial stiffness is a strong independent predictor of cardiovascular events and all-cause mortality (6, 13). However, there are still no therapies available to directly reduce large artery stiffness. This is in large part because the causative cellular and molecular mechanisms remain generally unknown.

The genetically modified mouse offers a powerful tool for investigating potential mechanisms. The shared physiology of human and mouse, the ability to knock out any particular gene of interest, and the wide availability of relevant disease models make it an ideal candidate for investigating novel pathways which could lead to increased stiffness.

Bearing this in mind, the scope of this thesis encompassed the development and employment of a new, high-fidelity, operator-independent technique for measuring aortic stiffness, by PWV, in the mouse and demonstrating the usefulness of this technique, in combination with myography and organ bath methods, in detecting functional changes in the aortas of different genetically modified mouse models.

9.1 Summary

9.1.1 Development of the method to measure aortic PWV in the mouse

Chapter 3 presents a review of several PWV-measurement techniques that were trialled before arriving to the final solution which was then used throughout this thesis. In brief, a 1.2F dual pressure sensing catheter with a fixed distance of 3 cm between pressure sensors was inserted into the aorta via the femoral artery to obtain precise transit time (TT) measurements. The foot-to-foot method was used to calculate PWV on a beat-by-beat basis. A venous line was inserted in the left femoral vein for infusion of blood pressure-altering drugs: *(i)* phenylephrine (PE), to raise blood pressure, and (ii) sodium nitroprusside (SNP), to lower blood pressure. To ascertain that infusion of drugs does not significantly affect mean arterial pressure (MAP) by increasing venous return, data were acquired over saline infusion and no changes in MAP were observed. PWV was measured during an active (SNP infusion) and passive (reducing venous return by occluding the vena cava) reduction of blood pressure. There were no statistical differences in PWV at any MAP between the two methods, indicating that the infusion of vasoactive drugs does not affect the vessel wall stiffness independently of its effects on blood pressure. It was also observed that there was a directional dependence in the PWV-MAP relationship such that PWV was higher at the same MAP when pressure was rising than when it was falling.

9.1.2 Characterizing the pressure-dependent PWV in the mouse

Chapter 4 explores some of the cardiovascular parameters that influence PWV measurements and provides, for the first time, high-fidelity pressure-dependent PWV across a wide range of physiological pressures in the mouse. The PWV-MAP relationship was characterised by a quadratic equation, indicating that the sensitivity of PWV to changes in MAP increases linearly. The incremental arterial stiffness along the length of the aorta was also measured by withdrawing the catheter in 0.5cm increments and calculating TT as the time delay between the R-wave of the ECG and the foot of the proximal pressure wave at each location. No changes in stiffness along the length of the aorta were observed. The pulse pressure amplification (PPA)-MAP relationship was also described. It was found that PPA remained at approximately 1 at pressures above 85 mmHg and dropped steadily as pressure decreased below this value. Finally, using a multiple linear regression approach, it was found that MAP, max dP/dt, pressure change direction, pulse pressure, and R-R interval all have a significant effect on PWV.

9.1.3 The effect of transglutaminase 2 on arterial stiffness

It was hypothesized that the ubiquitous and multifunctional enzyme, TG2, would play a role in large artery stiffness, due to its ability to crosslink proteins, such as collagen, in the ECM. In Chapters 5 and 6, the functional influence of TG2 on aortic stiffness, vascular reactivity, and cardiac function was assessed in $TG2^{-/-}$ mice and their WT littermate controls. Data from Chapter 5 were obtained at Macquarie University. No differences were observed in the baseline cardiovascular parameters, pressure sensitivity of PWV, PPA-MAP relationship, baroreflex sensitivity, vascular reactivity, histology, or aortic calcification. However, at pressures higher than 126 mmHg, WT did have high PWV compared to $TG2^{-/-}$. On the other hand, Chapter 6 results (obtained at Johns Hopkins University) demonstrated some minor

differences in baseline cardiovascular parameters, and no changes in most parameters of cardiac function, PWV-MAP relationship, pressure sensitivity of PWV, incremental aortic stiffness, or baroreflex sensitivity. However, WT mice had increased left ventricular mass and at some MAP, increased PPA. Therefore, findings from these chapters suggest that TG2 may play a role in large artery stiffness at high pressures and left ventricular hypertrophy, although this still requires further clarification. As TG2 is an inflammatory molecule and its activity is known to be suppressed by nitric oxide (NO), the nitric oxide synthase (NOS) inhibitor L-NAME was used to exacerbate the potential TG2-mediated cardiovascular effects. Two routes of administration were used: *(i)* via drinking water and *(ii)* via implanted osmotic mini pumps. In both instances, L-NAME did not produce an effect on any of the *in vivo* functional parameters that were examined. A compensatory mechanism involving prostacyclin and/or endothelium-derived hyperpolarizing factor (EDHF) was suggested. L-NAME administration did, in both studies, impair maximum constriction to PE and inhibit endothelium-dependent relaxation to ACh in *in vitro* organ bath experiments; however, there were no strain related differences observed in these impairments. In Chapter 6, WT mice treated with L-NAME had increased lumen-to-media ratios compared to untreated controls. $TG2^{-/-}$ mice did not experience this effect, indicating that there may also be a protective effect of TG2 regarding vascular remodelling.

9.1.4 Characterizing the PWV-MAP relationship in the apolipoprotein $E^{-/-}$ mouse

Pressure-dependent PWV was explored in the $apoE^{-/-}$ mouse, a widely used model of atherosclerosis. Significant differences in PWV between $apoE^{-/-}$ mice and WT controls were detected at mean blood pressures of 95 mmHg and above. This was the first study to be able to identify differences in mice at such a young age (12 weeks), demonstrating the sensitivity and utility of the developed technique, and also the importance of measuring PWV across a wide range of mean pressures. Administration of L-NAME has been previously shown to

intensify the progression of atherosclerosis in apoE$^{-/-}$ mice; therefore, it was decided to investigate arterial stiffness in apoE$^{-/-}$ mice which had been given L-NAME, hypothesizing that their aortas would be significantly stiffer after treatment. However, the PWV-MAP relationship after the treatment period was not different to that of untreated WT controls. This supported the previous notion that compensating mechanisms account for the reduced bioavailability of NO. As previously mentioned, there are the possible contributions of increased prostacyclin and EDHF. Additionally, the administration of L-NAME may provide a beneficial effect because it also inhibits iNOS and nNOS (in addition to eNOS). An upregulation of iNOS and nNOS has been shown to occur in atherosclerosis and excess NO generated by these enzymes can have detrimental effects on the vessel wall. As apoE$^{-/-}$ mice spontaneously develop atherosclerosis, it is possible that these processes were occurring and L-NAME treatment stopped them, thereby reducing aortic stiffness. The observed effects of L-NAME could also reflect the inhibition of uncoupled eNOS, or even nNOS which may also be highly expressed in the vascular endothelium. No differences were observed in the incremental aortic stiffness, PPA-MAP relationship, baroreflex sensitivity, histology or calcium content in the aorta. L-NAME treatment impaired constriction to PE in the apoE$^{-/-}$ compared to untreated apoE$^{-/-}$ and WT control. Both L-NAME treated and untreated apoE$^{-/-}$ had impaired endothelium-dependent relaxation to ACh compared to WT control. This indicates the presence of endothelial dysfunction in the apoE$^{-/-}$ mouse which likely leads to increased stiffness, as measured by PWV.

9.1.5 The effect of early aging on arterial stiffness in the mouse

Finally, as age is the most significant risk factor for increased vascular stiffness, preliminary investigations on the effects of aging on pressure-dependent PWV in the mouse aorta were performed. This analysis provided an interesting first glimpse into the effects of aging (between 8 and 46 weeks) on PWV at pressures of 60, 100, and 120 mmHg. There was almost

no effect of age within this range on PWV; however, the small effect of age was more apparent at lower pressures and diminished as pressure increased. This finding was not able to be readily interpreted as the data used for this analysis were acquired over a largely non-uniform group of mice. This led to the investigation of the effects of aging (between 12 and 36 weeks) on various parameters of vascular function in WT and apoE$^{-/-}$ mice. It was found that WT mice had increased pressure-dependent PWV at MAP of 100 mmHg and higher with age while apoE$^{-/-}$ mice did not develop age-associated changes in stiffness over this time period. These functional measurements were mirrored by the values for incremental elastic modulus which showed the same trends between groups. Incremental stiffness measurements yielded an increase with age in WT mice only immediately proximal to the aortic arch. There may be a difference in the rate of change of PWV with age between strains of mice that could explain the differential effects of age on functional aortic stiffness measurements. No significant differences in the pressure sensitivity of PWV, PPA-MAP relationship, or BRS were observed. Changes in stiffness in the WT mice with age may have been caused in part by increased medial thickness (as measured using histological cross-sections stained with H&E) and increased endothelial dysfunction (as indicated by the non significant reductions in maximum relaxation and sensitivity to ACh in isolated aortic ring preparations). This was the first study to provide high-fidelity pressure-dependent PWV data demonstrating the early effects of aging in WT and apoE$^{-/-}$ mice.

9.2 Limitations and future directions

Although attempts were made to address this, a major confounding factor in this study was the use of drugs to modify blood pressure. Findings in the mouse (Chapter 3) and in the rat (Appendix A2) suggest that the infusion of vasoactive drugs does not directly affect aortic stiffness and that the blood pressure altering effects are due to actions in the peripheral vasculature. Thus far it has not been possible to adequately increase MAP in a passive manner

to directly compare PWV measured over passive and active changes in pressure. It would be highly beneficial to determine a method of passively increasing mean blood pressure to remove any possible interactions between PE and the aortic wall. That being said, it is possible to lower PWV passively by occluding the vena cava. As PWV was not different whether pressure was lowered actively by SNP infusion or passively by venous occlusion, infusion was used throughout this thesis as venous occlusion is a highly invasive and complicated procedure.

Another potential limitation may come from the presence of the catheter itself. Positioning the catheter intravascularly may disrupt the fluid dynamics within the aorta or change wave transmission characteristics. However, using the "pull back" technique showed no major changes in MAP as the catheter was withdrawn from the aortic arch to the iliac bifurcation. Furthermore, the shape of the waveform measured proximal to the iliac bifurcation by the distal sensor when the catheter was fully inserted into the aorta was very similar to that measured by the proximal sensor pulled back to the same location. In addition, the baseline pressure and PWV measurements presented here fit well with values reported in the literature that had been measured noninvasively. It was also determined, based on an average value for the mouse thoracic aorta (1.29 mm) and abdominal aorta (0.72 mm), that a 1.2F catheter will cause a maximum of 30% reduction in cross-sectional area, which theoretically will not cause excessive flow disturbances to alter pressure measurement (233). Nevertheless, future studies could focus on validating these assumptions by computation fluid dynamics modelling or measuring changes in flow *in vivo* during catheter insertion.

As mentioned in Chapters 5, 6, 7, and 8, endothelium-dependent relaxation was impaired in all groups of animals to varying extents, including young, healthy, WT mice. While differences between strains could still be assessed, there is some cause for concern as there should generally be full relaxation (at least greater than 50%) to ACh in healthy mice. There

is the possibility that the surgical procedures activate or stress the endothelium, thereby affecting the *ex vivo* ring studies. It would be advantageous to compare vascular reactivity in aortas freshly harvested from mice to those obtained post-surgery to determine if this is the cause of the blunted relaxation response to ACh. This should be accompanied by immunohistochemical experiments indicating the presence (or absence) of an intact and healthy endothelium along the length of the aorta in mice after undergoing invasive PWV measurements. The aortic ring experiments were all performed in the absence of indomethacin, a drug which is commonly used to remove any contribution of prostanoids on endothelial-dependent relaxation. As endogenous prostacyclin was suggested to influence some of the results observed throughout this thesis, indomethacin should be included in subsequent ring studies as a future means to test for any redundancy of prostacyclin and other prostanoids.

There are limitations which arise due to the statistical methods used to evaluate the experimental measurements obtained throughout this study. The group sizes were small and, in some cases, several groups were compared, which may have limited the likelihood of finding statistically significant differences. Alternative statistical tests should be explored in future analyses, such as calculating the p-value for trends or the using non-parametric models rather than Student t-tests. Specifically, it would be beneficial to assess the PWV-MAP curves as a continuum, using a model that generates confidence intervals (CIs) for the complete range of values using all measurements in a single model. The method used in this thesis to test of differences in PWV-MAP curves between groups relies on the use of multiple comparisons at discrete pressure values which may not detect as accurately the point where the curves actually begin to separate.

It has already been shown that in WT mice treated with L-NAME there is increased TG2 activity and TG2-mediated crosslinks, while in $TG2^{-/-}$ mice there is not (16). However,

immunostaining of TG2 activity and crosslinks would also make a valuable contribution to this work. Similarly, while it is well known that the development of atherosclerotic plaques in apoE$^{-/-}$ mice progresses linearly from a young age, an assessment of the plaque area along the length of the aorta would further support the findings presented here.

This thesis provides a useful assessment of vascular function in different mouse models; however, evaluating cardiac function would complement these results nicely. High-fidelity pressure-volume catheters are available to measure pressure-volume loops and true maximum dP/dt in the heart chambers. Positioning flow probes around the aorta simultaneously with pressure measurement would also give a more complete quantitative description of the mouse vascular dynamics; allowing the determination of aortic impedance.

Throughout the thesis, it was observed that there was essentially no pulse pressure amplification at blood pressures of approximately 80 mmHg and above, with PPA falling quite dramatically as pressure was reduced below this value. Attention should be given to understanding the physiology of this relationship and its potential influence on PWV.

L-NAME is a non-specific inhibitor of NOS, inhibiting all three isoforms. Future work with TG2$^{-/-}$ mice could involve administration of a specific eNOS inhibitor or the creation of a TG2$^{-/-}$/eNOS$^{-/-}$ double knockout strain to examine the *in vivo* regulatory role of endothelium-derived NO in mediating TG2 activity and its impact on large artery stiffness. With respect to the apoE$^{-/-}$ mouse, it may be more useful to feed them a high-fat diet to accelerate atherosclerosis, than by L-NAME administration, as is often done in the literature.

There was no evidence of effect of L-NAME on TG2$^{-/-}$ and WT mice and in fact, in apoE$^{-/-}$ mice, a lowering of pressure-dependent PWV was observed. Several compensatory mechanisms were proposed and it is of great interest to confirm *in vivo* and *ex vivo* the presence of such mechanisms. For example, *ex vivo* measurements of vascular superoxide anion radical levels which are inhibited after L-NAME administration could address a

potential role for uncoupled NOS. It would also be interesting to understand why, in many cases, L-NAME causes significant increases in mean pressure as reported in a wide range of studies, yet in other instances either no or a beneficial effect is observed.

With the aging study, it is crucial that future work evaluate pressure-dependent functional stiffness measurements across a much wider age range. The range used in this thesis encompasses early aging; however, later stages comparable to an age where hypertension and markedly increased arterial stiffness are prevalent in humans would provide data which would be more clinically relevant. This type of longitudinal study would also clarify whether or not the mouse is truly a good model of the human aging vasculature.

Finally, focus should be placed in the future on using more mechanistic approaches to understand the pathophysiology behind the changes that were observed in various cardiovascular parameters in order to elucidate better the molecular determinants of arterial stiffness.

9.3 Concluding remarks

In summary, this thesis assesses the use of genetically modified mouse models to elucidate potential mechanisms of increased arterial stiffness. While the focus was primarily on WT, $TG2^{-/-}$, $apoE^{-/-}$, and aging mice, the techniques that have been described and used here could be applied to any knockout or disease model to acquire *in vivo* functional measurements which may aid in the identification of novel therapeutic targets that are necessary to develop treatments directed at reducing arterial stiffness. This study also highlights the importance of measuring pressure-dependent PWV. Not only does it allow for the comparison between different groups which may not have similar baseline mean pressures, but some differences only become apparent when MAP is higher or even lower than normal.

The key findings and outcomes of this thesis are:

(i) A new technique for measuring high-fidelity aortic PWV using a dual pressure catheter in the mouse was developed.

(ii) The pressure dependency of PWV in the wild type mouse aorta was characterised for the first time across a full physiological pressure range using high fidelity signals employing a dual pressure sensing catheter.

(iii) The enzyme, transglutaminase 2, plays a role in increased aortic stiffness at high mean arterial pressures, and in left ventricular hypertrophy.

(iv) ApoE$^{-/-}$ mice have increased PWV compared to control mice at mean arterial pressures greater than 95 mmHg as early as 12 weeks of age.

(v) NOS inhibition by L-NAME administration does not significantly increase pressure-dependent PWV in the mouse aorta, suggesting the presences of compensatory mechanisms in response to a reduction in nitric oxide bioavailability.

(vi) Early aging between 12 and 36 weeks induced significant increases in PWV at pressures of 100 mmHg and above in WT mice, but not in apoE$^{-/-}$ mice; the difference being related to the rate of change of PWV.

Appendices

A1: Measuring PWV using an intravascular catheter and an extravascular tonometer

Mice were anaesthetized as previously described in Section 3.3. Temperature was monitored and ECG obtained also in the same manner. A single 1.2F pressure sensor was introduced in the aortic arch via the carotid artery to record intravascular pressure. An incision was made in the abdomen, a section of abdominal aorta was isolated, and a second pressure sensor was positioned underneath the aorta to record extravascular pressure tonometrically. In order to obtain well-defined pressure waveform feet, the vessel had to be applanated. Pressure-dependent PWV was obtained as previously described. Following surgery, the mice were anaesthetized, and the distance between the two sensors was measured by laying a wetted suture along the aorta between the two sensors. This length was then measured with a ruler three times, and the average values were used. It was uncertain as to whether the applanation of the abdominal aorta would significantly affect the measurements of PWV, but as indicated in Figure 109, no significant differences were found between curves determined using this method, and the dual pressure sensor method. However, the surgery is much less invasive using only a single dual pressure sensor.

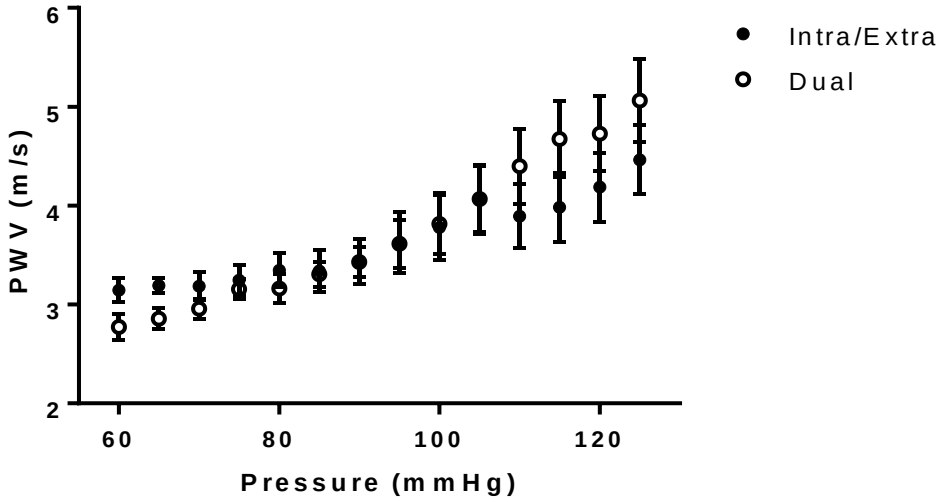

Figure 109: PWV-MAP curves obtained using two different measuring techniques as previously described. Intra/Extra refers to one proximal sensor placed into the arch via the carotid and one distal sensor placed underneath the abdominal aorta to record extravascular tonometric pressure. Dual refers to one dual pressure sensor placed in the aortic arch via the femoral artery. The data was analysed with 2-way ANOVA followed by Sidak's multiple comparisons test. There were no significant differences at any of the pressure bins.

A2: Measurement of aortic PWV in the rat: effects of vasoactive agents on the measurement

A2.1 Introduction

The stiffness of arteries depends on the pressure at which it is measured. Therefore, observed changes in pulse wave velocity (PWV) must always take into account the inherent effects of any changes in blood pressure, which often occur when investigating different treatment and disease groups, varying animal strains, or genetically modified organisms. To address this issue, aortic PWV is often measured over a range of physiological blood pressures induced by systemic infusion of vasoactive agents, sodium nitroprusside (SNP) and phenylephrine (PE). This is done under the assumption that these drugs alter blood pressure by acting on the peripheral circulation, and have negligible effects on the aorta. However, despite the fact that this technique is commonly used, the influence of vasoactive agents on the mechanical properties of the aorta itself remains highly unknown.

With a view to move into aortic stiffness measurement in mice to take advantage of gene knock-out models, PWV was measured in the rat using a combination of vasoactive agents and passive mechanisms to alter blood pressure. This was undertaken in order to test the validity of the assumption that SNP and PE do not primarily act in the aorta.

A2.2 Methods

A2.2.1 Animals

Male, Sprague Dawley (SD) rats (n=6, Animal Resource Centre, Perth), 12 weeks of age, were kept in a temperature controlled environment (21 ± 2^{o}C) with 12 hour light/dark cycles. Animals had *ad libitum* access to standard laboratory mouse feed and water. The animal protocol was approved by the Macquarie University Animal Ethics Committee (ARA 2010/044).

A2.2.2 Surgical preparation

Rats were anaesthetized with an intraperitoneal injection of urethane (1.3 g/kg). Once rats no longer responded to the pedal-withdrawal reflex, they were transferred to a thermoregulated heating pad and anaesthesia was maintained by bolus intravenous (IV) infusions of urethane as required. Temperature was monitored and maintained at 37± 1 ^{o}C with a rectal probe and thermoregulated heating pad. Three ECG electrodes were placed subcutaneously to provide heart rate.

A 1.6F high fidelity pressure sensor (Scisense, Canada) was positioned in the descending thoracic aorta via the carotid artery. A second sensor was positioned in the abdominal aorta via the femoral artery. The femoral vein was cannulated with a polyethelyne cannula (0.98 mm, Dow Corning) for IV infusion of blood-pressure altering agents. A section of vena cava proximal to the renal branches was exposed and isolated. A silk suture was then loosely tied around it.

Beat-to-beat arterial pressure waveforms were simultaneously recorded at 2 kHz using a CED 1401 data acquisition unit with Spike2 analysis software (CED, Cambridge). The transit time (TT) of the pressure pulse was defined as the time difference between the diastolic "feet" of the proximal and distal pressure waves. The foot of each pressure wave was located by detecting the peak of the second derivative of the pressure waveform. At the end of each experiment, the entire length of the aorta was exposed and the distance between the two sensors was measured using a wetted suture. PWV could then be calculated as distance divided by TT.

A2.2.3 PWV over active and passive changes in blood pressure

PWV was recorded over a range of physiological blood pressures. PE was infused at a rate of 30 μg/kg/min to raise mean arterial pressure (MAP) until it reached a plateau, and SNP was infused in the same manner to lower MAP.

The suture was then used to partially occlude the inferior vena cava in order to reduce venous return and lower pressure passively for comparison to the MAP range achieved with SNP. This was repeated during continuous infusion of phenylephrine to assess effect of phenylephrine on the aorta.

A2.2.4 Data and statistical analysis

Data are presented as mean ± standard error of the mean (SEM) and were analysed offline using a combination of Microsoft Excel, IBM SPSS Statistics 19, and R. *In vivo* PWV was averaged in 1 mmHg MAP bins. PWV was compared: *(i)* while MAP was returning to baseline after SNP infusion versus returning to baseline after partial venous occlusion, and *(ii)* while MAP was returning to baseline after cessation of PE infusion versus MAP being lowered to baseline by venous occlusion during PE infusion. Comparisons were made by robust analysis of covariance (ANCOVA). The slopes of the PWV-MAP curves were compared by fitting the 1 mmHg binned individual rat data with a second order polynomial by linear regression, and comparing the coefficients of the fit by paired t-tests.

A2.3 Results

Aside from three pressures bins no significant difference was found in arterial stiffness achieved with the vasoactive agents or with the venous occlusion methods of blood pressure manipulation (Figure 110). For MAP range 60-90 mmHg, PWV for SNP did not differ from PWV for venous occlusion (4.05±0.55 m/s, 4.05±0.51 m/s, p=0.99). For MAP 120-150 mmHg, PWV for phenylephrine did not differ from PWV with concurrent venous occlusion (6.37±0.87 m/s, 6.71±0.72 m/s, p=0.62).

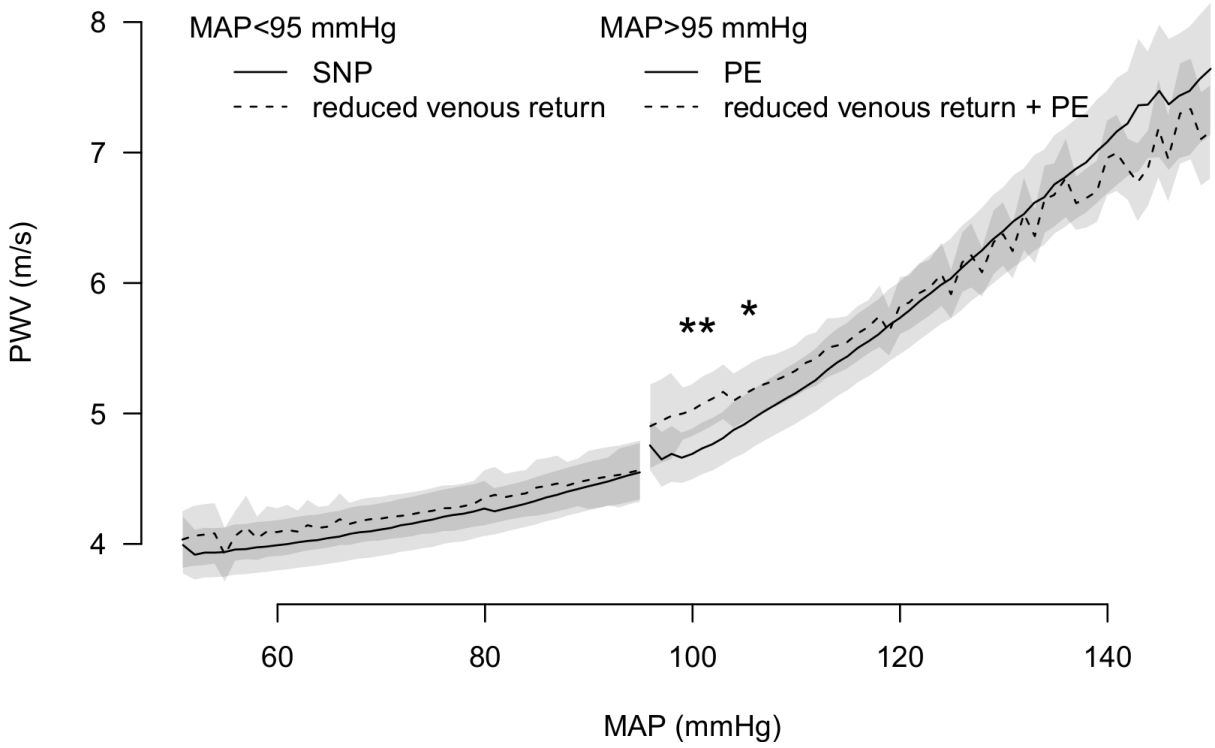

Figure 110: With the exception of three pressure bins, no significant difference was found in arterial stiffness achieved with the vasoactive agents or with the venous occlusion methods of blood pressure manipulation.*p<0.05.

A2.4 Discussion

The results indicate the concentration of SNP and PE infused did not significantly affect aortic smooth muscle in- vivo and all pressure dependent changes in PWV were mediated through effects on total peripheral resistance and not via active effects on the smooth muscle in the aortic wall. There is a small PE effect (~2%) at MAP close to 100 mmHg; however, this difference disappears at higher MAP.

A3: Comparison of PWV-MAP curves in TG2$^{-/-}$ and WT mice measured at Macquarie University and Johns Hopkins University.

As mentioned in Chapters 6, some of the findings based on measurements obtained at Johns Hopkins University (JHU) using TG2$^{-/-}$ mice and their WT controls (Chapter 6) were different than those made in the same strains of mice at Macquarie University (MQ) (Chapter 5). First, from Chapter 5, it was shown that PWV was higher in WT mice compared to TG2$^{-/-}$ mice at pressures higher than 126mmHg, while in Chapter 6, this was not found. Figure 111 shows a comparison of PWV-MAP results from JHU versus MQ. It can be seen that there are no differences between the two sets of experiments for the majority of the pressure range. However, at pressures of 125mmHg, WT mice from MQ have significantly higher PWV than those from JHU. It is unclear why this is the case.

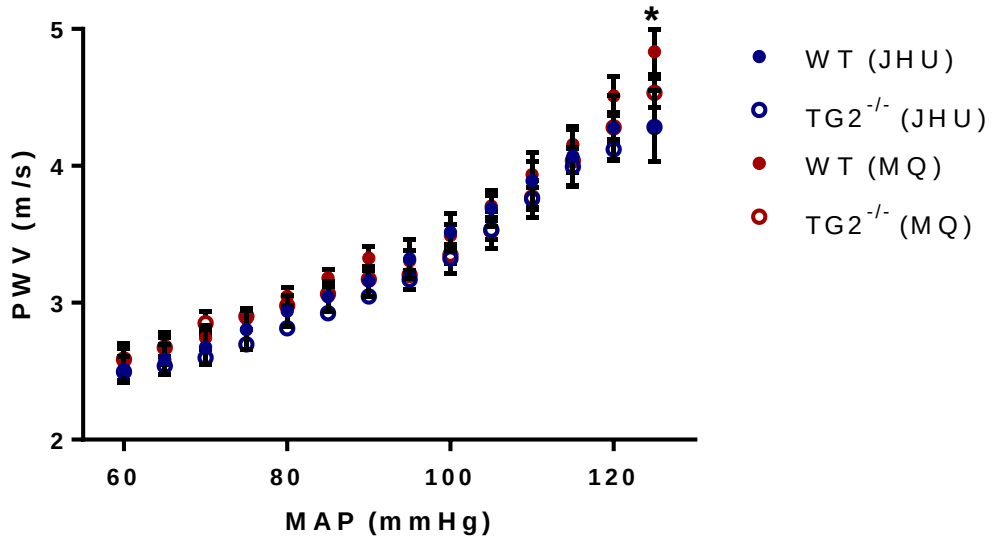

Figure 111: Comparison of the PWV-MAP relationship for WT and TG2$^{-/-}$ mice between experiments performed at JHU and MQ. There were only difference found occurred at a pressure of 125mmHg where WT mice from MQ had higher PWV than those from JHU (two-way ANOVA followed by Tukey's multiple comparisons test) *$p<0.05$ for WT (JHU) versus WT (MQ).

The other major discrepancy between the two studies involved the finding that $TG2^{-/-}$ mice were protected from left ventricular hypertrophy compared to WT controls at JHU while at MQ there were no differences in LV weight between the two animal strains.

Table 18: Body weight (g) of mice from JHU versus MQ. While $TG2^{-/-}$ mice have similar weights in both labs, WT mice from JHU are larger than from MQ, although this only reached statistical significance in the WT – L-NAME group. *p<0.05

	JHU	MQ
WT	34 ± 2	30 ± 4
WT – L-NAME	35 ± 1	29 ± 2*
$TG2^{-/-}$	29 ± 2	28 ± 2
$TG2^{-/-}$ - L-NAME	30 ± 2	30 ± 2

Table 19: Left ventricular weight normalized by body weight ($g/g \cdot 10^{-3}$) of mice from JHU versus MQ. In all cases, LVW/BW is smaller in mice from MQ compared to JHU; however this did not reach statistical significance in the WT – L-NAME group. *p<0.05

	JHU	MQ
WT	4.396 ± 0.457	3.202 ± 0.212*
WT – L-NAME	3.709 ± 0.310	3.076 ± 0.318
$TG2^{-/-}$	3.503 ± 0.226	3.139 ± 0.245*
$TG2^{-/-}$ - L-NAME	3.437 ± 0.381	3.109 ± 0.104*

While it is not known why these differences exist as the mice used in each location are genetically the same, it is important to note that findings can vary from laboratory to laboratory which may explain in part why the literature surrounding TG2 and its pathophysiological differences can be quite conflicting.

A4: Mouse demographics used for PWV-age study

The following table indicates the differences in strain, sex, anaesthesia, surgical method, weight, and age of the mice which were used for the preliminary analysis of the dependence of PWV on age. It is evident that there are many confounders between animals. However, in addition to the fact that this was simply intended to be an initial look into the influence of age, when PWV was plotted based on the differences in the factors listed here, the points generally overlapped and there did not appear to be major differences between groups.

Table 20: Summary details of mice used for aging analysis. Dual refers to measurements made with a dual pressure sensor. *Int/Ext* refers to measurements made with two separate sensors: one placed intravascularly and the other placed extravascularly as a tonometer. *Iso* is isoflurane, *U* is urethane, pent is sodium pentobarbital, and *A* refers to the administration of atropine which was sometimes required to reduce respiratory difficulties.

Date used	Method	Anaesthesia	Strain	Sex	Weight	Age (weeks)
22/12/2012	Dual	Iso	SJL	F	19	8
26/01/2012	Int/Ext	Iso	WT	M	36	19
07/08/2012	Dual	Iso	WT	M	25	12
15/08/2012	Dual	Iso	WT	M	28	12.5
10/08/2012	Dual	Iso	TG2-/-	M	25	12.5
13/08/2012	Dual	Iso	TG2-/-	M	25	12.5
17/08/2012	Dual	Iso	TG2-/-	M	27	11.5
20/08/2012	Dual	Iso	TG2-/-	M	29	12
22/11/2012	Dual	Iso	C57	M	24	11
24/11/2012	Dual	Iso	C57	M	26	11
30/11/2012	Dual	Iso	C57	M	30	12
03/12/2012	Dual	Iso	C57	M	27	12.5
05/12/2012	Dual	Iso	C57	M	25	12.5
17/12/2012	Dual	Iso	C57	M	29	14
23/07/2012	Dual	Iso	VR1+/+	F	26	46
25/07/2012	Dual	Iso	VR1+/+	F	28	46
06/06/2012	Dual	Iso	VR1+/+	F	24	41
30/05/2012	Int/Ext	Iso	VR1-/-	F	24	43
25/05/2012	Int/Ext	Pent+Iso	VR1-/-	F	29	43
12/04/2012	Int/Ext	Pent+Iso	VR1-/-	F	30	36.5
02/02/2012	Int/Ext	Iso+A	TG2-/-	M	30	17

Date used	Method	Anaesthesia	Strain	Sex	Weight	Age (weeks)
26/01/2012	Int/Ext	Iso +A	WT	M	35	19
13/01/2012	Int/Ext	U+A	VR1-/-	F	24	30
15/11/2011	Dual	U	VR1-/-	F	21	13
04/10/2011	Dual	U+A	C57	F	24	11
30/01/2013	Dual	Iso	SJL	F	21	13
28/01/2013	Dual	Iso	SJL	F	21	13

A5: Final Ethics Approval Letters

From: **Animal Ethics** <animal.ethics@mq.edu.au>
Date: 6 December 2013 14:54
Subject: Outcome of 5 December 2013 AEC Meeting - Final Report - ARA 2011/036
To: Melissa Farnham <melissa.farnham@mq.edu.au>

Dear Dr Farnham,

2011/036	**Dr Melissa Farnham** (ASAM)	**Surgical preparation of mice: Establishment of the current rat preparation in mice**

Final Report

Decision

The Committee accepted the final report.

Your Final Report for the above project was considered and accepted at the Animal Ethics Committee meeting of 5 December 2013.

Thank you and all the best for your future research endeavours.

This email serves as official notification of the AEC decision. Please keep a copy for your records. Should you have any queries or require clarification, please contact the AEC Secretariat.

Regards,

Professor Mark Connor
Chair, AEC

Office of the Deputy Vice Chancellor (Research)
Research Office
Level 3, Research Hub, Building C5C East
Macquarie University
NSW 2109 Australia
T: +61 2 9850 7758
F: +61 2 9850 4465
Email: animal.ethics@mq.edu.au
http://www.mq.edu.au/research

From: **Animal Ethics** <animal.ethics@mq.edu.au>
Date: 17 April 2014 15:51
Subject: Outcome of 17 April 2014 AEC Meeting - Final Report - ARA 2011/017
To: Alberto Avolio <alberto.avolio@mq.edu.au>, Mark Butlin <mark.butlin@mq.edu.au>, Kayla Dawn Viegas <kayla.viegas@mq.edu.au>, Ann Goodchild <ann.goodchild@mq.edu.au>
Cc: Christine Sutter <christine.sutter@mq.edu.au>

Dear Professor Avolio,

2011/017	**Professor Alberto Avolio** (ASAM)	**Effect of transglutaminase 2 on large artery structure and stiffness in TG2 knockout mice**

Final Report

Decision

The Committee accepted the final report.

Your Final Report for the above project was considered and accepted at the Animal Ethics Committee meeting of 17 April 2014.

Thank you and all the best for your future research endeavours.

This email serves as official notification of the AEC decision. Please keep a copy for your records. Should you have any queries or require clarification, please contact the AEC Secretariat.

Regards,

Professor Mark Connor
Chair, AEC

Office of the Deputy Vice Chancellor (Research)
Research Office
Level 3, Research Hub, Building C5C East
Macquarie University
NSW 2109 Australia
T: +61 2 9850 7758
F: +61 2 9850 4465
Email: animal.ethics@mq.edu.au
http://www.mq.edu.au/research

From: **Animal Ethics** <animal.ethics@mq.edu.au>
Date: 19 April 2013 12:28
Subject: Outcome of 18 April 2013 AEC Meeting - Final Report - ARA 2011/002
To: Mark Butlin <mark.butlin@mq.edu.au>, Alberto Avolio <alberto.avolio@mq.edu.au>, Ann Goodchild <ann.goodchild@mq.edu.au>
Cc: Christine Sutter <christine.sutter@mq.edu.au>

Dear Dr Butlin,

2011/002	***Dr Mark Butlin (ASAM)***	***Effect of gender on large artery structure and stiffness in wild type mice***

Final Report

Decision
The Committee accepted the final report.

Your Final Report for the above project was considered and accepted at the Animal Ethics Committee meeting of 18 April 2013.

Thank you and all the best for your future research endeavours. This email serves as official notification of the AEC decision. Please keep a copy for your records. Should you have any queries or require clarification, please contact the AEC Secretariat.

Regards,

Professor Mark Connor
Chair, AEC

Office of the Deputy Vice Chancellor (Research)
Animal Ethics Secretariat
Research Office
Level 3 C5C Research Hub East
Macquarie University NSW 2109

+61 2 9850 7758 / 4456
animal.ethics@mq.edu.au

From: **Animal Ethics** <animal.ethics@mq.edu.au>
Date: 18 August 2014 09:03
Subject: Outcome of 14 August 2014 AEC Meeting - Final Report - ARA 2010/044
To: Mark Butlin <mark.butlin@mq.edu.au>, Alberto Avolio <alberto.avolio@mq.edu.au>, Parisa Kouchaki <zahra.kouchaki@students.mq.edu.au>, George Lindesay <george.lindesay@mq.edu.au>, Kayla Dawn Viegas <kayla.viegas@mq.edu.au>, Omar-Al-Adhami <omar.al-adhami@mq.edu.au>, Cara Hildreth <cara.hildreth@mq.edu.au>

Dear Dr Butlin,

2010/044	***Dr Mark Butlin*** *(ASAM)*	***Large artery dimension, structure and stiffness in development of hypertension***

Final Report

Decision

The Committee accepted the final report.

Your Final Report for the above project was considered and accepted at the Animal Ethics Committee meeting of 14 August 2014.

Thank you and all the best for your future research endeavours.

This email serves as official notification of the AEC decision. Please keep a copy for your records. Should you have any queries or require clarification, please contact the AEC Secretariat.

Regards,

Professor Mark Connor
Chair, AEC

Office of the Deputy Vice Chancellor (Research)
Research Office
Level 3, Research Hub, Building C5C East
Macquarie University
NSW 2109 Australia
T: +61 2 9850 7758
F: +61 2 9850 4465
Email: animal.ethics@mq.edu.au
http://www.mq.edu.au/research

References

1. Alwan A. Global status report on noncommunicable diseases 2010: World Health Organization; 2011.

2. Heart Foundation Data and Statistics. [16/10/2013]; Available from: http://www.heartfoundation.org.au/information-for-professionals/data-and-statistics/Pages/default.aspx.

3. Nichols W, O'Rourke M, C V. McDonald's Blood Flow in Arteries: Theoretical, Experimental and Clinical Principles. 6 ed. Boca Raton, Fl: CRC Press Taylor & Francis Group; 2011.

4. Blacher J, Asmar R, Djane S, London GM, Safar ME. Aortic pulse wave velocity as a marker of cardiovascular risk in hypertensive patients. Hypertension. 1999;33(5):1111-7.

5. Laurent S, Katsahian S, Fassot C, Tropeano AI, Gautier I, Laloux B, et al. Aortic stiffness is an independent predictor of fatal stroke in essential hypertension. Stroke. 2003;34(5):1203-6.

6. Laurent S, Boutouyrie P, Asmar R, Gautier I, Laloux B, Guize L, et al. Aortic stiffness is an independent predictor of all-cause and cardiovascular mortality in hypertensive patients. Hypertension. 2001;37(5):1236-41.

7. Blacher J, Pannier B, Guerin AP, Marchais SJ, Safar ME, London GM. Carotid arterial stiffness as a predictor of cardiovascular and all-cause mortality in end-stage renal disease. Hypertension. 1998;32(3):570-4.

8. Blacher J, Guerin AP, Pannier B, Marchais SJ, Safar ME, London GM. Impact of aortic stiffness on survival in end-stage renal disease. Circulation. 1999;99(18):2434-9.

9. Blacher J, Safar ME, Guerin AP, Pannier B, Marchais SJ, London GM. Aortic pulse wave velocity index and mortality in end-stage renal disease. Kidney International. 2003;63(5):1852-60.

10. Meaume S, Benetos A, Henry O, Rudnichi A, Safar M. Aortic pulse wave velocity predicts cardiovascular mortality in subjects> 70 years of age. Arteriosclerosis, Thrombosis, and Vascular Biology. 2001;21(12):2046-50.

11. Cruickshank K, Riste L, Anderson SG, Wright JS, Dunn G, Gosling RG. Aortic Pulse-Wave Velocity and Its Relationship to Mortality in Diabetes and Glucose Intolerance: An Integrated Index of Vascular Function? Circulation. 2002;106(16):2085-90.

12. Mattace-Raso FUS, van der Cammen TJM, Hofman A, van Popele NM, Bos ML, Schalekamp MADH, et al. Arterial stiffness and risk of coronary heart disease and stroke: the Rotterdam Study. Circulation. 2006;113(5):657.

13. Mitchell GF, Hwang S-J, Vasan RS, Larson MG, Pencina MJ, Hamburg NM, et al. Arterial Stiffness and Cardiovascular Events: The Framingham Heart Study. Circulation. 2010;121(4):505-11.

14. Liao D, Arnett DK, Tyroler HA, Riley WA, Chambless LE, Szklo M, et al. Arterial stiffness and the development of hypertension. The ARIC study. Hypertension. 1999;34(2):201-6.

15. Sutton-Tyrrell K, Najjar SS, Boudreau RM, Venkitachalam L, Kupelian V, Simonsick EM, et al. Elevated aortic pulse wave velocity, a marker of arterial stiffness, predicts cardiovascular events in well-functioning older adults. Circulation. 2005;111(25):3384-90.

16. Santhanam L, Tuday EC, Webb AK, Dowzicky P, Kim JH, Oh YJ, et al. Decreased S-nitrosylation of tissue transglutaminase contributes to age-related increases in vascular stiffness. Circulation Research. 2010;107(1):117-25.

17. Jandu SK, Webb AK, Pak A, Sevinc B, Nyhan D, Belkin AM, et al. Nitric oxide regulates tissue transglutaminase localization and function in the vasculature. Amino Acids. 2013;44(1):261-9.

18. van Popele NM, Grobbee DE, Bots ML, Asmar R, Topouchian J, Reneman RS, et al. Association Between Arterial Stiffness and Atherosclerosis: The Rotterdam Study. Stroke. 2001;32(2):454-60.

19. Avolio A, Deng F, Li W, Luo Y, Huang Z, Xing L, et al. Effects of aging on arterial distensibility in populations with high and low prevalence of hypertension: comparison between urban and rural communities in China. Circulation. 1985;71(2):202.

20. O'Rourke MF, Hashimoto J. Mechanical Factors in Arterial AgingA Clinical Perspective. Journal of the American College of Cardiology. 2007;50(1):1-13.

21. Shadwick RE. Mechanical design in arteries. Journal of Experimental Biology. 1999;202(23):3305-13.

22. Greenwald SE. Ageing of the conduit arteries. Journal of Pathology. 2007;211(2):157-72.

23. Zieman S, Melenovsky V, Kass D. Mechanisms, pathophysiology, and therapy of arterial stiffness. Arteriosclerosis, Thrombosis, and Vascular Biology. 2005;25(5):932.

24. Belz GG. Elastic properties and Windkessel function of the human aorta. Cardiovascular Drugs and Therapy. 1995;9(1):73-83.

25. Chirinos JA. Arterial stiffness: basic concepts and measurement techniques. Journal of Cardiovascular Translational Research. 2012;5(3):243-55.

26. McEniery CM, Wilkinson IB, Avolio AP. Age, hypertension and arterial function. Clinical and Experimental Pharmacology and Physiology. 2007;34(7):665-71.

27. Bramwell JC, Hill AV. The Velocity of the Pulse Wave in Man. Proceedings of the Royal Society of London Series B, Containing Papers of a Biological Character. 1922;93(652):298-306.

28. Fitch RM, Vergona R, Sullivan ME, Wang YX. Nitric oxide synthase inhibition increases aortic stiffness measured by pulse wave velocity in rats. Cardiovascular Research. 2001;51(2):351-8.

29. Butlin M. Structural and functional effects on large artery stiffness: an in-vivo experimental investigation: University of New South Wales; 2007.

30. Farrar DJ, Bond MG, Riley WA, Sawyer JK. Anatomic correlates of aortic pulse wave velocity and carotid artery elasticity during atherosclerosis progression and regression in monkeys. Circulation. 1991;83(5):1754-63.

31. Wilkinson IB, Qasem A, McEniery CM, Webb DJ, Avolio AP, Cockcroft JR. Nitric oxide regulates local arterial distensibility in vivo. Circulation. 2002;105(2):213-7.

32. Latson TW, Hunter WC, Katoh N, Sagawa K. Effect of nitroglycerin on aortic impedance, diameter, and pulse-wave velocity. Circulation Research. 1988;62(5):884-90.

33. Avolio A, O'rourke M, Mang K, Bason P, Gow B. A comparative study of pulsatile arterial hemodynamics in rabbits and guinea pigs. American Journal of Physiology -- Legacy Content. 1976;230(4):868-75.

34. Avolio A, O'Rourke M, Webster M. Pulse-wave propagation in the arterial system of the diamond python Morelia spilotes. American Journal of Physiology- Regulatory, Integrative and Comparative Physiology. 1983;245(6):831.

35. O'Rourke MF. Pressure and flow waves in systemic arteries and the anatomical design of the arterial system. Journal of Applied Physiology. 1967;23(2):139-49.

36. Avolio AP, Nichols WW, O'Rourke MF. Propagation of pressure pulse in kangaroo arterial system. American Journal of Physiology - Regulatory, Integrative and Comparative Physiology. 1985;249(3):R335-R40.

37. Hartley CJ, Reddy AK, Madala S, Entman ML, Michael LH, Taffet GE. Doppler velocity measurements from large and small arteries of mice. American Journal of Physiology - Heart and Circulatory Physiology. 2011;301(2):H269-H78.

38. Hartley CJ, Reddy AK, Entman ML, Michael LH, Taffet GE, editors. Noninvasive assessment of vascular mechanics in mice. Annual International Conference of the IEEE Engineering in Medicine and Biology - Proceedings; 2002; Houston, TX.

39. Reddy AK, Li Y-H, Pham TT, Ochoa LN, Treviño MT, Hartley CJ, et al. Measurement of aortic input impedance in mice: effects of age on aortic stiffness. American Journal of Physiology-Heart and Circulatory Physiology. 2003;285(4):H1464-H70.

40. Anea CB, Irfan Ali M, Osmond JM, Sullivan JC, Stepp DW, Merloiu AM, et al. Matrix metalloproteinase 2 and 9 dysfunction underlie vascular stiffness in circadian clock mutant mice. Arteriosclerosis, Thrombosis, and Vascular Biology. 2010;30(12):2535-43.

41. Tham DM, Martin-McNulty B, Wang YX, Da Cunha V, Wilson DW, Athanassious CN, et al. Angiotensin II injures the arterial wall causing increased aortic stiffening in apolipoprotein E-deficient mice. American Journal of Physiology - Regulatory Integrative and Comparative Physiology. 2002;283(6 52-6):R1442-R9.

42. Hartley CJ, Reddy AK, Madala S, Martin-McNulty B, Vergona R, Sullivan ME, et al. Hemodynamic changes in apolipoprotein E-knockout mice. American Journal of Physiology - Heart and Circulatory Physiology. 2000;279(5 48-5):H2326-H34.

43. Lim HK, Ryoo S, Benjo A, Shuleri K, Miriel V, Baraban E, et al. Mitochondrial arginase II constrains endothelial NOS-3 activity. American Journal of Physiology - Heart and Circulatory Physiology. 2007;293(6):H3317-H24.

44. Hartley CJ, Taffet GE, Michael LH, Pham TT, Entman ML. Noninvasive determination of pulse-wave velocity in mice. American Journal of Physiology - Heart and Circulatory Physiology. 1997;42(1):H494-H500.

45. Fitch RM, Rutledge JC, Wang YX, Powers AF, Tseng JL, Clary T, et al. Synergistic effect of angiotensin II and nitric oxide synthase inhibitor in increasing aortic stiffness in mice. American Journal of Physiology - Heart and Circulatory Physiology. 2006;290(3):H1190-H8.

46. Monassier L, Combe R, Fertak LE. Mouse models of hypertension. Drug Discovery Today: Disease Models. 2006;3(3):273-81.

47. Zuurbier CJ, Emons VM, Ince C. Hemodynamics of anesthetized ventilated mouse models: aspects of anesthetics, fluid support, and strain. American Journal of Physiology-Heart and Circulatory Physiology. 2002;282(6):H2099.

48. Parczyk M, Herold V, Klug G, Bauer WR, Rommel E, Jakob PM. Regional in vivo transit time measurements of aortic pulse wave velocity in mice with high-field CMR at 17.6 Tesla. Journal of Cardiovascular Magnetic Resonance. 2010;12(1).

49. Herold V, Parczyk M, Morchel P, Ziener CH, Klug G, Bauer WR, et al. In vivo measurement of local aortic pulse-wave velocity in mice with MR microscopy at 17.6 tesla. Magnetic Resonance in Medicine. 2009;61(6):1293-9.

50. Zhao X, Pratt R, Wansapura J. Quantification of aortic compliance in mice using radial phase contrast MRI. Journal of Magnetic Resonance Imaging. 2009;30(2):286-91.

51. Wang YX, Halks-Miller M, Vergona R, Sullivan ME, Fitch R, Mallari C, et al. Increased aortic stiffness assessed by pulse wave velocity in apolipoprotein E-deficient mice. American Journal of Physiology - Heart and Circulatory Physiology. 2000;278(2 47-2):H428-H34.

52. Segers P, Georgakopoulos D, Afanasyeva M, Champion HC, Judge DP, Millar HD, et al. Conductance catheter-based assessment of arterial input impedance, arterial function, and ventricular-vascular interaction in mice. American Journal of Physiology - Heart and Circulatory Physiology. 2005;288(3 57-3):H1157-H64.

53. Maizel J, Six I, Slama M, Tribouilloy C, Sevestre H, Poirot S, et al. Mechanisms of aortic and cardiac dysfunction in uremic mice with aortic calcification. Circulation. 2009;119(2):306-13.

54. Marque V, Kieffer P, Gayraud B, Lartaud-Idjouadiene I, Ramirez F, Atkinson J. Aortic wall mechanics and composition in a transgenic mouse model of Marfan syndrome. Arteriosclerosis, Thrombosis & Vascular Biology. 2001;21(7):1184-9.

55. Transonic. Solid-State Sensors vs. Fluid-Filled Transducers. 2010 [18/13/2013]; Available from: http://www.scisense.com/education/ssp-solid-vs-fluid.html.

56. DSI. DSI Pressure Sensing Technologies in Small Animals. [18/10/2013]; Available from: http://www.datasci.com/solutions/cardiovascular/dsi-pressure-sensing-technologies-in-small-animals.

57. Wagenseil JE, Mecham RP. Vascular extracellular matrix and arterial mechanics. Physiological Reviews. 2009;89(3):957-89.

58. Ross MH, Pawlina W. Histology: A Text and Atlas. 6 ed. Philadelphia: Lippincott Williams & Wilkins: Wolters Kluwer; 2010.

59. Kingwell B, Boutouyrie P. Genetic influences on the arterial wall. Clinical and Experimental Pharmacology and Physiology. 2007;34(7):652-7.

60. Yasmin, O'Shaughnessy KM. Genetics of arterial structure and function: Towards new biomarkers for aortic stiffness? Clinical Science. 2008;114(11-12):661-77.

61. Laurent S, Boutouyrie P, Lacolley P. Structural and genetic bases of arterial stiffness. Hypertension. 2005;45(6):1050-5.

62. Lacolley P, Challande P, Osborne-Pellegrin M, Regnault V. Genetics and pathophysiology of arterial stiffness. Cardiovascular Research. 2009;81(4):637.

63. Lakatta EG, Levy D. Arterial and cardiac aging: major shareholders in cardiovascular disease enterprises part I: aging arteries: a “set up” for vascular disease. Circulation. 2003;107(1):139-46.

64. Xu C, Zarins CK, Pannaraj PS, Bassiouny HS, Glagov S. Hypercholesterolemia Superimposed by Experimental Hypertension Induces Differential Distribution of Collagen and Elastin. Arteriosclerosis, Thrombosis, and Vascular Biology. 2000;20(12):2566-72.

65. Martyn C, Greenwald S. Impaired synthesis of elastin in walls of aorta and large conduit arteries during early development as an initiating event in pathogenesis of systemic hypertension. The Lancet. 1997;350(9082):953-5.

66. Davis EC. Elastic lamina growth in the developing mouse aorta. Journal of Histochemistry & Cytochemistry. 1995;43(11):1115-23.

67. Dao H, Essalihi R, Bouvet C, Moreau P. Evolution and modulation of age-related medial elastocalcinosis: impact on large artery stiffness and isolated systolic hypertension. Cardiovascular Research. 2005;66(2):307.

68. Lemarié CA, Tharaux PL, Lehoux S. Extracellular matrix alterations in hypertensive vascular remodeling. Journal of Molecular and Cellular Cardiology. 2010;48(3):433-9.

69. Langille LB. Remodeling of developing and mature arteries: endothelium, smooth muscle, and matrix. Journal of Cardiovascular Pharmacology. 1993;21:S11-S7.

70. Mulvany MJ. Small artery remodelling in hypertension. Basic & Clinical Pharmacology & Toxicology. 2012;110(1):49-55.

71. Wang YX, Fitch RM. Vascular stiffness: Measurements, mechanisms and implications. Current Vascular Pharmacology. 2004;2(4):379-84.

72. McNulty M, Mahmud A, Feely J. Advanced Glycation End-Products and Arterial Stiffness in Hypertension. American Journal of Hypertension. 2007;20(3):242-7.

73. Aronson D. Cross-linking of glycated collagen in the pathogenesis of arterial and myocardial stiffening of aging and diabetes. Journal of Hypertension. 2003;21(1):3-12.

74. Norton GR, Candy G, Woodiwiss AJ. Aminoguanidine prevents the decreased myocardial compliance produced by streptozotocin-induced diabetes mellitus in rats. Circulation. 1996;93(10):1905-12.

75. Huijberts M, Wolffenbuttel B, Boudier H, Crijns F, Kruseman A, Poitevin P, et al. Aminoguanidine treatment increases elasticity and decreases fluid filtration of large arteries from diabetic rats. Journal of Clinical Investigation. 1993;92(3):1407.

76. Asif M, Egan J, Vasan S, Jyothirmayi GN, Masurekar MR, Lopez S, et al. An advanced glycation endproduct cross-link breaker can reverse age-related increases in myocardial stiffness. Proceedings of the National Academy of Sciences. 2000;97(6):2809-13.

77. Wolffenbuttel BH, Boulanger CM, Crijns FR, Huijberts MS, Poitevin P, Swennen GN, et al. Breakers of advanced glycation end products restore large artery properties in experimental diabetes. Proceedings of the National Academy of Sciences. 1998;95(8):4630-4.

78. Kass DA, Shapiro EP, Kawaguchi M, Capriotti AR, Scuteri A, Lakatta EG. Improved arterial compliance by a novel advanced glycation end-product crosslink breaker. Circulation. 2001;104(13):1464-70.

79. Blumenthal H, Lansing A, Wheeler P. Calcification of the media of the human aorta and its relation to intimal arteriosclerosis, ageing and disease. American Journal of Pathology. 1944;20:665-79.

80. Edmonds M. Medial arterial calcification and diabetes mellitus. Zeitschrift Kardiologie 2000;89(Suppl. 2):101-4.

81. Guerin A, London G, Marchais S, Metivier F. Arterial stiffening and vascular calcifications in end-stage renal disease. Nephrology Dialysis Transplantation. 2000;15:1014-21.

82. Ng K, Hildreth CM, Avolio AP, Phillips JK. Angiotensin-converting enzyme inhibitor limits pulse-wave velocity and aortic calcification in a rat model of cystic renal disease. American Journal of Physiology-Renal Physiology. 2011;301(5):F959-F66.

83. Sutliff RL, Walp ER, El-Ali AM, Elkhatib S, Lomashvili KA, O'Neill WC. Effect of medial calcification on vascular function in uremia. American Journal of Physiology-Renal Physiology. 2011;301(1):F78-F83.

84. Henrion D, Chillon JM, Godeau G, Muller F, Capdeville-Atkinson C, Hoffman M, et al. The consequences of aortic calcium overload following vitamin D3 plus nicotine treatment in young rats. Journal of Hypertension. 1991;9(10):919-26.

85. Nakamura U, Iwase M, Nohara S, Kanai H, Ichikawa K, Iida M. Usefulness of brachial-ankle pulse wave velocity measurement: correlation with abdominal aortic calcification. Hypertension Research: Official Journal of the Japanese Society of Hypertension. 2003;26(2):163.

86. Weber C, Zernecke A, Libby P. The multifaceted contributions of leukocyte subsets to atherosclerosis: lessons from mouse models. Nature Reviews Immunology. 2008;8(10):802-15.

87. Hansson GK, Hermansson A. The immune system in atherosclerosis. Nature Immunology. 2011;12(3):204-12.

88. Weber C, Noels H. Atherosclerosis: current pathogenesis and therapeutic options. Nature Medicine. 2011;17(11):1410-22.

89. Stocker R, Keaney JF. Role of Oxidative Modifications in Atherosclerosis. Physiological Reviews. 2004;84(4):1381-1478.

90. Bozec E, Lacolley P, Bergaya S, Boutouyrie P, Meneton P, Herissé-Legrand M, et al. Arterial stiffness and angiotensinogen gene in hypertensive patients and mutant mice. Journal of Hypertension. 2004;22(7):1299-307.

91. Tsilimingas N, Warnholtz A, Wendt M, Münzel T. Angiotensin II and Oxidative Stress. Angiotensin Vol II: Springer Berlin Heidelberg; 2004. p. 3-20.

92. Dzau VJ. Significance of the vascular renin-angiotensin pathway. Hypertension. 1986;8(7):553-9.

93. Daugherty A, Manning MW, Cassis LA. Angiotensin II promotes atherosclerotic lesions and aneurysms in apolipoprotein E–deficient mice. The Journal of Clinical Investigation. 2000;105(11):1605-12.

94. Ng K, Butlin M, Avolio AP. Persistent effect of early, brief angiotensin-converting enzyme inhibition on segmental pressure dependency of aortic stiffness in spontaneously hypertensive rats. Journal of Hypertension. 2012;30(9):1782-90.

95. Mahmud A, Feely J. Reduction in arterial stiffness with angiotensin II antagonist is comparable with and additive to ACE inhibition. American Journal of Hypertension. 2002;15(4):321-5.

96. Lantelme P, Mestre C, Lievre M, Gressard A, Milon H. Heart Rate: An Important Confounder of Pulse Wave Velocity Assessment. Hypertension. 2002;39(6):1083-7.

97. Cines DB, Pollak ES, Buck CA, Loscalzo J, Zimmerman GA, McEver RP, et al. Endothelial cells in physiology and in the pathophysiology of vascular disorders. Blood. 1998;91(10):3527-61.

98. Soulis JV, Giannoglou GD, Parcharidis GE, Louridas GE. Flow parameters in normal left coronary artery tree. Implication to atherogenesis. Computers in Biology and Medicine. 2007;37(5):628-36.

99. Hahn C, Schwartz MA. Mechanotransduction in vascular physiology and atherogenesis. Nature Reviews Molecular Cell Biology. 2009;10(1):53-62.

100. Davies PF. Flow-mediated endothelial mechanotransduction. Physiological Reviews. 1995;75(3):519.

101. Foster M, Hess D, Stamler J. Protein S-nitrosylation in health and disease: a current perspective. Trends in Molecular Medicine. 2009;15(9):391-404.

102. Thomas SR, Witting PK, Drummond GR. Redox control of endothelial function and dysfunction: molecular mechanisms and therapeutic opportunities. Antioxidants & Redox Signaling. 2008;10(10):1713-66.

103. Thomas SR, Chen K, Keaney Jr JF. Oxidative stress and endothelial nitric oxide bioactivity. Antioxidants and Redox Signaling. 2003;5(2):181-94.

104. Hess D, Matsumoto A, Kim S, Marshall H, Stamler J. Protein S-nitrosylation: purview and parameters. Nature Reviews Molecular Cell Biology. 2005;6(2):150-66.

105. Stamler JS, Lamas S, Fang FC. Nitrosylation: the prototypic redox-based signaling mechanism. Cell. 2001;106(6):675-83.

106. Santhanam L, Gucek M, Brown TR, Mansharamani M, Ryoo S, Lemmon CA, et al. Selective fluorescent labeling of S-nitrosothiols (S-FLOS): A novel method for studying S-nitrosation. Nitric Oxide. 2008;19(3):295-302.

107. Hare JM. Nitroso-redox balance in the cardiovascular system. New England Journal of Medicine. 2004;351(20):2112-4.

108. Chirinos JA, David R, Bralley JA, Zea-Díaz H, Muñoz-Atahualpa E, Corrales-Medina F, et al. Endogenous Nitric Oxide Synthase Inhibitors, Arterial Hemodynamics, and Subclinical Vascular Disease The PREVENCION Study. Hypertension. 2008;52(6):1051-9.

109. Andrew PJ, Mayer B. Enzymatic function of nitric oxide synthases. Cardiovascular Research. 1999;43(3):521-31.

110. KrÖncke, Fehsel, Kolb B. Inducible nitric oxide synthase in human diseases. Clinical & Experimental Immunology. 1998;113(2):147-56.

111. Zhou L, Zhu D-Y. Neuronal nitric oxide synthase: Structure, subcellular localization, regulation, and clinical implications. Nitric Oxide. 2009;20(4):223-30.

112. Rees D, Palmer R, Schulz R, Hodson H, Moncada S. Characterization of three inhibitors of endothelial nitric oxide synthase in vitro and in vivo. British Journal of Pharmacology. 1990;101(3):746-52.

113. Colonna VDG, Bianchi M, Pascale V, Ferrario P, Morelli F, Pascale W, et al. Asymmetric dimethylarginine (ADMA): an endogenous inhibitor of nitric oxide synthase and a novel cardiovascular risk molecule. Medical Science Monitor. 2009;15(4):RA91-RA101.

114. Cayatte AJ, Palacino JJ, Horten K, Cohen RA. Chronic inhibition of nitric oxide production accelerates neointima formation and impairs endothelial function in

hypercholesterolemic rabbits. Arteriosclerosis, Thrombosis, and Vascular Biology. 1994;14(5):753-9.

115. Kameyama H, Takeda K, Kusaba T, Narumiya H, Tanda S, Kuwahara N, et al. Augmentation of Pulse Wave Velocity Precedes Vascular Structural Changes of the Aorta in Rats Treated with N ω-Nitro-L-Arginine Methyl Ester. Hypertension Research. 2005;28(5):439-45.

116. Joannides R, Richard V, Haefeli WE, Benoist A, Linder L, Lüscher TF, et al. Role of Nitric Oxide in the Regulation of the Mechanical Properties of Peripheral Conduit Arteries in Humans. Hypertension. 1997;30(6):1465-70.

117. Parkington HC, Tare M, Coleman HA. The EDHF Story The Plot Thickens. Circulation research. 2008;102(10):1148-50.

118. Vliet BN, Chafe LL, Montani JP. Characteristics of 24 h Telemetered Blood Pressure in eNOS-Knockout and C57Bl/6J Control Mice. The Journal of Physiology. 2003;549(1):313-25.

119. Soucy KG, Ryoo S, Benjo A, Lim HK, Gupta G, Sohi JS, et al. Impaired shear stress-induced nitric oxide production through decreased NOS phosphorylation contributes to age-related vascular stiffness. Journal of Applied Physiology. 2006;101(6):1751-9.

120. Jung SM, Jandu S, Steppan J, Belkin A, An SS, Pak A, et al. Increased tissue transglutaminase activity contributes to central vascular stiffness in eNOS knockout mice. American Journal of Physiology-Heart and Circulatory Physiology. 2013;305(6):H803-H10.

121. Lorand L, Graham R. Transglutaminases: crosslinking enzymes with pleiotropic functions. Nature Reviews Molecular Cell Biology. 2003;4(2):140-56.

122. Bakker E, Pistea A, VanBavel E. Transglutaminases in vascular biology: relevance for vascular remodeling and atherosclerosis. Journal of Vascular Research. 2008;45(4):271-8.

123. Karpuj MV, Becher MW, Springer JE, Chabas D, Youssef S, Pedotti R, et al. Prolonged survival and decreased abnormal movements in transgenic model of Huntington disease, with administration of the transglutaminase inhibitor cystamine. Nature Medicine. 2002;8(2):143-9.

124. Lampasona V, Bonfanti R, Bazzigaluppi E, Venerando A, Chiumello G, Bosi E, et al. Antibodies to tissue transglutaminase C in type I diabetes. Diabetologia. 1999;42(10):1195-8.

125. Reif S, Lerner A. Tissue transglutaminase—the key player in celiac disease: a review. Autoimmunity Reviews. 2004;3(1):40-5.

126. Haroon ZA, Wannenburg T, Gupta M, Greenberg CS, Wallin R, Sane DC. Localization of tissue transglutaminase in human carotid and coronary artery atherosclerosis: implications for plaque stability and progression. Laboratory Investigation. 2001;81(1):83-93.

127. Pistea A, Bakker ENTP, Spaan JAE, Hardeman MR, Van Rooijen N, VanBavel E. Small artery remodeling and erythrocyte deformability in L-NAME-induced hypertension: Role of transglutaminases. Journal of Vascular Research. 2008;45(1):10-8.

128. Ou H, Haendeler J, Aebly MR, Kelly LA, Cholewa BC, Koike G, et al. Retinoic acid–induced tissue transglutaminase and apoptosis in vascular smooth muscle cells. Circulation Research. 2000;87(10):881-7.

129. Iismaa S, Mearns B, Lorand L, Graham R. Transglutaminases and disease: lessons from genetically engineered mouse models and inherited disorders. Physiological reviews. 2009;89(3):991.

130. Chen JS, Mehta K. Tissue transglutaminase: an enzyme with a split personality. The International Journal of Biochemistry & Cell Biology. 1999;31(8):817-36.

131. Gaudry C, Verderio E, Jones R, Smith C, Griffin M. Tissue Transglutaminase Is an Important Player at the Surface of Human Endothelial Cells: Evidence for Its Externalization and Its Colocalization with the [beta] 1 Integrin. Experimental Cell Research. 1999;252(1):104-13.

132. Lorand L, Dailey J, Turner P. Fibronectin as a carrier for the transglutaminase from human erythrocytes. Proceedings of the National Academy of Sciences. 1988;85(4):1057-9.

133. Sane DC, Moser TL, Pippen AM, Parker CJ, Achyuthan KE, Greenberg CS. Vitronectin is a substrate for transglutaminases. Biochemical and Biophysical Research Communications. 1988;157(1):115-20.

134. Aeschlimann D, Paulsson M. Cross-linking of laminin-nidogen complexes by tissue transglutaminase. A novel mechanism for basement membrane stabilization. Journal of Biological Chemistry. 1991;266(23):15308-17.

135. Kleman J-P, Aeschlimann D, Paulsson M, van der Rest M. Transglutaminase-catalyzed crosslinking of fibrils of collagen V/XI in A204 rhabdomyosarcoma cells. Biochemistry. 1995;34(42):13768-75.

136. Griffin M, Casadio R, Bergamini C. Transglutaminases: nature's biological glues. Biochemical Journal. 2002;368(Pt 2):377.

137. Telci D, Collighan R, Basaga H, Griffin M. Increased TG2 Expression Can Result in Induction of Transforming Growth Factor 1, Causing Increased Synthesis and Deposition of Matrix Proteins, Which Can Be Regulated by Nitric Oxide. Journal of Biological Chemistry. 2009;284(43):29547.

138. Bergamini C, Griffin M, Pansini F. Transglutaminase and vascular biology: physiopathologic implications and perspectives for therapeutic interventions. Current Medicinal Chemistry. 2005;12(20):2357-72.

139. Shin DM, Jeon JH, Kim CW, Cho SY, Kwon JC, Lee HJ, et al. Cell type-specific activation of intracellular transglutaminase 2 by oxidative stress or ultraviolet irradiation: Implications of transglutaminase 2 in age-related cataractogenesis. Journal of Biological Chemistry. 2004;279(15):15032-9.

140. Auld GC, Ritchie H, Robbie LA, Booth NA. Thrombin Upregulates Tissue Transglutaminase in Endothelial Cells A Potential Role for Tissue Transglutaminase in Stability of Atherosclerotic Plaque. Arteriosclerosis, Thrombosis, and Vascular Biology. 2001;21(10):1689-94.

141. Aeschlimann D, Thomazy V. Protein crosslinking in assembly and remodelling of extracellular matrices: The role of transglutaminases. Connective Tissue Research. 2000;41(1):1-27.

142. Lai T, Hausladen A, Slaughter T, Eu J, Stamler J, Greenberg C. Calcium regulates S-nitrosylation, denitrosylation, and activity of tissue transglutaminase. Biochemistry. 2001;40(16):4904-10.

143. Bernassola F, Rossi A, Melino G. Regulation of transglutaminases by nitric oxide. Annals of the New York Academy of Sciences. 1999;887(1):83-91.

144. Engholm M, Eftekhari A, Chwatko G, Bald E, Mulvany MJ. Effect of Cystamine on Blood Pressure and Vascular Characteristics in Spontaneously Hypertensive Rats. Journal of Vascular Research. 2011;48(6):476-84.

145. Bakker EN, Buus CL, Spaan JA, Perree J, Ganga A, Rolf TM, et al. Small artery remodeling depends on tissue-type transglutaminase. Circulation Research. 2005;96(1):119-26.

146. van den Akker J, VanBavel E, van Geel R, Matlung HL, Guvenc Tuna B, Janssen GMC, et al. The redox state of transglutaminase 2 controls arterial remodeling. PLoS ONE. 2011;6(8).

147. Stamnaes J, Pinkas DM, Fleckenstein B, Khosla C, Sollid LM. Redox Regulation of Transglutaminase 2 Activity. Journal of Biological Chemistry. 2010;285(33):25402-9.

148. Eftekhari A, Rahman A, Schæbel LH, Chen H, Rasmussen CV, Aalkjær C, et al. Chronic cystamine treatment inhibits small artery remodelling in rats. Journal of Vascular Research. 2007;44(6):471-82.

149. Lorand L, Conrad S. Transglutaminases. Molecular and Cellular Biochemistry. 1984 58(1-2):9-35.

150. Bakker ENTP, Pistea A, Spaan JAE, Rolf T, de Vries CJ, van Rooijen N, et al. Flow-dependent remodeling of small arteries in mice deficient for tissue-type transglutaminase. Circulation Research. 2006;99(1):86-92.

151. Nanda N, Iismaa SE, Owens WA, Husain A, Mackay F, Graham RM. Targeted inactivation of Gh/tissue transglutaminase II. Journal of Biological Chemistry. 2001;276(23):20673-8.

152. Deasey S, Shanmugasundaram S, Nurminskaya M. Tissue-specific responses to loss of transglutaminase 2. Amino Acids. 2011:1-9.

153. Sarang Z, Tóth B, Balajthy Z, Köröskényi K, Garabuczi E, Fésüs L, et al. Some lessons from the tissue transglutaminase knockout mouse. Amino Acids. 2009;36(4):625-31.

154. Szondy Z, Mastroberardino P, Varadi J, Farrace M, Nagy N, Bak I, et al. Tissue transglutaminase (TG2) protects cardiomyocytes against ischemia/reperfusion injury by regulating ATP synthesis. Cell Death & Differentiation. 2006;13(10):1827-9.

155. Iwai N, Shimoike H, Kinoshita M. Genes up-regulated in hypertrophied ventricle. Biochemical and Biophysical Research Communications. 1995;209(2):527-34.

156. Small K, Feng JF, Lorenz J, Donnelly ET, Yu A, Im MJ, et al. Cardiac specific overexpression of transglutaminase II (Gh) results in a unique hypertrophy phenotype independent of phospholipase C activation. Journal of Biological Chemistry. 1999;274(30):21291.

157. Zhang Z, Vezza R, Plappert T, McNamara P, Lawson JA, Austin S, et al. COX-2–dependent cardiac failure in Gh/tTG transgenic mice. Circulation Research. 2003;92(10):1153-61.

158. Hwang K-C, Gray CD, Sweet WE, Moravec CS, Im M-J. α1-Adrenergic receptor coupling with Gh in the failing human heart. Circulation. 1996;94(4):718-26.

159. Johnson TS, El-Koraie AF, Skill NJ, Baddour NM, El Nahas AM, Njloma M, et al. Tissue transglutaminase and the progression of human renal scarring. Journal of the American Society of Nephrology. 2003;14(8):2052-62.

160. Grenard P, Bresson-Hadni S, El Alaoui Sd, Chevallier M, Vuitton DA, Ricard-Blum S. Transglutaminase-mediated cross-linking is involved in the stabilization of extracellular matrix in human liver fibrosis. Journal of Hepatology. 2001;35(3):367-75.

161. Boisvert W, Rose D, Boullier A, Quehenberger O, Sydlaske A, Johnson K, et al. Leukocyte transglutaminase 2 expression limits atherosclerotic lesion size. Arteriosclerosis, Thrombosis, and Vascular Biology. 2006;26(3):563-9.

162. Sumi Y, Inoue N, Azumi H, Seno T, Okuda M, Hirata K-i, et al. Expression of tissue transglutaminase and elafin in human coronary artery: implication for plaque instability. Atherosclerosis. 2002;160(1):31-9.

163. Matlung HL, Neele AE, Groen HC, van Gaalen K, Tuna BG, van Weert A, et al. Transglutaminase activity regulates atherosclerotic plaque composition at locations exposed to oscillatory shear stress. Atherosclerosis. 2012.

164. Johnson KA, Polewski M, Terkeltaub RA, Johnson KA, Polewski M, Terkeltaub RA. Transglutaminase 2 is central to induction of the arterial calcification program by smooth muscle cells.[Erratum appears in Circ Res. 2008 May 23;102(10):e106]. Circulation Research. 2008;102(5):529-37.

165. Faverman L, Mikhaylova L, Malmquist J, Nurminskaya M. Extracellular transglutaminase 2 activates β-catenin signaling in calcifying vascular smooth muscle cells. FEBS letters. 2008;582(10):1552-7.

166. Beazley KE, Deasey S, Lima F, Nurminskaya MV. Transglutaminase 2–Mediated Activation of β-Catenin Signaling Has a Critical Role in Warfarin-Induced Vascular Calcification. Arteriosclerosis, Thrombosis, and Vascular Biology. 2012;32(1):123-30.

167. Chabot N, Moreau S, Mulani A, Moreau P, Keillor JW. Fluorescent probes of tissue transglutaminase reveal its association with arterial stiffening. Chemistry & Biology. 2010;17(10):1143-50.

168. Tuday EC, Nyhan D, Shoukas AA, Berkowitz DE. Simulated microgravity-induced aortic remodeling. Journal of Applied Physiology. 2009;106(6):2002-8.

169. Schaertl S, Prime M, Wityak J, Dominguez C, Munoz-Sanjuan I, Pacifici RE, et al. A profiling platform for the characterization of transglutaminase 2 (TG2) inhibitors. Journal of Biomolecular Screening. 2010;15(5):478-87.

170. Lesort M, Lee M, Tucholski J, Johnson GVW. Cystamine Inhibits Caspase Activity: Implications for the treatment of polyglutamine disorders. Journal of Biological Chemistry. 2003;278(6):3825-30.

171. Wang Y-X. Cardiovascular functional phenotypes and pharmacological responses in apolipoprotein E deficient mice. Neurobiology of Aging. 2005;26(3):309-16.

172. Plump AS, Smith JD, Hayek T, Aalto-Setälä K, Walsh A, Verstuyft JG, et al. Severe hypercholesterolemia and atherosclerosis in apolipoprotein E-deficient mice created by homologous recombination in ES cells. Cell. 1992;71(2):343-53.

173. Nakashima Y, Plump AS, Raines EW, Breslow JL, Ross R. ApoE-deficient mice develop lesions of all phases of atherosclerosis throughout the arterial tree. Arteriosclerosis, Thrombosis, and Vascular Biology. 1994;14(1):133-40.

174. Reddick RL, Zhang SH, Maeda N. Atherosclerosis in mice lacking apo E. Evaluation of lesional development and progression. Arteriosclerosis, Thrombosis, and Vascular Biology. 1994;14(1):141-7.

175. Kauser K, Da Cunha V, Fitch R, Mallari C, Rubanyi GM. Role of endogenous nitric oxide in progression of atherosclerosis in apolipoprotein E-deficient mice. American Journal of Physiology - Heart and Circulatory Physiology. 2000;278(5 47-5):H1679-H85.

176. Hodgin JB, Knowles JW, Kim H-S, Smithies O, Maeda N. Interactions between endothelial nitric oxide synthase and sex hormones in vascular protection in mice. The Journal of Clinical Investigation. 2002;109(4):541-8.

177. Kuhlencordt PJ, Gyurko R, Han F, Scherrer-Crosbie M, Aretz TH, Hajjar R, et al. Accelerated Atherosclerosis, Aortic Aneurysm Formation, and Ischemic Heart Disease in Apolipoprotein E/Endothelial Nitric Oxide Synthase Double-Knockout Mice. Circulation. 2001;104(4):448-54.

178. Sindler AL, Fleenor BS, Calvert JW, Marshall KD, Zigler ML, Lefer DJ, et al. Nitrite supplementation reverses vascular endothelial dysfunction and large elastic artery stiffness with aging. Aging Cell. 2011;10(3):429-37.

179. Tan I, Butlin M, Liu YY, Ng K, Avolio AP. Heart Rate Dependence of Aortic Pulse Wave Velocity at Different Arterial Pressures in RatsNovelty and Significance. Hypertension. 2012;60(2):528-33.

180. Salum E, Kampus P, Zilmer M, Eha J, Butlin M, Avolio AP, et al. Effect of vitamin D on aortic remodeling in streptozotocin-induced diabetes. Cardiovascular Diabetology. 2012;11:58.

181. Mitchell GF, Pfeffer MA, Finn PV, Pfeffer JM. Comparison of techniques for measuring pulse-wave velocity in the rat. Journal of Applied Physiology. 1997;82(1):203-10.

182. Butlin M, Hammond A, Lindesay G, Viegas K, Avolio AP. 138 In-Vitro and in-Vivo Use of Vasoactive Agents in Characterising Aortic Stiffness in Rats: Testing the Assumptions. Journal of Hypertension. 2012;30:e42.

183. Viegas K, Lindesay G, Butlin M, Avolio A, editors. Aortic Stiffness is Dependent on Direction of Mean Arterial Pressure Change. Hypertension. 2012;60:497.

184. Lichtenstein O, Safar ME, Mathieu E, Poitevin P, Levy BI. Static and dynamic mechanical properties of the carotid artery from normotensive and hypertensive rats. Hypertension. 1998;32(2):346-50.

185. Bonyhay I, Jokkel G, Karlocai K, Reneman R, Kollai M. Effect of vasoactive drugs on carotid diameter in humans. American Journal of Physiology-Heart and Circulatory Physiology. 1997;273(4):H1629-H36.

186. Coleridge HM, Coleridge JC, Poore ER, Roberts AM, Schultz HD. Aortic wall properties and baroreceptor behaviour at normal arterial pressure and in acute hypertensive resetting in dogs. The Journal of Physiology. 1984;350(1):309-26.

187. Hironaka K, Yano M, Kohno M, Tanigawa T, Obayashi M, Konishi M, et al. In vivo aortic wall characteristics at the early stage of atherosclerosis in rabbits. American Journal of Physiology - Heart and Circulatory Physiology. 1997;273(3):H1142-H7.

188. Lénárd Z, Fülöp D, Visontai Z, Jokkel G, bor a, Reneman R, et al. Static versus dynamic distensibility of the carotid artery in humans. Journal of Vascular Research. 2000;37(2):103-11.

189. Eckberg DL, Sleight P. Human baroreflexes in health and disease: Clarendon Press Oxford; 1992.

190. O'Leary DD, Steinback CD, Cechetto AD, Foell BT, Topolovec JC, Gelb AW, et al. Relating drug-induced changes in carotid artery mechanics to cardiovagal and sympathetic baroreflex control. Canadian Journal of Physiology and Pharmacology. 2005;83(5):439-46.

191. Studinger P, Goldstein R, Taylor JA. Mechanical and neural contributions to hysteresis in the cardiac vagal limb of the arterial baroreflex. The Journal of Physiology. 2007;583(3):1041-8.

192. Kroeker EJ, Wood EH. Comparison of simultaneously recorded central and peripheral arterial pressure pulses during rest, exercise and tilted position in man. Circulation Research. 1955;3(6):623-32.

193. Wilkinson IB, Mohammad NH, Tyrrell S, Hall IR, Webb DJ, Paul VE, et al. Heart rate dependency of pulse pressure amplification and arterial stiffness. American Journal of Hypertension. 2002;15(1):24-30.

194. Rowell LB, Brengelmann GL, Blackmon JR, Bruge RA, Murray JA. Disparities between aortic and peripheral pulse pressures induced by upright exercise and vasomotor changes in man. Circulation. 1968;37(6):954-64.

195. Cosson E, Herisse M, Laude D, Thomas F, Valensi P, Attali J-R, et al. Aortic stiffness and pulse pressure amplification in Wistar-Kyoto and spontaneously hypertensive rats. American Journal of Physiology-Heart and Circulatory Physiology. 2007;292(5):H2506-H12.

196. Safar ME, Levy BI, Struijker-Boudier H. Current Perspectives on Arterial Stiffness and Pulse Pressure in Hypertension and Cardiovascular Diseases. Circulation. 2003;107(22):2864-9.

197. Vanbavel E, Bakker EN, Vanbavel E, Bakker ENTP. A vascular bone collector: arterial calcification requires tissue-type transglutaminase. Circulation Research. 2008;102(5):507-9.

198. Santhanam L, Berkowitz DE, Belkin AM. Nitric oxide regulates non-classical secretion of tissue transglutaminase. Communicative & Integrative Biology. 2011;4(5):584-6.

199. Elhage R, Bayard F, Richard V, Holvoet P, Duverger N, Fiévet C, et al. Prevention of Fatty Streak Formation of 17β-Estradiol Is Not Mediated by the Production of Nitric Oxide in Apolipoprotein E– Deficient Mice. Circulation. 1997;96(9):3048-52.

200. Obst M, Grossa V, Luft FC. Systemic hemodynamics in non-anesthetized L-NAME- and DOCA-salt-treated mice. Journal of Hypertension. 2004;22(10):1889-94.

201. Johnson KB, Petersen-Jones H, Thompson JM, Hitomi K, Itoh M, Bakker EN, et al. Vena cava and aortic smooth muscle cells express transglutaminases 1 and 4 in addition to transglutaminase 2. American Journal of Physiology-Heart and Circulatory Physiology. 2012;302(7):H1355-H66.

202. Moncada S. Prostacyclin and arterial wall biology. Arteriosclerosis, Thrombosis, and Vascular Biology. 1982;2(3):193-207.

203. Osanai T, Fujita N, Fujiwara N, Nakano T, Takahashi K, Guan W, et al. Cross talk of shear-induced production of prostacyclin and nitric oxide in endothelial cells. American Journal of Physiology - Heart and Circulatory Physiology. 2000;278(1):H233-H8.

204. Merkus D, Houweling B, Zarbanoui A, Duncker DJ. Interaction between prostanoids and nitric oxide in regulation of systemic, pulmonary, and coronary vascular tone in exercising swine. American Journal of Physiology - Heart and Circulatory Physiology. 2004;286(3):H1114-H23.

205. Puybasset L, Béa M-L, Ghaleh B, Giudicelli J-F, Berdeaux A. Coronary and Systemic Hemodynamic Effects of Sustained Inhibition of Nitric Oxide Synthesis in Conscious Dogs: Evidence for Cross Talk Between Nitric Oxide and Cyclooxygenase in Coronary Vessels. Circulation Research. 1996;79(2):343-57.

206. Sun D, Huang A, Smith CJ, Stackpole CJ, Connetta JA, Shesely EG, et al. Enhanced Release of Prostaglandins Contributes to Flow-Induced Arteriolar Dilation in eNOS Knockout Mice. Circulation Research. 1999;85(3):288-93.

207. Busse R, Edwards G, Félétou M, Fleming I, Vanhoutte PM, Weston AH. EDHF: bringing the concepts together. Trends in Pharmacological Sciences. 2002;23(8):374-80.

208. Garland CJ, McPherson GA. Evidence that nitric oxide does not mediate the hyperpolarization and relaxation to acetylcholine in the rat small mesenteric artery. British Journal of Pharmacology. 1992;105(2):429-35.

209. Cohen RA, Vanhoutte PM. Endothelium-Dependent Hyperpolarization: Beyond Nitric Oxide and Cyclic GMP. Circulation. 1995;92(11):3337-49.

210. Nagao T, Vanhoutte PM. Hyperpolarization as a mechanism for endothelium-dependent relaxations in the porcine coronary artery. The Journal of Physiology. 1992;445(1):355-67.

211. Shimokawa H, Yasutake H, Fujii K, Owada M, Nakaike R, Fukumoto Y, et al. The importance of the hyperpolarizing mechanism increases as the vessel size decreases in endothelium-dependent relaxations in rat mesenteric circulation. Journal of Cardiovascular Pharmacology. 1996;28(5):703.

212. Garland CJ, Hiley CR, Dora KA. EDHF: spreading the influence of the endothelium. British Journal of Pharmacology. 2011;164(3):839-52.

213. Waldron GJ, Ding H, Lovren F, Kubes P, Triggle CR. Acetylcholine-induced relaxation of peripheral arteries isolated from mice lacking endothelial nitric oxide synthase. British Journal of Pharmacology. 1999;128(3):653-8.

214. Buxton IL, Cheek DJ, Eckman D, Westfall DP, Sanders KM, Keef KD. NG-nitro L-arginine methyl ester and other alkyl esters of arginine are muscarinic receptor antagonists. Circulation Research. 1993;72(2):387-95.

215. Kass DA, Hare JM, Georgakopoulos D. Murine Cardiac Function A Cautionary Tail. Circulation Research. 1998;82(4):519-22.

216. Janssen BJ, De Celle T, Debets JJ, Brouns AE, Callahan MF, Smith TL. Effects of anesthetics on systemic hemodynamics in mice. American Journal of Physiology-Heart and Circulatory Physiology. 2004;287(4):H1618-H24.

217. Pollick C, Hale SL, Kloner RA. Echocardiographic and cardiac doppler assessment of mice. Journal of the American Society of Echocardiography. 1995;8(5, Part 1):602-10.

218. Lorenz JN. A practical guide to evaluating cardiovascular, renal, and pulmonary function in mice. American Journal of Physiology-Regulatory, Integrative and Comparative Physiology. 2002;282(6):R1565-R82.

219. Choy K, Beck K, Png FY, Wu BJ, Leichtweis SB, Thomas SR, et al. Processes involved in the site-specific effect of probucol on atherosclerosis in apolipoprotein E gene knockout mice. Arteriosclerosis, Thrombosis, and Vascular Biology. 2005;25(8):1684-90.

220. Thomas SR, Leichtweis SB, Pettersson K, Croft KD, Mori TA, Brown AJ, et al. Dietary cosupplementation with vitamin E and coenzyme Q10 inhibits atherosclerosis in apolipoprotein E gene knockout mice. Arteriosclerosis, Thrombosis, and Vascular Biology. 2001;21(4):585-93.

221. Hofker MH, van Vlijmen BJ, Havekes LM. Transgenic mouse models to study the role of APOE in hyperlipidemia and atherosclerosis. Atherosclerosis. 1998;137(1):1-11.

222. Buday A, Őrsy P, Godó M, Mózes M, Kökény G, Lacza Z, et al. Elevated systemic TGF-β impairs aortic vasomotor function through activation of NADPH oxidase-driven superoxide production and leads to hypertension, myocardial remodeling, and increased plaque formation in apoE−/− mice. American Journal of Physiology - Heart and Circulatory Physiology. 2010;299(2):H386-H95.

223. Chen X, Zhang H, McAfee S, Zhang C. The reciprocal relationship between adiponectin and LOX-1 in the regulation of endothelial dysfunction in ApoE knockout mice. American Journal of Physiology-Heart and Circulatory Physiology. 2010;299(3):H605-H12.

224. Wilcox JN, Subramanian RR, Sundell CL, Tracey WR, Pollock JS, Harrison DG, et al. Expression of Multiple Isoforms of Nitric Oxide Synthase in Normal and Atherosclerotic Vessels. Arteriosclerosis, Thrombosis, and Vascular Biology. 1997;17(11):2479-88.

225. Nathan C. Nitric oxide as a secretory product of mammalian cells. The FASEB Journal. 1992;6(12):3051-64.

226. Beckman JS, Beckman TW, Chen J, Marshall PA, Freeman BA. Apparent hydroxyl radical production by peroxynitrite: implications for endothelial injury from nitric oxide and superoxide. Proceedings of the National Academy of Sciences. 1990;87(4):1620-4.

227. Kuhlencordt PJ, Chen J, Han F, Astern J, Huang PL. Genetic Deficiency of Inducible Nitric Oxide Synthase Reduces Atherosclerosis and Lowers Plasma Lipid Peroxides in Apolipoprotein E–Knockout Mice. Circulation. 2001;103(25):3099-104.

228. Huang Z, Huang P, Panahian N, Dalkara T, Fishman M, Moskowitz M. Effects of cerebral ischemia in mice deficient in neuronal nitric oxide synthase. Science. 1994;265(5180):1883-5.

229. Crauwels HM, Van Hove CE, Holvoet P, Herman AG, Bult H. Plaque-associated endothelial dysfunction in apolipoprotein E-deficient mice on a regular diet. Effect of human apolipoprotein AI. Cardiovascular Research. 2003;59(1):189-99.

230. Bentzon JF, Pasterkamp G, Falk E. Expansive Remodeling Is a Response of the Plaque-Related Vessel Wall in Aortic Roots of ApoE-Deficient Mice: An Experiment of Nature. Arteriosclerosis, Thrombosis, and Vascular Biology. 2003;23(2):257-62.

231. Donato AJ, Walker AE, Magerko KA, Bramwell RC, Black AD, Henson GD, et al. Life-long caloric restriction reduces oxidative stress and preserves nitric oxide bioavailability and function in arteries of old mice. Aging Cell. 2013;12(5):772-83.

232. Goyal V. Changes with age in the aorta of man and mouse. Experimental Gerontology. 1982;17(2):127-32.

233. Huo Y, Guo X, Kassab G. The flow field along the entire length of mouse aorta and primary branches. Annals of Biomedical Engineering. 2008;36(5):685-99.